



National Library
of Canada

Acquisitions and
Bibliographic Services Branch

395 Wellington Street
Ottawa, Ontario
K1A 0N4

Bibliothèque nationale
du Canada

Direction des acquisitions et
des services bibliographiques

395, rue Wellington
Ottawa (Ontario)
K1A 0N4

Acquisitions and Bibliographic Services

Direction des acquisitions et des services bibliographiques

NOTICE

The quality of this microform is heavily dependent upon the quality of the original thesis submitted for microfilming. Every effort has been made to ensure the highest quality of reproduction possible.

If pages are missing, contact the university which granted the degree.

Some pages may have indistinct print especially if the original pages were typed with a poor typewriter ribbon or if the university sent us an inferior photocopy.

Reproduction in full or in part of this microform is governed by the Canadian Copyright Act, R.S.C. 1970, c. C-30, and subsequent amendments.

AVIS

La qualité de cette microforme dépend grandement de la qualité de la thèse soumise au microfilmage. Nous avons tout fait pour assurer une qualité supérieure de reproduction.

S'il manque des pages, veuillez communiquer avec l'université qui a conféré le grade.

La qualité d'impression de certaines pages peut laisser à désirer, surtout si les pages originales ont été dactylographiées à l'aide d'un ruban usé ou si l'université nous a fait parvenir une photocopie de qualité inférieure.

La reproduction, même partielle, de cette microforme est soumise à la Loi canadienne sur le droit d'auteur, SRC 1970, c. C-30, et ses amendements subséquents.

Canada

UNIVERSITY OF ALBERTA

A SHEAR-FRICTION TRUSS MODEL FOR REINFORCED
CONCRETE BEAMS SUBJECTED TO SHEAR

BY

SIMON AIMIAN CHEN



A THESIS

SUBMITTED TO THE FACULTY OF GRADUATE STUDIES AND
RESEARCH IN PARTIAL FULFILLMENT OF THE REQUIREMENTS
FOR THE DEGREE OF DOCTOR OF PHILOSOPHY

DEPARTMENT OF CIVIL ENGINEERING

EDMONTON, ALBERTA

FALL, 1993



National Library
of Canada

Acquisitions and
Bibliographic Services Branch

395 Wellington Street
Ottawa, Ontario
K1A 0N4

Bibliothèque nationale
du Canada

Direction des acquisitions et
des services bibliographiques

395, rue Wellington
Ottawa (Ontario)
K1A 0N4

Votre lieu - Votre référence

Our file - Notre référence

The author has granted an irrevocable non-exclusive licence allowing the National Library of Canada to reproduce, loan, distribute or sell copies of his/her thesis by any means and in any form or format, making this thesis available to interested persons.

L'auteur a accordé une licence irrévocable et non exclusive permettant à la Bibliothèque nationale du Canada de reproduire, prêter, distribuer ou vendre des copies de sa thèse de quelque manière et sous quelque forme que ce soit pour mettre des exemplaires de cette thèse à la disposition des personnes intéressées.

The author retains ownership of the copyright in his/her thesis. Neither the thesis nor substantial extracts from it may be printed or otherwise reproduced without his/her permission.

L'auteur conserve la propriété du droit d'auteur qui protège sa thèse. Ni la thèse ni des extraits substantiels de celle-ci ne doivent être imprimés ou autrement reproduits sans son autorisation.

ISBN 0-315-88194-1

Canada

Aimian Chen
Dept. of Civil Engineering
University of Alberta
Edmonton, Alberta
Canada T6G 2G7

March 21, 1993

Professor Scordelis, A.C.
Dept. of Civil Engineering
University of California
Berkeley, California
USA

Dear Professor Scordelis:

I am a Ph.D student in the Dept. of Civil Engineering, University of Alberta. My supervisor is Professor MacGregor, James G. I am writing to you asking for your permission to use the test data and the crack patterns of the reinforced concrete beams you tested. They are going to be used in my Ph.D thesis to examine the shear-friction truss model I developed in the thesis. The test data and the crack patterns that I am using were published in the following articles:

"Shear strength of reinforced concrete beams," by B. Bresler and A.C. Scordelis, 1961,

"Shear strength of reinforced concrete beams-Series II," by B. Bresler and A.C. Scordelis, 1964

"Shear strength of reinforced concrete beams-Series III," by B. Bresler and A.C. Scordelis, 1966

Thank you very much for your kindest help. I am looking forwards to your your reply.

Thank you very much.

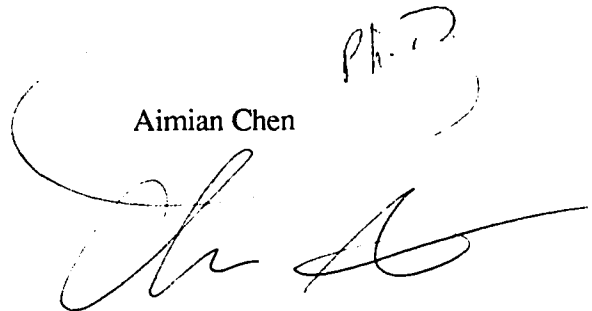
MARCH 31, 1993

DEAR MR. CHEN:

YOU ARE WELCOME TO USE THE
TEST DATA IN THE ABOVE REPORTS
IN YOUR RESEARCH STUDIES.
GOOD LUCK IN YOUR WORK.

Alex Scordelis

Aimian Chen

Ph.D.


UNIVERSITY OF ALBERTA

RELEASE FORM

NAME OF AUTHOR: Simon Aimian Chen

TITLE OF THESIS: A Shear-Friction Truss Model for Reinforced
Concrete Beams Subjected to Shear

DEGREE: Doctor of Philosophy

YEAR THIS DEGREE GRANTED: 1993

Permission is hereby granted to the UNIVERSITY OF ALBERTA LIBRARY to reproduce single copies of this thesis and to lend or sell such copies for private, scholarly or scientific research purposes only.

The author reserves other publication rights, and neither the thesis nor extensive extracts from it may be printed or otherwise reproduced without the author's written permission.



417 Michener Park

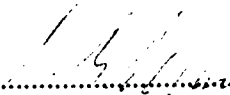
Edmonton, Alberta

Canada T6M 4M5

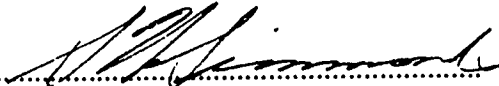
DATE June 28, 1993

UNIVERSITY OF ALBERTA
FACULTY OF GRADUATE STUDIES AND RESEARCH

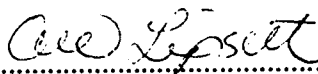
The undersigned certify that they have read, and recommend to the Faculty of Graduate Studies And Research for acceptance, a thesis entitled A SHEAR-FRICTION TRUSS MODEL FOR REINFORCED CONCRETE BEAMS SUBJECTED TO SHEAR submitted by SIMON AIMIAN CHEN in partial fulfillment of the requirements for the degree of Doctor of Philosophy in Civil Engineering.


.....
Dr. J.G. MacGregor, Supervisor


.....
Dr. A.E. Elwi


.....
Dr. S.H. Simmonds


.....
Dr. P. Robertson


.....
Dr. A.W. Lipsett


.....
Dr. J.K. Wight

DATE Jun. 18 1993

ABSTRACT

The objective of this thesis was first to develop a model to calculate the shear transferred across an inclined crack, and second to determine the effective strength of concrete in the web of a beam when diagonal crushing of concrete governs. Fifty-seven tests were carried out to aid in the development of this objective.

The experimental program included two series of tests. The first series consisted of seventeen concrete cantilevers tested to investigate the shear-friction on an inclined crack. The major variables were the angle of the inclined crack, the longitudinal compressive force and the conditions of the crack interface. The specimens generally failed due to the loss of the shear transfer across the crack interface. The ratio of the shear transferred by shear-friction across the inclined cracks to the longitudinal compression force on the crack face increased as the angle of inclination of the failure crack increased. The ratio varied from 0.114 to 1.778.

Based on the tests, a shear-friction truss model was developed. In this model the function of the stirrups is represented by the truss analogy and the concrete contribution is modelled by shear-friction. Both the truss model and the shear-friction model are based on a constant angle of the inclined crack. The shear-friction truss model was used to examine twenty seven test beams and gave a good prediction of the shear strength of the beams. Based on the shear-friction truss model, a design procedure for shear was developed.

The second series of tests consisted of forty concrete panels subjected to longitudinal compression and transverse tension. The major variables were the gross transverse tensile strain and the loading history. The specimens generally failed due to longitudinal crushing. It was found that the effective compressive strength decreased as the gross transverse tensile strain increased. The loading history had no effect on the effective compressive strength of concrete. The decrease in compressive strength was caused by the number and the width of the cracks in the concrete. Because the gross transverse tensile strain is a measure of the cracks in the concrete, the effective compressive strength of the concrete is expressed as a function of the gross transverse tensile strain. A new equation for the principal tensile strain in the web of beam was derived based on the strains in a compression field. A constant efficiency factor of 0.75 is recommended in the shear design of slender beams.

ACKNOWLEDGEMENTS

This study was carried out in the Structural Division of the Department of Civil Engineering at the University of Alberta. The author wishes to thank all the professors for their excellent lectures and his fellow graduate students for their friendly help.

The author wishes to express his special thanks and deep appreciation to his supervisor, Professor James G. MacGregor, for his invaluable support, encouragement and guidance throughout this study.

The assistance of the technical staff of the I.F. Morrison Structural Laboratory at the University of Alberta is acknowledged.

Financial support was provided by the Natural Science and Engineering Research Council of Canada.

My deep gratitude goes to my parents and my wife for their understanding and encouragement throughout the course of this study.

TABLE OF CONTENTS

1. INTRODUCTION	1
1.1 Problem Statement.....	1
1.2 Objectives and Scope.....	2
1.3 Outline of Problem Solution	3
2. LITERATURE REVIEW AND DISCUSSION.....	6
2.1 Behaviour of Beams Failing in Shear.....	6
2.2 Principle of B and D Regions	8
2.3 Truss Models.....	9
2.3.1 Traditional Truss Model.....	9
2.3.2 The Procedures Used in ACI and CSA Codes	11
2.3.3 Variable Angle Truss Model.....	15
2.3.4 The Strut-and-Tie Model.....	17
2.4 The Modified Compression Field Theory.....	19
2.5 Shear-friction	22
2.5.1 Initially Uncracked Interfaces.....	23
2.5.2 Initially Cracked Interfaces.....	23
2.5.3 Difference between Shear Friction Specimen and Beam	26
2.5.4 Crist Analysis for Deep Beam.....	28

2.5.5 Collins and Vecchio's Expression for Shear Carried across a Crack	3 1
2.6 Effective Concrete Strength.....	3 2
2.7 Summary of the Unsolved Issues.....	3 7
3. EXPERIMENTAL PROGRAM.....	5 7
3.1 Overview of Experimental Program.....	5 7
3.2 Test Series 1: Tests on Shear Transferred by Friction.....	5 8
3.2.1 Objectives	5 8
3.2.2 The Specimens.....	6 0
3.2.3 Material Properties	6 4
3.2.4 Test Set-up and Procedure	6 6
3.2.5 Instrumentation	6 8
3.3 Test Series 2: Tests on Concrete Softening.....	7 1
3.2.1 Objectives	7 1
3.3.2 Test Specimens.....	7 2
3.3.3 The materials.....	7 6
3.3.4 Test Set-up.....	7 7
3.3.5 Instrumentation	7 9
4. TEST RESULTS OF THE SHEAR SPECIMENS.....	1 0 3
4.1 Principal Test Results.....	1 0 3
4.2 Specimen Behavior.....	1 0 4

4.2.1 Group 1: Specimens with $\theta = 45^\circ$	104
4.2.2 Group 2: Specimens with $\theta = 60^\circ$	112
4.2.3 Group 3: Specimens with $\theta = 30^\circ$	116
4.2.4 Group 4: Specimens with $\theta = 90^\circ$	120
4.2.5 Group 5: Specimens with Undesigned Inclined Crack	122
4.3 The Effect of Dowel Action.....	127
4.4 The Effect of Uncracked Compression Zone.....	130
4.5 Combined Truss and Shear Friction Action.....	132
4.6 Relationship between V_u and N_u	134
4.7 Summary of the Test Results.....	134
5. THE SHEAR-FRICTION TRUSS MODEL.....	161
5.1 Introduction.....	161
5.2 The Internal Forces in a Cracked R/C Beam.....	161
5.3 Shear Friction Analogy.....	165
5.4 The Coefficient of Shear Friction of Concrete.....	169
5.5 The Shear-Friction Truss Model.....	172
5.6 The Computational Approach of Shear-Friction Truss Model.....	177
5.7 Application of the SFTM in Bresler and Scordelis' Tests.....	180
5.8 Design Procedure and Example.....	185

5.9 Extension of the Application of SFTM.....	190
5.9.1 Beam with External Axial Load.....	190
5.9.2 Prestressed Concrete Beams.....	192
5.9.3 Deep Beam Loaded Indirectly.....	193
5.10 Summary	195
6. RESULTS OF TESTS ON CONCRETE SOFTENING.....	218
6.1 Presentation of Test Data.....	218
6.2 Group I: General Study of the Reduction of Compressive Strength of Concrete due to Transverse Tension	220
6.2.1 Specimen Group II: Study of the Mechanism of Concrete Softening.....	225
6.3 Specimen Group II: Study of the Mechanism of Concrete Softening.....	226
6.4 Group III: Study of the Concrete Softening due to Non-uniform Stresses.....	233
6.5 Summary of Test Results.....	236
7. THE MECHANISM OF CONCRETE SOFTENING AND THE EFFECTIVE STRENGTH OF CONCRETE.....	269
7.1 Factors Effecting Concrete Softening	269
7.2 The Effective Strength of Concrete.....	272
7.3 Proposal for the Design of Reinforced Concrete Beams	277
7.4 The Mechanism of Concrete Softening due to Transverse Tension.....	281

7.4.1 The Shearing Softening Mechanism.....	282
7.4.2 The Buckling Softening Mechanism.....	284
7.4.3 The Difference between the Concrete Softening of Plain Concrete and Reinforced Concrete.....	285
7.5 Softening due to Non-uniform Compressive Strain.....	288
7.6 Summary.....	291
8. SUMMARY AND CONCLUSIONS.....	303
8.1 Experimental Observations.....	303
8.1.1 Tests on Shear-friction.....	303
8.1.2 Tests on Concrete Softening.....	305
8.2 Conclusions (Shear-friction Truss Model).....	306
8.3 Conclusions (The Effective Strength of Concrete under Transverse Tension).....	308
8.3.1 The Effective Strength of Concrete in Beam Web	310
REFERENCES	311
APPENDIX A: PHOTOGRAPHS OF THE SHEAR-FRICTION SPECIMENS AFTER FAILURE.....	318
APPENDIX B: PHOTOGRAPHS OF THE SPECIMENS FOR CONCRETE SOFTENING TESTS.....	329
APPENDIX C: CRACK PATTERNS OF THE TEST BEAMS BY SCORDELIS AND BRESLER	350

LIST OF TABLES

2.1	Values of v proposed in literature	40
3.1	Properties of the shear specimens.....	82
3.2	Properties of the concrete softening specimens.....	83
4.1	Principal test results of shear test.....	137
4.2	The internal forces on the failure crack for S15, S16 and S17.....	138
5.1	The properties of the test beams by Scordelis.....	198
5.2	The strengths predicted by SFTM.....	199
5.3	The strengths predicted by ACI procedure and CSA general method.....	200
5.4	The comparisons of the CSA simplified method, the CSA general method and the shear-friction truss model in the design of stirrups.....	201
6.1	Major results of tests on concrete softening.....	237
7.1	Comparison of measured and computed effective strength of concrete.....	294

LIST OF FIGURES

2.1	Effect of a/d ratio on shear strength of beams without web reinforcement.....	4 1
2.2	Stress trajectories in a beam.....	4 2
2.3	Example of B-region and D-region in a beam.....	4 2
2.4	The truss analogy.....	4 3
2.5	45° truss model - equilibrium conditions.....	4 4
2.6	Variable angle truss model for a beam.....	4 4
2.7	Forces in tension and compression chords of a truss.....	4 5
2.8	Comparison of load paths in a deep beam and in a slender beam.....	4 6
2.9	Equilibrium in the Compression Field Theory.....	4 7
2.10	The modified compression field theory.....	4 8
2.11	Force transmission models in concrete.....	4 9
2.12	Pushoff test.....	5 0
2.13	Shear Friction Model by Walraven.....	5 1
2.14	Truss models for pushoff/pulloff specimens.....	5 2
2.15	Comparison between the shear interfaces in a pushoff specimen and a beam.....	5 3
2.16	Shear friction analogy for deep beams by Crist.....	5 4
2.17	ACI code shear-friction method.....	5 5

2.18	Concrete Strength under Bi-axial Stresses.....	5 5
2.19	The efficiency factors for isolated struts from Schlaich's analysis.....	5 6
3.1	Series 1: Tests on shear transferred by friction.....	8 5
3.2	Series 2: Tests on concrete softening.....	8 5
3.3	Specimens with Inclined Crack.....	8 6
3.4	Specimens S9, S10 and S11 with expected crack of 90 degree "inclination".....	8 7
3.5	Specimens S15, S16 and S17.....	8 7
3.6	Details of the groove.....	8 8
3.7	Comparison of Dowel Action Between Bars with and without Foam Insulation.....	8 8
3.8	The set-up for the pre-cracking.....	8 9
3.9	Stress-strain curves for the steels.....	8 9
3.10	Concrete strength.....	9 0
3.11	Loading Frame for Test Series 1.....	9 0
3.12	Test Set-up for Shear Friction.....	9 1
3.13	Layouts of demec gauge targets and LVDTs.....	9 2
3.14	Layouts of strain gauges for the reinforcements.....	9 3
3.15	The concrete panel tested by Collins and Vecchio.....	9 4
3.16	The specimens for concrete softening tests.....	9 5
3.17	Load paths for the tests on concrete softening.....	9 6

3.18 The specimens with grooves.....	97
3.19 Loading system for Group 3.....	98
3.20 Concrete strengths during the testing period.....	99
3.21 Loading Frame and Test Set-up for Concrete Softening Investigation.....	100
3.22 The mechanical wedge clamp.....	101
3.23 Instrumentation for Group I and II.....	101
3.24 Instrumentation for Group III.....	102
4.1 Load vs. steel strain, S1, S2 and S3.....	139
4.2 Load vs. horizontal relative movement of the two crack faces, S1, S2 and S3.....	139
4.3 Load vs. strains measured across the crack, S1.....	140
4.4 Load vs. strains measured across the crack, S2.....	141
4.5 Load vs. strains measured across the crack, S3.....	142
4.6 Load history, S4 and S5.....	143
4.7 Load vs. horizontal relative movement of the two crack faces, S4 and S5.....	143
4.8 Load vs. strain in the compression zone, S3 and S5.....	144
4.9 Load vs. steel strain, S6 and S7.....	145
4.10 Load vs. horizontal relative movement of the two crack faces, S6 and S7.....	145
4.11 Load vs. strains measured across the crack, S6.....	146
4.12 Load vs. strains measured across the crack, S7.....	147

4.13	Load vs. strain in the compression zone for specimen S6 and S7.....	148
4.14	Test result of specimen S8.....	149
4.15	Load vs. steel strain for specimens S12 and S13.....	150
4.16	Load vs. horizontal relative movement of the two crack faces, S2 and S13.....	150
4.17	Re-testing of specimens S12 and S13.....	151
4.18	Test result of specimen S14.....	152
4.19	Load history, S9, S10 and S11.....	153
4.20	Load vs. horizontal relative of the two crack faces, S9, S10 and S11.....	153
4.21	Load vs. strains measured across the crack, S9.....	154
4.22	Load vs. strains measured across the crack, S10.....	155
4.23	Load vs. strains measured across the crack, S11.....	156
4.24	Strain in the longitudinal reinforcement, S16.....	157
4.25	Strain in the stirrups, S16.....	157
4.26	Strain in the longitudinal reinforcement, S15.....	158
4.27	Strain in the stirrups, S15.....	158
4.28	Load history, S17.....	159
4.29	Strain in the longitudinal reinforcement, S17.....	159
4.30	Strain in the stirrups, S17.....	160

4.31	The relationship between $\frac{V_u}{N_u}$ and θ	160
5.1	Internal forces in a cracked beam.....	202
5.2	The simplified internal forces in the crack plane.....	203
5.3	A truss system account for the concrete contribution.....	203
5.4	Dry friction analogy for the cross section of a reinforced concrete beam.....	204
5.5	Dry Friction analogy in an inclined section of a reinforced concrete beam.....	205
5.6	Force transformation	206
5.7	Analysis of the coefficient of shear-friction.....	206
5.8	Force transfer across the crack between two diagonal struts.....	207
5.9	Shear strengths vs. angle of inclination.....	208
5.10	The differences among Crist's shear-friction model, ACI's shear-friction method and the shear-friction truss Model.....	209
5.11	Relationship between $\frac{V}{A_v f_y d}$ and θ	210
5.12	Shear strength predicted by SFTM using $\beta_o=3.0$	211
5.13	The prediction by SFTM using Eqn. (5.13).....	212
5.14	The prediction by the ACI procedure.....	212
5.15	The prediction of variable angle truss model.....	213

5.16	The prediction of Equation (5.24).....	213
5.17	Design charter.....	214
5.18	Forces in a beam with external axial force.....	215
5.19	Forces in a Prestressed Concrete Beam.....	216
5.20	Shear transfer mechanism in deep beams loaded indirectly	217
6.1	Examples of transverse deformations measured by the demec Gauges and LVDT's.....	239
6.2	Examples of LVDT readings at different heights.....	240
6.3	Photos of Specimens #1 and #10 after failure	241
6.4	Test results, Specimens #1 to #4.....	242
6.5	Test results, Specimens #5 to #8.....	244
6.6	Test results, Specimens #9 to #12.....	246
6.7	Test results, Specimens #13 to #18.....	248
6.8	The effective compressive strengths for specimens of Group I.....	250
6.9	Test results, Specimens #19 to #22.....	251
6.10	Test results, Specimens #23 and #24.....	253
6.11	Test results, Specimens #25 and #26.....	255
6.12	Test results, Specimens #27 to #29.....	257
6.13	Test results, Specimens #30 and #31.....	259
6.14	Test results, Specimens #32 and #33.....	261

6.15	Test results, Specimens #34 to 36 and #40.....	263
6.16	Test results, Specimens #37 to #39.....	265
6.17	The effective compressive strengths for the test specimens	268
7.1	The relationship between $\frac{f'_{ce}}{f'_c}$ and ϵ_t	296
7.2	Collins and Vecchio's test results.....	296
7.3	The strains in the web of beams.....	297
7.4	Concrete softening due to divergent cracks.....	298
7.5	Diagonal crushing in a R.C. beam.....	299
7.6	Comparison of plain concrete and reinforced concrete.....	299
7.7	Comparison of diagonal strains distributions between slender and deep beams.....	300
7.8	The mechanism of concrete softening due to non-uniform compressive strain.....	301
7.9	Compressive force paths in non-uniformly stressed concrete.....	302

NOTATION

a	shear span; or size of aggregate
A_g	gross area of beam section
A_h	area of horizontal web reinforcement within a distance s_h
A_s	area of longitudinal tension reinforcement
A_{st}	area of the cross section of isolated strut in a strut and tie model
A_v	area of vertical stirrups within a distance s
a_x	X-component of the contact area for one piece of aggregate
A_x	X-component of the average contact area for a unit crack area
A_y	Y-component of the average contact area for a unit crack area
a_y	Y-component of the contact area for one piece of aggregate
b	width of the compression face of member
b_w	width of the web of member
C	longitudinal compressive force in concrete
d	effective depth
D	diagonal compressive force due to shear
f_c	compressive stress in the uncracked concrete

d_v	equivalent to $j d$
F_c	resultant of f_c over the uncracked compression zone
F_{cx}	horizontal component of F_c
F_{cy}	vertical component of F_c
f'_c	specified compressive strength of concrete
f_{cd}	diagonal compressive stress in concrete
f_{ce}	effective compressive strength of concrete
f_{cr}	cracking strength of concrete
f_d	compressive stress distributed on crack plane
F_d	resultant of f_d over the cracked face
F_{dx}	horizontal component of F_d
F_{dy}	vertical component of F_d
F_{DT}	normal force on the inclined crack
f_s	stress in reinforcement
F_{vi}	force in the web reinforcement
f_y	yield strength of reinforcement
h	overall depth of member

$j d$	distance between the resultants of the internal compressive and tensile forces on a cross section
k	the ratio of principal tensile stress to principal compressive stress
M	bending moment
M_f	factored bending moment
n	normal compressive stress in the contact area
N	tensile force in longitudinal reinforcement, or normal compressive force on an interface
N_e	external axial force
N_s	tensile force in the longitudinal reinforcement
N_u	compressive force on the crack surface in the longitudinal direction ($N_u = N_s + N_e$)
N_v	axial force due to shear
N_θ	compressive force normal to the interface of an angle of inclination θ
s	vertical stirrup spacing
S	shear force parallel to and on a crack face
s_h	spacing of horizontal web reinforcement

s_{θ}	crack spacing
t	the ratio of the uniaxial ultimate compressive strength to the uniaxial ultimate tensile strength
T	Tensile force in reinforcement
v	shear stress, or coefficient of standard deviation
V	shear force
V_c	shear contribution from the concrete
V_c^e	shear contribution from the concrete in beams with external axial force
V_c^p	shear contribution from the concrete in prestressed concrete beams
v_{ci}	shear stress on crack surface in the modified compression field theory
V^{cal}	predicted ultimate shear force
V_{cr}	shear force at cracking
V_d	shear contribution from dowel action
V_f	factored shear force
V_r	factored shear resistance
V_n	normal shear strength

V_s	shear contribution from the stirrups
V_{top}	shear strength of deep beams loaded at the top
V^t	ultimate shear force measured from the tests
v_u	shear stress at the ultimate state
V_u	shear force at the ultimate state
V_θ	compressive force on the interface of an angle of θ with the axial
w	width of crack
\bar{x}	mean value of V^t/V^{cal}
α_t	the inclination of the web reinforcement with beam axis
β_0	equivalent coefficient of shear-friction of an inclined crack, defined by the dry friction law on an inclined interface
β_θ	coefficient of shear-friction of an inclined crack (V_c/N)
ϵ_c	longitudinal compressive strain
ϵ_d	diagonal compressive strain; or principal compressive strain
ϵ_h	strain in the direction of beam axis
ϵ_v	strain in the direction perpendicular to beam axis
ϵ_t	gross transverse tensile strain computed using a gauge length that includes the cracks in the concrete

ϵ_{tu}	ϵ_t at ultimate state
ϕ_c	material resistance factor for concrete
ϕ_s	material resistance factor for reinforcement
η	regression factor
κ	ratio of the factored shear force to the factored shear contribution by the stirrups
λ	correction factor to account for unit weight of concrete
μ	coefficient of friction
μ_s	coefficient of static friction
μ_θ	coefficient of static friction of an inclined interface
v	effectiveness factor of concrete (ratio of effective strength to specified compressive strength)
v^{cal}	effectiveness factor calculated by proposed equations
v^t	effectiveness factor calculated from the tests
θ	angle of diagonal compression struts, inclined cracks and principal compressive stress to the longitudinal axis of a beam
ρ	ratio of steel area to concrete area
σ	standard deviation
σ_1	principal tensile stress

σ_2 principal compressive stress

σ_d diagonal compressive stress

σ_{pu} compressive stress normal to the contact area

σ_v vertical compressive stress in the concrete

τ_{pu} shear stress on the contact area

1. INTRODUCTION

1.1 Problem Statement

Shear failure of reinforced concrete beams is frequently sudden and brittle compared to flexural failure. Much research has been conducted since the turn of the century to develop simple but conceptually understandable design procedures. Among the various methods developed, the truss model is an excellent conceptual model that provides an understanding of the flow of internal forces and the failure mechanism in a cracked concrete beam. In the truss model, the concrete web in the shear span of a beam is divided into a number of diagonal struts by the inclined cracks. Shear failure is caused due to either the loss of the force transfer across the inclined cracks due to yield of the stirrups or by the crushing of the diagonal struts.

In the traditional truss model, beam stirrups act as vertical tension ties and the entire shear is transferred across an inclined crack by the stirrups. However, other mechanisms also provide resistance to shear, including shear in the uncracked concrete compression zone, shear transfer by aggregate interlock across the crack, and dowel action of the longitudinal reinforcement. If this additional shear capacity, traditionally called the "concrete contribution" is neglected, the truss model can be unnecessarily conservative. The shear design procedure in the ACI¹ Code and the Simplified Method in the CSA² Code account for the conservatism by

adding a concrete contribution V_c to the capacity of a truss action with compression diagonals at 45° . Although these code methods usually lead to a satisfactory design, they are highly empirical and do not provide designers with a rational model for the shear strength. A variable angle truss model like the General Method in the CSA Code selects a flatter inclination for the truss struts so that more stirrups are taken account of in the shear resistance, but it does not directly consider any contribution of the concrete shear transfer mechanism to shear strength.

If excess vertical ties are provided, the shear failure is caused by crushing of the diagonal struts and the shear strength is governed by the concrete compressive strength. Because the concrete is transversely tensioned and cracked, the effective strength of the concrete is usually lower than the concrete cylinder strength. This is referred to as concrete softening. The General Method in the CSA Code uses the effective strength of concrete developed by Collins and Vecchio³. Although concrete softening under transverse tension is generally accepted, the mechanism by which it occurs is not well understood yet.

1.2 Objectives and Scope

Two general objectives are involved in this thesis. The first is to develop a rational procedure to calculate the shear transferred across an inclined crack. The shear transfer mechanism should include the shear transferred by the stirrups and by the concrete contribution. The stirrup contribution is calculated by the truss model. The

concrete contribution is based on the shear-friction method. Both contributions should be based on a consistent angle of the inclined cracks. Since the truss model has been well developed, the first objective of this thesis is to establish the shear-friction method to calculate the concrete contribution and to develop a rational procedure to select the angle of the critical inclined cracks for the truss model and shear-friction method. Seventeen tests were used to study the mechanism of shear-friction and the coefficient of shear-friction across inclined cracks having various angles of inclination. The shear-friction truss model is developed based on the tests.

The second objective is to determine the effective strength of concrete in the web of the beam when diagonal crushing of concrete governs. The detailed work includes an investigation of the mechanism of concrete softening due to transverse tension and to determine the variables causing the concrete softening, to develop an expression from the experimental results to calculate the effective strength of concrete. A constant concrete efficiency factor is proposed for use in the design of slender reinforced concrete beams. Forty tests were involved in this phase of the study.

1.3 Outline of Problem Solution

In Chpt. 2 of this thesis, the basic behavior of concrete beams subjected to shear is discussed and various models which describe the mechanisms of shear transfer across a inclined crack and the ACI and CSA code shear design procedures are presented and discussed.

In addition, previous studies on the effective strength of concrete under transverse tension are presented.

The two experimental programs which deal with the shear-friction and the effective strength of concrete under transverse tension, respectively, are described in Chpt. 3. The tests for shear-friction consisted of 17 cantilever beams. The tests provided the coefficient of shear-friction for the inclined cracks with various angles of inclination. The second test program, related to the effective compressive strength of concrete under transverse tension, involved tests of 40 concrete panels with longitudinal compression and transverse tension to investigate aspects of the mechanism of concrete softening and to provide test data to establish the relationship between the effective strength of concrete and the gross transverse tensile strain. The results of the two experimental programs are presented and interpreted in Chpt. 4 and Chpt. 6, respectively.

The shear-friction truss model is developed in Chpt. 5. The model is used to examine the results of the tests by Bresler and Scordelis⁴⁻⁶ on reinforced concrete beams and is compared with the CSA Simplified and General methods, respectively. A design example is also given in this chapter.

In Chpt. 7, conceptual models are developed to explain the mechanisms of concrete softening due to transverse tension. An empirical equation is established to calculate the effective strength of

concrete under transverse tension. A constant efficiency factor is proposed for the shear design of slender reinforced concrete beams.

A summary and conclusions are presented in Chpt. 8.

Photographs of the specimens after failure are presented in Appendices A and B. Appendix C includes the crack patterns of the beams tested by Bresler and Scordelis which are used to examine the shear-friction truss model.

2. LITERATURE REVIEW AND DISCUSSION

2.1 Behaviour of Beams Failing in Shear

The shear strength of reinforced concrete beams is often investigated by testing simply supported beams subjected to symmetrical two point loading. Tests performed on beams without web reinforcement have indicated that the mode of failure is highly dependent on the shear span ratio a/d , as shown in Fig. 2.1. At small a/d ratios the ultimate shear capacity increases substantially beyond the initial diagonal cracking⁷. The differences in behaviour shown in Fig. 2.1 suggests that beams can be divided into four categories, typically referred to as very short, short, slender or very slender beams.

Beams with short or very short shear spans are commonly referred to as deep beams. Very short spans, having $a/d < 1$, develop inclined cracks jointing the load and support and resist load by arch action. Failure can occur by crushing of the compression strut, or by yielding or loss of anchorage of the longitudinal tension chord. Relatively short shear spans, with a/d from 1 to about 2.5, resist load by a combination of arch and beam action. The internal force redistribution after cracking permits further increases in loads. Failure may occur either by distress in the longitudinal tension bars, described as a "shear-tension" failure, or by crushing of compression

zone above the inclined crack, commonly referred to as "shear-compression" failure.

Most practical beams are slender beams having a/d ratios from 2.5 to 6 which transmit shear primarily by beam action. In slender beams without web reinforcement, flexural cracks form prior to any diagonal crack, however, the development of inclined cracks disrupts the equilibrium and failure occurs suddenly. Very slender beams with a/d greater than 6 are characterized by flexural failure prior to inclined cracking.

Because of inclined cracking, the shear capacity of beams without web reinforcement having a/d less than 6 is much lower than the flexural capacity. To ensure that the full flexural capacity can be developed, web reinforcement is provided in beams. This is particularly important in slender beams, where the formation of an inclined crack can cause immediate failure if no web reinforcement is provided. Generally, beams will have enough web reinforcement to fail in flexure. For beams with less web reinforcement than that corresponding to flexural failure, shear failure occurs gradually due to the yielding of web reinforcement after inclined cracking. If a very small amount of web reinforcement is provided, the formation of an inclined crack may cause immediate yielding of web reinforcement, resulting in a sudden failure. If excess web reinforcement is provided, the beam may fail due to web crushing prior to yielding of the web reinforcement. Both of the two failure modes are brittle and undesirable.

2.2 Principle of B and D Regions

The behaviour and shear resisting mechanism are very different from region to region in a concrete structure. Figure 2.2 shows the principal stress trajectories in half of a simply supported beam. It shows that at the support or at the load application point the stress trajectory pattern is severely disturbed. A relatively new concept in the design of concrete structures presented by Schlaich et al.⁸ is the division of a structure into separate design regions based on the type of load path and strain distribution. Those regions of a beam in which the Bernoulli hypothesis of plane strain distribution is assumed to be valid are referred to as B-regions, where B denotes beam or Bernoulli. B-regions display primarily beam action. At disturbed or discontinuous regions of a structure such as corners, openings or concentrated loads and supports, plane sections do not remain plane, and the behaviour is very different from that in B-region. Those disturbed portion are designated D-regions, where D denotes discontinuity or disturbance. Figure 2.3 shows beams with both B and D-regions.

D-regions, which extend about one member-depth on each side of a discontinuity, transfer load by in-plane compression such as arch action. Typical structures in which D-region behaviour dominates are brackets and deep beams. In such members the load carrying mechanism may be idealized as a truss made up of concrete compression struts and steel ties. Crushing of the concrete struts is one of the major failure modes for D-regions and the ultimate load is very dependent on the compressive strength of concrete. Because of

the transverse tension and cracking in the region of the strut, an effective concrete strength, generally less than the cylinder strength, must be used in the design of concrete strut.

Most reinforced concrete beams are sufficiently slender that their behaviour is dominated by B-region behaviour. The post-cracking behaviour of these regions can be determined from a truss model. Yielding of web reinforcement is the major shear failure mode.

2.3 Truss Models

As mentioned previously, a given portion of a reinforced concrete beam under loading displays either D-region behaviour or B-region behaviour. The response of uncracked D and B-region can be determined by elastic analysis, or much more easily by elastic beam theory. However, cracking of the concrete causes stress redistribution and the elastic methods are no longer applicable. Researchers have developed a number of mechanical-mathematical models to express the behaviour of concrete beams after cracking. Among the best of these is the truss model which provides an excellent conceptual model to show the forces existing in a cracked concrete beam.

2.3.1 Traditional Truss Model

At the turn of the century, Ritter⁹ and Mörsch¹⁰ independently developed truss analogies for the design of web reinforcement in

concrete beams. Ritter visualized diagonal concrete struts acting from the top of one stirrup to the bottom of the next. Mörsch introduced the concept that inclined compression fields, not discrete diagonal struts, could be used to model the flow of forces. In its simplest form, several stirrups are collected into one vertical tension member, and several inclined concrete struts are combined into one diagonal member, as shown in Fig. 2.4b. This model assumes that after cracking the diagonal compression stresses remain at an inclination θ . Although Mörsch recognized the possible re-orientation of the principal compression stress and the flatter inclination of crack that occurs as loading progresses, he recommended the $\theta=45^\circ$ truss model as a conservative approach in design.

If the joints are assumed to be hinged, the truss shown in Fig. 2.4b is statically determinate. For the free body diagram shown in Fig. 2.5a, the shear force can be calculated as

$$V = \frac{A_v f_y j d}{s} \quad (2.1)$$

where A_v is the area of vertical reinforcement within the distance s , f_y is the yielding strength of steel and $j d$ is the internal lever arm.

As shown in Fig. 2.5b, the shear force V can be resolved into a diagonal compression force D and an axial tension N_v . If the shear stresses are assumed to be uniformly distributed over $b_w j d$, where b_w is the web width, the shear force can be expressed as

$$V = 0.5 f_{cd} b_w j d \quad (2.2)$$

where f_{cd} is the diagonal compression stress. The shear strength of a reinforced concrete beam reaches its maximum value when $f_{cd}=f_{ce}$, where f_{ce} is the effective compressive strength of the concrete, no matter how much web reinforcement is provided, i.e.

$$V = \frac{A_v f_y j d}{s} \leq 0.5 f_{ce} b_w j d \quad (2.3)$$

Although the analysis of the traditional pin-jointed truss is very simple, it neglects the shear transferred by the uncracked compression zone, aggregate interlock on the crack surface and dowel action of longitudinal reinforcement. These mechanisms can provide a significant portion of the total shear resistance. Moreover, the assumed angle of 45° for the inclined cracks is usually larger than observed in tests, which underestimates the contribution of vertical web reinforcement and makes the shear capacity predicted by Eqn. (2.3) more conservative.

2.3.2 The Procedures Used in ACI and CSA Codes

The ACI Code¹ shear design procedure and the Simplified Method in the CSA Code² are based on the 45° truss model, with an empirical correction to account for the conservatism of the model. Both codes have the same formulas for shear design except that ACI Code uses a single strength reduction factor, ϕ , for the shear resistance while CSA Code uses different reduction factors ϕ_c and ϕ_s for concrete and steel. For simplicity the ACI Code procedures are illustrated and the Imperial Unit System is used in this section.

The ACI Code does not consider a whole member approach where an entire beam is visualized as a truss, but instead derives a sectional approach from the basic truss concepts, where any section of a beam can be examined independently of other portions. In the code, the nominal shear resistance V_n is equal to the sum of two components namely

$$V_n = V_c + V_s \quad (2.4)$$

where V_c is the shear carried by concrete and V_s is the shear resisted by web reinforcement. V_s is calculated based on the 45° truss model.

$$V_s = \frac{A_v f_y d}{s} \quad (2.5)$$

V_s in Eqn. (2.5) is the sum of the forces in the web reinforcement intersected by an ideal 45° inclined crack, which is similar to Eqn. (2.1) obtained from the simple truss model, except that the codes assume the horizontal projection of the crack is equal to the effective depth.

The concrete contribution V_c in Eqn. (2.4) is assumed equal to the strength of a concrete beam without any web reinforcement, or the shear causing inclined cracking. As a result, the effects of uncracked compression zone, aggregate interlock, and dowel action are combined into one V_c term. For members subject to shear and flexure the code expresses V_c as:

$$V_c = 2\sqrt{f'_c} b d \quad (2.6)$$

or in SI units
$$V_c = \sqrt{f'_c} b d / 6 \quad (2.6a)$$

Equation (2.6) was developed from test results. Compared with the test results on simply supported beams without web reinforcement, Equation (2.6) generally underestimates the shear capacity for beams with large longitudinal reinforcement ratios and overestimates the shear strength for small steel percentages¹¹. For a beam with web reinforcement, the shear strength is

$$V_n = 2\sqrt{f'_c} b d + \frac{A_v f_y d}{s} \quad (2.7)$$

or in SI units
$$V_n = \frac{1}{6} \sqrt{f'_c} b d + \frac{A_v f_y d}{s} \quad (2.7a)$$

As indicated in previous sections, diagonal compression stresses exist in the web of a beam. In very thin-walled beams, these may lead to crushing of the web. According to Eqn. (2.2), the diagonal compressive stress f_{cd} is related to the shear stress. A number of codes limit the shear stress to 0.2-0.25 times the compressive strength of the concrete. The ACI Code limits on V_s , originally given for crack control, provide adequate safety against web crushing in reinforced concrete beams.

$$V_{s(max)} = 8\sqrt{f'_c} b d \quad (2.8)$$

Axial forces or prestressing change the cracking load of a beam. Axial tensile forces tend to increase the tensile stress in the concrete

which decreases the cracking load, while axial compressive forces tend to decrease the tensile stress in the concrete and as a result increase the cracking load. The effects of axial forces on the ultimate shear capacity have been reported but not been well explained. Members with axial tensile forces have lower shear strength than those subjected to shear and moment only. In the ACI Code, the nominal shear carried by the concrete of members with axial tension is given by

$$V_c = 2(1 + \frac{N_e}{500A_g}) \sqrt{f'_c} bd \quad (2.9)$$

where N_e is the axial tensile force and A_g is the gross area of the section. N_e/A_g is expressed in psi and is negative in tension. V_c in Equation (2.9) becomes zero when the average axial tensile stress on the section reaches or exceeds 500 psi in tension, which is roughly the tensile strength of concrete.

Axial compression tends to increase the shear strength. The ACI Code presents the following equation for calculating V_c for reinforced concrete members subjected to combined shear, moment and axial compression:

$$V_c = 2(1 + \frac{N_e}{2000A_g}) \sqrt{f'_c} bd \quad (2.10)$$

where N_e/A_g is positive in compression and has units of psi.

2.3.3 Variable Angle Truss Model

Some researchers attribute the conservatism to the assumption of 45° inclination. They suggest that the 45° truss model be adjusted by considering that θ is typically less than 45° . This modification is referred to as variable angle truss model. A variable angle truss model departs from the traditional assumption that the inclination of the diagonal compression struts is constant at 45° , and provides a more realistic model of the behaviour of a beam in shear.

Variable angle truss models can incorporate the different types of behaviour in the B-regions and D-regions in a beam. In a B-region, it is suitable to model the internal flow of force as a continuous field of parallel diagonal struts, having a constant angle of inclination θ . In D-regions, a fan shaped stress field or compression fan provides a better representation of the internal force flow, as illustrated in Fig. 2.6. A compression fan is usually statically indeterminate, although it becomes statically determinate if the stirrups are all assumed to yield. The plastic truss model presented by MacGregor and Rogowsky¹² can be used to calculate the internal forces in a compression fan. In the plastic truss model, the stirrups are assumed to yield at failure and the forces in the longitudinal reinforcement can be calculated from the moments using the method of sections.

The internal forces in the parallel diagonal field of a variable angle truss model can be derived similarly to those in the 45° truss model in Section 2.3.1, except the angle of inclination θ is usually less

than 45° . Referring to Fig. 2.5 and replacing the 45° by θ , the shear force can be calculated as:

$$V = \frac{A_v f_y j d}{s \tan \theta} \quad (2.11)$$

all the variables in Eqn. (2.11) are as previously defined. If the forces in the stirrups are assumed uniformly distributed over a length of $j d / \tan \theta$, the moment equilibrium of the free body in Fig. 2.5a gives

$$T = \frac{M}{j d} + 0.5 \frac{V}{\tan \theta} \quad (2.12)$$

Equation (2.12) indicates that the tensile force in the longitudinal reinforcement is $(0.5V/\tan \theta)$ larger than that responding to the bending moment. This is a result of truss action. Alternatively the vertical shear can be resolved into an inclined compression force D and a horizontal tension force N_v , as shown in Fig. 2.5b. The tension force N_v is equal to

$$N_v = \frac{V}{\tan \theta} \quad (2.13)$$

Since the shear is assumed to be distributed uniformly over the depth of the beam, N_v acts at mid-height and $N_v/2$ will act on both the top and the bottom chord of the truss. These forces will be added to those caused by flexure. As a result, the force in the compression chord of the truss will be reduced and the force in the tension chord will be increased, as shown in Eqn (2.12) and illustrated in Fig. 2.7. The inclined force D induces compressive

stress in the struts which may cause the crushing of the web. The corresponding shear strength is

$$V = f'_{ce} bd \sin\theta \cos\theta \quad (2.14)$$

With the variable angle truss model, the designer can choose any reasonable angle of inclination. As indicated in Eqn. (2.11) a smaller angle allows more stirrups to be intercepted by the crack and the shear carried by the stirrups is increased, however the compression stress in the diagonal strut increases as θ decreases. To ensure that stirrups will yield prior to the diagonal struts crushing in compression, the maximum compression stress must be less than the allowable compression stress and the minimum permissible angle chosen for design is limited. The CSA Code General Method for shear design is a member of the variable truss model family.

2.3.4 The Strut-and-Tie Model

In a structure, forces tend to take the shortest possible path to transfer load. In a beam subjected to concentrated loads, the shortest paths to transfer load are the straight lines connecting the points of loading and the supports. For deep beams, those shortest paths are also the possible paths, see Fig. 2.8a. The load is directly transferred to the supports through compression in the web concrete which acts as compressive struts. However for slender beams, as shown in Fig. 2.8b, those shortest paths are not possible paths. This is because the large a/d ratio makes the compressive stress trajectory in the web very flat and the vertical component is not

large enough to equilibrate the vertical shear. Furthermore, flexural cracks may intercept the diagonal struts. Hence other paths are needed to transfer the vertical force. Vertical web reinforcement provides those force paths. The truss model assumes that the compression chord is horizontal and carries no vertical force. As a result all the vertical force is carried by the vertical tension ties.

From Figures 2.8c and 2.8d, we can see that the strut-and-tie model is a special case of the truss model in which no vertical tie is needed statically. If anchorage and bearing failures are prevented and ties do not yield, the shear failure of a strut-and-tie system is caused by the crushing of the struts and the shear strength is governed by the compressive strength of the concrete. According to the strut-and-tie model shown in Fig. 2.8c, the shear strength V can be calculated as

$$V = A_{st} f'_{ce} \sin\theta \quad (2.15)$$

where A_{st} is the cross section area of the strut, f'_{ce} is the effective compressive strength of the concrete and θ is the inclination of the strut. Because the strut-and-tie model is a special case of the truss model, Eqn. (2.15) is similar to Eqn. (2.14), except in the truss model the strut is a continuous compression field with its cross section area equal to $(bdcos\theta)$.

A number of researchers have studied shear strength of deep beams using the strut-and-tie model¹³⁻¹⁶. The size of the struts is usually determined according to the bearing areas of the loading and supporting regions. Since the concrete struts and the truss nodes are

under a complicated state of stress, the effective strength of the concrete is generally reported to be lower than its cylinder strength. Usually f_{ce} is defined as $f_{ce} = v f'_c$, where v is an efficiency factor between 0 and 1.0. This will be discussed in more detail in Section 2.6.

2.4 The Modified Compression Field Theory

The Modified Compression Field Theory³ developed by Collins and Vecchio is an extension of the Compression Field Theory originally developed for concrete in torsion and shear^{17,18}. In both models, the cracked concrete is treated as a new material with its own stress-strain characteristics. Equilibrium, compatibility, and stress-strain relationships are formulated in terms of average stresses and average strains. While the original compression field theory ignored tension in the cracked concrete, the modified compression field theory takes into account transverse tensile stresses in the concrete between the cracks.

The compression field theory models a cracked concrete beam as a continuous field of diagonal compression, as illustrated in Fig. 2.9. The equilibrium equations are established according to the Mohr's circle in Fig. 2.9c. Since the tension in concrete is ignored, the principal tensile stress σ_1 is zero. According to the Mohr's circle, the shear stress v can be expressed as

$$v = \sigma_v / \tan\theta \quad (2.16)$$

where σ_v is the vertical compression in the concrete. σ_v is in equilibrium with the tension in the vertical reinforcement:

$$\sigma_v = \frac{A_v f_s}{b s} \quad (2.17)$$

where A_v is the vertical steel area within the distance s and f_s is the stress in the vertical steel. Hence, the shear force is

$$V = \frac{A_v f_s d}{s \tan \theta} \quad (2.18)$$

The compression field theory yields the same expression for shear strength as the variable angle truss model, except in the compression field theory, the inclination of the diagonal compression field θ is calculated through solving a nonlinear system of equations based on equilibrium, compatibility and material properties. Because tension in the concrete is ignored, the shear transferred by the concrete is not considered in the model.

The modified compression field theory extended the compression field theory by taking into account the average tensile stress in the concrete between two cracks. It assumes that there is no tension in the concrete at a crack. Due to bond, tension in the reinforcement causes tensile stresses in the concrete that reach a maximum value midway between the cracks. Figure 2.10 shows the stresses in an element and its Mohr's circle in which the concrete tensile stresses exceed zero. According to the Mohr's circle, the shear stress v can be calculated:

$$v = (\sigma_1 - \sigma_v) / \tan\theta \quad (2.19)$$

where the vertical tensile stress in the concrete is in equilibrium with the stress in the vertical reinforcement, as shown by Eqn. (2.17). Substituting Eqn. (2.17) into Eqn. (2.19) and letting $V = vbd$ gives

$$V = \frac{A_v f_s d}{s \tan\theta} + \frac{b d \sigma_1}{\tan\theta} \quad (2.21)$$

The first term on the righthand side of Eqn. (2.21) is the same as the shear strength calculated through both the variable angle truss model expressed by Eqn.(2.11) and the compression field theory expressed by Eqn.(2.18), which is the shear carried by the vertical reinforcement. The second part is the contribution of the concrete in terms of average principal tensile stress in concrete.

Figure 2.11 shows the mechanism of shear transferred by concrete. In Fig. 2.11a the section is cut along an idealized inclined crack. In Fig. 2.11b the section is at an average location between two inclined cracks. The modified compression field theory assumes a tensile stress σ_1 acts on section B-B along with the stirrup forces $A_v f_s$. A shear stress v_{ci} is assumed to act along the crack accompanied by stirrup forces $A_v f_y$. As a result, the concrete contribution can be expressed in two ways, either in terms of tensile stresses in concrete between the cracks or as an aggregate interlock mechanism. The vertical equilibrium of forces in Fig. 2.11b yields the same equation as Eqn. (2.21) which is derived directly from the

Mohr's circle, while the free body diagram in Fig. 2.11a yields the following equilibrium equation:

$$V = \frac{A_v f_y d}{s \tan \theta} + v_{ci} b d \quad (2.22)$$

Equations (2.21) and (2.22) show that the modified compression field theory considers both the concrete contribution and the possible reorientating of the inclined struts from 45° . However calculation of θ and v_{ci} or σ_1 is a tedious procedure of solving a system of nonlinear equations which are based on a number of assumptions.

2.5 Shear-friction

Research has shown that the concrete contribution to the shear strength in a reinforced concrete beam can not be ignored. The concrete contribution usually consists of three parts: shear transferred by aggregate interlock, shear transferred by the uncracked compression zone and shear carried by dowel action of the reinforcement. Among these three components, aggregate interlock plays the major role in carrying shear. The mechanism of aggregate interlock has been well described. When a crack is developed in a concrete mass, the surfaces of the crack are usually rough and irregular. The majority of the coarse aggregate particles remain embedded in one or the other of the crack faces. When this crack forms along a continuous plane a displacement parallel to the plane of the crack is possible and when it occurs, projecting particles from one face of the crack come into contact with the matrix of the other face. Further movement is then restricted by the bearing and

friction of the aggregate particles on the crack surface. Provided that restraint is available to prevent large increases in the crack width, substantial shear forces can be transmitted across the crack interface. This is aggregate interlock action. Aggregate interlock is also referred to as shear-friction.

2.5.1 Initially Uncracked Interfaces

Extensive tests have been carried out by Mattock, Paulay and others¹⁹⁻²³, using specimens of the general configuration shown in Fig. 2.12a. The specimens were either intentionally cracked along the expected interface prior to testing, or were uncracked. For uncracked specimens shear is transmitted across the interface. At higher loads, a series of diagonal tension cracks occur across the interface. Further load was resisted by stirrups and the diagonal compression struts between the cracks, which act as a truss system. In the tests, failures were usually observed due to the crushing of the diagonal compression struts. No continuous crack along the interface was formed. Although shear is transferred across a defined plane, this mechanism is not strictly shear friction since appreciable shear is not transferred across a crack.

2.5.2 Initially Cracked Interfaces

For an initially cracked surface, shear is transmitted only if lateral confinement or transverse steel exists. The irregularities of the surfaces of the two sides of crack ride up on each other. This tends to open the crack and create forces in the transverse steel. For

equilibrium a compressive stress is induced on the crack surfaces. The shear transferred across the crack is expressed in terms of this compressive stress and a coefficient of friction. Failures were observed due to sliding along the crack, combined with slight crushing in the crack surfaces.

Test results obtained by Mattock and his co-workers²¹ are shown in Fig. 2.12b. The compressive stress on the interface was assumed to be produced by the tension in the stirrups across the interface. In Fig. 2.12b the shear stress at failure, v_u , is plotted against ρf_y , where ρ is the ratio of the stirrups across the interface to the area of the interface. The ultimate shear strength increases almost linearly with the index ρf_y . With a monolithic shear plane, the strength is considerably higher than with a pre-cracked shear plane. The forces in the stirrups were not measured in the tests. If the stirrups are assumed to yield at failure the tangents of the curves in Fig. 2.12b are the coefficients of shear friction.

Fenwick and Paulay²⁰ studied shear transfer in pre-cracked unreinforced pushoff specimens. The confinement on the interface was applied externally. The variables in the tests included crack width and aggregate size. The test results indicated that variations in the size of the aggregate, from 1cm to 2cm, had no effect on the shear stress-slip curve or the ultimate strength. There was a continuous degradation of the aggregate interlock mechanism on the shear plane with an increase of the crack width. Fenwick and Paulay suggested the mean value of coefficient of friction be 1.7.

Taylor²³ simulated the deformation at an inclined crack in a beam by testing concrete blocks in a device that maintained a constant ratio between the opening normal to the crack, ΔN , and the shearing movement along the crack, ΔS . Both the ultimate shear strength and the deformation decreased linearly as $\Delta N/\Delta S$ increased. The shear transfer strength was a function of the roughness of the crack surface. Other researchers also carried out tests using cyclic loads or using stirrups inclined with the interface.

Walraven²⁴ studied the fundamentals of aggregate interlock by simplifying the aggregate particles to rigid spheres of different sizes, protruding from a flat crack plane, as shown in Fig. 2.13a. The force condition in the contact area is shown in Fig. 2.13b. According to the force equilibrium along the crack, the shear stress v can be expressed as:

$$v = \sigma_{pu} (A_y + \mu A_x) \quad (2.23)$$

where A_x and A_y are the average contact areas for a unit crack area, σ_{pu} is compressive stress normal to the contact area, and μ is the coefficient of friction of the contact area. A_x is equal to Σa_x and A_y is equal to Σa_y , where a_x and a_y are the contact area on one piece of aggregate. Walraven established the parameters σ_{pu} and μ by fitting Eqn. (2.23) to the experimental results of his pushoff tests on externally restrained specimens. He found that the best value for the friction coefficient was $\mu=0.4$ and the matrix yielding stress σ_{pu} could be expressed as

$$\sigma_{pu} = 6.39 f'_c{}^{0.56} \quad (\text{N/mm}^2) \quad (2.24)$$

By substituting Eqn. (2.24) into Eqn. (2.23), the shear stress can be expressed as

$$v = 6.39 f'_c{}^{0.56} (A_y + 0.4A_x) \quad (2.25)$$

Equation (2.25) indicates that shear friction or aggregate interlock action increases as the concrete strength f'_c and the contact area increase.

2.5.3 Difference between Shear Friction Specimen and Beam

Most of the research on shear friction was carried out by testing pushoff or pulloff specimens with the general configuration shown in Fig. 2.12a. However, the shear transfer mechanism of these specimens is quite different from that of a beam. The load carrying mechanisms of typical pushoff or pulloff specimens can be modelled as a truss system shown in Fig. 2.14a and b. Failures of the specimens were usually caused by either the crushing of the diagonal compression struts or the yielding of the tension ties. However, shear friction in a beam is a shear transferring mechanism additional to the truss system, as shown in Fig. 2.14c. The failure of shear friction may not cause the failure of the truss system.

The initial cracks on the specimens tested by the above researchers were usually formed by applying a line load along the interface on both sides of the specimens. There are several

differences between these initial cracks in a pushoff or pulloff specimen and the inclined cracks in a concrete beam.

1) The overall initial crack in a pushoff or pulloff specimen is approximately straight. The roughness is mainly due to the aggregate. The overall shape of the inclined crack in a beam is zigzag. The roughness is results from both the aggregate and the overall zigzag shape. Therefore, the shear crack in a beam has stronger shear friction action.

2) The pushoff or pulloff specimens were completely cracked throughout the interface before the shear forces were applied. The two halves of the specimen started to slide relatively along the crack once the shear forces were applied and kept continued to slide as the shear force increased. This is a process of losing the fit between aggregate and matrix. The looseness of fit of aggregate particles due to both initial cracking and the sliding during loading tends to degrade the stiffness and the strength of the shear friction along the crack. However, in a reinforced concrete beam, a crack is formed gradually with the loading. Before failure there always is an uncracked zone, large or small, which can prevent the crack faces from losing fit. Hence, the shear friction of the crack in a beam is more effective than that in the pushoff specimens.

3) In the pushoff specimens, the interface is not subjected to any bending moment. The relative sliding along the crack and widening of the crack is the necessary condition to develop the compression on the crack surfaces. The compressive stress on the crack plane

increases as the crack width increases. As observed by many researchers, the shear friction mechanism degrades as the crack width increases. So the coefficient of friction decreases as the compression on the crack surface increases. However, in a reinforced concrete beam, the compression is due to the bending moment.

4) The initial crack in a pushoff or pulloff specimen is an artificial crack which does not correspond with the stress state under the loading. This initial crack tends to change and weaken the load carrying system in the specimen. However, in a reinforced concrete beam, the shear crack is formed naturally due to the loading. It corresponds with the load carrying system formed in the beam. This load carrying system has a higher capacity than that corresponding with pre-cracked specimens.

5) The concrete contribution to shear in a reinforced concrete beam includes aggregate interlock action, the effect of the uncracked zone and dowel action. For the pushoff or pulloff specimens, the shear transfer along the interface only includes the aggregate interlock.

2.5.4 Crist's Analysis for Deep Beam

Crist²⁵ applied the shear friction mechanism to reinforced concrete deep beams. He assumed that the sole function of the vertical and the horizontal web reinforcement, is to induce a compression force on the crack plane which then creates shear friction action. Figure 2.16a shows the forces in the stirrups across a

crack plane. From the geometry of the forces, the component of the tension resultant normal to the crack plane can be expressed as:

$$F_{DT} = \Sigma F_{vi} \sin(\alpha_i + \theta) \quad (2.25)$$

F_{DT} creates an equal normal compressive force on the crack plane, as shown in Fig. 2.16b. This normal compressive force is required by the friction along the crack. According to the shear friction analogy, the shear force along the crack can be expressed as:

$$S = \mu \Sigma F_{vi} \sin(\alpha_i + \theta) \quad (2.26)$$

The vertical component of S is the shear resistance of the inclined section. Therefore the shear force can be expressed as:

$$V = \Sigma \mu F_{vi} \sin(\alpha_i + \theta) \sin \theta \quad (2.27)$$

If the web reinforcement consists of both vertical and horizontal reinforcement, the inclination α_i is equal to either 90° for the vertical ones or 0° for the horizontal ones. Assuming that both the vertical and the horizontal reinforcements are uniformly distributed, with a spacing of s and s_h respectively, then Equation (2.27) can be rewritten as

$$V = \frac{A_v f_y d}{s} (\mu \cos^2 \theta) + \frac{A_h f_y d}{s_h} (\mu \sin^2 \theta) \quad (2.28)$$

where A_v and A_h are the area of the vertical and horizontal reinforcement respectively. The reinforcements are assumed to yield at the ultimate state, with a yielding strength f_y .

In Crist's shear friction model, the component of the tensile force in the web reinforcement parallel to the crack plane is ignored. The ACI shear friction method²⁶ considers the contribution of tensile force in the reinforcement parallel to the crack plane. This analysis is based on Mattock's work²⁷. Figure 2.17a shows the forces on a crack plane. The shear force along the crack plane can be expressed by ACI Eqn.(11.27):

$$S = \mu A_w f_y \sin\alpha + A_w f_y \cos\alpha \quad (2.29)$$

The first term in Eqn. (2.29) is the shear friction due to the normal compression on the crack plane, which is equivalent to the shear friction of Crist's method, as expressed by Eqn. (2.26). The second term of Eqn. (2.29) is the component of the tension in the web reinforcement which is parallel to the crack plane. If the crack under consideration is an inclined crack in a beam, as shown in Fig. 2,17b, the vertical shear force V can be written as:

$$V = (\mu A_w f_y \sin\alpha + A_w f_y \cos\alpha) \sin\theta \quad (2.30)$$

Equation (2.30) can be expressed in terms of vertical and horizontal reinforcement:

$$V = \frac{A_v d f_y}{s} (\mu \cos^2\theta + \cos\theta \sin\theta) + \frac{A_h d f_y}{s_h} (\mu \sin^2\theta - \sin\theta \cos\theta) \quad (2.31)$$

According to Eqn. (2.28) and (2.31), both Crist and Mattock's shear friction methods assume that the primary function of web reinforcement is to induce a normal compression force on the crack plane and then to produce shear friction. It is well known that in a

structure, force always tends to take the shortest possible path. According to this principle, all the elements of a structure tend to form the shortest possible path to carry the load. In a beam, the most direct possible load carrying path involving the vertical reinforcement, or the vertical component of web reinforcement, is to carry the vertical shear force directly by tension, as do the tension ties described by the truss model. The vertical reinforcement, or the vertical component of web reinforcement, in a beam does not transfer vertical load by inducing a compressive force on the crack plane to form shear friction along the crack, and then the vertical component of the shear friction carrying the vertical load.

Crist's shear friction analysis is only applicable to the case where the applied load is parallel to the crack plane and the shear reinforcement under consideration is perpendicular to the crack plane. It can not be used in the design of reinforced concrete where the the applied load and the shear reinforcement are at an angle with the inclined crack.

2.5.5 Collins and Vecchio's Expression for Shear Carried Across a Crack

Collins and Vecchio³ applied the shear friction concept in their modified compression field theory, as shown by Fig. 2.11 and Eqn. (2.22). Based on Walraven's work²⁴, they derived the following relationship for the shear stress v_{ci} across a crack of width w :

$$v_d = 0.18 v_{dmax} + 1.64 f_d - 0.82 \frac{f_d^2}{v_{dmax}} \quad (2.32)$$

where

$$v_{dmax} = \frac{\sqrt{f'_c}}{0.31 + 24 w / (a + 16)} \quad (2.33)$$

and a is the maximum aggregate size in mm and the stresses are in MPa. The crack width w is related to the crack spacing s_θ measured perpendicular to the crack and the principal tensile strain ϵ_1 perpendicular to the crack.

$$w = \epsilon_1 s_\theta \quad (2.34)$$

where s_θ depends on both the location and the amount of the reinforcement.

$$s_\theta = \frac{1}{\frac{\sin\theta}{S_x} + \frac{\cos\theta}{S_y}} \quad (2.35)$$

In the modified compression field theory, the shear friction stress is expressed as a function of crack width, and the crack width is a function of tension strain and the crack spacing. So far there are no good methods to calculate all these variables for a concrete beam, making the method difficult to apply.

2.6 Effective Concrete Strength

As mentioned in previous sections, if excess web reinforcement is provided, the beam may fail due to web crushing prior to yield of

the stirrups. In this case the shear strength is governed by the compressive strength of concrete in the web. The concept of an effective concrete strength was introduced when researchers developed the truss models and observed that the concrete strength of the struts at the ultimate state is usually less than the cylinder strength f'_c . This behaviour was later referred to as concrete softening. Softening of concrete is considered in the truss models by using the effective concrete strength f_{ce} in Eqn. (2.3) and (2.14) instead of the cylinder strength f'_c to calculate the strut strength. The effective concrete strength is frequently expressed as:

$$f_{ce} = v f'_c \quad (2.36)$$

where v is an efficiency factor which has values between 0 and 1.0. Many researchers have investigated this issue. The major cause of concrete softening was reported to be the transverse tension perpendicular to the compression. Table 2.1 shows the values of v proposed by some of the researchers³²⁻⁵⁶. Only a few of them will be discussed in more detail.

The behaviour of plain concrete under bi-axial stresses has been well investigated by many researchers²⁸⁻³¹. The strength of plain concrete under bi-axial tension-compression decreases as the transverse tensile stress σ_t increases, as shown in Fig. 2.18. Slate³⁰ suggested a linear relationship between the compressive strength and the transverse tensile stress as:

$$\frac{f_{ce}}{f'_c} = \frac{1}{1 + k t} \quad (2.37)$$

where t is the ratio of the uniaxial ultimate compressive strength, f'_c , to the uniaxial ultimate tensile strength, f'_t ; k is the ratio of the principal tensile stress, σ_2 which is equal to f_{ce} at failure, to the principal compressive stress, σ_1 . Equation (2.37) can be rewritten as:

$$\frac{f_{ce}}{f'_c} = 1 - \frac{\sigma_1}{f'_t} \quad (2.37a)$$

What needs to be mentioned here is that the plain concrete element in Fig. 2.18 fails once the concrete cracks transversely. The failure may not be due to the concrete crushing and the strength predicted by Eqn. (2.37) may not be the compressive strength of the concrete. However, for reinforced concrete, cracking may not immediately cause failure but reduces the compressive strength.

Based on their experimental tests on uniformly strained panels, Collins and his co-workers⁴⁵⁻⁴⁷ discovered that the principal compressive strength decreased as the gross principal tensile strain ϵ_1 increased, where ϵ_1 is the average strain including the widths of the crack. The lowest strength in their tests was about 20% of the cylinder strength. According to their tests, Collins and his co-workers developed an empirical equation to calculate the effective strength of concrete. The empirical equation was modified in the Modified Compression Field Theory as:

$$f'_{ce} = \frac{f'_c}{0.8 + 170 \epsilon_1} \quad (2.38)$$

where the principal tensile strain, ϵ_1 , is obtained from a Mohr's circle for strain relating the horizontal strain ϵ_x parallel to the axis of the beam, the inclination θ of the compression strut and $\epsilon_2 = -0.002$. In lieu of an analysis for ϵ_x Collins and Mitchell suggested it can be taken as 0.002. Thus v varies almost linearly from 0 when $\theta = 0$ to 0.55 when $\theta = 45^\circ$, and back to 0 when $\theta = 90^\circ$. Equation (2.38) is used by the CSA Code.

Based on their tests, Schafer et al⁵⁸ stated that the reduction of the compressive strength due to transverse tension may generally assumed around 20% if the reinforcement is designed according to the codes. In 1990 Kollegger and Mehlhorn⁵⁷ published the result of tests of 47 panels carried out in the University of Kassel. They found that the maximum reduction of the concrete compressive strength due to transverse tension was 20%, which was consistent with Schlaich and Schafer's conclusion. No influence of loading history or reinforcement properties on the panel strength was observed in the tests. They reviewed the experiments by Vecchio and Collins and concluded that the majority of the panels failed due to yielding of both reinforcements or load introduction problems. They claimed that only three panels of the Vecchio and Collins test series experienced a compressive failure of the concrete. The maximum reduction of the concrete compressive strength of these three panels was 21%. Kollegger and Mehlhorn suggested that the effective strength of concrete under transverse tension be more accurately described as a function of tensile transverse tensile stress than a function of tensile strain as suggested by Vecchio and Collins.

The specimens tested by the above researchers were generally uniformly stressed concrete panels. These panels are able to model the B-regions in slender beams which are usually modelled as continuous fields of uniform compression. However, for isolated struts as in D-regions which usually are modelled as strut-and-tie system, the stresses are highly localized. Schlaich and his colleagues⁸ observed that the isolated compression struts have their least width at the node points, and, in the real case, can increase in width between the node points. The bulging in width of the strut induces tensile stresses transverse to the strut which limit the compressive strength of the strut. Schlaich et al. then gave a mini-truss model for the strut itself and analyzed the effective strength of the struts. The result of the analysis is shown in Fig. 2.19. In fact, bulging of isolated strut has two effects on the strength of the struts. First, the bulging induces transverse tensile stresses perpendicular to the compression and as a result reduces the compressive strength of the concrete. Second the bulging increases the area of cross section of the strut and as a result increases the capacity.

The softening truss model theory developed by Hsu⁵¹⁻⁵⁴ et al. is very similar to the compression field theory of Collins. In the softening truss model theory, Hsu uses Collins' earlier work⁴⁶ on concrete softening to compute the effective strength of concrete:

$$v = \sqrt{\frac{\epsilon_h + \epsilon_v - 2\epsilon_d}{\epsilon_d} - 0.3} \quad (2.39)$$

In 1993, Hsu⁵⁵ developed a new equation for effective compressive strength of concrete according to their tests:

$$v = \frac{0.9}{\sqrt{1+600\varepsilon_t}} \quad (2.40)$$

The effective strength predicted by Eqn. (2.40) is very close to that by Collins Eqn. (2.38).

The concrete softening originated by Collins and Schlaich are both due to transverse tension, either from transverse loading or from the strut bulging. In reinforced concrete beams, transverse tensions are usually caused by the crossing of web reinforcement. The distributed web reinforcement has two opposing functions: to restrain the struts or to transfer tension to the struts. If the web reinforcement is not a major part of the load paths, as in deep beams, it tends to restrain the struts transversely and hence increase the strength of the struts. When the web reinforcement participates in transferring load, as in the case of vertical stirrups in slender beams, it applies transverse tension to the struts and as a result reduces the strength of the concrete.

2.7 Summary of the Unsolved Issues

The traditional truss model can provide an excellent conceptual model to show the forces existing in a cracked concrete beam. However, it neglects the concrete contribution and assumes a conservative angle of 45° for the inclined cracks. The shear design procedure in the ACI and CSA Codes accounts for the conservatism

by adding a concrete contribution V_c to the capacity of the 45° truss action. Although the code method usually leads to a satisfactory design, it is highly empirical and does not provide designers with a rational model for the shear strength. A variable truss model selecting a flatter inclination for the truss struts provides a better representation of forces in a cracked beam, but it does not directly consider any contribution of the concrete shear transfer mechanism to shear strength. Although the modified compression field theory considers both the variation of the truss inclination and the concrete contribution, it describes the concrete contribution as a function of crack width, crack spacing and concrete strains which can not be easily determined. Moreover the modified compression field theory itself involves a tedious procedure of solving a nonlinear system of equations which is not convenient in design practice.

The shear-friction model provides a very good understanding for the concrete shear transfer mechanism. However, the experimental tests were limited to pushoff or pulloff specimens whose cracks are geometrically and statically different from those in a beam. The existing applications of the shear friction method to concrete beams are only applicable when the applied shear force is parallel to the crack face and the reinforcement is perpendicular to the crack.

Although many researchers have studied the effective compressive strength of concrete under transverse tension, the concrete efficiency factors, v , were usually established by fitting a certain theory to test results on specific members. These efficiency factors must absorb the shortcomings of the theory used and include

the structural behaviours of the members tested. These factors actually become the correction factors for the theories, rather than a material property. The mechanism of concrete softening under transverse tension is still unknown.

In summary, the variable angle truss model is the best model of the function of vertical stirrups, however, it needs a supplement to account for the concrete shear transfer mechanism. The shear friction method, if expressed in terms of the coefficient of friction and the forces in the crack plane, is a very understandable and simple model to describe the concrete shear transfer mechanism. The shear strength corresponding to web crushing is governed by the effective concrete strength. In the light of the above, two experimental test series were designed and conducted to investigate the mechanism and behaviours of both the shear friction across an inclined crack and the concrete softening under transverse tension. Based on the test results, a shear-friction truss model which combines the variable angle truss model with the shear friction method and takes into account the concrete softening in the web will be developed.

Table 2.1 Value of v proposed in literature

Investigator(s)	Proposed value for v	year and comments
Mattock and Kaar ³²	No explicit value	1961; Influenced by a/d , A_v
Leonhart and Walther ³³	0.6 - 0.8	1961; Quoted in terms of prism strength ($\approx 0.9f_c$)
Taylor ³⁴	0.4	1963; Influenced by b_w , d , f_c
Bennett and Balasooriya ³⁵	0.92	1971; from tests
Placas and Regan ³⁶	$(25 + 500\rho_u) / \sqrt{f}$	1971; Imperial units;
Lyngberg ³⁷	0.85	1976; Plastic approach
Nielson and Brastrup ³⁸	0.72	1975; Plastic approach
Hilsen, et al. ³⁹	$(0.8 - f_c/200)$	1978; dependent on section and reinforcement detail
Exner ⁴⁰	$3.2\sqrt{f_c}$	1979; in MPa
Thurlimann ⁴¹	0.6	1979, Proposed for CEB Code
Campbell et al. ⁴²⁻⁴³	≈ 0.92 Observed 0.85 recommended	1976-80; Plasticity and variable angle truss model
Batchelor ⁴⁴	0.6 recommend	1986; Regression analysis; influenced by a/d
Marti ⁴⁸⁻⁵⁰	0.55-0.6	1985-87; used in application of truss model
	$\frac{3.6}{1 + \gamma_m / \epsilon_c}$	1979; γ_m average value of max. shear strain
Collins ^{3,45-47} et al.	$\sqrt{\frac{\epsilon_h + \epsilon_v - 2\epsilon_d}{\epsilon_d}} - 0.3$	1981, from tests
	$1 / (0.8 - 0.34 \frac{\epsilon_1}{\epsilon_0})$	1988, Modified from empirical equation developed in 1983
Hsu & Mau ⁵¹⁻⁵⁵	$1 / \sqrt{0.7 - \frac{\epsilon_1}{\epsilon_2}}$	1985-88; Simplified from Collins' earlier work
	$\frac{0.9}{\sqrt{1 + 600\epsilon_t}}$	1993; very close to Collins work (3)
Rogowsky ⁵⁶	0.85	1983; Influenced by the selection of truss
Schlaich et al. ⁸	0.8	1987; Using strut-and-tie model

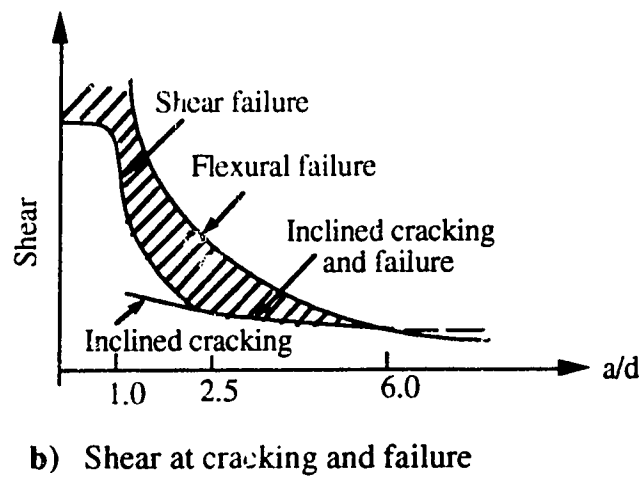
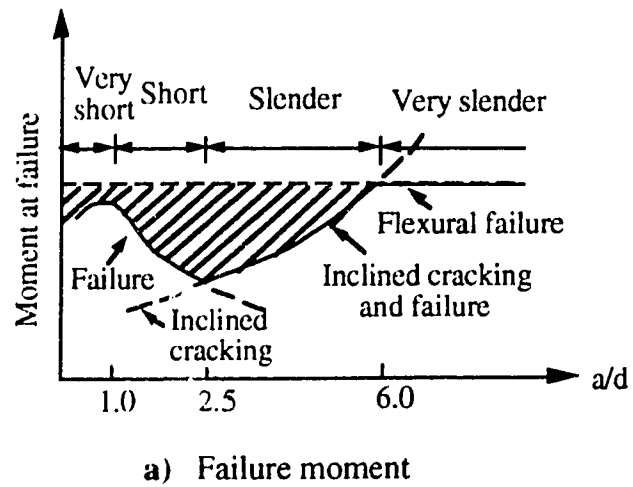


Figure 2.1 Effect of a/d ratio on shear strength of beams without web reinforcement

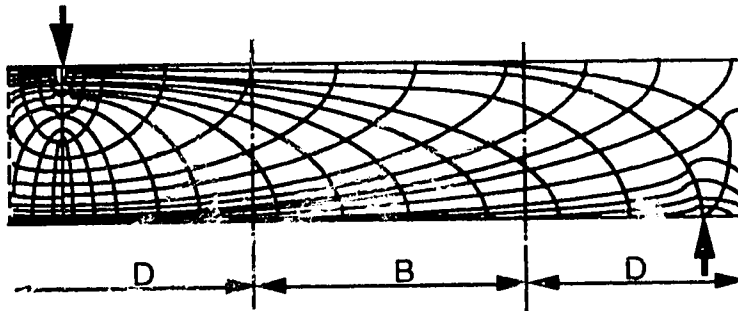
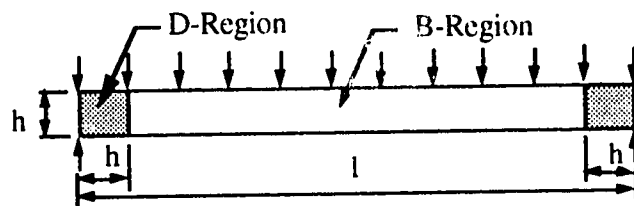
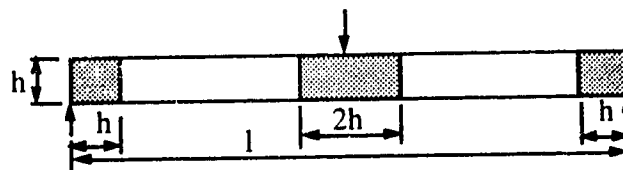


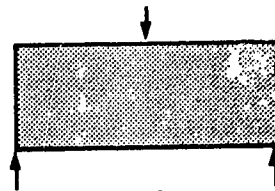
Figure 2.2 Stress trajectories in a beam;



a) Beam under line load

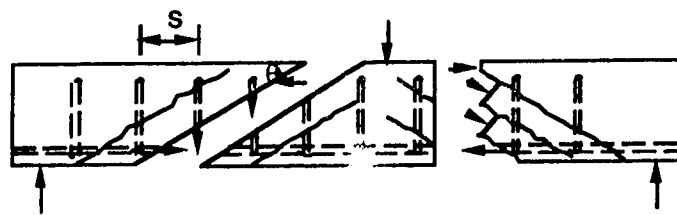


b) Beam under concentrated load

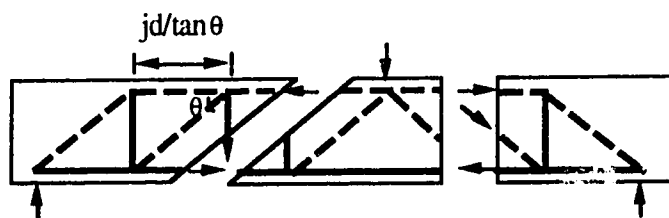


c) Deep beam

Figure 2.3 Examples of B-regions and D-regions in beams



a) Internal forces in a cracked beam



b) Pin-jointed truss

Figure 2.4 The truss analogy

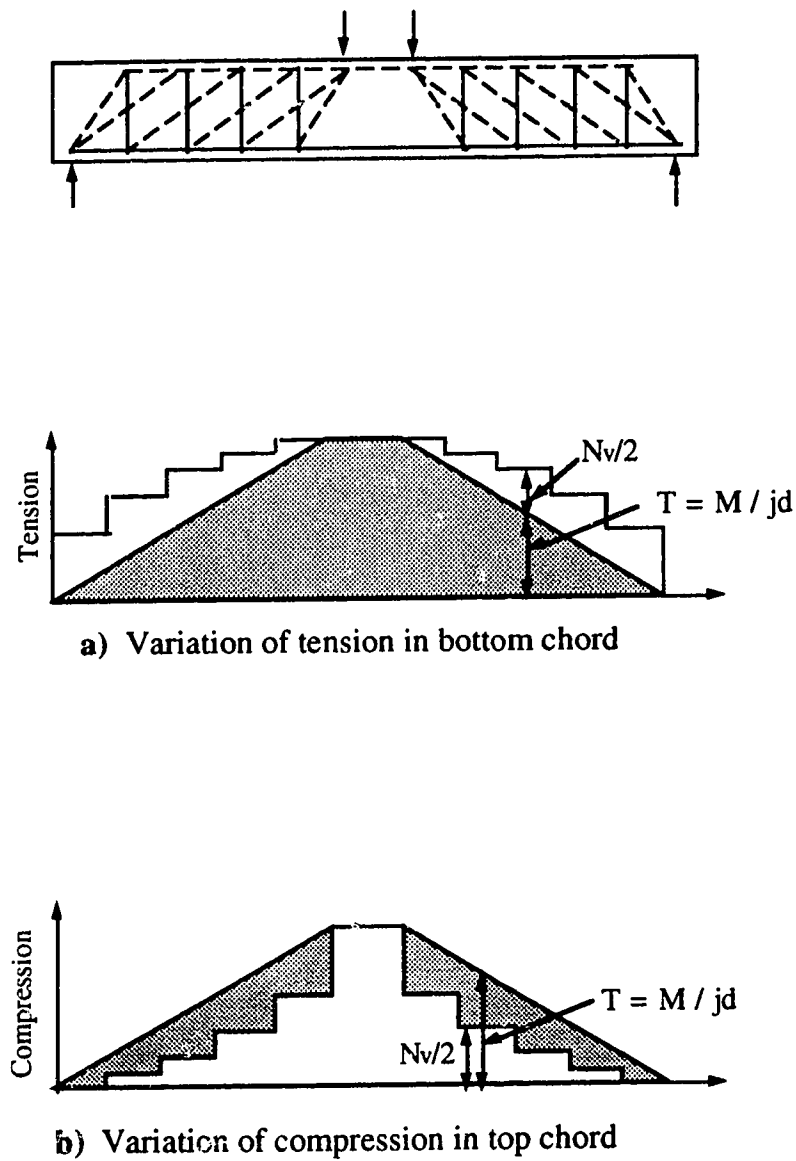
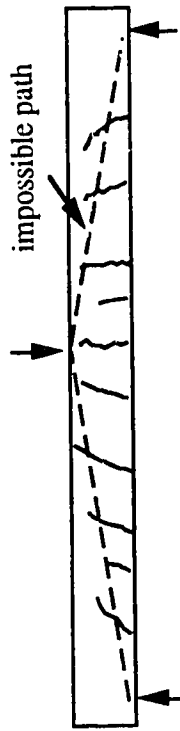
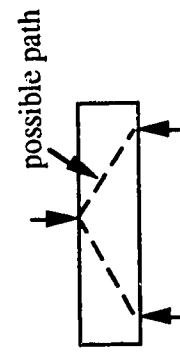


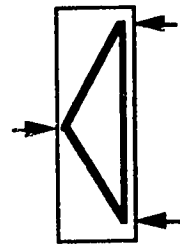
Figure 2.7 Forces in tension and compression chords of a truss



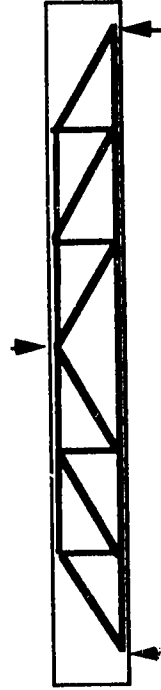
a) The shortest path in deep beam



b) The shortest path in slender beam



c) Strut-and-tie model for deep beam



d) Truss model for slender beam

Figure 2.8 Comparison of load paths in a deep beam and in a slender beam

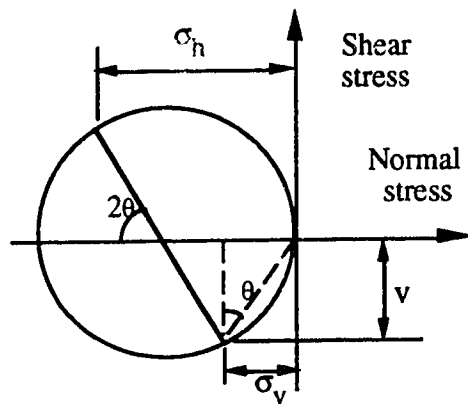
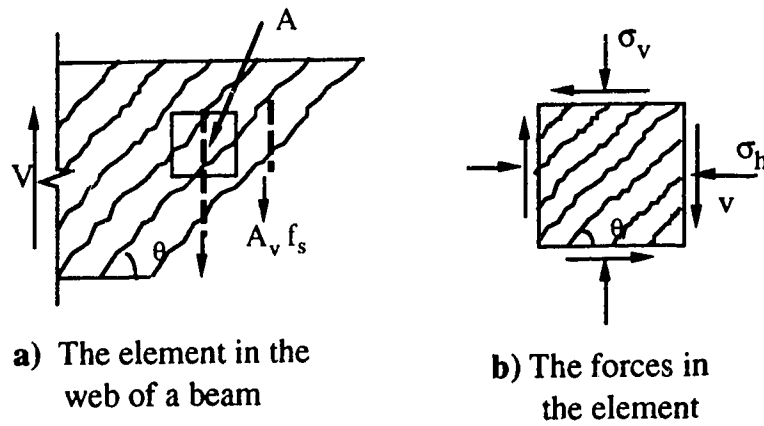


Figure 2.9 Equilibrium in the Compression Field Theory

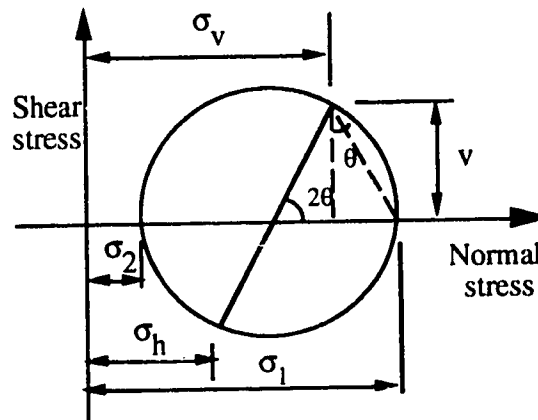
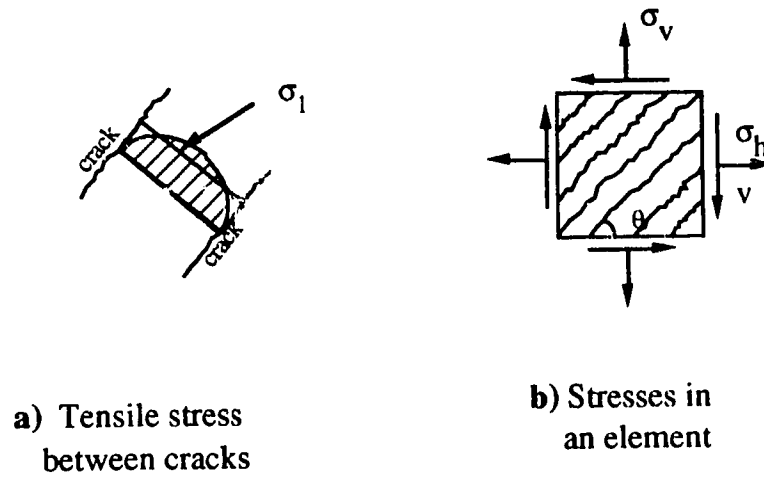
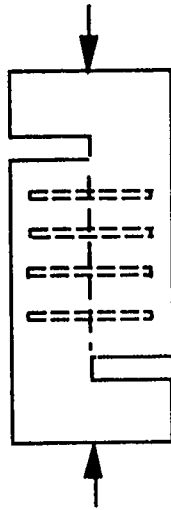
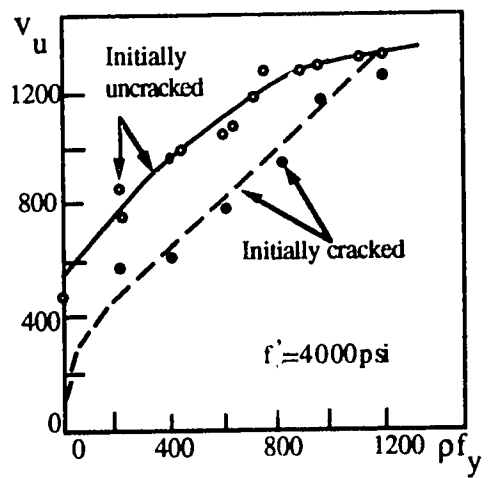


Figure 2.10 The Modified Compression Field Theory

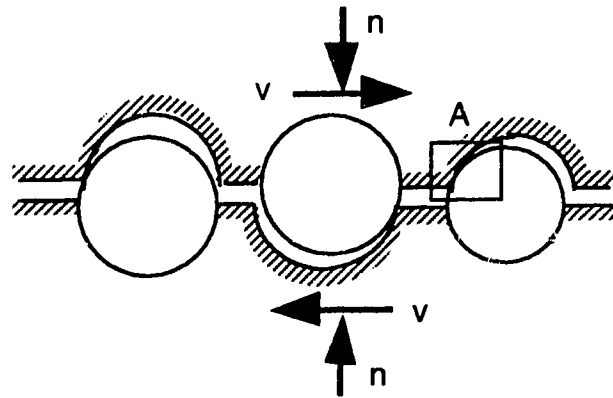


a) Shear transfer specimen

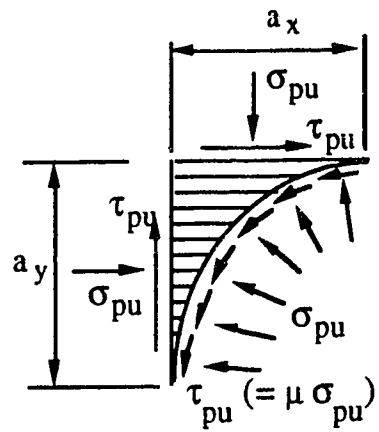


b) Variation of shear strength with reinforcement ratio

Figure 2.12 Pushoff test



a) Simplified crack surface



b) Forces in the contact area A

Figure 2.13 Shear friction model by Walraven²⁴

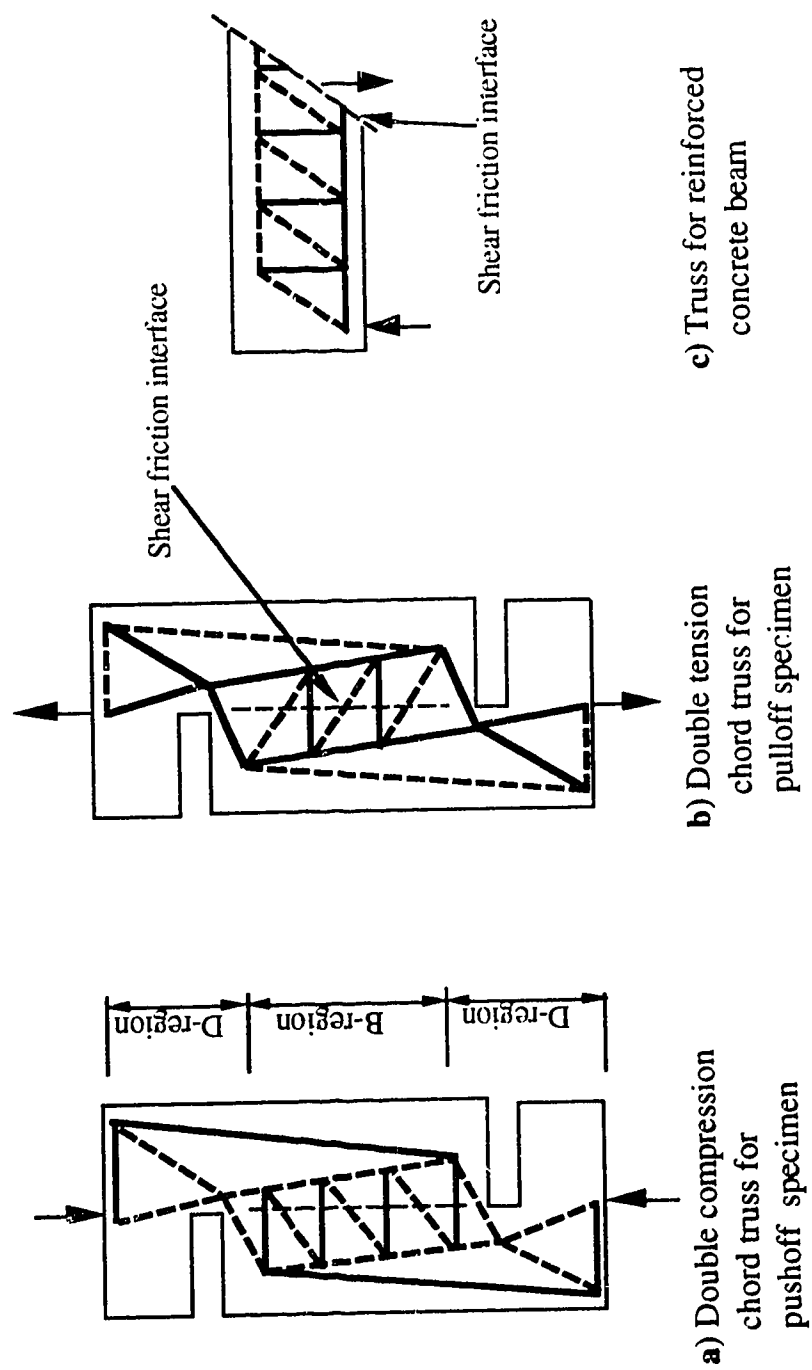
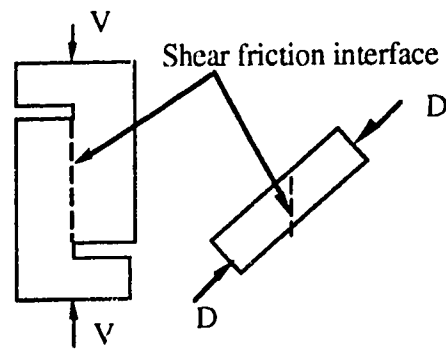
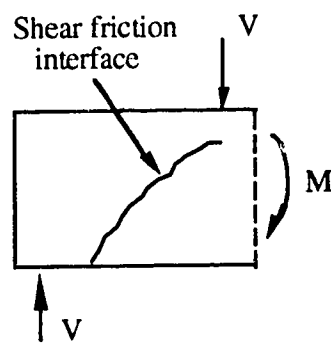


Figure 2.14 Truss models for pushoff and pulloff specimens and a reinforced concrete beam

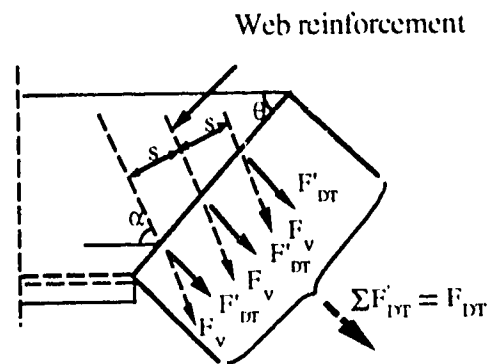


a) Initial crack in a pushoff specimen

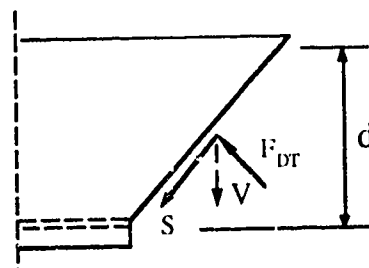


b) Inclined crack in a beam

Figure 2.15 Comparison between the shear interfaces in a pushoff specimen and a beam



a) Forces in stirrups
across a crack plane



b) Forces on a inclined plane

Figure 2.16 Shear friction analogy for deep beams by Crist²⁵

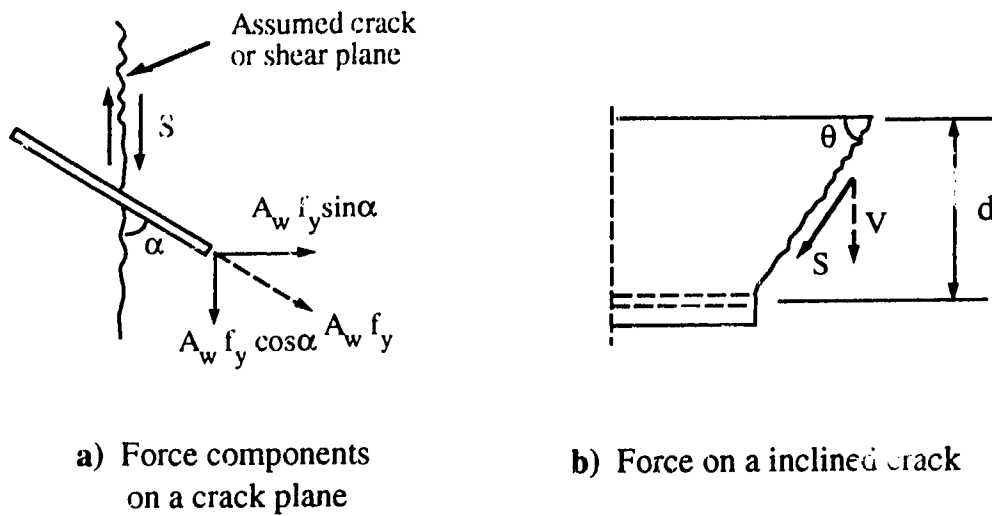


Figure 2.17 ACI code shear-friction method

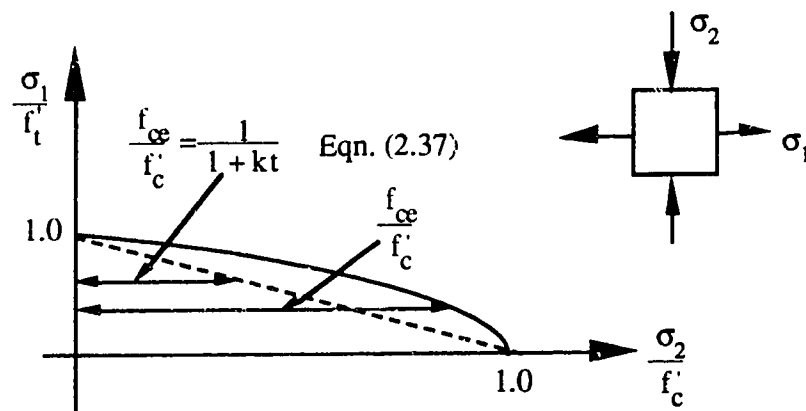


Figure 2.18 Concrete strength under bi-axial stresses

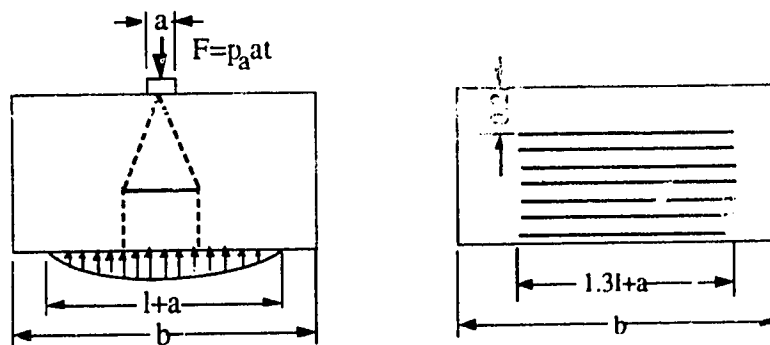
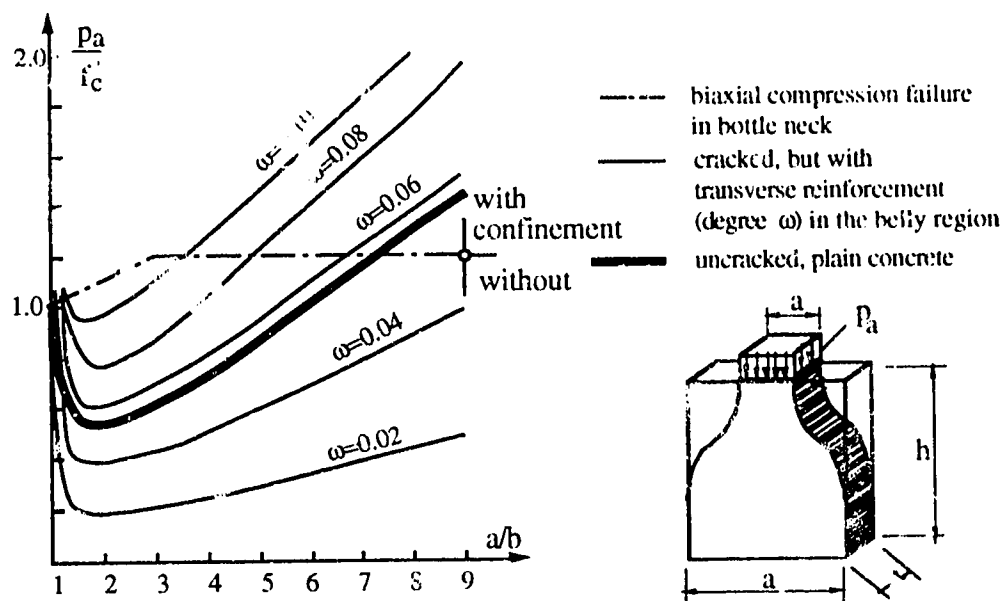


Figure 2.19 The efficiency factors for isolated struts from Schlaich's analysis

3. EXPERIMENTAL PROGRAM

3.1 Overview of Experimental Program

Based on the findings of the literature review, an experimental program was designed. The overall objectives of the experimental program were first, to investigate the shear transferred by friction on an inclined crack and second, to investigate the reduction in the compressive strength of concrete due to transverse tension, referred to as concrete softening. Two test series were involved in the experimental program to achieve the two overall objectives respectively. The first consisted of tests on shear transferred by friction, referred to for convenience as shear-friction. They consisted of tests of 17 reinforced concrete cantilevers subjected to transverse shear force, simulating the shear spans of reinforced concrete beams, as illustrated in Fig. 3.1. The cross section of the cantilever was 320x160 mm. The specimens were tested with different angles of the inclined crack, and various interface conditions. The inclination of the crack and the forces on the crack plane were well defined and directly measured in the test. Using the test results, the relationship between the ultimate shear-friction force and the longitudinal compressive force on the crack plane was derived as a function of the crack inclination.

The second test series consisted of tests on concrete softening. This series included tests of 40 concrete panels subjected to combined longitudinal compression and transverse tension to

simulate the diagonal compression field in a cracked concrete beam web, as illustrated in Fig. 3.2. The typical dimensions of the panels were 420 mm wide, 640 mm high and 70 mm thick. The specimens were loaded longitudinally to crushing under various degrees of transverse tension. Different loading histories, crack patterns and stress distributions were selected in the tests to investigate the effects of these variables. Using the test results, the mechanism of concrete softening was investigated and a relationship between the effective compressive strength of concrete and transverse tensile strain was developed.

The detailed descriptions of the test specimens, the test set-ups and testing procedures of both test series are presented in this chapter. The results of the first test series are presented and discussed in Chpt. 4. Based on the test results a shear-friction truss model is developed in Chpt. 5. The test results of the second series on concrete softening are presented and discussed in Chpt. 6. The behavior and the mechanisms of concrete softening under transverse tension are discussed and an equation for calculating the effective strength is proposed in Chpt. 7.

3.2 Test Series 1: Tests on Shear Transferred by Friction

3.2.1 Objectives

As mentioned in the previous chapter, prior experimental investigations on shear friction have focused on tests of pushoff and pulloff specimens whose shear transferring interfaces were parallel

to the shear forces and subjected to zero bending moment. The shear transferring mechanisms in these tests were very different from that existing along an inclined crack of a reinforced concrete beam. The existing applications of the shear friction method in deep beam design were a misunderstanding of the force paths in a reinforced concrete beam. The experimental program presented here was intended to investigate the shear friction behavior of an inclined crack subjected to bending moment. The internal and external forces and the inclinations of the cracks were well defined in the test. The variables investigated included the inclination of crack, the longitudinal compressive force on the crack plane, the reinforcement and cracking conditions with the following objectives:

1. To investigate the behaviour of shear transfer by friction along inclined cracks with various inclinations. The inclinations selected for the tests were 30, 45, 60, 90 degrees and undefined.
2. To investigate the effects of bond conditions on shear friction and the shear contribution of dowel action.
3. To investigate the influence of cracking in the compression zone and the shear contribution of the uncracked compression zone.
4. To derive a relationship between the shear-friction force and the longitudinal compression on the crack planes based on the dry friction theory.

5. To develop a shear-friction truss model which accounts for the shear contribution of stirrups using a truss model and the shear contribution of concrete using the shear-friction method.

3.2.2 The Specimens

Seventeen reinforced concrete cantilevers subjected to transverse loading were tested. The cross section of the specimens was 320x160 mm (see Fig. 3.3), which were the average dimensions of the interfaces of the pushoff specimens tested by Mattock^{21,22} and Paulay^{19,20}. The inclinations selected for the specimens were 30°, 45°, 60° and 90°. The clear shear span of the specimens were then chosen so that a shear crack with the designated inclination could occur within the clear shear span. The actual shear-span ratios of the specimens were from 0.5 to 3.0. Since the objectives of the tests were to investigate the shear transfer by friction on a defined inclined crack under known forces, the shear-span ratio was not a primary variable in the study.

The reinforcing steel in the specimens consisted of Grade 400 15M bars as the longitudinal reinforcement and 6 mm, 8.5 mm and 11.3 mm diameter bars as the stirrups. The geometry and reinforcing of the specimens are shown in Figs. 3.3 to 3.5. The typical steel cage was divided into upper and lower halves with heavy reinforcement in the regions where the load and the reaction acted respectively. The inclined strip between the two halves was either unreinforced or more lightly reinforced to allow the shear-

friction testing. All the specimens except S15, S16 and S17 had no stirrups across the inclined crack zone. In this region shear forces were resisted only by the shear transferred by friction. The specimens were reinforced with longitudinal tensile reinforcement which either extended across the expected crack or was cut at the crack, as shown in Figs. 3.3 to 3.5. In the specimens with longitudinal reinforcement across the crack, the tension in the reinforcement produced the confinement on the crack planes which was needed to mobilize the shear friction. For those without longitudinal reinforcement across the interfaces, an external normal force was applied on the end of the specimens as shown in Fig. 3.3c to produce the compression on the crack plane necessary to induce shear-friction on the crack. Specimens S15, S16 and S17 were reinforced with both the longitudinal and transverse reinforcement across the cracks. Both truss action and shear-friction contributed to resist the shear.

Several special details were incorporated in the specimens to achieve various specified purposes. They are described in the following paragraphs and summarized in Table 3.1.

Grooving along the specimen surface: Except for specimens S5, S11, and S15 to S17, the specimen surfaces were grooved on both the faces along the expected inclined crack and, in addition, had a 10 mm deep cut on the tension edge of the specimens, as shown in Fig. 3.6. The purpose was to make the crack have an approximate straight overall shape so that the inclination of the crack was well defined and the strain gauges on the longitudinal reinforcement could be

located at the crack to measure the forces on the crack planes. The width of the groove was 40 mm which was 4 times the aggregate size so that the zigzag nature of the crack was not eliminated.

Reduction of dowel action: Dowel action has been considered as one of the shear resisting mechanism. Dowel action is the shear force developed in the reinforcement itself, as illustrated in Fig. 3.7a. To reduce the dowel action in some of the specimens, the portion of the longitudinal reinforcement intercepting the inclined crack was wrapped with an annulus of foam insulation 150 mm long and 10 mm thick. The mechanism of dowel action reduction is shown in Fig. 3.7b. The foam insulation increased the shearing length of the reinforcement and in this way it decreased the shear force developed in the reinforcement.

Pre-cracking in the compression zone: The shear transferring mechanism of the compression zone has been traditionally considered as the shear in the uncracked concrete mass. However, shear friction is the shear transferring mechanism on a physical interface. To study the differences between the shear transferring mechanisms of uncracked concrete and shear friction along a crack plane, the specimens with both pre-cracked and uncracked compression zones were tested. The compression zones were pre-cracked by applying an opposite bending moment to the specimens to produce tension and cracking in the "uncracked compression zone", as shown in Fig. 3.8. The pre-cracks were about 1/3 of the specimen depth and were located within the groove along the

extension of the expected crack. They were invisible to the naked eye after removing the opposite moment.

The specimens with the expected inclined crack of 45° consisted of five specimens from S1 to S5. Specimen S1, S2 and S3 had two 15M longitudinal bars across the inclined crack, while S4 and S5 had no reinforcement across the inclined crack. To investigate the effects of cracking in the compression zone, S3 was pre-cracked in the compression zone. In S2 the longitudinal reinforcement was wrapped with foam insulation to investigate the effects of the dowel action. Except for S5, the specimens were grooved to define the failure crack. The geometry and reinforcing were shown in Fig. 3.3.

The specimens with the expected inclination of crack of 60° included S6 to S8. Specimens S6 and S7 had two 15M bars across the inclined crack, while there was no reinforcement across the crack in S8. In S7 the compression zone was pre-cracked. The reinforcement was wrapped with foam insulation in S6. All three specimens were grooved in the surfaces to define the crack.

Specimens S12, S13 and S14 had inclined cracks at 30° . Both S12 and S13 were reinforced with two 15M bars across the inclined crack but in S12 the reinforcement was wrapped with the foam insulation to reduce the dowel action. S14 had no reinforcement across the inclined crack. All three specimens were grooved on the surface to define the crack.

Specimens S9, S10 and S11 shown in Fig. 3.4 had their "inclined" cracks at 90° . No reinforcement was provided across the crack in

these specimens. The confinement of the interface was introduced by the external longitudinal force. Different external forces were applied in the three specimens respectively. These three specimens were tested to provide a comparison with the pushoff tests.

Specimens S15, S16 and S17 shown in Fig. 3.5 were the last three specimens tested in the series. They were reinforced as normal reinforced concrete beams. Four 15M were used as the longitudinal reinforcement and closed 6 mm, 8.5 mm and 11.3 mm stirrups were used in the three specimens, respectively. The stirrup spacings were 100 mm. These specimens were not grooved or pre-cracked and the bars were not wrapped with foam. The objectives of these three specimens were to study the push behavior and the effect of the stirrups on shear friction.

3.2.3 Material Properties

All the reinforcement used in the test specimens consisted of deformed bars. The Grade 400 15M bars were supplied locally and the 6 mm, 8.5 mm and 10M (11.3 mm) reinforcement was taken from laboratory stock. Tension coupon tests were performed on samples of the all reinforcement to determine their mechanical properties. The coupon tests were done in the MTS test machine using an electrical resistance strain gage and calipers to determine the strain. Figure 3.9 shows the stress-strain curves for all the reinforcement.

The concrete mix was designed to produce a 28 day cylinder strength of about 40 MPa. Normal Type 10 portland cement and normal weight washed river aggregates were used. The maximum aggregate size was 10 mm. All of 17 specimens in this test series were cast from the same batch of concrete. The concrete was mixed by a local concrete supplier and delivered by ready-mix truck.

The specimens were cast in a horizontal position. The forms were removed approximately 24 hours after the concrete was placed. The specimens were then cured with moisture under burlap and polyethylene sheeting for the first week. Following this curing the specimens were stored in the lab without special curing procedure. Concrete test cylinders were cast at the same time as the specimens and then cured in a similar manner.

A few of the cylinders were tested at 14 and 28 days to assess the quality of the concrete. The remaining cylinders were tested during the period of the specimen testing, which was from 37 days to 103 days after casting. Three cylinders were tested approximately every week. The average compressive strength of 3 cylinders is plotted against the concrete age in Fig. 3.10. The cylinder strengths were quite consistent and about 45 MPa during the testing period. Figure 3.10 was used directly to determine the concrete strength of each of the specimens according to their age.

3.2.4 Test Set-up and Procedure

Each specimen was tested in the loading frame shown in Fig. 3.11. The details of the load application and the supports are illustrated schematically in Fig. 3.12. The specimens were placed vertically on a stiff beam and fixed at the bottom. The fixing confinement was applied by three high strength concrete blocks, two of which served as wedges. The fixing wedges were pre-loaded vertically to introduce a restraint on the specimens to prevent the specimens from overall rotation under horizontal load. To avoid bearing failure, the fixing length was designed to be 420 mm which was about $4/3$ the overall depth of the cross section of the specimen.

Both the transverse shear force and the longitudinal compression, if any, were applied by hydraulic jacks. Loads in the two jacks were measured by two load cells. Rollers and half rounds were used for both the vertical and horizontal loadings to ensure that no horizontal force component was induced by the vertical jack and no vertical force component was produced by the horizontal jack during the deforming of the specimens. The load was applied in increments, with approximately 8 load stages to failure. Near the ultimate strength of the specimens, smaller increments were used. During each load stage, all the readings including loads, displacement and strains were taken either manually or using the computer data acquisition system and cracks were marked. Each load stage was also divided into 3 or 4 sub-stages at which only the electrical readings were recorded. After failure each of the specimens was photographed.

For the specimens with longitudinal reinforcement across the inclined crack, except specimen S15 and S17, only transverse load was applied. The bending moment caused by the transverse load was resisted by the internal moment resulting from the tension in the longitudinal bar and the compression in the concrete. The latter at the same time contributed to the shear friction. For those specimens without longitudinal reinforcement across the inclined crack, an external longitudinal load was applied. This played a role similar to the longitudinal reinforcement in resisting the moment caused by the transverse load. The transverse load was applied monotonically. In the specimens with longitudinal load, the load was applied in such a way that its magnitude was approximately equal to the tensile force in the longitudinal reinforcement at the corresponding transverse load stage in the test of the reinforced specimen with the same configurations which had been tested earlier.

Specimens S9, S10 and S11 were designed with cracks at 90° . The ultimate external longitudinal forces were chosen equal to 80 KN, 160 KN and 240 KN, respectively. These loads represented the yielding force of one, two and three 15M bars. The longitudinal load was originally designed to increase at the same rate as the transverse load. However, because of the small shear span depth ratio of the three specimens, there was no crack observed in the original test of S9 at a very large load stage. To fulfill the investigation into the shear-friction on a crack, these three specimens were pre-cracked by applying the transverse load only.

The specimens were then tested under both the longitudinal and transverse loads following the designed longitudinal/transverse load path. The pre-cracks occurred at a transverse load about 50 KN and extended about 9/10 of the gross section depth.

For Specimens S15 and S17 in which closed 8.5 mm and 10M (11.3 mm) stirrups at 100 mm spacing were used, respectively, the longitudinal reinforcement started to yield before any shear failure phenomenon was observed. To ensure that the specimens would fail in shear, an external longitudinal force was applied to these two specimens. The external force played a role similar to additional reinforcement.

3.2.5 Instrumentation

In all tests in this series, the loads applied by both hydraulic jacks were measured by load cells and recorded using the Fluke computer data acquisition system. Each load cell was calibrated with the same hydraulic jack and the same Fluke system channel as used in the test.

Two LVDTs were used to monitor the relative sliding of the crack planes on each face of the specimens. The LVDT lengths extended across the inclined crack horizontally between targets mounted onto both edges of the specimens, as shown in Fig. 3.13. They gave measures of the horizontal component of relative sliding. The difference of the two LVDT readings on each of the specimen faces showed the relative rotation of the two crack planes. The

LVDTs had a stroke of 20 mm and were sensitive to 0.002 mm. They were calibrated and read using the same Fluke data acquisition system.

Concrete strains were recorded manually using 5" length Demec gauges. The gauge was sensitive to 0.002 mm. The targets were fastened to the concrete using sealing wax and arranged to form a 45° strain rosette. For all specimens except S9, S10 and S11, the strain rosettes consisted of horizontal, vertical and 45° diagonal gauge lengths, while for S9, S10 and S11 the lengths of the strain rosette were in the directions of vertical and 45° diagonal each way, (see Fig. 3.13).

Three Demec rosettes were mounted on each face of the specimens. The centers of the rosettes were located along the expected cracks, at a horizontal spacing of $1/4$ of the specimen depth. The readings of the rosettes show the crack width and the relative movement of the two crack planes. Besides the rosettes, three 5" Demec gage lengths were longitudinally arranged in the compression zones to measure the compressive strains in concrete. For those specimens with pre-crack in the compression zone, the displacements of the gauge lengths across the pre-crack were measured before the pre-cracking, after the pre-cracking and at each of the load stages of the testing.

The strains in the reinforcing steel were measured using electrical resistance strain gages. The strain gage results were recorded using the computer data acquisition system.

The electrical resistance strain gauges on reinforcement were always mounted in pairs on opposite sides of the bar to eliminate any effects due to bending strains in the reinforcement. The gauges used were 5 mm gauge length foil gauges with a nominal resistance of 120 ohms and gauge factor of $2.11 \pm 1\%$. Each gauge was installed using the three-wire system and calibrated using a shunt resistor. As is the standard in the lab, each gauge uses a "dummy" gauge for temperature compensation. In the aggressive environment within a concrete specimen, the gauges need adequate protection. Black electrical tape was used wrapping around and through the leads to insulate the leads from each other and from the steel. Both gauges were then wrapped again and then sealed using sealant to resist water. None of the gauges failed to function at the start of the test.

For the specimens S1 to S14 which had 2-15M longitudinal bars, the strains in both of the bars were measured. The average strains of the four gauges were used in the analysis. Since the locations of the inclined cracks in these specimens were well defined, the strain gauges could be attached to the portion of the reinforcement intercepting the expected inclined cracks, as shown in Fig. 3.14a. The forces on the crack planes were then calculated from the strains measured and the reinforcement properties.

Specimens S15, S16 and S17 were reinforced with both the longitudinal reinforcement and the stirrups. To calculate the forces on the crack plane, the strains in both the longitudinal bars and the

stirrups at the crack planes were measured. Strain gauges were mounted onto two of the longitudinal bars and one leg of each of the stirrups expected to be crossed by the crack. The strain gradient along the longitudinal reinforcement was measured by strain gauges on the longitudinal reinforcement at 200 mm spacing. The layout of the strain gauges was shown in Fig. 3.14b.

3.3 Test Series 2: Tests of Concrete Softening

3.2.1 Objectives

As reviewed in the previous chapter, the upper bound of shear capacity for a reinforced concrete beam is that causing the concrete struts between cracks in the web to crush. The upper bound of the shear strength is then governed by the compressive strength of the concrete. The transverse tension and cracking in the concrete cause significant reductions in the compressive strength. This is referred to as concrete softening. The tests described in this section are to study the behavior and the mechanism of concrete softening. The investigation included 40 concrete panels under longitudinal compression and transverse tension with the following objectives:

1. To investigate the behavior and the mechanism of concrete softening under transverse tension and cracking.

2. To determine the effects of transverse tensile strains, tensile stresses and transverse cracking on the concrete strength. The specimens were tested under different transverse tensile strains and stresses and with various crack patterns.

3. To study the effect of loading paths on the concrete strength. Various loading paths were arranged in the tests.

4. To determine the effect of non-uniform distribution of compressive stresses. Three non-uniform distributions of the compressive stresses were tested to compare with the uniform distributed stresses.

5. To propose an equation to calculate the effective strength of concrete for use in design.

3.3.2 Test Specimens

The test panels all had the same configuration of 70 mm thick, 420 mm wide and 640 mm high, except Specimens #34 to #40, inclusive, which were 560 mm high. The dimensions of the specimens were chosen to be equivalent to the center rectangular portion within the concrete panels tested by Collins and Vecchio⁴⁷, as shown in Fig. 3.15. In the Collins and Vecchio tests, the ratio of the compression to transverse tension was varied over a narrow range. Most of the panels were subjected to pure shear along the four edges thus the ratio of compression to transverse tension was equal to unity. In their tests the stresses were calculated using the compression field theory. In the specimens presented in this section the compression and transverse tension were applied by two individual loading systems and the ratio of compression/transverse tension was chosen freely. The stresses and strains were measured.

The specimens were tested vertically, with the height parallel to the vertical compressive load and the width parallel to horizontal tension. The vertical direction was identified as longitudinal, while the horizontal direction as transverse. To eliminate the effects other than those from transverse tension and cracking, the specimens were only reinforced transversely, as shown in Fig. 3.16. Thus, the longitudinal compressive load was resisted entirely by the compression in the concrete.

The functions of the transverse reinforcement in the specimens were to introduce transverse tensile strains and stresses to the specimens and then to distribute them over the concrete through the bonding action between the concrete and the reinforcement. To perform the above functions, either two or eight 10 mm deformed bars at a spacing of 80 mm were placed in the specimens as shown in Fig. 3.16. The reinforcement was placed at the mid-thickness of the specimen, with an 80 mm length extending out of the concrete on each side to introduce the transverse tension, as shown in Fig. 3.16a. Six specimens were constructed with reinforcement only at the top and bottom edges and the major part of the panel was plain concrete, (see Fig. 3.16b). They were tested under uniaxial compression as plain concrete panels. The compressive strength of the plain concrete panels were compared with the concrete cylinder strength to determine the shape effect in the specimens. To prevent the corners of the specimen from breaking off at the loading edges, a 8 mm thick steel plate was welded to the reinforcement and cast with the concrete at the four corners, as shown in Fig. 3.16.

The specimens were divided into three groups. The first group which included specimens #1 to #18 was designed with the concrete strength approximately 25 MPa. They were loaded to crushing under various transverse tensile strains to investigate the relationship between the effective strength of concrete f'_{ce} and the transverse strain ϵ_t . The ultimate average transverse tensile strains ranged from 0 to 0.02 which was about 9 times the steel yield strain. In the course of the test, both the longitudinal and the transverse loads were monotonically increased from zero to failure. The transverse load was increased in such a way that the ratio of longitudinal compressive stress to transverse tensile strain was approximately constant in the course of each of the specimen tests. The ratios of longitudinal compressive stress to transverse tensile strain were different from specimen to specimen so that different ultimate transverse strains were reached. The load paths were illustrated in Fig. 3.17a.

Panels #5 and #17 were reinforced only at the top and bottom edges and were tested under uniaxial compression. The strengths of these panels together with the concrete cylinder strengths were used to determine the unsoftened concrete strengths in the analysis. As mentioned in the literature review, the presence of reinforcement softens the concrete if it introduces transverse tension to the concrete, and strengthens the concrete if it introduces transverse restraint to the concrete. Specimens #4 was reinforced with transverse steel but they were tested under uniaxial longitudinal

compression to investigate the transverse restraining effect of the reinforcement.

Groups II and III were designed after the tests of the first group were finished. Both groups were designed with the concrete strength of 35 MPa. Group II which included specimens #19 to #33 was tested to investigate the effects of load path and crack patterns. Specimens #19 to #22 were tested following the load paths shown in Fig. 3.17b. The longitudinal compression and the transverse tension were increased alternatively in two steps to the failure. In the tests of these specimens, the crushing of concrete was observed as the direct result of either the increasing of the transverse tension or the increasing of the longitudinal compression. Specimens #23 to #28, inclusive, experienced repeated transverse tension. The load paths were shown in Fig. 3.17c. The tension in the transverse reinforcement was repeated from zero to either a pre-yield stress or a post-yield stress. Therefore, different numbers and patterns of cracks might occur under the same transverse tensile strain in different cycles and different transverse tensile strains might occur under the same transverse tensile stress. The purpose of this group was to determine the real factor which reduced the concrete strength among transverse tensile stress, transverse tensile strain and transverse cracking.

Specimens #30 to #33 were cast with 5 mm deep and 10 mm wide grooves on both sides to result in different crack patterns to investigate their effects on concrete softening. The grooves are shown in Fig. 3.18.

The third group of tests, which consisted of specimens #34 to #40, was tested to investigate concrete softening due to a non-uniform distribution of the compression stresses. The non-uniform distributions of stresses were produced by one center force P and two side forces nP , as shown in Fig. 3.19. Three configurations of stress distributions, ($n=0.25$, $n=0.5$ and $n=0.75$) were tested. The test results were compared with those of Group I and II which had $n=1$. Specimens #34 to #36 were tested with uniaxial compression while #37 to #39 were tested under compression and transverse tension.

3.3.3 The Materials

The reinforcement used in the specimens was 10M deformed bars supplied locally. Tension coupon tests performed on samples of the reinforcement indicated the yield strength was 350 MPa and the yield strain was 0.0022. The stress-strain curve for the 10M bars is shown in Fig. 3.9.

The 40 specimens were cast in two batches. The first batch of concrete for the 18 specimens of Group I was produced in the laboratory. The concrete mix was designed to produce a 28 day cylinder strength of about 25 MPa. After the first 18 specimens had been tested, The remaining specimens, from #19 to #40, were cast. The 28 day strength of the concrete was designed to be about 35 MPa. The concrete mix was batched by a local concrete supplier. For both batches of concrete, normal Type 10 Portland cement and

normal weight washed river aggregates with a maximum aggregate size of 10 mm were used.

The specimens were cast in a horizontal position and then cured in the same method used for the specimens of the shear-friction series as described in Sec. 3.2.3. Concrete test cylinders were cast at the same time as the specimens and then cured in a similar manner. The cylinders were tested during the period of the testing. Three cylinders were tested approximately every week. The average compressive strength of the three cylinders was plotted against the concrete age in Fig. 3.20. The concrete strength for each specimen was determined directly from Fig. 3.20 according to the age at the day of testing.

3.3.4 Test Set-up

Figure 3.21 shows the loading frame and test set-up for the specimens. The specimens were placed vertically on the stiff base beam which was bolted to the floor. The longitudinal compressions were applied to the top of the specimens by three 500 KN hydraulic jacks. To distribute the compression uniformly to the specimens, three jacks were connected to a single loading pump. Each jack force was then divided into two by a distributing plate. Six bearing plates 60 mm wide were used to reduce the bearing confinement on the concrete. A set of rollers and half rounds were used between the jacks and the bearing plates to guarantee only vertical forces were applied. Same type of bearing plates, rollers and half rounds were used on the bottom to support the specimens. To ensure a uniformly

distributed reaction, the bottom bearing plates were leveled carefully to fit the edge of the specimens.

For the specimens of Group III, the bottom reactions were produced by three 500 KN jacks of the same type as used on the top in order to produce reactions with the same distribution as the load applied at the top, (see Fig. 3.19). The center jacks on both the top and the bottom were connected to one jack and the side jacks on both the top and the bottom were connected to another jack. Thus both the top and the bottom edges had the same stress distribution. The ratios of the center force to side force remained constant in the course of testing.

The specimens were loaded transversely by the tensile forces applied to the transverse reinforcement extending out of the specimens. There were eight extended bars per side, (see Fig. 3.21). The forces on the extended reinforcement were applied through sixteen loading bars and mechanical wedge clamps which connected the loading bars to the extended transverse reinforcement. The mechanical wedge clamps were designed to clamp the deformed bars through the wedges and to link the loading bars through the threads, as shown in Fig. 3.22. Sixteen 120 KN center hole hydraulic jacks, eight on each side, were used to produce the tension. All the sixteen jacks were connected to a manifold and a single loading pump so that uniform forces were applied to the specimens. The transverse tensile forces on both sides of the specimens, the vertical compressive forces on the top of the specimens and the reactions on

the bottom were all applied on the same plane as the middle of the thickness of the specimen.

The load was applied in increments, following the load paths described in Fig. 3.17, with approximately 8 load stages to failure. Near the ultimate strength of the specimens, smaller increments were used. At each load stage, loading was halted by shutting off the hydraulic system while all the various strain, load cell, and displacement were recorded. During each load stage, cracks on the concrete were marked and all pertinent observations noted. Loading was then resumed. After failure each specimen were photographed.

3.3.5 Instrumentation

Measurements of strain in the specimens were made using mechanical Demec gages and LVDTs. The Demec gages were sensitive to 0.0025 mm displacements, and had strokes of approximately 5 mm. The LVDTs were sensitive to 0.002 mm and had strokes of approximately 20 mm. The Demec gauges and LVDTs monitored strains in the specimen by measuring relative displacement between the targets over known gauge or LVDT lengths.

LVDTs were used to measure the gross average transverse strain across the specimen width. The targets of each of the LVDTs were fastened to both edges of the specimens and the LVDT length was in the transverse direction, as shown in Fig. 3.23. For each of the specimens in Groups 1 and 2, five LVDTs were arranged on each face

of the specimen, at a spacing of 80 mm. The average readings of the two LVDTs at the same height at the two faces of the panel were used in the analysis. The readings of the two LVDTs at the mid-height were used to control the transverse loading during the tests. The layout of the LVDTs is shown in Fig. 3.23.

Two inch gauge length Demec gauges were used to measure the transverse strains of the concrete. Brass targets were attached to the concrete surface. The targets of the 2 inch gauge were arranged on the both faces of the specimen as shown in Fig. 3.23, 8 gauge lengths per row and totally 16 gauge lengths for each face. The longitudinal compressive strains in the specimens of Group I were monitored using 200 mm gauge length Demec gauge on the both faces. The targets were fixed to the concrete surface along the center line of the specimen, 2 gauge lengths per face, as shown in Fig. 3.23a. The longitudinal compressive strains in the specimens of Group II were measured by LVDTs along the center line of the specimen at both faces (see Fig. 3.23b)

For the specimens of Group I, a 5 inch Demec gauge was used to measure the strain in the reinforcement. Targets were mounted using sealing wax onto 6 mm diameter steel lugs which were brazed onto the steel. These lugs were isolated from the concrete by using a short piece of rubber hose. The hose was lubricated with Vaseline and wrapper with polyethylene so that it could be removed after the forms were stripped. The layout of the targets is shown in Fig. 3.23a.

For the specimens of Group III which were subjected to non-uniform longitudinal compression, the distribution of compressive strain in the concrete was monitored by 200 mm gauge length Demec gauge. The gauge lengths were arranged longitudinally, at a spacing of 52 mm across the specimen width. Both faces of the specimen had the same Demec gauge targets layout. The average transverse strain was monitored using LVDTs mounted on both sides of the specimen, in the same manner as used in the testing of Groups I and II. Four LVDTs were used for each of the faces. The layout is shown in Fig. 3.24.

All the sixteen 120 KN hydraulic jacks which produced the transverse tension were connected to a single hydraulic pump and the load was measured by a load cell. The 500 KN jacks producing the longitudinal compression were connected to another pump and the load was measured in the same way as for the transverse tension. In the testing of Group III, the forces in the side jacks and center jacks were measured individually.

Table 3.1 Properties of the shear specimens

Specimen	θ	A_s	A_v	f'_c MPa	Dowel action*	Pre-crack	Groove	External Longi. load
S1	45°	2-15M	0	45	F		✓	
S2	45°	2-15M	0	45	R		✓	
S3	45°	2-15M	0	45	F	✓	✓	
S4	45°	0	0	45	0		✓	✓
S5	45°	0	0	45	0			✓
S6	60°	2-15M	0	45	R		✓	
S7	60°	2-15M	0	45	F	✓	✓	
S8	60°	0	0	45	0		✓	✓
S9	90°	0	0	45	0		✓	✓
S10	90°	0	0	45	0		✓	✓
S11	90°	0	0	45	0			✓
S12	30°	2-15M	0	45	R		✓	
S13	30°	2-15M	0	45	F		✓	
S14	30°	0	0	45	0		✓	✓
S15	Not designed	4-15M	2x8.5mm @ 100		F			
S16	Not designed	4-15M	2x6mm @ 100		F			✓
S17	Not designed	4-15M	2x11.3mm @ 100		F			✓

* F: Full dowel action; R: Reduced dowel action; 0: No dowel action

Table 3.2 Properties of the concrete softening specimens

Specimen No.	f'_c MPa	Transv. reinf.*	Loading**	No. of Grooves	n ***
#1	20.6	8-10M	P	0	1
#2	21.0	8-10M	P	0	1
#3	22.3	8-10M	P	0	1
#4	22.6	8-10M	Uni.	0	1
#5	23.0	2-10M	Uni.	0	1
#6	23.6	8-10M	P	0	1
#7	24.1	8-10M	P	0	1
#8	24.5	8-10M	P	0	1
#9	24.9	8-10M	P	0	1
#10	25.1	8-10M	P	0	1
#11	25.7	8-10M	P	0	1
#12	26.0	2-10M	Uni.	0	1
#13	26.2	8-10M	P	0	1
#14	26.4	8-10M	P	0	1
#15	26.5	8-10M	P	0	1
#16	26.8	8-10M	P	0	1
#17	26.8	2-10M	Uni.	0	1
#18	26.8	8-10M	S	0	1
#19	33.7	8-10M	S	0	1
#20	33.9	8-10M	S	0	1

* The yielding strength was 350 MPa for panels #1 to #18 and 423 MPa for #19 to #40

** P: Longitudinal compressive stress and transverse tensile strain were proportional; S: Longitudinal compressive stress and transverse tensile strain were stepwise; Uni: Uniaxial compression

*** n was the ratio of the center force to the side force (see Fig. 3.19)

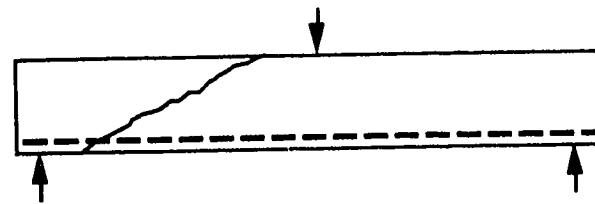
Table 3.2 Continued

Specimen No.	f'_c MPa	Transv. reinf.*	Loading**	No. of Grooves	n ***
#21	34.0	8-10M	S	0	1
#22	34.0	8-10M	S	0	1
#23	34.3	8-10M	R	0	1
#24	34.5	8-10M	R	0	1
#25	35.0	8-10M	R	0	1
#26	35.1	8-10M	R	0	1
#27	35.2	8-10M	S	0	1
#28	35.3	8-10M	S	0	1
#29	35.3	2-10M	Uni.	0	1
#30	35.4	8-10M	S	1	1
#31	35.5	8-10M	S	1	1
#32	35.7	8-10M	S	2	1
#33	35.7	8-10M	S	2	1
#34	36.0	2-10M	Uni.	0	0.50
#35	36.0	2-10M	Uni.	0	0.75
#36	36.0	2-10M	Uni.	0	0.25
#37	36.0	6-10M	S	0	0.50
#38	36.0	6-10M	S	0	0.75
#39	36.0	6-10M	S	0	0.50
#40	36.0	2-10M	Uni.	0	1

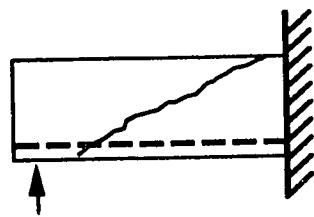
* The yielding strength was 350 MPa for panels #1 to #18 and 423 MPa for #19 to #40

** S: Longitudinal compressive stress and transverse tensile strain were stepwise; Uni: Uniaxial compression; R: Transverse tension was repeated

*** n was the ratio of the center force to the side force (see Fig. 3.19)

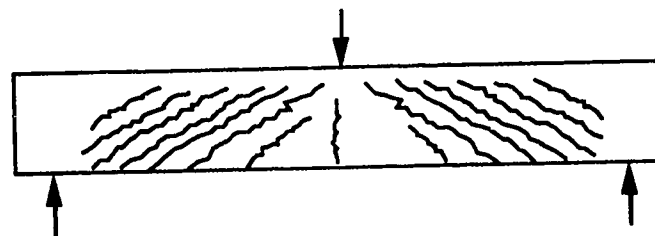


a) A reinforced concrete beam

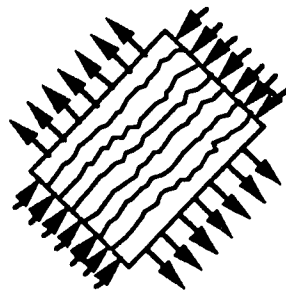


b) The specimen tested

Figure 3.1 Series 1: Tests on shear transferred by friction

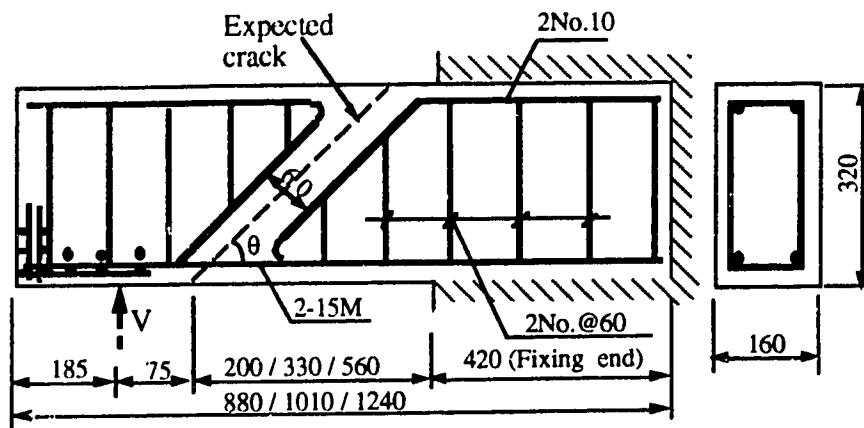


a) Cracks in a reinforced concrete beam



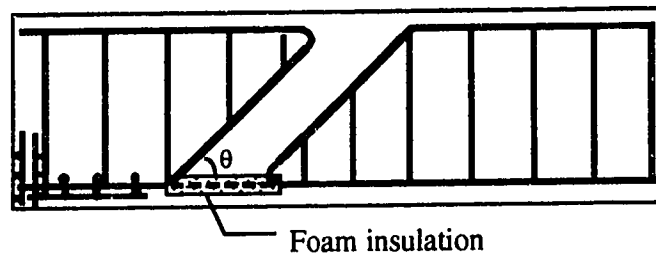
b) The specimen tested

Figure 3.2 Series 2: Tests on concrete softening



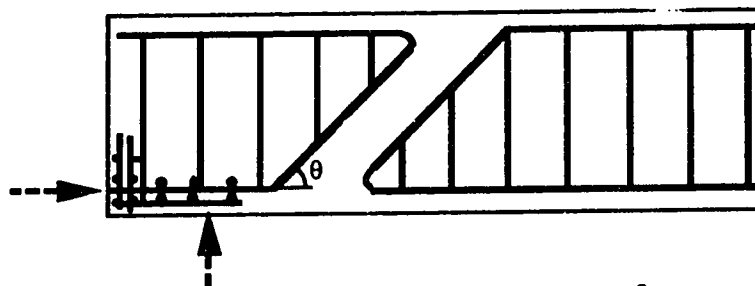
$\theta = 30^\circ$: S13; $\theta = 45^\circ$: S1, S3; $\theta = 60^\circ$: S7

a) Specimens with $A_s=2-15M$



$\theta = 30^\circ$: S12; $\theta = 45^\circ$: S2; $\theta = 60^\circ$: S6

b) Specimens with $A_s=2-15M$ unbonded in the crack area



$\theta = 30^\circ$: S14; $\theta = 45^\circ$: S4, S5; $\theta = 60^\circ$: S8

b) Specimens with $A_s=0$

Figure 3.3 Specimens with inclined crack

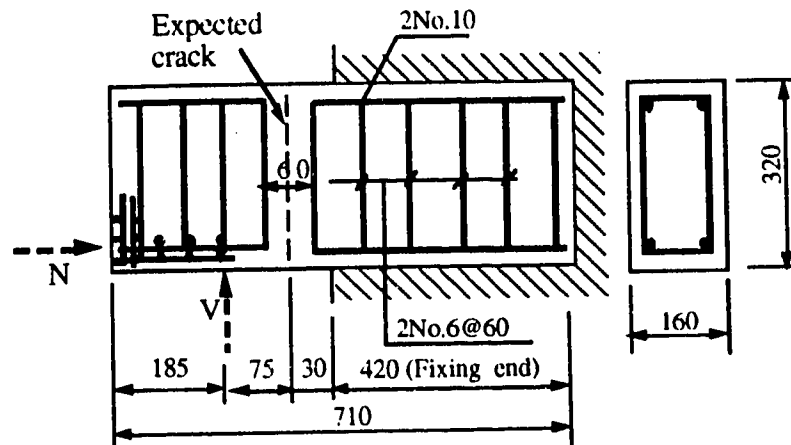
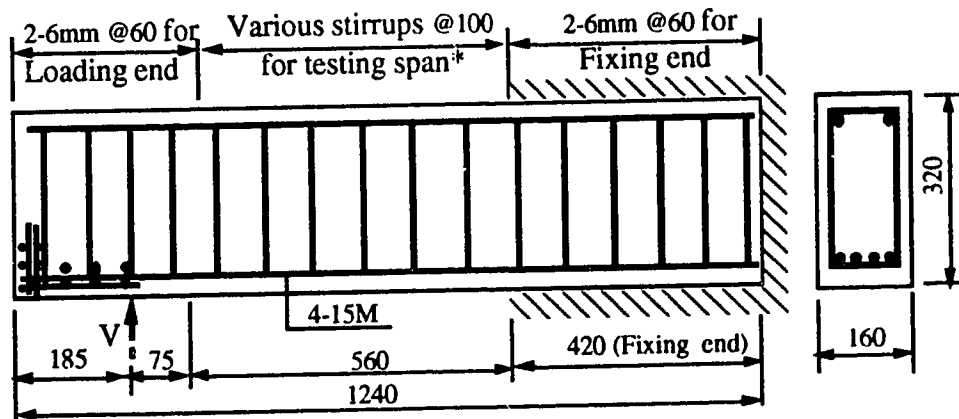


Figure 3.4 Specimens S9, S10 and S11 with expected crack of 90 degree inclination



* The closed stirrups were 6 mm for S16, 8.5 mm for S15 and 11.3 mm for S17.

Figure 3.5 Specimens S15, S16 and S17

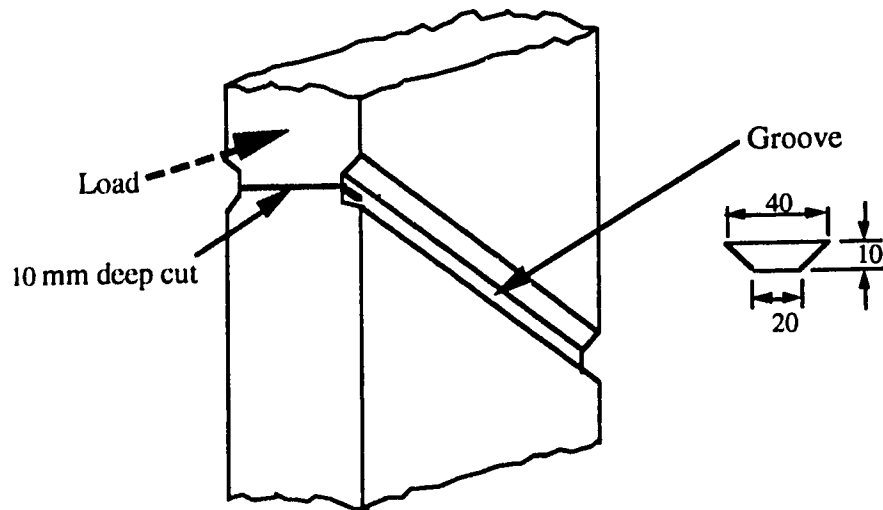


Figure 3.6 Details of the groove

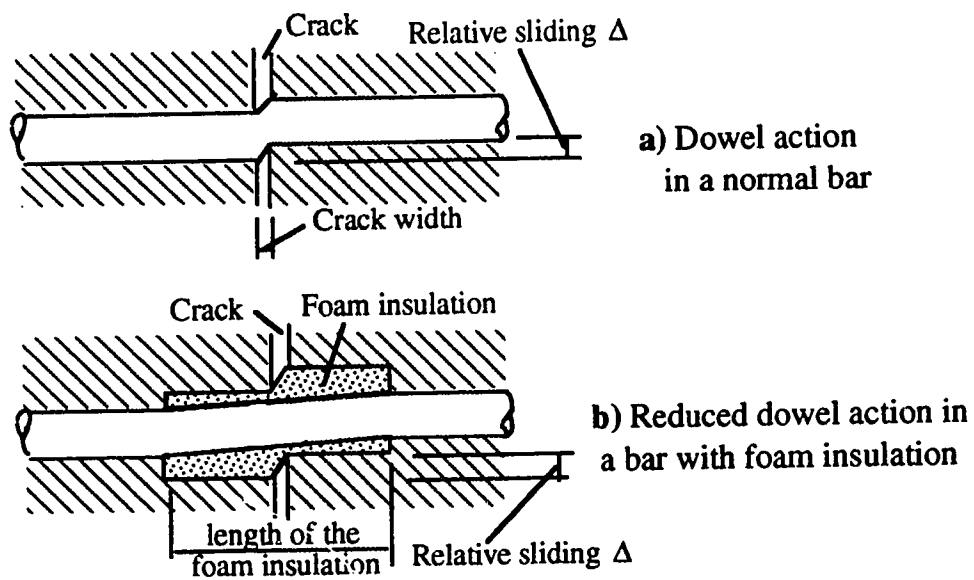


Figure 3.7 Comparison of dowel action between bars with and without foam insulation

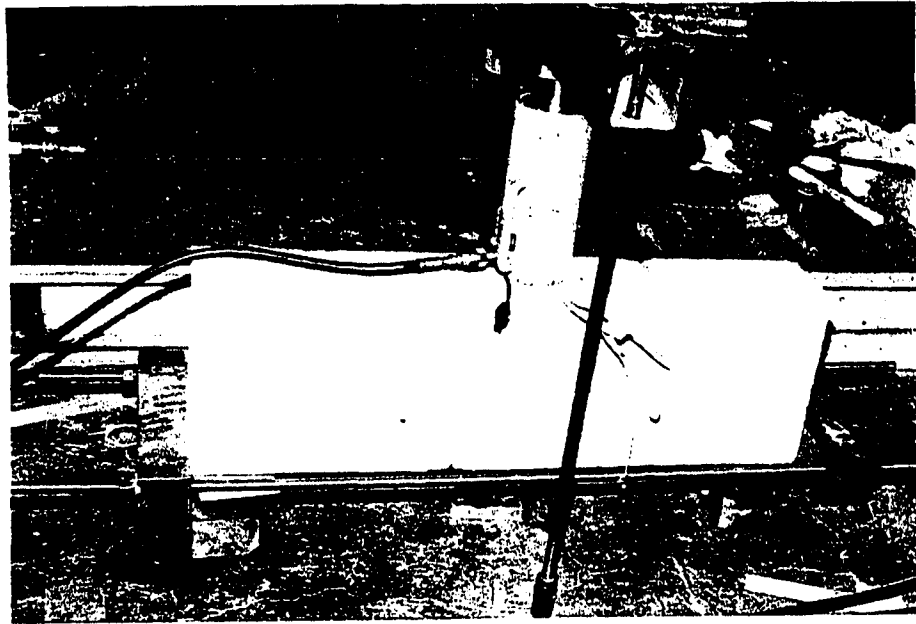


Figure 3.8 The set-up for the pre-cracking

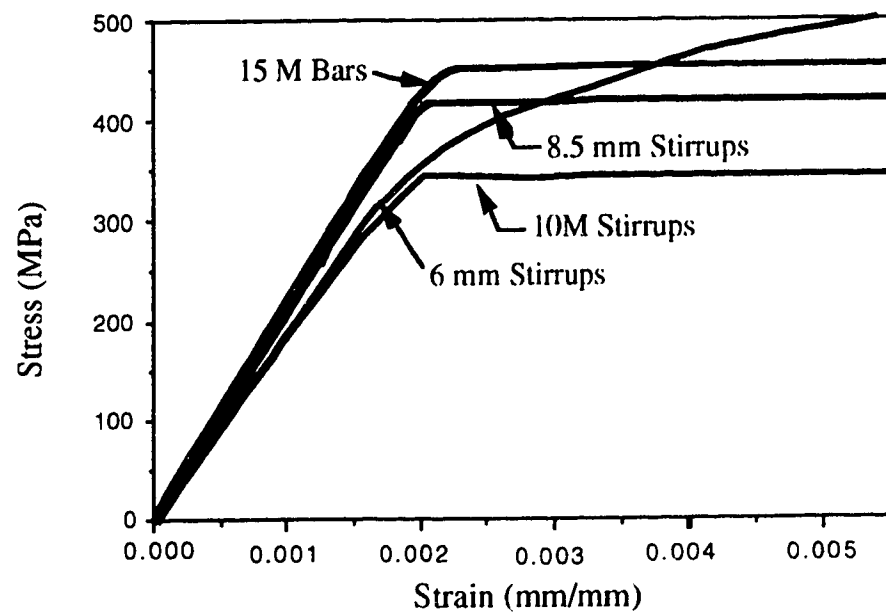


Figure 3.9 Stress-strain curves for the steels

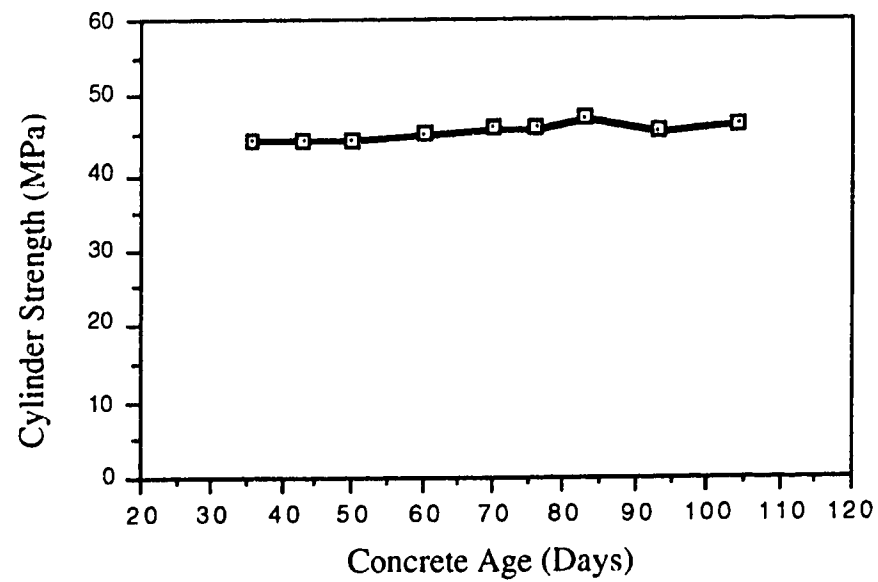


Figure 3.10 Concrete strength

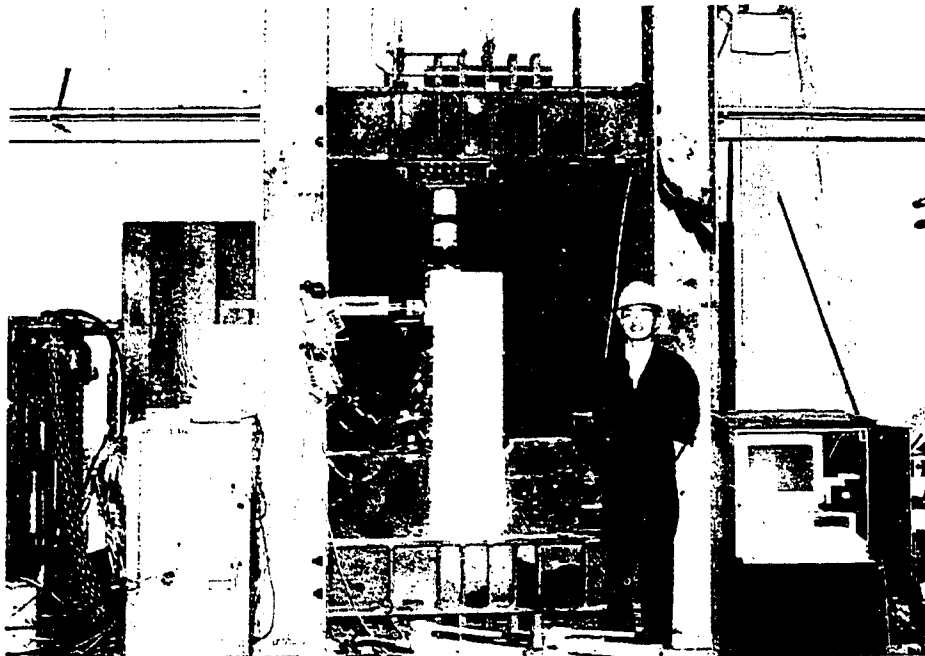


Figure 3.11 Loading frame for test series 1

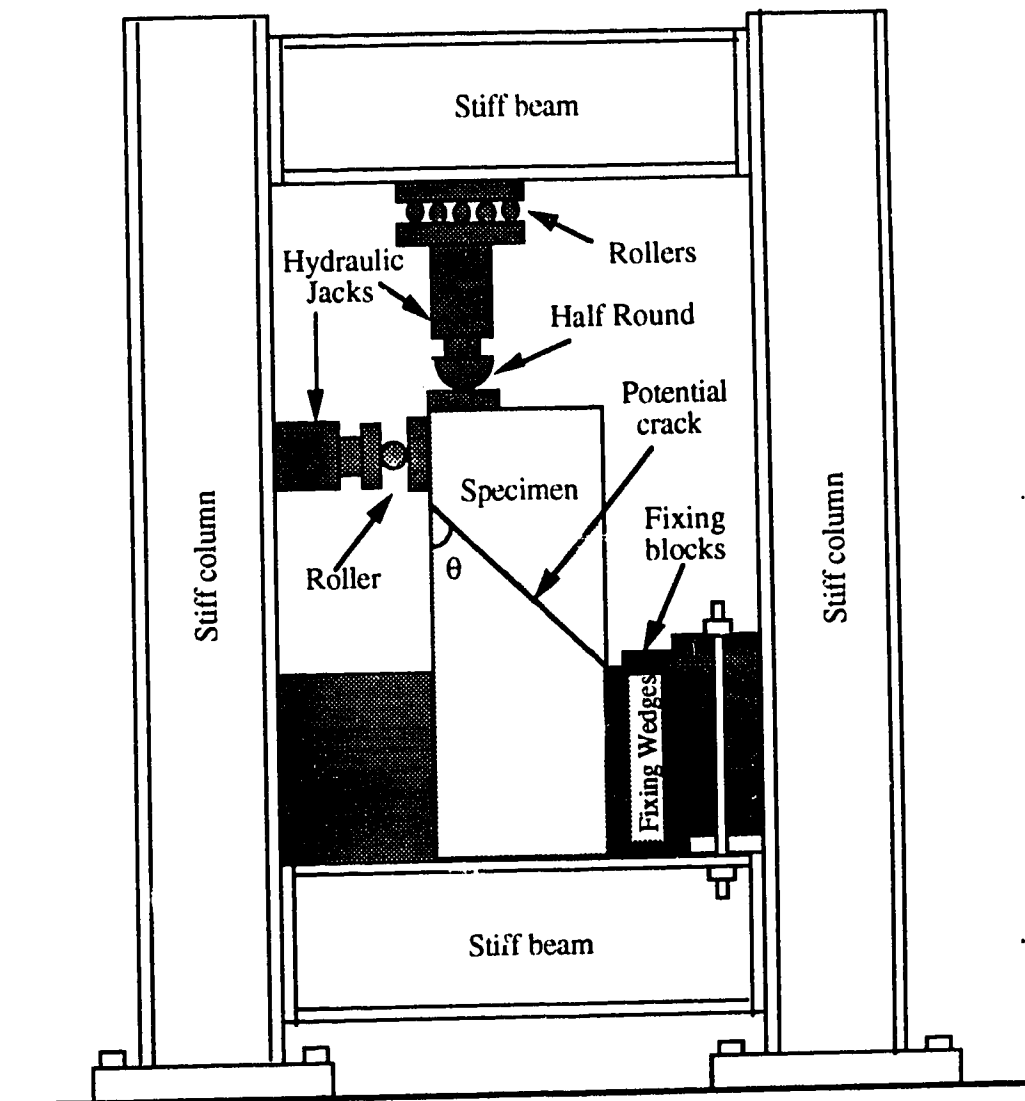


Figure 3.12 Test set-up for shear friction

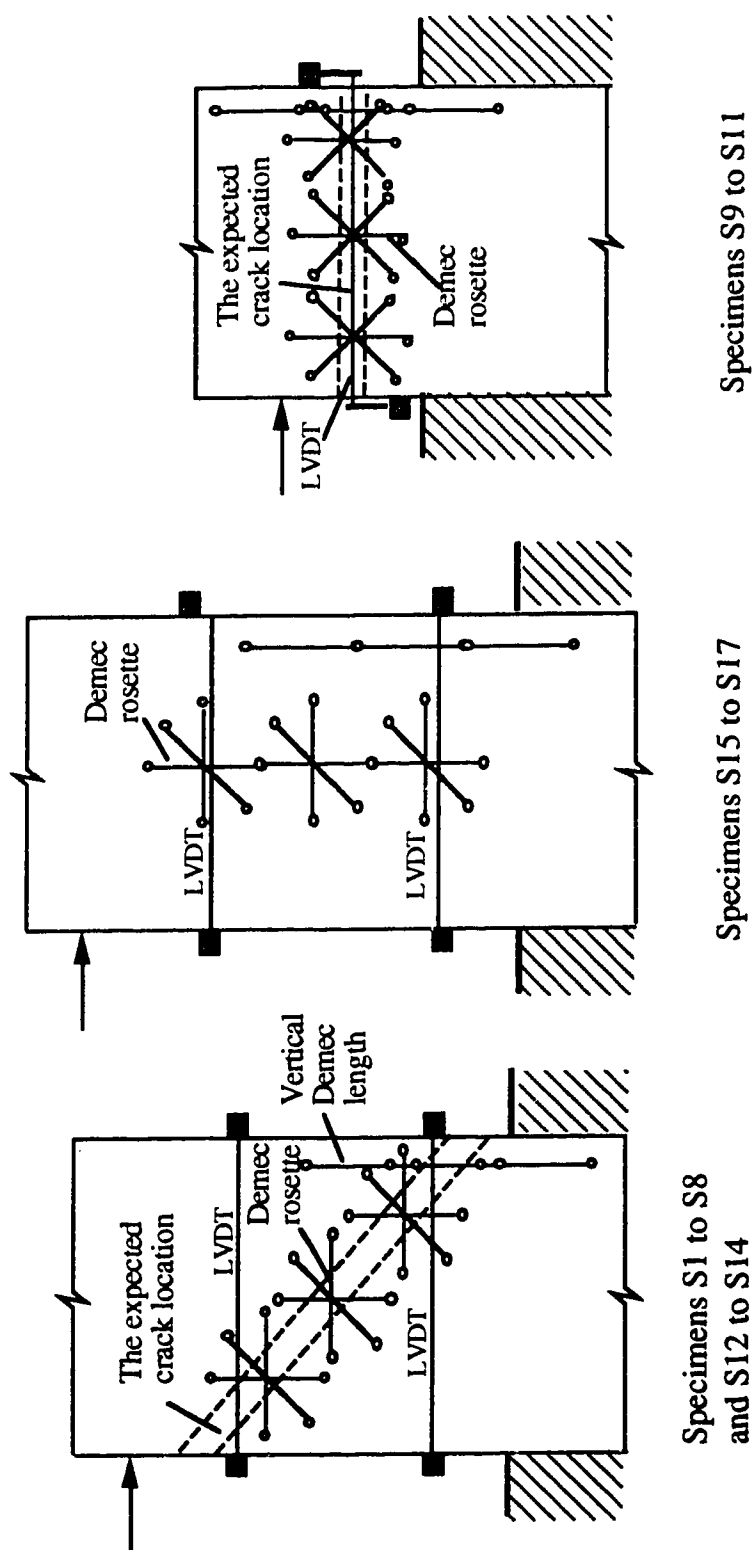
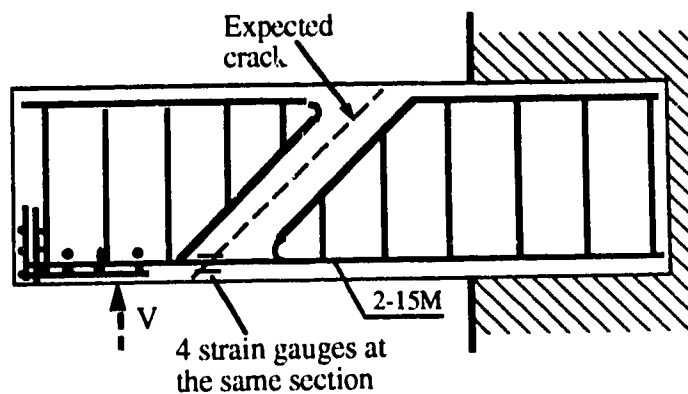
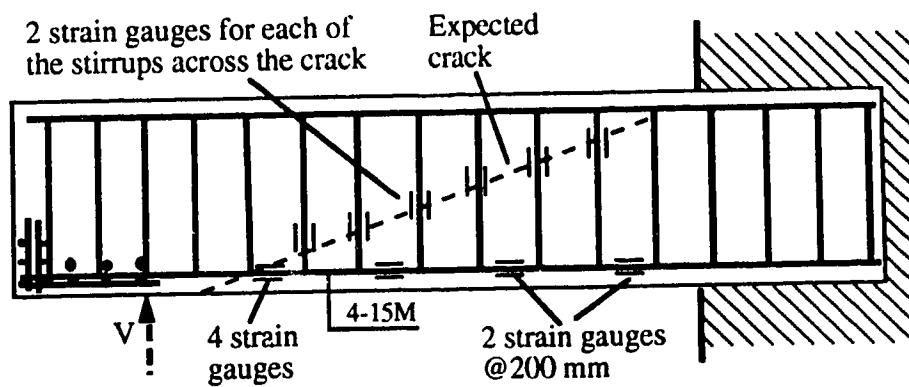


Figure 3.13 Layouts of demec gauge targets and LVDTs



a) Strain gauge layouts for the specimens with longitudinal reinforcement only



b) Strain gauge layouts for the specimens with both longitudinal reinforcements and stirrups

Figure 3.14 Layouts of strain gauges on the reinforcement

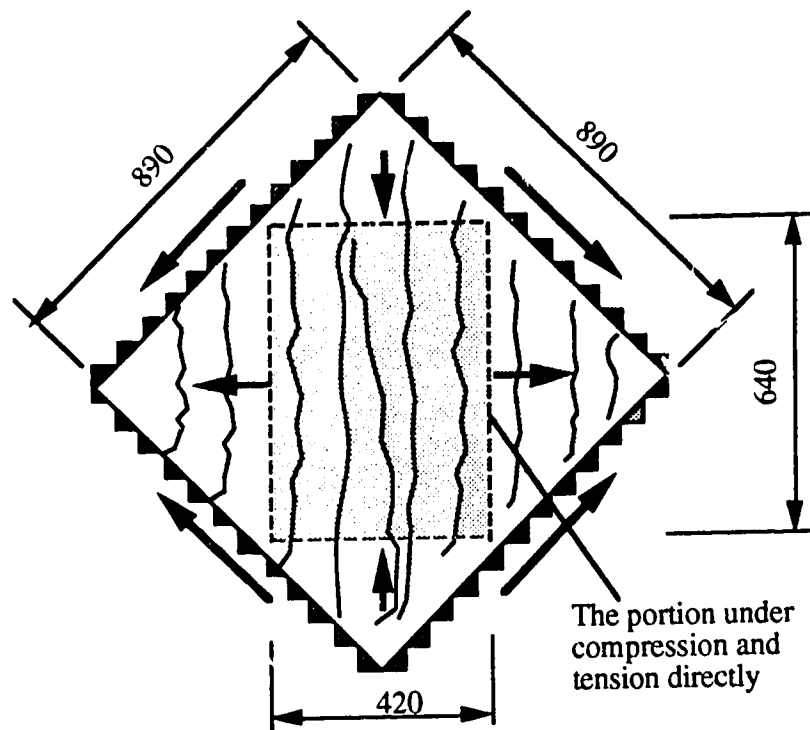
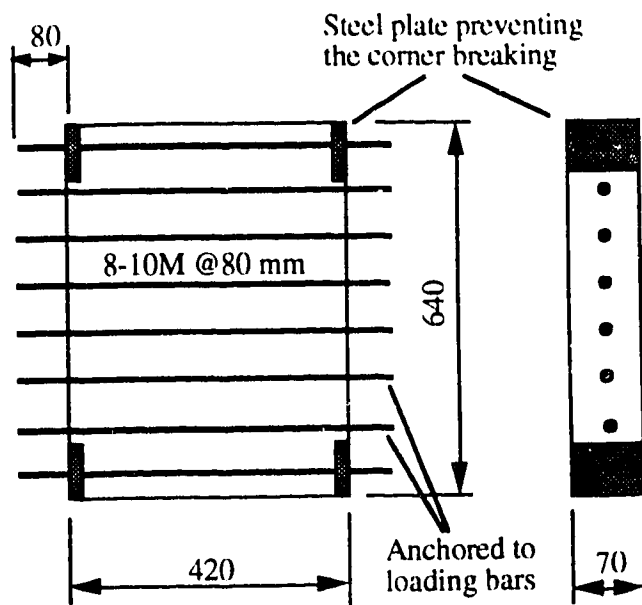
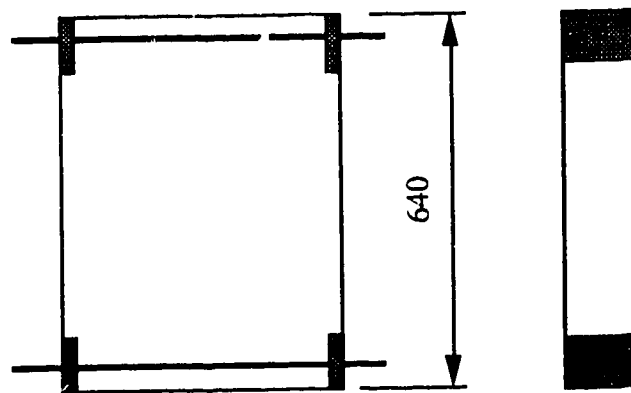


Figure 3.15 The concrete panel tested by Collins and Vecchio⁴⁷

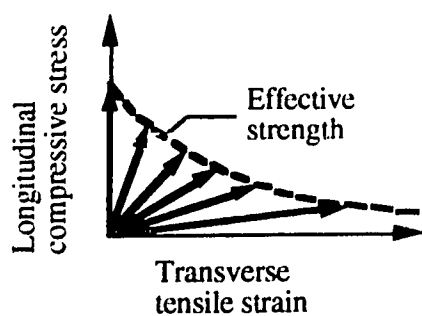


a) Specimens subjected to longitudinal compression and transverse tension

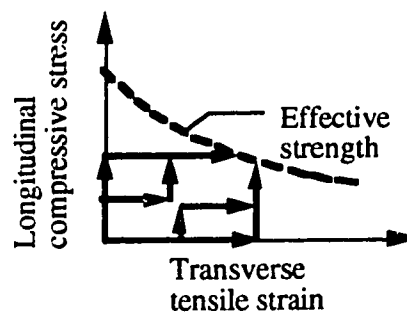


b) Specimens subjected to longitudinal compression only

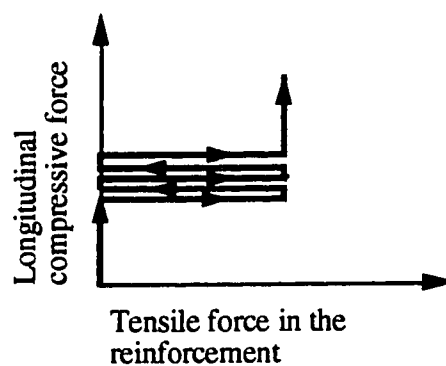
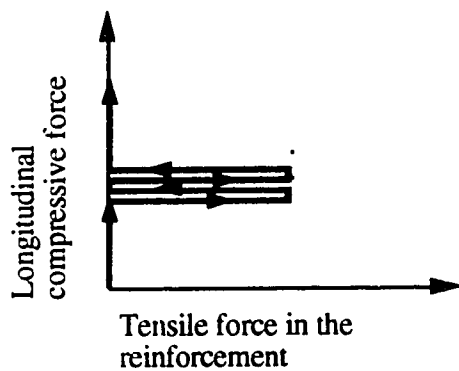
Figure 3.16 The specimens for concrete softening tests



a) Load paths for group 1,
group 3 and specimens
#30 to #33

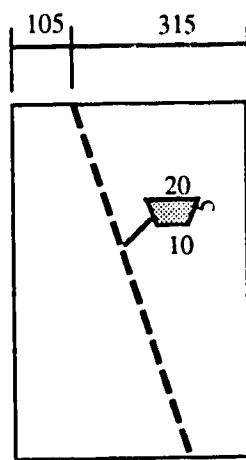


b) Load paths for
specimens #19 to #22

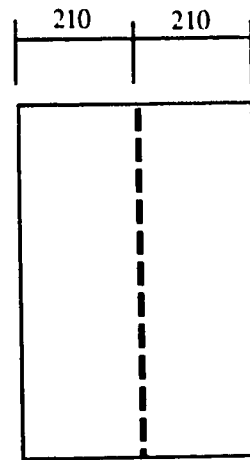


c) Load paths for specimens #23 to #28

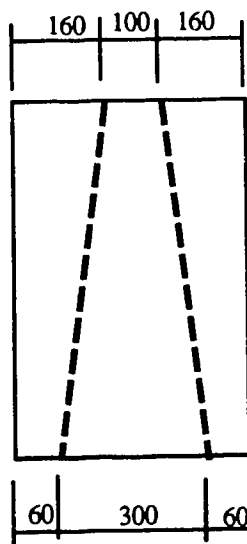
Figure 3.17 Load paths for the tests on concrete softening



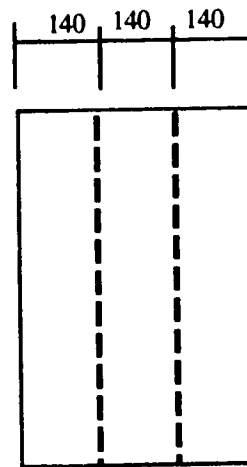
Specimen #30



Specimen #31



Specimen #32



Specimen #33

Figure 3.18 The specimens with grooves

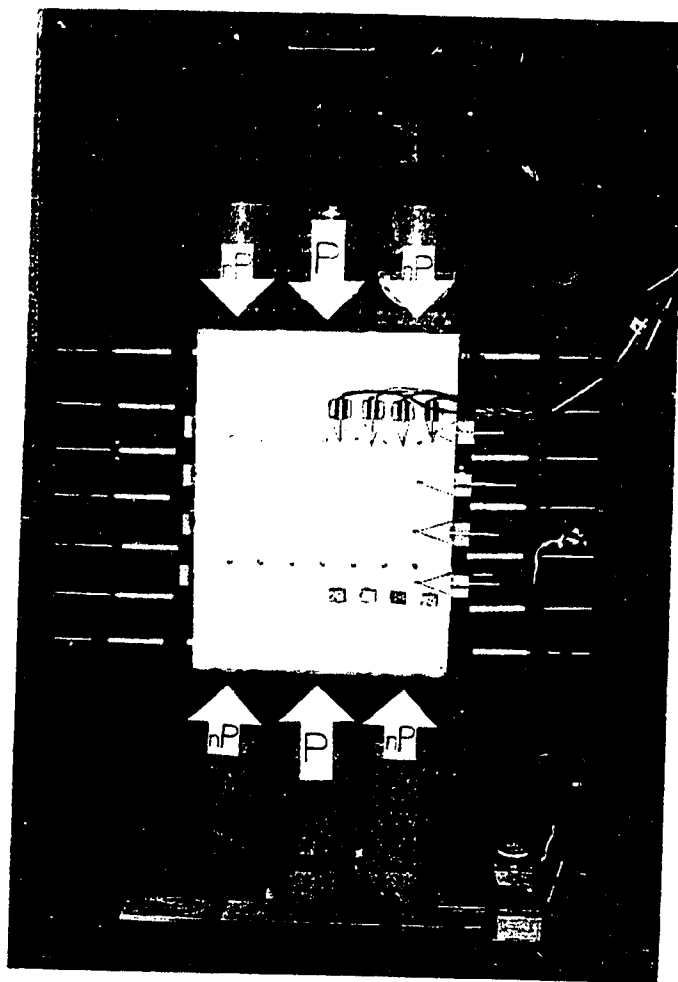
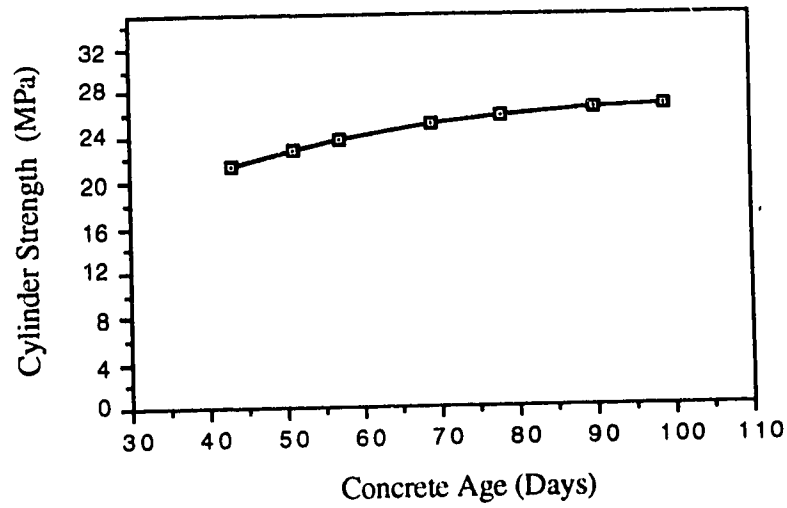
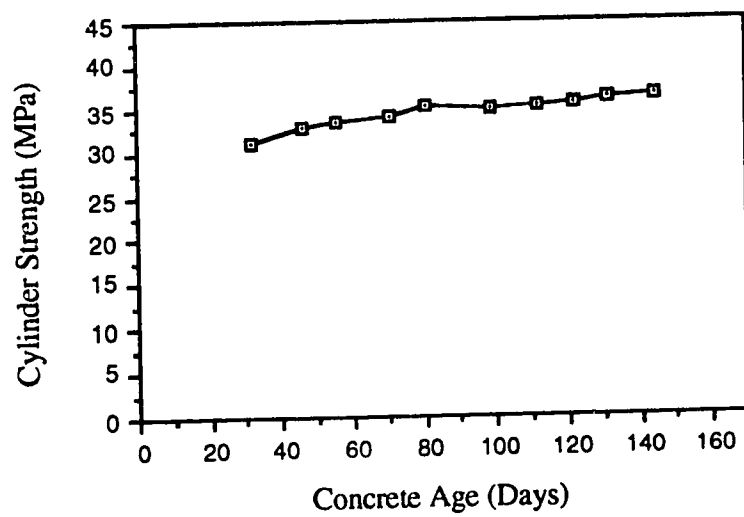


Figure 3.19 Loading system for Group III



a) Concrete strength for specimens from #1 to #18



b) Concrete strength for specimens from #19 to #40

Figure 3.20 Concrete strengths during the testing period

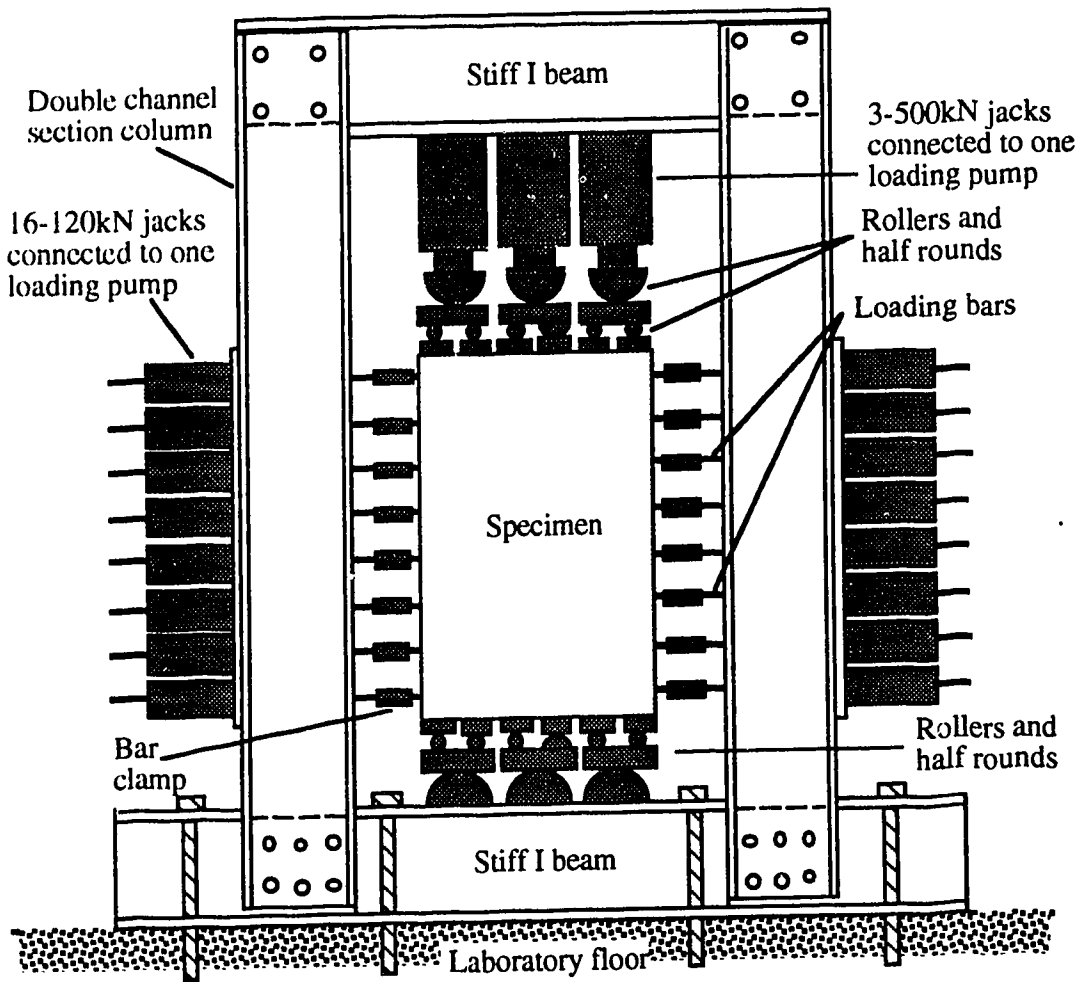


Figure 3.21 Loading frame and test set-up for concrete softening investigation

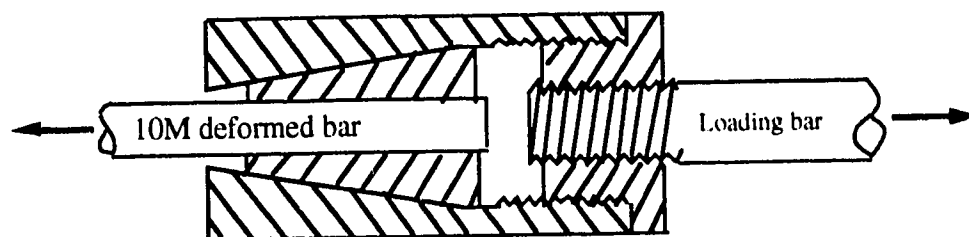


Figure 3.22 The mechanical wedge clamp

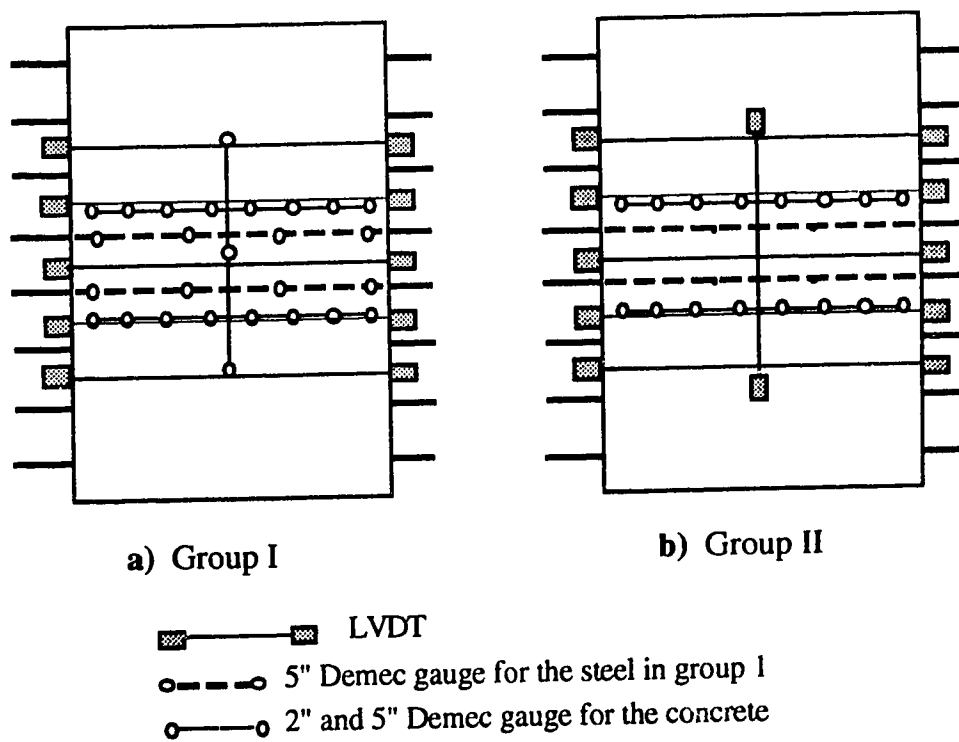


Figure 3.23 Instrumentation for Group I and II

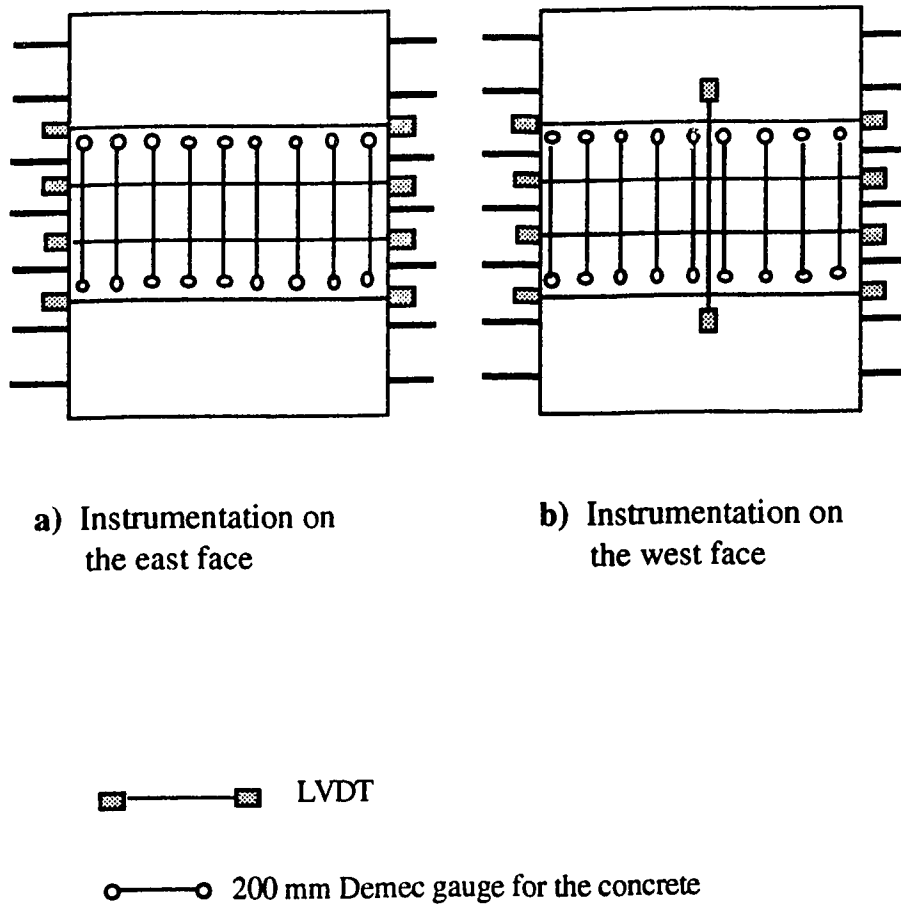


Figure 3.24 Instrumentation for Group III

4. TEST RESULTS OF THE SHEAR SPECIMENS

4.1 Principal Test Results

All seventeen specimens experienced shear failure. The principal test results presented in Table 4.1 consist of the measured angle of inclination of the failure crack along with the designed inclination, loads at first inclined cracking, V_{cr} , failure load, V_u , force in the longitudinal reinforcement at the crack, N_s , external longitudinal force at failure, N_e , the longitudinal compression force on the crack plane N_u , the ratio of V_u/N_u and the types of failure.

For most of the specimens, the failure crack developed within the groove and was straight overall. The inclination of these cracks could be easily measured. They were usually very close to the designed inclinations. A few of the specimens had an overall curved failure crack. For these specimens, the measured inclination was the inclination of the straight line linking the two points where the crack crossed the tension longitudinal reinforcement and compression reinforcement or extension line of the compression reinforcement respectively. The cracking load was the shear force under which an inclined crack became visible to the naked eye, which was usually observed later than that indicated by the strains in the reinforcement and concrete. The failure was reached when the specimen was not able to carry any additional shear force. Failure load was the maximum shear force corresponding to the failure. The

longitudinal compressive force on the failure crack plane was equal to the sum of the tension force in the reinforcement at the crack and the applied external longitudinal force, if any. The failure modes observed in this test program were shear-friction failure which is referred to as SF in Table 4.1, diagonal compressive crushing of the web, referred to as DC and combined shear-friction and diagonal crushing, referred to as SF+DC. A detailed description of the failure modes is given in the presentation of the test results of each group of specimens.

The following sections present the most significant test results for each group of specimens to illustrate the behavior of the specimens. These results consist of photographs of the specimens after failure, strains in the reinforcement at the failure crack, the horizontal relative movement of the two crack faces measured by the LVDT's mounted on the two edges of the specimen and the strains in the concrete perpendicular and parallel to the crack which were measured by the 5" strain rosettes across the crack. All the data has been reduced to graphical form for ease of interpretation.

4.2 Specimen Behavior

4.2.1 Group 1: Specimens with $\theta = 45^\circ$

Forty five degrees was the intermediate failure crack inclination among those considered in the tests. This group included five specimens. Specimens S1, S2 and S3 had 2-15M bars as longitudinal reinforcement while S4 and S5 were unreinforced in the test section,

(See Fig. 3.3). Specimens S1 to S3 had no externally applied compression load ($N_e=0$) while such a load was applied in the case of S4 and S5.

Figure A.1 (in Appendix A) shows specimen S1 after failure. The first crack was observed within the groove at $V=48$ kN which corresponded to about 48% of the failure load. The crack started from the edge of the loading plate and extended into about 7/10 of the cross section. As the load increased, the crack extended into the compression zone and new cracks formed in the shear span. At $V=80$ kN, about 80% of the failure load, the inclined crack penetrated through the compression zone and the test section was completely cracked. At higher loads the shear was carried only by the shear friction across the crack. At $V=92$ kN the longitudinal tension reinforcement started to yield at the failure crack. The specimen failed at a load of $V=99$ kN by loss of the shear transfer across the crack. The failure was accompanied by a sudden visible relative sliding between the two crack faces and slight damage of the crack surface. This failure is referred to as a shear-friction failure (SF) in Table 4.1. Near failure a few inclined cracks were observed in the fixed end of the specimen. The ratio of the failure shear force to the longitudinal compression force was $V_u/N_u=0.55$.

The load vs. steel strain relationship at the failure crack is shown in Fig. 4.1. Figure 4.2 shows the load versus the horizontal relative movement between the two crack faces. Figure 4.3 shows plots of load versus the strains perpendicular and parallel to the failure crack at the quarter points along the crack. All the curves are

essentially a straight line up to the start of cracking. In this stage the specimen remained elastic and the deformations were not measurable. This stage is referred as "uncracked stage". The cracking of concrete initiated the non-linear behavior of the specimen. After cracking, the opening and relative sliding of the crack as well as the tension in the reinforcement increased very rapidly as the load increased. The change of stiffness at this stage is due to the initial looseness of fit caused by the cracking. A certain displacement must occur before the aggregate particles, projecting across the crack, can firmly bear against the matrix of the opposite face. This stage is referred to as the "stage of initial looseness of fit". Once bearing of the two crack faces was developed, a relatively stiffer shear transfer mechanism was established. This is represented by the steeper curves after about $V=60$ kN in Fig. 4.1 to 4.3. At this stage, the crack became relatively stable. This stage is referred to as the "shear-friction stage" in which the transverse load was resisted by the shear-friction across the failure crack. The term shear-friction as used here includes the aggregate interlock action along the crack, the shear transferred in the uncracked compression zone and the dowel action of the longitudinal reinforcement. The strains perpendicular and parallel to the crack at the quarter points in Fig. 4.3 indicate that the opening and the sliding of the crack decreased as the location approached the compression zone. This suggests that the two faces of the failure cracks had both relative sliding and relative rotation.

Specimen S2 had the same properties as S1 except that in S2 the longitudinal reinforcement were wrapped with foam insulation at the failure crack to reduce the dowel action. Specimen S2 had much lower ultimate strength than S1. Figure A.2 shows the photograph of the specimen after failure. The load-steel strain relationship at the crack is shown in Fig. 4.1. Figure 4.2 shows the horizontal relative movement of the two crack faces and Figure 4.4 shows the strain of the concrete perpendicular and parallel to the failure crack.

The first inclined crack in S2 was observed within the groove at $V=45$ kN which corresponded to 78% of the failure load. This load was very close to the cracking load of S1 suggesting that the foam insulation had little effect on the cracking load. The crack extended from the edge of the loading plate to about 6/10 height of the cross section, with the largest width about 0.6 mm at the tension edge. As the load increased the crack extended into the compression zone quickly. At $V=57$ kN the specimen suddenly failed by the instantaneous separation of the two crack faces. Up to failure no new cracks were observed. The longitudinal reinforcement had not yet yielded at the failure. The strain in the steel was 0.00125 which corresponded to $N_s=112$ kN in the reinforcement at the crack. Although the ultimate strength of S2 was much lower than that of S1, the ratio of shear force to the longitudinal compression force in the crack plane, V_u/N_u , was 0.51 which was very close to that of S1. The similar values of V_u/N_u ratio for S1 and S2 suggests that the shear strength is almost linearly proportional to the longitudinal compression force on the crack plane.

The load-deformation curves in Fig. 4.1, 4.2 and 4.4 show that before cracking specimen S2 had elastic behavior and the load-deformation curves were essentially linear with very small deformations. This stage was the uncracked stage. The second stage, the stage of initial looseness of fit, started as the failure crack formed. In this stage the strain in the concrete and steel increased very rapidly as the load increased. Because the reinforcement was wrapped with the form insulation at the failure crack, tension in the reinforcement was not developed as quickly as in S1 to confine the crack. This behavior is explained in Sec. 4.3. The specimen failed before the third stage, the shear friction stage, started.

Specimen S3 had the same geometric configuration as S1 and S2 except that in S3 the compression zone had been pre-cracked to investigate the significance of the uncracked compression zone in resisting the shear force. The tension steel was not wrapped with the foam. Figure A.3 shows specimen S3 with precrack before test. The precrack extended about 1/5 height of the specimen. The specimen after failure is shown in Fig. A.4.

Due to the precrack, the specimen had smaller monolithic section than S1 and S2. As a result the first crack in S3 was observed earlier than in S1 and S2. The first crack occurred near but outside the groove at $V=32$ kN which corresponded to 31% of the failure load. The crack started from the edge of the loading plate and extended to about half of the height of the cross section. As load increased, the crack extended into the compression zone. At $V=50$ kN the crack

joined with the precrack and the test section was completely separated by the crack. After this stage the load was carried only by the shear friction across the crack. About $V=95$ kN the longitudinal reinforcement start to yield at the failure crack. As the load increased to 102 kN the specimen failed by loss of the shear-friction across the crack. The failure was accompanied by a sudden visible relative sliding between the two crack planes and slight damage of the roughness of the crack planes. Near failure a few inclined cracks were observed at the fixing end. The ratio of the shear force to the longitudinal compression force in the crack plane was $V_u/N_u=0.57$.

The load-steel strain relationship at the failure crack and the load-horizontal relative movement of the two crack faces for specimen S3 are shown in Fig. 4.1 and 4.2 respectively. Figure 4.5 shows the curves for the load-strain responses perpendicular and parallel to the failure crack for this specimen. In the first stage, the elastic behavior stage, all the curves, except the concrete strains across the precrack, were essentially linear. Negative strains were read across the precrack due to the closing of the precrack under positive moment. The second stage, the stage of initial looseness of fit, started as the test section cracked. This was shown by the load-deformation curves in Fig. 4.1, 4.2 and 4.5 at about $V=30$ kN. In this stage the opening and relative sliding of the crack as well as the tension in the reinforcement increased very rapidly as the load increased. The strain across the precrack in the compression zone started to become positive (tensile). The the initial looseness of fit caused by the cracking reduced the stiffness of the specimen. After

about $V=60$ kN the shear-friction stage started. In this stage a relatively stiffer shear transfer behavior was observed, as shown in Fig. 4.1, 4.2 and 4.5. The strains perpendicular and parallel to the crack at the quarter points in Fig. 4.5 indicated that the quarter point closest to the tensile steel bar had the largest opening and sliding. The third quarter point had the smallest opening and sliding while the second point was in between.

Specimens S4 and S5 had the same geometric configuration as the rest of the specimens in the same group, but in S4 and S5 no reinforcement was used in the testing section. S4 was grooved in the surface of the specimen. The confinement in the crack plane was provided by an external longitudinal force, N_e . The line of action of this force coincided with the axis of the longitudinal reinforcement in the reinforced specimens. Figure 4.6 shows the load history (N_e vs. V) for the two specimens. The two forces, V and N_e , were increased alternatively in 5 steps. The specimens were then loaded to failure by increasing V only. Figure 4.7 shows the horizontal relative movement of the two crack faces for the both specimens. The Demec strain gauge readings across the crack have been disregarded because the Demec gauge readings in the vertical and 45° directions were very erratic due to the nature of the loading change. As V was increased, the Demec readings increased. Then, when N was increased, the Demec gauge reading decreased.

Unlike the specimens with a reinforced test section in which the tension in the reinforcement developed as a result of the cracking of the concrete as the shear force was applied, S4 and S5 were loaded

with the external longitudinal force before the concrete cracked in order to prevent the specimens from failing instantaneously following the cracking. Because of the longitudinal compression in the concrete prior to the cracking, S4 and S5 had relatively longer uncracked stages than S1 to S3. The first crack in S4 was observed near the groove at $V=73$ kN and $N_c=135$ kN. The initial crack extended from the tension edge of the specimen to about 6/10 of the height of the cross section. The cracking was accompanied by a drop in the transverse load V and an increase in the longitudinal force N_c . As the load increased the crack split into two cracks and both extended into the compression zone. At $V=85$ kN, 9/10 of the section was cracked. The specimen failed at $V=96$ kN and $N_c=179$ kN by loss of the shear transfer across the crack. A sudden slip was observed at failure. The ratio of V_u/N_u at failure was 0.54.

Specimen S5 had similar behavior to S4. The first crack was observed at $V=65$ kN and $N_c=130$ kN. The crack extended from the edge of the loading plate to about 7/10 of the height of the cross section, with a drop in V and a increase in N_c . As the load increased the crack extended into the compression zone. At $V=70$ kN, 9/10 of the section was cracked. The specimen failed at $V=76$ kN and $N_c=151$ kN by loss of the shear transfer across the crack. A sudden slip was observed at failure. The ratio of V_u/N_u at failure was 0.50.

Figure 4.7 shows the curves of load-horizontal relative movement of the two crack faces for S4 and S5. Up to the first cracking no opening was recorded. The cracking initiated the nonlinear behavior in the specimens. However, unlike the specimens

with reinforcement across the failure crack, the second and the third stages, the initial looseness of fit stage and the shear-friction stage, were not distinguishable from the load-deformation curves.

The concrete strain along the compression edge were measured in two of the specimens in this group, S3 and S5. They are shown in Figure 4.8. Strains were measured by three Demec gauge lengths along the compression edge. Gauge 2 in both specimens was crossed by the failure crack. Before cracking all three gauge lengths experienced compression strain due to the flexural moment. The magnitude of the strains increased as the location of the gauge getting closer to the fixing end. In specimen S3 gauge length 2 was crossed by the precrack and experienced larger compression strain than others due to the closing of the precrack. As the specimens cracked and the crack extended into the compression zone, gauge 2 in both specimens developed tension strain, while the adjacent gauges still had compression strains. This behavior indicated that although the compression zones were cracked, they were still under compression. The tensile strain in gauge 2 resulted from a separation of the crack surfaces resulting from relative slip along the crack and the roughness of the surfaces.

4.2.2 Group 2: Specimens with $\theta = 60^\circ$

This group consisted of three specimens. S6 and S7 had 2-15M bars as longitudinal reinforcement while S8 was unreinforced in the test section. In S6 the reinforcement was wrapped with foam

insulation at the failure crack to reduce the dowel action. S7 was pre-cracked at the compression zone.

Figure A.7 shows specimen S6 after failure. The first crack was observed within the groove at $V=47$ kN which corresponded to 44% of the failure load. The crack started from the edge of the loading plate and extended across about 6/10 of the cross section. As the load increased, the crack extended into the compression zone and new cracks formed in the shear span. At $V=95$ kN the inclined crack extended to about 95% of the cross section. As the load increased to 107 kN the specimen failed by loss of the shear transfer across the crack. The failure was accompanied by a sudden visible relative sliding between the two crack planes. The strain in the steel at the crack at failure was 0.0014 which corresponded to $N_s=124$ kN in the reinforcement. Near failure a few inclined cracks were observed at the fixed end. The ratio of the shear force to the longitudinal force in the crack plane was $V_u/N_u=0.86$ which was higher than those of the specimens with $\theta=45^\circ$.

The load-steel strain relationship at the crack for specimen S6 is shown in Fig. 4.9. Figure 4.10 shows the load-horizontal relative movement of the two crack faces. Figure 4.11 shows the curves of load vs. the strains perpendicular and parallel to the failure crack at the quarter points. In the uncracked stage the deformations were nearly zero. After cracking the specimen underwent the stage of initial looseness of fit. In this stage the opening and relative sliding of the failure crack as well as the tension in the reinforcement increased very rapidly as the load increased. Due to the unbonded

length wrapped by the foam insulation, force in the reinforcement did not develop quickly and the specimen experienced very little of the shear-friction stage. The strains perpendicular and parallel to the crack at the quarter points in Fig.4.11 indicate that the opening and the sliding of the crack decreased as the location approached the compression zone. This suggests both relative sliding and rotation between the two crack faces.

Due to the precrack in the compression zone, specimen S7 had a smaller monolithic section than S6. As a result the first crack in S7 was observed earlier than in S6. The first crack occurred at $V=37$ kN which was 25% of the failure shear. The crack extended from the tension edge of the specimen to about 4/10 of the cross section. As the load increased, the crack extended, parallel to the groove, into the compression zone. The crack did not join the precrack in the compression zone but penetrated through the compression zone underneath the precrack. At about $V=130$ kN the longitudinal reinforcement start to yield. At a load of $V=149$ kN the specimen failed by loss of the shear-friction across the crack. The failure was accompanied by a sudden visible relative sliding between the two crack faces and slight diagonal crushing in the compression zone, as shown in Fig. A.9. This failure mode is referred as to combined shear-friction failure and diagonal crushing, (SF+DC). Near failure a few inclined cracks were observed at the fixing end. Although S7 had pre-cracked in the compression zone, it had higher shear strength than S6. The ratio of the failure shear force to the

longitudinal force in the crack plane was $V_u/N_u=0.83$, close to that of S6.

The load-steel strain relationship at the crack and the load-horizontal relative movement of the two crack faces for specimen S7 are shown in Fig. 4.9 and 4.10 respectively. Figure 4.12 shows the curves for the load-strain response perpendicular and parallel to the failure crack. In the first stage, the uncracked behaviour stage, all the curves, except the concrete strains across the precrack in the compression zone, were essentially linear. The negative strains of the Demec gauge across the precrack were due to the closing of the precrack under positive moment. The second stage, the stage of initial looseness of fit, started as the first inclined crack occurred. This was indicated by the load-deformation curves and load-strain curves in Fig. 4.9 and 4.10 at about $V=30$ kN. In this stage the crack developed rapidly and the two faces of the crack became separated and lose their initial fit. The strain across the precrack in the compression zone started to become positive (tensile). The shear friction stage started about at $V=80$ kN. In this stage a relative stiffer shear transfer behavior was observed, as shown in Fig.4.9, 4.10 and 4.12.

Figure 4.13 shows the load-strain relationships along the compression edge for S6 and S7. Gauge 2 in S6 and gauges 2 and 3 in S7 were crossed by the cracks. Before cracking all the gauges experienced compression strain due to the flexural moment. The strains increased as the location of the gauge approached the fixed end. In S7 gauge length 2 was crossed by the precrack and

experienced larger compression strain than others due to the closing of the precrack. As the specimens cracked and the cracks extended into the compression zone the gauge lengths intercepted by the cracked started to have tension strains, while the adjacent gauges still had compression strains.

Specimen S8 had the same geometric configuration as S6 and S7 but it was unreinforced in the test section. The confinement of the crack plane was provided by an external longitudinal force, N_e . Figure 4.14a shows the load history of the test. Figure 4.14b and 4.14c show the horizontal opening of the failure crack and the compression strain in the compression zone. The specimen after failure is shown in Fig. A.10. The first crack in S4 was observed near the groove at $V=85$ kN and $N_e=40$ kN. It extended from the tension edge of specimen into about 7/10 of the cross section. Accompanied with the cracking was a drop in the transverse load V and an increase in the longitudinal load N_e . As the load increased the crack extended into the compression zone. The specimen failed at $V=118$ kN and $N_e=120$ kN by loss of the shear transfer across the crack. A sudden slip was observed at failure. The ratio of V_u/N_u at failure was 0.98

4.2.3 Group 3: Specimens with $\theta = 30^\circ$

Three specimens were included in this group. S12 and S13 had 2-15M bars as longitudinal reinforcement while S14 was unreinforced in the test section. In S13 the reinforcement was

wrapped with foam insulation at the failure crack to reduce the dowel action.

The first crack in S12 was a flexural crack in the middle of the shear span, with a height about 5/10 of the cross section. As load increased to $V=54$ kN this crack extended a bit and no new crack was observed. At $V=54$ kN an inclined crack suddenly appeared within the groove and the specimen failed instantaneously by the separation of the two crack faces. At the failure the strain in the reinforcement was only 0.00052 which corresponding to $N_s=48$ kN in the reinforcement. The ratio of V_u/N_u at failure was 1.13.

The unexpected large V_u/N_u ratio and the instant failure following the cracking of concrete indicated that failure of the specimen was resulted from loss the tension in the concrete. The inclined cracking load was larger than the shear friction capacity across the crack. As a result the cracking load exceeded the capacity of shear transfer across the crack in the cracked section and therefore the specimen failed instantly after cracking. Thus, the ratio of V_u/N_u was much higher than expected.

In order to determine the shear-shear friction capacity S12 was retested. The upper half of the specimen was pushed back to the original position using an opposite shear force. An external longitudinal force was then applied to induce the confinement on the crack. The load history (V vs. N_e) of the retest is shown in Fig. 4.17a. The longitudinal load, N_e , was increased to about 180 kN before V was loaded. The specimen was then loaded to failure by increasing V

only. Figure 4.17b shows the load-horizontal relative movement of the two crack faces in the retest. No relative movement was recorded up to $V=10$ kN. After $V=10$ kN the two faces of the crack start to have measurable slip. The specimen reached the failure at $V=24$ kN because no additional shear force could be applied. During the retest the strains in the longitudinal reinforcement at the failure crack were either near zero or negative. This suggests that no tensile force was developed in the reinforcement at the failure crack in the retest ($N_s=0$). The non-tensile strain in the reinforcement at the crack may be due to the application of the compressive force N_e and the small angle between the reinforcement and the crack. No new crack was observed in the retest. Figure A.15 shows S12 after failure. The ratio of V_u/N_u at the failure was 0.133.

Specimen S13 had similar behavior to S12. The first crack was a flexural crack in the mid shear span. At $V=48$ kN an inclined crack suddenly appeared within the groove and the specimen failed instantaneously by the separation of the two crack faces. The strain in the reinforcement was only 0.0006 which corresponding to $N=50$ kN in the reinforcement. The ratio of V_u/N_u was 0.96.

S13 was retested to achieve the shear-friction capacity. The load history (V vs. N_e) of the retest is shown in Fig. 17a. The longitudinal load, N_e , was increased to 227 kN before V was loaded. The specimen was then loaded to failure by increasing V only. Figure 4.17b shows the load-horizontal relative movement of the two crack faces in the retest. Very small relative movement was recorded up to $V=27$ kN. After $V=27$ kN the two faces of the crack start to have

measurable slip. The specimen failed at $V=46$ kN because no additional shear force could be applied. In the retest the strain in the reinforcement at the failure crack was negative and no new crack was observed. Figure A.12 shows S13 after failure. The ratio of V_u/N_u at the failure was 0.203.

Specimen 14 had the same configuration as S12 and S13 but was unreinforced in the test section. Like S12 and S13, S14 was pre-cracked and then retested to achieve the shear-friction capacity. Figure 4.18 shows the test results of both the original test to create the failure crack and the retest for the shear friction. In the original test, the concrete cracked and suddenly failed at $V=42$ kN and $N_e=30$ kN by the separation of the two crack faces. The ratio of V_u/N_u at the failure was 1.4.

The load history (V vs. N_e) of the retest for S14 is also shown in Fig. 4.18a. The longitudinal load, N_e , was increased to about 150 kN before V was loaded. The specimen was then loaded to failure by increasing V only. Figure 4.18b shows the load-horizontal relative movement of the two crack faces in the retest. Very small relative movement was recorded up to $V=15$ kN. After $V=15$ kN the two faces of the crack started to have measurable slip. The specimen reached the failure at $V=69.4$ kN and $N_e=179$ kN because no additional shear force could be added. In the retest no new crack was observed. Figure A.13 shows S12 after failure. The ratio of V_u/N_u at the failure was 0.388

The significance of the failure behavior of this group specimens is that for an inclined crack with 30° or less the capacity of the shear transfer across the crack is less than the shear that causes the crack. For many slender beams the failure cracks are about 30° . For these beams the shear strength may be overestimated if the concrete contribution V_c is taken equal to the inclined cracking load.

4.2.4 Group 4: Specimens with $\theta=90^\circ$

This specimen group included Specimens S9, S10 and S11. The specimens were designed to fail along a crack parallel to the transverse shear force. No reinforcement was placed across the failure crack. The confinement on the crack plane was induced by the external longitudinal force N_e . These three specimens were tested to provide a comparison with the pushoff tests by Mattock^{21,22} and Paulay^{19,20}.

The longitudinal force N_e was originally designed to increase simultaneously as the transverse load V increased. However, because of the small shear span depth ratio, no crack had occurred in the original test of S9 at a very large shear force stage. To fulfill the investigation into the shear-friction on a crack, these three specimens were pre-cracked by applying the transverse load only. The specimens were then tested under both the longitudinal and transverse loads. The pre-cracks in the three specimens occurred at about $V=60$ kN and extended about 9/10 of the gross section. The cracks were inclined, rather than parallel to the shear force. Figure A.11 shows the example of the precrack (S9).

Fig. 4.19 shows the load history (V vs. N_e) for the three specimens after the precracking. The longitudinal load, N_e , was increased to a certain amount (50 kN for S9, 80 kN for S10 and 140 kN for S11) before V was loaded. The specimen was then loaded to failure by increasing V only, with the jack applying N_e locked. However the application of V caused the rotation of the specimens, as a result N_e increased slightly as V increased. Figure 4.20 shows the load-horizontal relative movement of the two crack faces for the three specimens.

Figure A.12 shows S9 after failure. Very small relative movement was recorded up to $V=120$ kN. After $V=120$ kN the two faces of the crack start to have measurable slip. The specimen failed at $V=281$ kN and $N_e=158$ kN because no additional shear force could be applied. The failure was accompanied with a visible slip between the two crack planes and diagonal compression crushing in the compression zone, (SF+DC). No new crack was observed in the test. The angle of the failure was 75° and the ratio of V_u/N_u at the failure was 1.78.

S10 had higher longitudinal force N_e than S9. As a result S10 had stiffer behavior than S9, as shown in Fig. 4.20. Up to about $V=300$ kN the failure crack had a stable relative movement. After $V=300$ kN the failure crack started to undergo larger relative movement. The failure was reached at $V=359$ kN and $N_e=208$ kN when no additional V could be applied. The failure was accompanied by diagonal crushing of the concrete along the failure crack, (SF+DC).

The angle of the failure was 75° and the ratio of V_u/N_u at the failure was 1.73. Figure A.13 shows S10 after failure.

S11 had the smallest longitudinal force, ($N_e=88$ kN). As a result S11 had much lower shear capacity and softer behavior than S9 and S10. The specimen started to develop significant slip at about $V=100$ kN. Once the slip started it continuously increased without any stable stage. The specimen failed at $V=140$ kN and $N_e=88$ kN. Unlike S9 and S10, no diagonal crushing was observed in S11 at failure. The angle of the failure was 75° and the ratio of V_u/N_u at the failure was 1.60. Figure A.14 shows S11 after failure.

Figures 4.21 to 4.23 show the load-strain response perpendicular and parallel to the failure crack for the three specimens. The zero strain in Fig. 4.21 to 4.23 was taken at the start of the application of V . The curves indicate that the opening and the sliding of the crack decreased as the location approached the compression zone. This suggests that the two faces of the failure cracks had both relative sliding and relative rotation.

4.2.5 Group 5: Specimens with Undesigned Inclined Crack

Three specimens, S15, S16 and S17, were included in this group. All of them had the same geometric configuration and were reinforced with both longitudinal reinforcement and stirrups. The specimens did not have inclined grooves to define the failure crack. The edge of the loading plate used to apply the shearing load was located so that a 30 degree crack could form (See the insets to Fig.

4.24 to 4.27). The longitudinal reinforcement in the three specimens were four 15M deformed bars. Six mm, 8.5 mm and 10M closed stirrups @ 100 mm were used in S16, S15 and S17 respectively.

Figure A.19 shows Specimen S16 after failure. The first crack was a flexural crack observed near the fixed end at $V=40$ kN. At $V=70$ kN which corresponds to 44% of the failure shear force the first inclined crack was observed in the shear span. The crack started from the tension edge and extended into about half of the cross section. As the load increased to 88 kN, a new inclined crack developed above the first one, starting from the edge of the support plate and extending about $7/10$ of the cross section height. As the load increased the cracks extended into the compression zone and new cracks formed in the shear span and in the fixing zone. The first inclined crack increased at a faster rate than the second inclined crack and formed the failure crack. At $V=135$ kN the failure crack extended to about $9/10$ of the cross section. At $V=154$ kN the longitudinal reinforcement started to yield at the fixed end which corresponds to the largest bending moment. The specimen failed at $V=159$ kN by loss of shear transfer across the failure crack. This was accompanied by a sudden visible relative sliding along the crack and compressive crushing in the diagonal direction, (SF+DC). At failure three of the four stirrups intercepted by the failure crack yielded.

The load-strain relationships for the longitudinal reinforcement are shown in Fig. 4.24. Strain gauge 1 was located at the failure crack; Strain gauge 4 was located at maximum bending moment section at the fixed end and strain gauges 2 and 3 were in between.

The yield strain of the reinforcement was 0.0022. Figure 4.24 indicates that the tension in the longitudinal reinforcement increased as the sectional flexural moment increased until the steel yielded at $V=154$ kN. Figure 4.25 shows the curves of load-strain relationships for the stirrups intercepted by the failure crack. All the curves are essentially a straight line with zero strain up to the start of inclined cracking. The inclined cracking in the shear span increased the strain in the stirrups greatly. Although Stirrup 1 responded to the cracking later than Stirrups 3 and 4, they had larger strain than Stirrups 3 and 4 after the cracking. At failure Stirrup 2 had the largest tension and Stirrup 1 had the second largest tension. Stirrup 4 which intercepted the failure crack at the compression zone had the smallest tension. At failure the strains in stirrups 1, 2 and 3 exceeded 0.002 and the strain in stirrup 2 was very close to 0.002.

Specimen S15 had 8.5 mm stirrups compared to 6 mm in S16. Figure A.17 shows S15 after failure. The first crack was a flexural crack observed near the fixed end at $V=45$ kN. At $V=75$ kN the first inclined crack was observed in the shear span. As load increased to $V=95$ kN, a second inclined crack developed above and parallel to the first one. As the load increased the cracks extended into the compression zone and new cracks formed in the shear span and in the fixing zone. At $V=155$ kN the longitudinal reinforcement start to yield at the fixed end. At $V=163$ kN the yield length of the reinforcement exceeded $1/3$ of the shear span and visible curvature of the specimen was observed. In order to ensure shear failure would be reached, an external longitudinal force was applied at the

end of the specimen to increase the flexural strength of the specimen. The external force was loaded to 170 kN in one step. The shear force V was then increased again after the application of N_e . As V increased new cracks were observed between the two previous inclined cracks. The specimen failed at $V=223$ kN by the diagonal crushing of the concrete between the two major inclined cracks, (DC). At failure the tension strain in the four stirrups intercepting the failure crack were from 0.0010 to 0.0022, compared to a yield strain of 0.0021.

Figure 4.26 shows the load-strain relationships for the longitudinal reinforcement. Before the external longitudinal force was applied the specimen had a load-strain relationship similar to Specimen S16. The tension strain increased as the flexural moment increased. The application of the external longitudinal force ($N_e=170$ kN) decreased the strains in the longitudinal reinforcement. The strain changes at gauges 1 and 2 were 0.0004 and 0.00048 respectively. The corresponding change in N_s was about $\Delta N_s=75$ kN and 90 kN respectively. This indicated that about half of the external force was introduced to the concrete and the other half acted to reduce the tension in the reinforcement. Figure 4.27 shows the load-strain curves for the stirrups intercepted by the inclined cracks. Similar to S16, the stirrups intercepted by the crack near the tension face experienced larger tension than the others. The application of N_e seemed to have little effect on the strain in the stirrups. At failure the two stirrups intercepted by the crack at the tension zone yielded. The yield strain for the stirrups was 0.0021.

Since the stirrups in S17 were larger than those in S15 and S16, S17 was expected to failed by flexure if no external longitudinal force was applied. To avoid flexural failure, an external longitudinal force N_e was applied. N_e was increased as V was increased. Figure 4.28 shows the load path (V vs. N_e).

Figure A.20 shows Specimen S17 after failure. Due to the application of the longitudinal force, cracking in S17 was observed later than in S15 and S16. The first crack was a flexural crack observed near the fixed end at $V=63$ kN. At $V=120$ kN the first inclined crack was observed in the shear span. The crack started from the tension edge to about half of the cross section height. As load increased several new inclined cracks developed parallel to the first one and above it. As the load increased diagonal cracks in the opposite direction were observed in the fixing zone. Near failure the concrete in the compression zone and in the web crushed diagonally in the both direction. The failure was reached at $V=366$ when no additional shear force could be applied. At failure a large area of the compression zone crushed, (referred as DC in Table 4.1). At failure the longitudinal reinforcement had yielded at the fixed end.

The load-strain relationships for the longitudinal reinforcement are shown in Fig. 4.29. The reduction of the strain at $V=55$ kN and 200 were due to the large increase in the longitudinal force N_e . The reinforcement had yielded at failure near the fixed end at failure. The load-strain relationships for the stirrups intercepted by the failure crack are shown in Fig.4.30. The large change of the

longitudinal force did not have a notable effect on these curves. Similar to what observed in the test of S15 and S16, all the curves are essentially a straight line with zero strain up to the start of inclined cracking. The inclined cracking in the shear span resulted in a large increase of the strain in the stirrups. At failure no stirrups were yielded.

4.3 The Effect of Dowel Action

Three types of specimens were involved in the investigation of the effect of dowel action on the shear transfer across the failure crack. The first type was specimens with normal dowel action. They were S1 and S3 in the specimen group with $\theta=45^\circ$, S7 in the specimen group with $\theta=60^\circ$ and S13 in the specimen group with $\theta=30^\circ$. The second type was specimens with the reinforcement wrapped with foam insulation at the failure crack. They were S2, S6 and S12 for the specimen groups with $\theta=45^\circ$, 60° and 30° , respectively. The third type was specimens without reinforcement crossing the failure crack. These specimens included S4 and S5 with $\theta=45^\circ$, S8 with $\theta=60^\circ$ and S14 with $\theta=30^\circ$.

The mechanism of the reduction of the dowel action for the second type of specimens is illustrated in Fig. 3.7 of Chpt. 3. The length of the wrapped reinforcement was 150 mm. The dowel action was reduced by increasing the shearing length of the reinforcement. Since no reinforcement intercepted the failure crack in the third type of specimens, no dowel action was involved in the shear transfer across the failure crack. The behavior of these two types of

specimens was compared with the first type of specimens (normal dowel action) in the following aspects. In all cases the strain gauges on the longitudinal bars were mounted on the sides of the bars to minimize the effects of flexural strains due to the dowel action.

The effect of the reduced dowel action on the strain of the reinforcement at the failure crack are shown in Fig. 4.1, 4.9 and 4.15 for the specimen groups with $\theta=45^\circ$, 60° and 30° respectively. Before cracking, both types of the specimens had no measurable strain. After cracking the specimens with normal dowel action developed longitudinal reinforcement strain faster than those with reduced dowel action. Two reasons may explain this behavior. In the specimens with reduced dowel action the reinforcement had an unbonded length at the failure crack. Once the concrete cracked, the deformation of the crack was distributed over the unbonded length of the reinforcement, while in the specimens with normal dowel action the deformation from the crack was concentrated in a small length of reinforcement adjacent to the crack. Secondly, in the specimens with normal dowel action the reinforcement at the failure crack was more effective in holding the two faces of the crack together than that wrapped with foam insulation, and as a result the former had larger tension in the reinforcement at the crack. At failure the reinforcement yielded at the failure crack for the specimens with normal dowel action in the specimen group of $\theta=45^\circ$ and 60° , while the tension strains were only 0.00125 for S2 and 0.0014 for S6 at the same group. In the specimen group with $\theta=30^\circ$, the reinforcement of both S12 and S13 did not yield at failure. The

reduction of dowel action had little effect on the steel strain at the failure crack in specimens with $\theta=30^\circ$.

Reduction of dowel action decreased the failure shear force of the specimens. In the specimen group with $\theta=45^\circ$, S1 and S3 failed at $V=99$ kN and 102 kN respectively but the failure shear force of S2 was only 57 kN. In the specimen group with $\theta=60^\circ$, S7 failed at $V=149$ kN while S6 failed at $V=107$ kN. Dowel action had no significant effect on the ultimate shear strength of the specimens with $\theta=30^\circ$ because these specimens failed due to cracking of the concrete rather than the failure of shear friction.

Although the reduction of dowel action affected the ultimate strength and the tension in the reinforcement at the failure crack, it had very little effect on the ratio of V_u/N_u . For the specimens with $\theta=45^\circ$ the ratios of V_u/N_u for the three reinforced specimens were 0.55 , 0.51 and 0.57 respectively. The ratio of V_u/N_u for the two reinforced specimens with $\theta=60^\circ$ were 0.86 and 0.83 respectively. The ratio of V_u/N_u of the retest for the two specimens S12 and S13, with $\theta=30^\circ$ were 0.13 and 0.20 respectively. The ratio of V_u/N_u increased as θ increased.

Specimens S4, S5, S8 and S14 did not have any reinforcement across the failure crack. These specimens developed the compression on the failure crack plane through the external longitudinal force N_e but had no dowel action in the failure crack. The shear transfer across the crack is attributed to the aggregate interlock and shear in the uncracked compression zone. Due to different $N_e \sim V$ loading

history the unreinforced specimens had different behavior from the reinforced specimens before the failure. However, this parameter had no significant effect on the failure shear force V_u . For Specimen S4 the external longitudinal force at the failure was 179 kN which was about the tensile force in the reinforcement at failure of S1 and S3. S4 failed at $V=96$ kN which was only slight lower than the shear force at failure of S1 and S3. For the rest of the unreinforced specimens, since N_e at failure was different from N_s in the reinforced specimens, the failure shear force were different. However, the ratios of V_u/N_u were very close to those from the reinforced specimens in the same group.

As summary, the major contribution of the longitudinal reinforcement to the shear transfer across the failure crack is its ability to hold the two faces of the crack together and induce the shear-friction across the crack, rather than direct transfer shear by the shear stress in the cross section of reinforcement. The bonding condition of the reinforcement at the crack affects this ability of the reinforcement. Reinforcement with poor bonding condition at the crack has less ability to develop its tension and, as a result, the crack transfers less shear.

4.4 The Effect of Uncracked Compression Zone

Two specimens were pre-cracked in the compression zone to compare with the monolithic specimens to investigate the significance of the uncracked compression zone in the shear transfer mechanism. Specimen S3 had $\theta=45^\circ$ while S7 had $\theta=60^\circ$. The pre-

cracks were about 1/3 of the cross section height and located at the extension line of the groove used to force the location of the failure crack in order to join with the failure crack. Figures A.3 and A.7 show the precrack for the two specimens respectively.

The precracking in the compression zone reduced the cracking load of the specimens by decreasing the monolithic section of the specimens. However, the precrack did not reduce the shear force at failure of the specimens. The failure loads for the tested specimens are listed in Table 4.1. For the specimens with $\theta=45^\circ$, the only difference between S1 and S3 was that S3 was precracked but S1 was not. Both specimens had the same behavior and failure mode at the ultimate state. S3 failed at $V=102$ kN which was a little higher than the 99 kN at which S1 failed. In the specimen group with $\theta=60^\circ$, S7 (precracked) failed at $V=149$ kN while S6 and S8 failed at $V=107$ kN and 118 kN respectively. Direct comparison between the failure loads of S7 and the other two specimens is not practical because S6 had the reinforcement wrapped with foam insulation at the failure crack and S8 was unreinforced at the failure crack. However, as discussed in Sec. 4.3 the condition of the dowel action does not affect the ratio of V_u/N_u . The fact that the V_u/N_u ratio of S7 was approximately equal to that of S6 and S8 indicates that the precrack did not reduce the failure shear force of S7. Actually, the failure crack in S7 did not join the precrack but extended underneath it. The failure shear was the shear transfer capacity across the failure crack and thus was not effected by the precrack.

In a summary, precracking the compression zone reduced the cracking load but did not affect the failure load. The cracking in the compression zone was the extension of the cracks from the tension zone. The concrete of the compression zone was still in compression. The contribution of the compression zone to the shear strength in a reinforced concrete beam is because it is under compression. The compression on the concrete induces shear friction to resist the applied shear force.

4.5 Combined Truss and Shear Friction Action

For the three specimens (S15, S16 and S17) with stirrups, the shear transfer across an inclined crack consists of two parts: the shear-friction mechanism and the truss action. The shear-friction mechanism includes the dowel action of the reinforcement, the aggregate interlock and the shear transferred by the uncracked compression zone. According to the test observations and the discussions in Sec. 4.3 and 4.4, the aggregate interlock (the friction on the rough crack faces) is the major part of the shear friction. The truss action results from the stirrups acting as transverse tension ties in a truss to transfer shear force.

Two objectives were involved in the tests of S15, 16 and 17. The first objective was to determine the ratio of V_c/N_u and compare this to the ratio of V_u/N_u in the specimens without stirrups. The second objective was to investigate the effect of the amount of stirrups on the angle of the truss strut θ , because, according to the truss model, θ

increases as the ratio of the stirrup amount to the longitudinal reinforcement amount increases. Because the application of the longitudinal force N_e in S15 and S17 in effect increased the longitudinal reinforcement, the second investigation was not successful. Actually the angles of the diagonal struts for the three specimens were very close (about 35°).

The strains in the stirrups of the three specimens were measured by the strain gauges which were attached to the stirrups in the vicinity of where the failure crack intercepted the stirrups. The stresses in the stirrups were then calculated using the stress-strain curves of the steel shown in Fig. 3.9. Six stirrups were arranged in the shear span while only the four in the middle were intercepted by the failure crack. The shear transferred by the stirrups through truss action was the force in these four stirrups:

$$V_s = \Sigma A_v f_s \quad (4.1)$$

where A_v is the area of one stirrup and f_s is the stress in the stirrups. The shear force carried by the shear friction was

$$V_c = V_u - V_s \quad (4.2)$$

The longitudinal compression on the failure crack plane was the sum of the tension force in the longitudinal reinforcement at the crack, N_s , and the external force, N_e . The stress in the longitudinal reinforcement can be determined using the stress-strain curve of the steel in Fig. 3.9. Although destressing occurred in the longitudinal reinforcement of S15 and S17 when the external longitudinal force

was applied, the strains in the longitudinal reinforcement at the failure crack did not exceed the yield strain and thus the stress-strain curve in Fig. 3.9 was still applicable.

Table 4.2 shows the forces in the steel at the failure crack, the shear transferred by the shear friction and the ratio of V_c/N_u for S15, S16 and S17.

4.6 Relationship between V_c/N_u and N_u

The ratios of V_c/N_u are plotted in open symbols in Fig. 4.31 for the 14 specimens without stirrups. The shear transferred varies from approximately zero for small θ to twice the longitudinal compression force for large angles.

The ratios of V_c/N_u for S15, S16 and S17 are also plotted in Fig. 4.31. Comparisons indicate that for S16, which failed by shear-friction failure, the ratio of V_c/N_u is close to the V_u/N_u ratio of the specimens without stirrups. S15 and S17 had lower V_c/N_u ratio since they failed by diagonal crushing of the concrete before the shear friction failure was reached.

4.7 Summary of the Test Results

Based on the evaluation of the test results, the following conclusions are made.

1. All the specimens failed in shear. The failures were due to either the loss of the shear transfer across the failure cracks (shear-

friction failure) or the diagonal crushing of the concrete (diagonal strut failure of the truss). The ratio of the shear transferred by the shear-friction to the longitudinal compression on the crack face (V_u/N_u for S1 to S14 and V_c/N_u for S15 to S17) increased as the angle of inclination of the failure crack, θ , increased.

2. Test results of the specimens with $\theta=30^\circ$ indicate that the cracking shear of a inclined section with $\theta=30^\circ$ is larger than the shear friction strength of the crack under the same longitudinal compression force. Thus the specimens with $\theta=30^\circ$ failed instantaneously after the failure crack formed if no stirrups were provided. For many slender reinforced concrete beams the inclination of the failure cracks are 30° or less. This suggests that using the inclined cracking load as the shear contribution of the concrete may overestimate the shear strength of the beams if V_s is based on the actual angle θ .

3. Test results of the specimens with $\theta=90^\circ$ indicated that it was not possible to develop a crack in the shear span which was parallel to the applied shear force. Since in reinforced concrete beams the failure cracks of shear are always inclined, it is not practical to apply the test results of the pushoff specimens to them.

4. The shear contribution of dowel action in reinforcement is its ability to hold the two faces of the crack together and induce shear friction across the crack, rather than the shear stress in the cross section of the reinforcement. Reduction of the dowel action in the

specimens tested reduced the failure shear force by decreasing the shear friction across the crack.

5. The uncracked compression zone contributes to the shear resistance of reinforced concrete beams because it is under compression. The compression zone may crack due to the extension of the crack in the tension zone. However it is still under compression. The compression induces the shear friction to resist the shear.

6. For the specimens with stirrups, the shear force was resisted by both the stirrups intercepted by the failure crack and the shear-friction across the failure crack. The stirrups participated in resisting the shear by direct tension across the inclined cracks. The longitudinal reinforcement and the external longitudinal force, if any, induce the confining force on the failure crack surfaces necessary to mobilize the shear friction across the crack.

Table 4.1 Principal test results of shear tests (Units: Degree and kN)

Specimen	Designed θ	Measured θ	V_{cr}	V_u	N_s	N_e	N_u	$\frac{V_u}{N_u}$	Failure condition ^{***}
S1	45	46	48.0	99.0	180.0	0	180.0	0.550	SF
S2	45	44	45.0	57.0	112.0	0	112.0	0.509	SF
S3	45	49	32.0	102.0	180.0	0	180.0	0.567	SF
S4	45	44	73.0	96.0	0	179.0	179.0	0.536	SF
S5	45	47	65.0	76.0	0	151.0	151.0	0.503	SF
S6	60	57	47.0	107.0	124.0	0	124.0	0.863	SF
S7	60	60	35.0	149.0	180.0	0	180.0	0.828	SF+DC
S8	60	65	85.0	118.0	0	120.0	120.0	0.983	SF
S9	90	80	58.0	281.0	0	158.0	158.0	1.778	SF+DC
S10	90	74	63.0	359.0	0	208.0	208.0	1.726	SF+DC
S11	90	80	61.0	140.0	0	88.0	88.0	1.602	SF
S12	30	30	54.0	24.0*	0	180.0	180.0	0.133	SF
S13	30	33	48.0	46.0*	0	227.0	227.0	0.203	SF
S14	30	39	45.0	69.4*	0	179.0	179.0	0.388	SF
S15	not designed	39	75.0	158.5	189.0	171.5	360.5**	0.215	DC
S16		34	70.0	223.0	270.4	0	270.4**	0.276	SF+DC
S17		35	120.0	266.0	114.0	331.0	445.0	0.114	DC

* The failure shear force for S12, S13 and S14 is the failure shear in the re-test.

** For S15, S16 and S17 V_c/N_u is used instead of V_u/N_u in the analysis. Table 4.2 shows the procedure to determine V_c .

*** SF = Shear friction failure, DC = Diagonal crushing.

Table 4.2 The internal forces on the failure crack for S15, S16 and S17

Forces	S15	S16	S17
N_e	171.5	0	331.0
N_s	189.0	270.4	114.0
$N_u = N_s - N_e$	360.5	270.4	445.0
V_s	145.7	86.8	215.0
V_u	223.0	159.0	266.0
$V_c = V_u - V_s$	77.3	72.2	51.0
V_c / N_u	0.214	0.267	0.115

* All the Forces are in kN

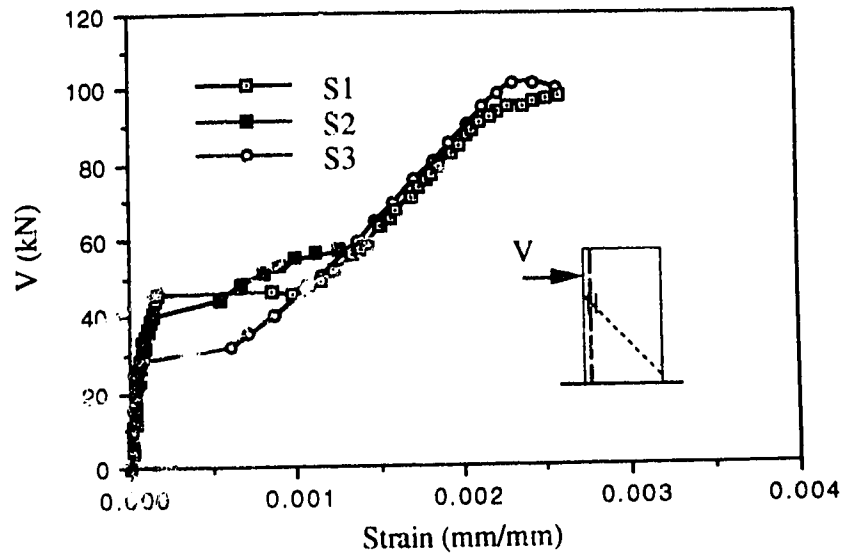


Figure 4.1 Load vs. steel strain, S1, S2 and S3;

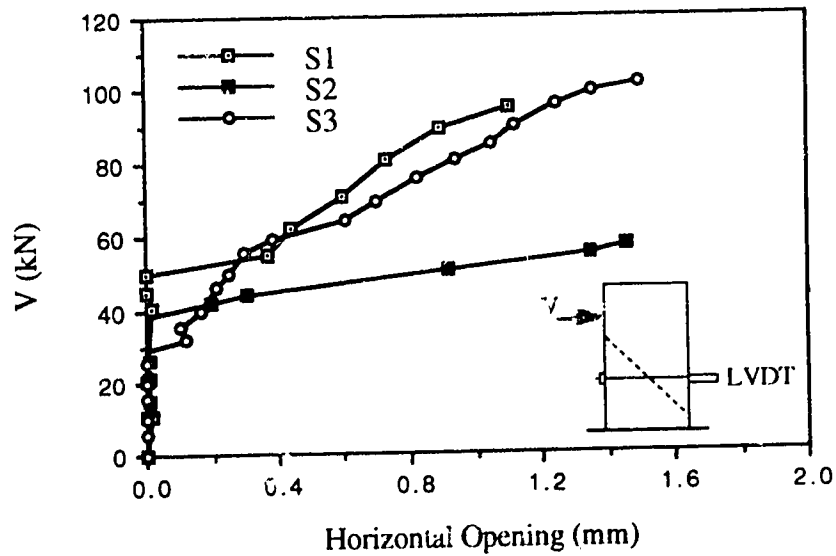
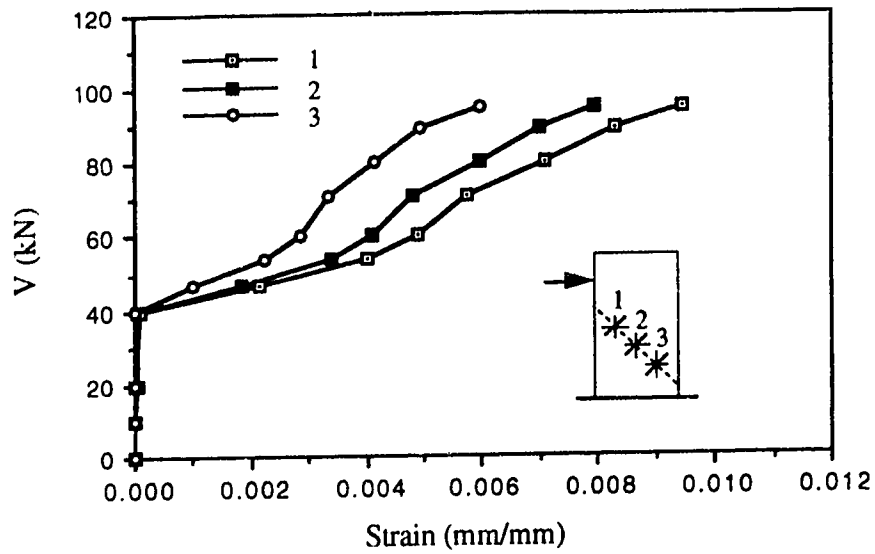
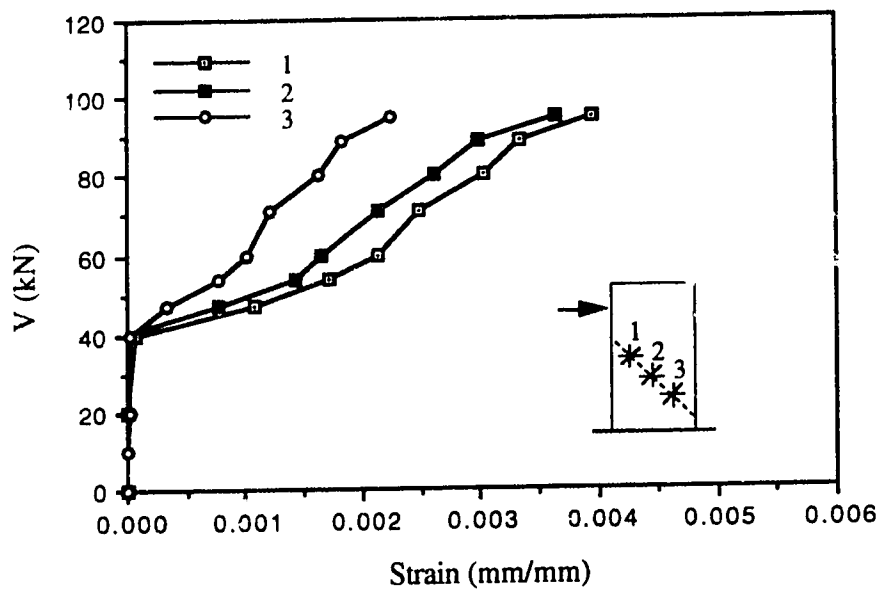


Figure 4.2 Load vs. horizontal relative movement of the two crack faces, S1, S2 and S3

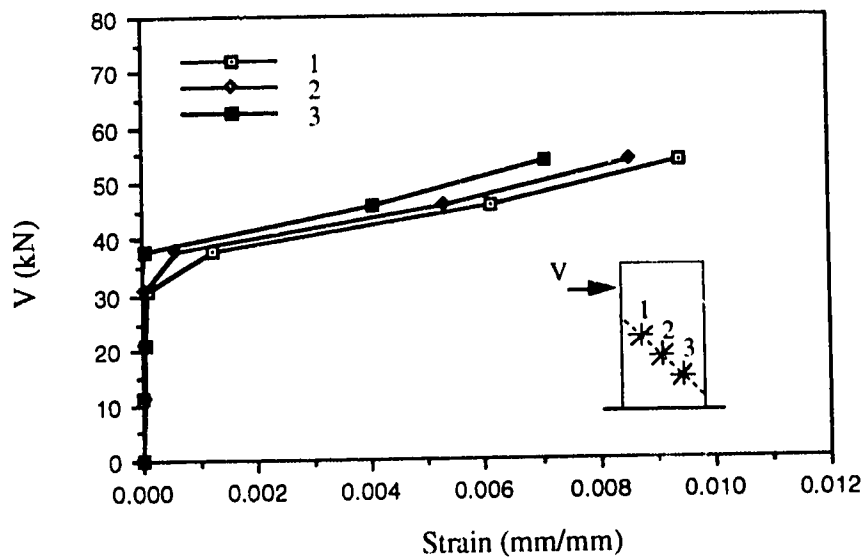


(a) Strain perpendicular to the crack

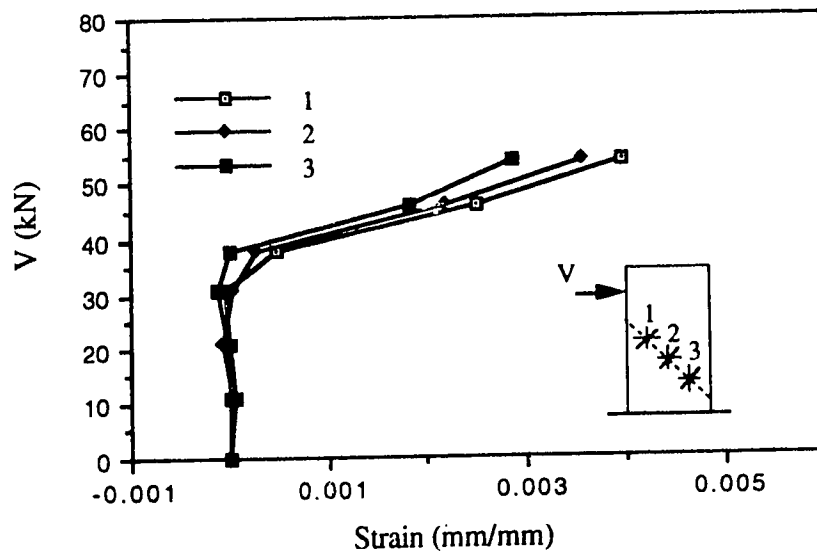


(b) Strain parallel to the crack

Figure 4.3 Load vs. strains measured across the crack, S1;

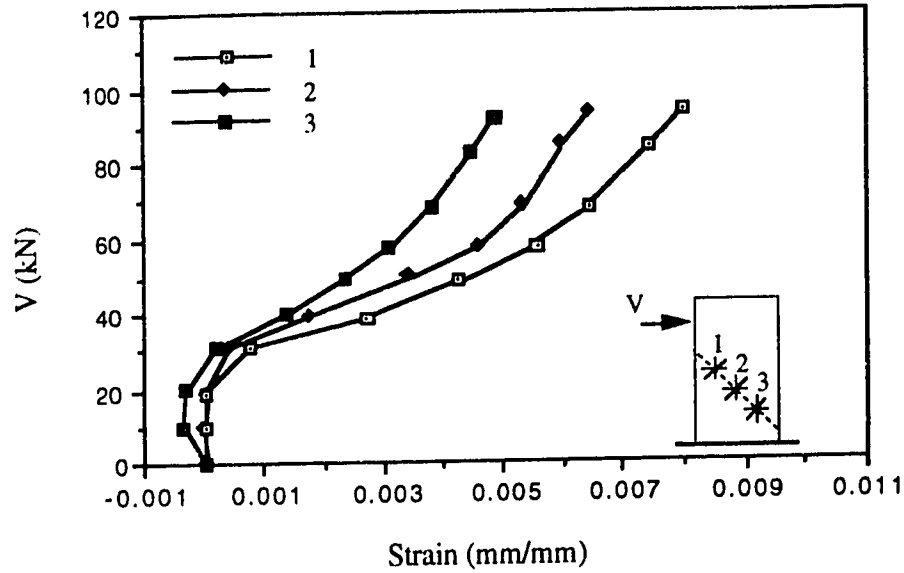


(a) Strain perpendicular to the crack

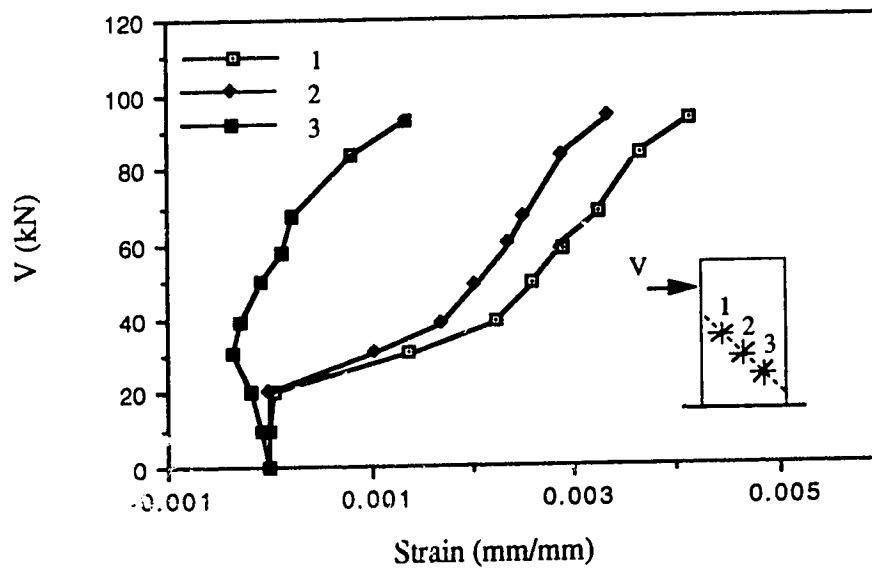


(b) Strain parallel to the crack

Figure 4.4 Load vs. strains measured across the crack, S2;



(a) Strain perpendicular to the crack



(b) Strain parallel to the crack

Figure 4.5 Load vs. strains measured across the crack, S3;

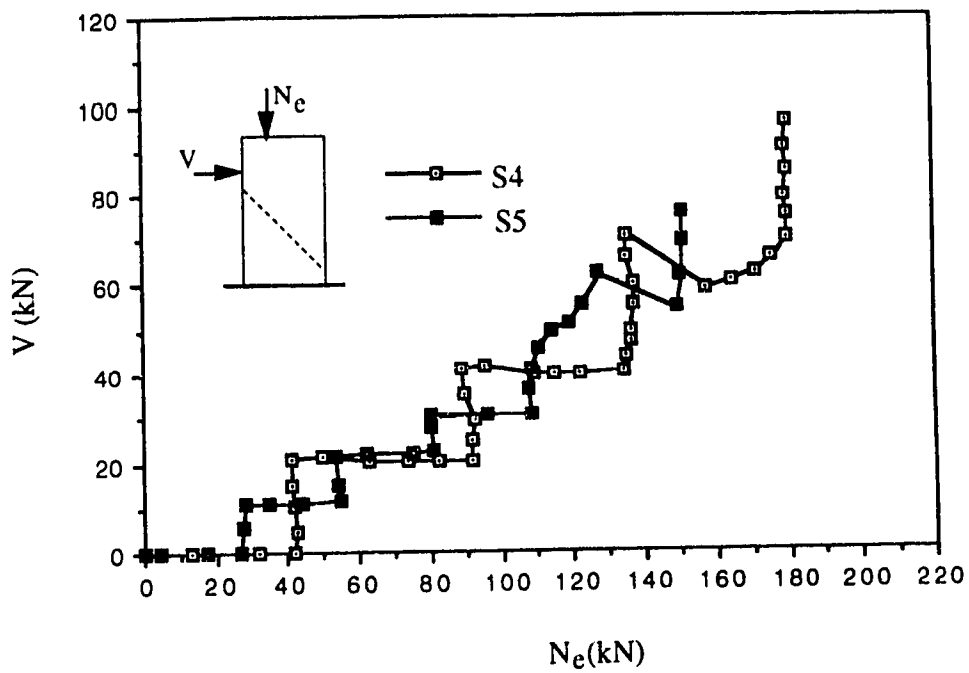


Figure 4.6 Load history, S4 and S5

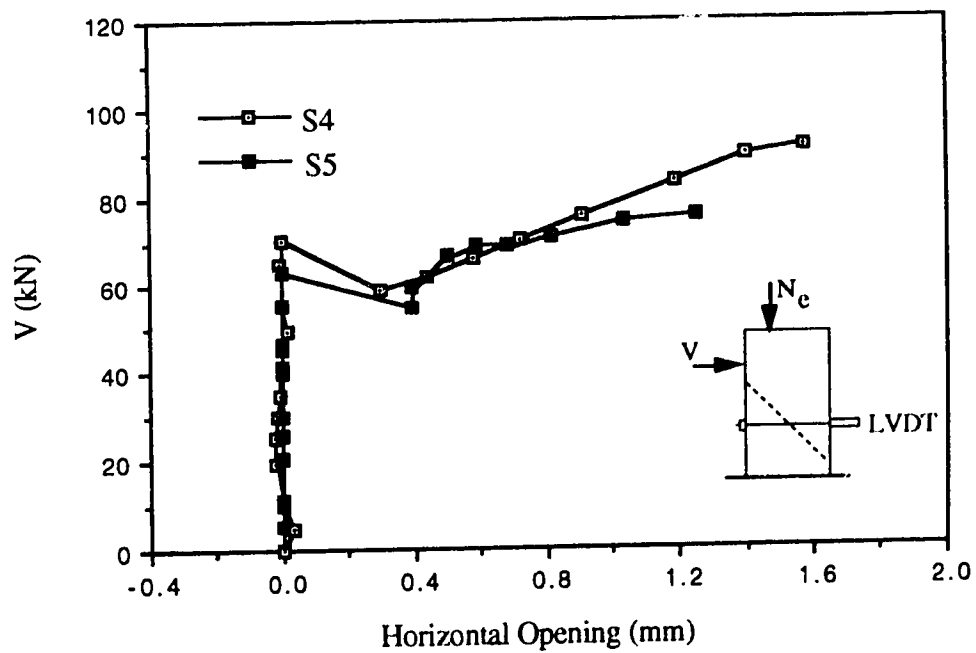
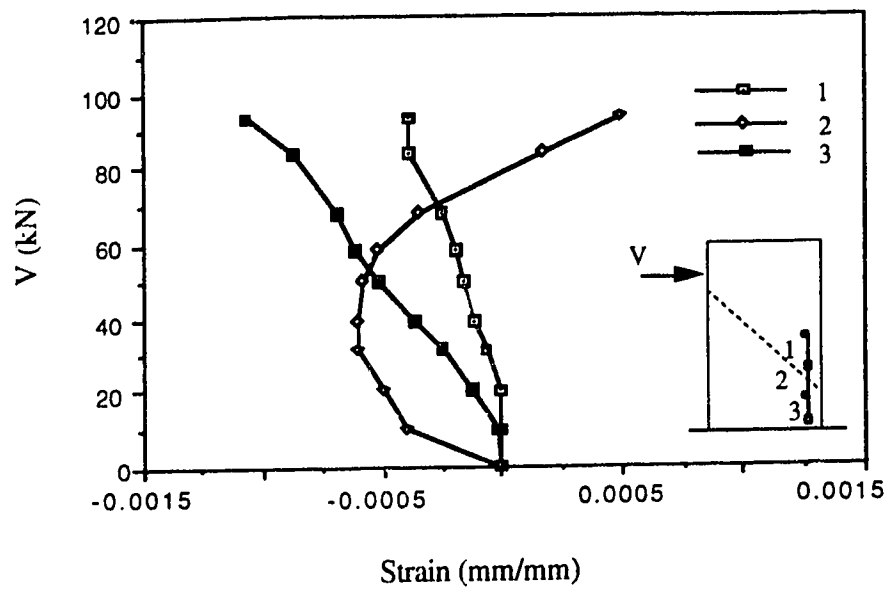
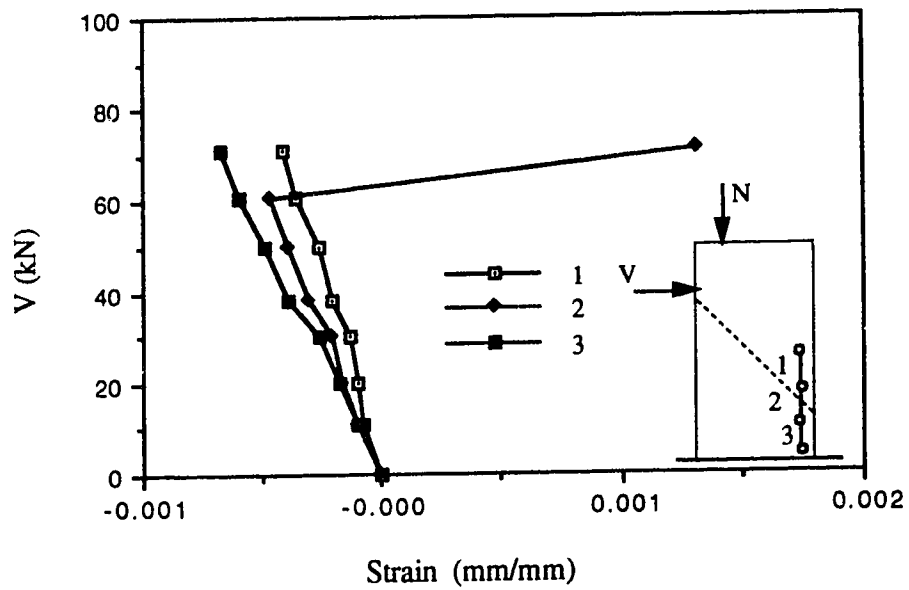


Figure 4.7 Load vs. horizontal relative movement of the two crack faces, S4 and S5



a) Specimen S3



b) Specimen S5

Figure 4.8 Load vs. strain in the compression zone, S3 and S5;

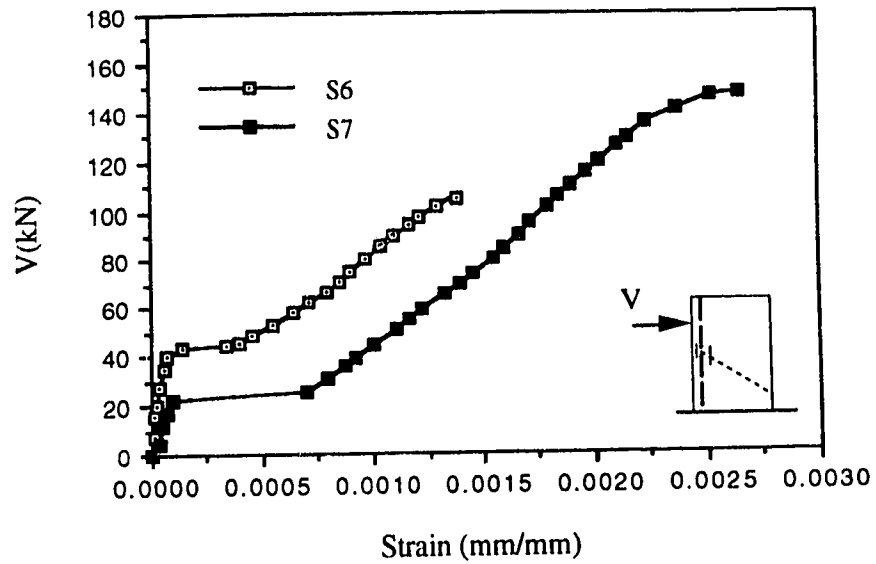


Figure 4.9 Load vs. steel strain, S6 and S7;

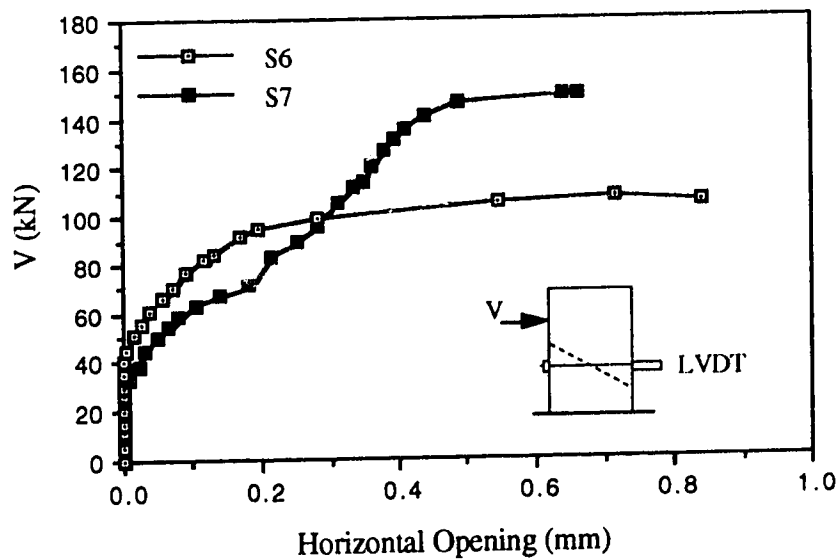
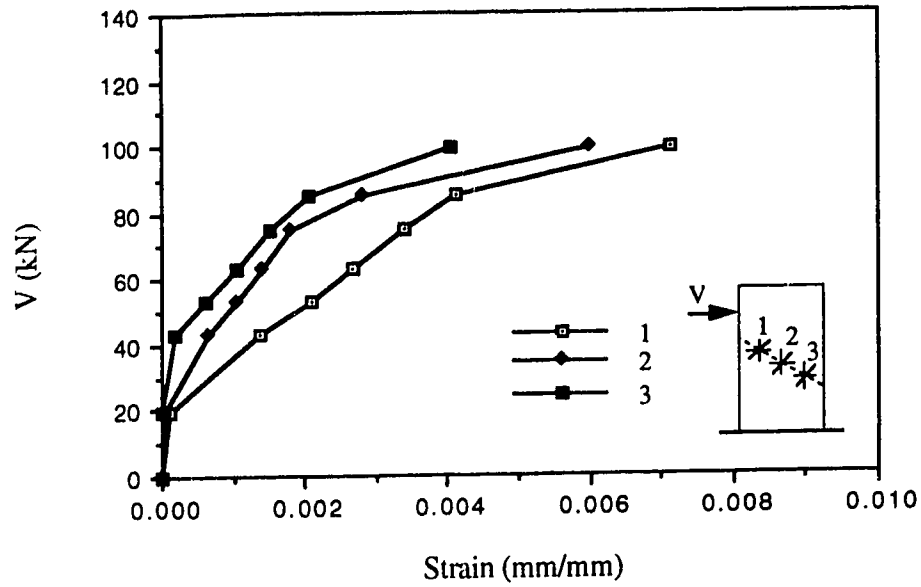
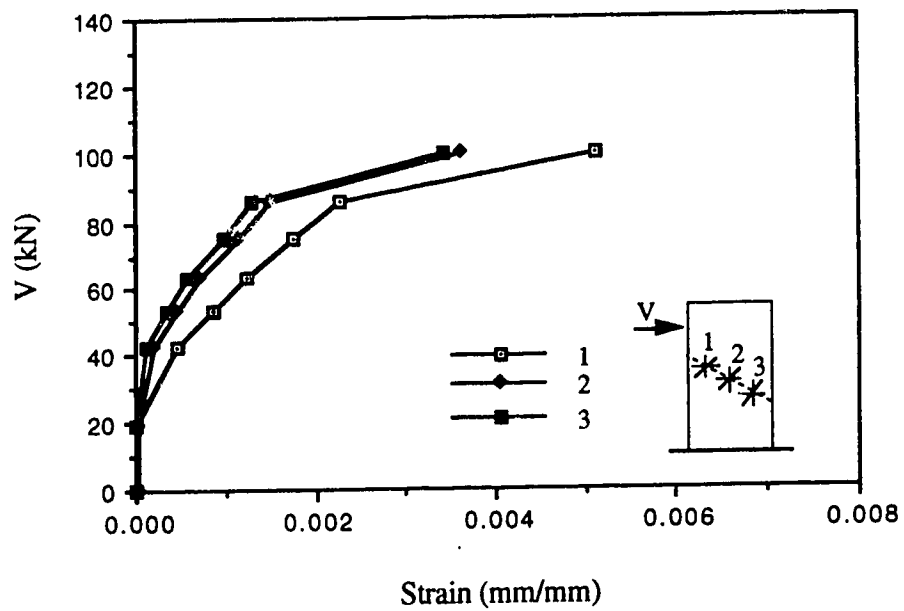


Figure 4.10 Load vs. horizontal relative movement of the two crack faces, S6 and S7

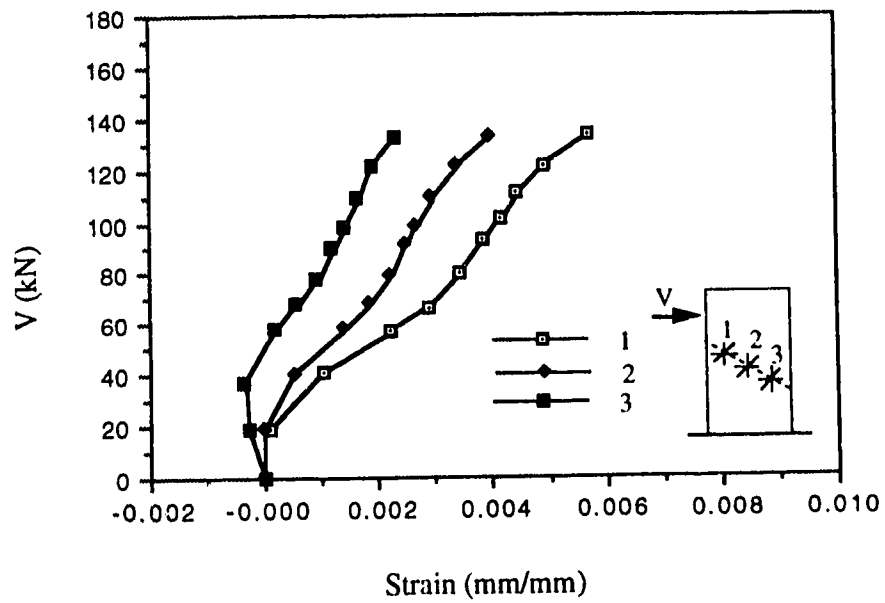


(a) Strain perpendicular to the crack

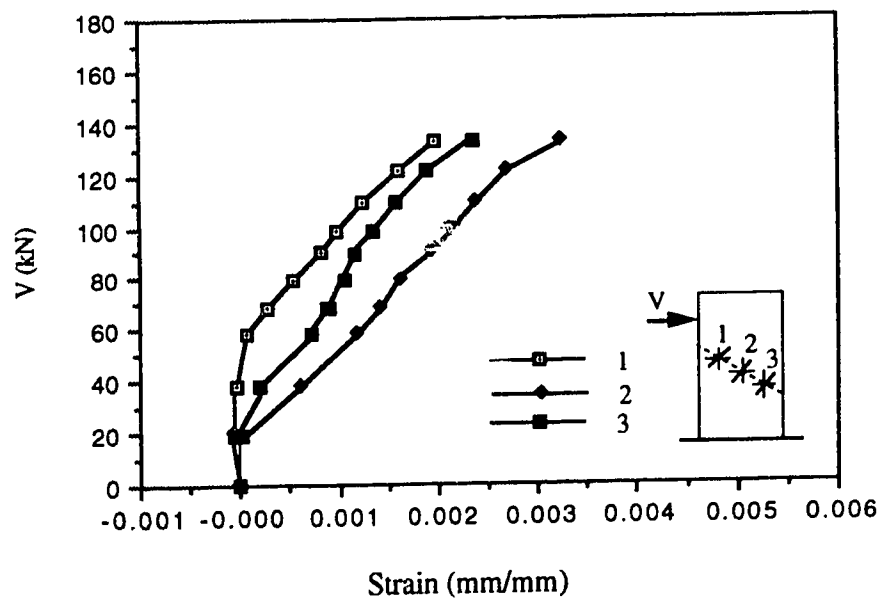


(b) Strain parallel to the crack

Figure 4.11 Load vs. strains measured across the crack, S6;

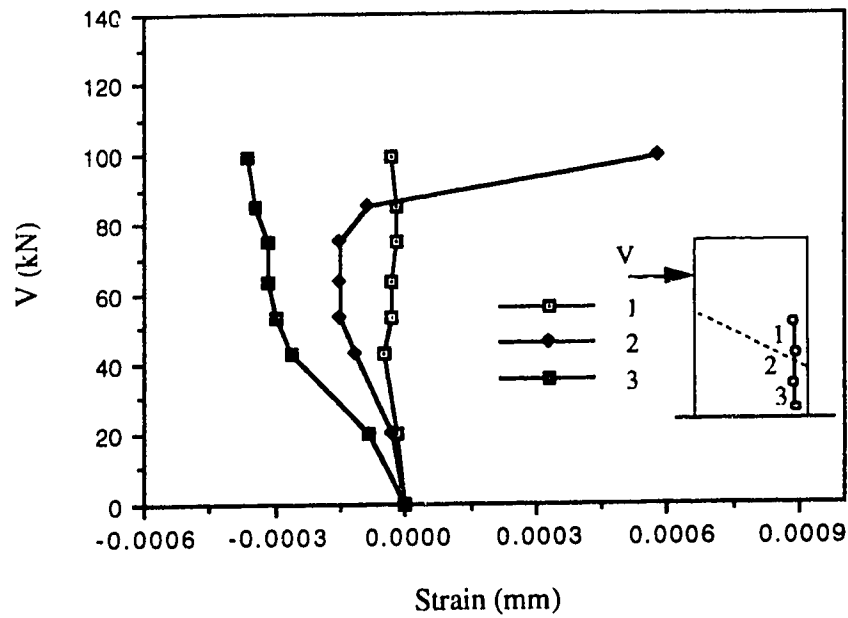


a) Strain perpendicular to the crack

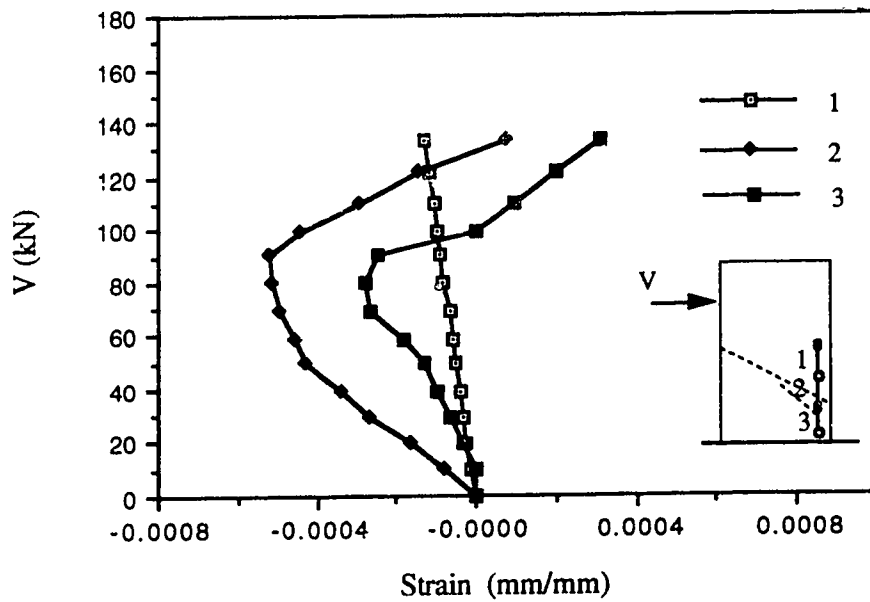


b) Strain parallel to the crack

Figure 4.12 Load vs. strains measured across the crack, S7

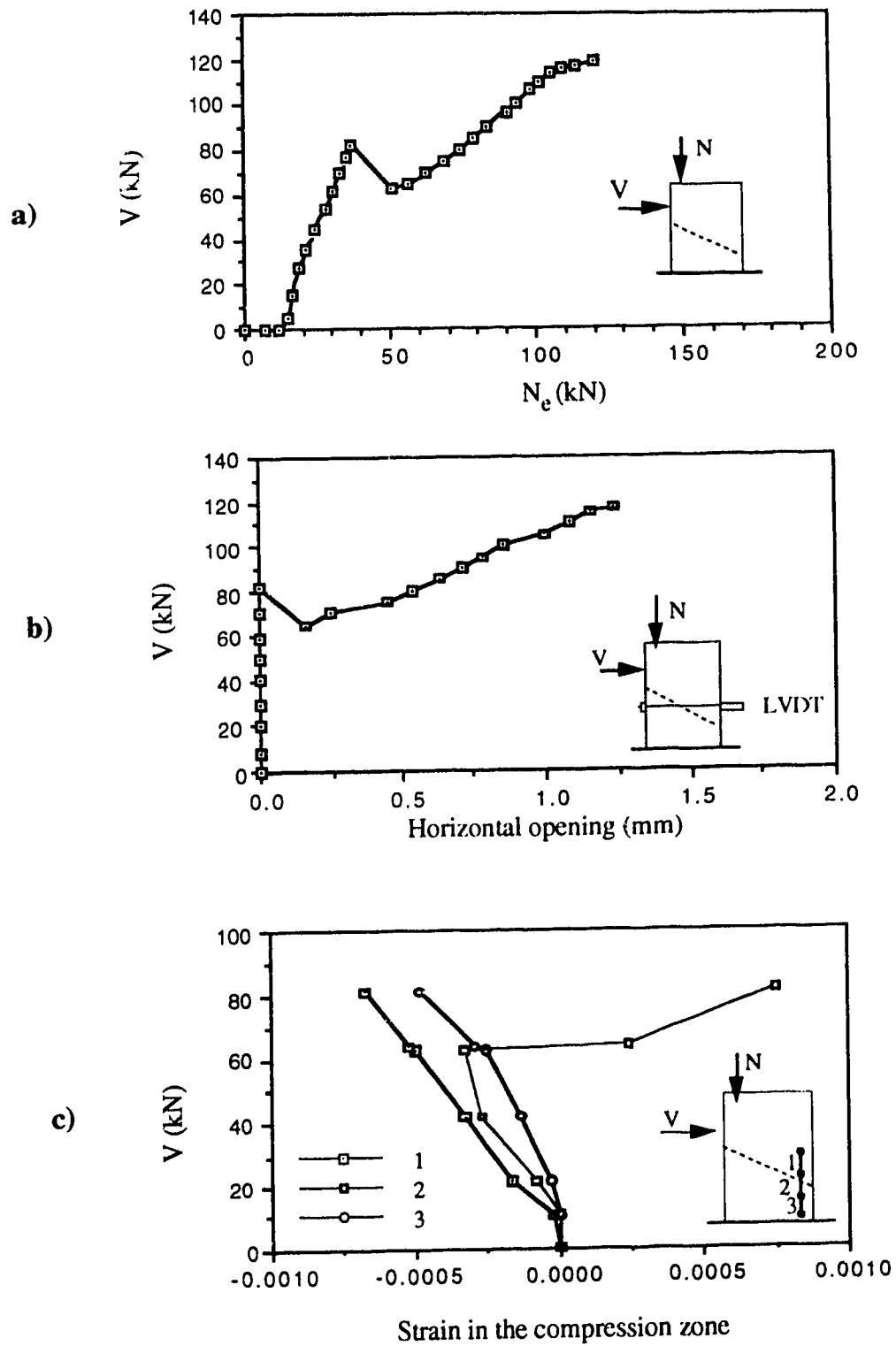


a) Specimen S6



b) Specimen S6

Figure 4.13 Load vs. strain in the compression zone for specimen S6 and s7



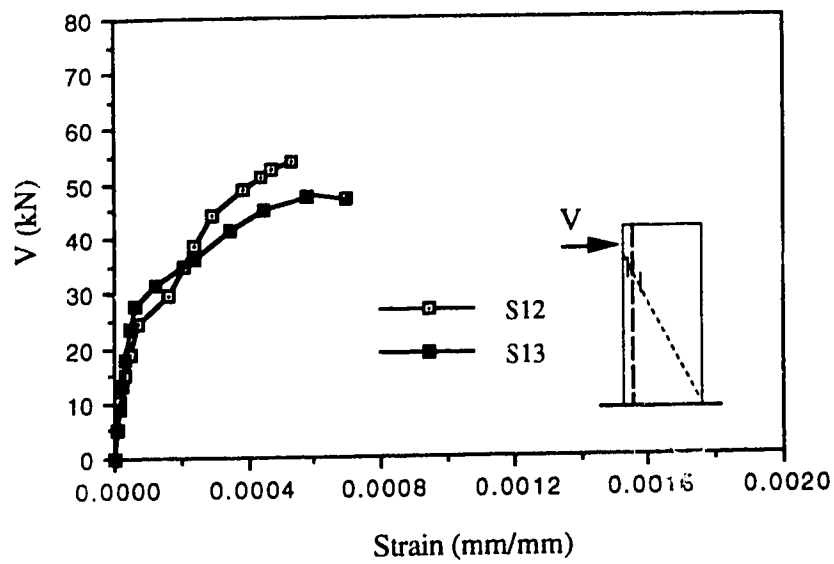


Figure 4.15 Load vs. steel strain for specimens S12 and S13;

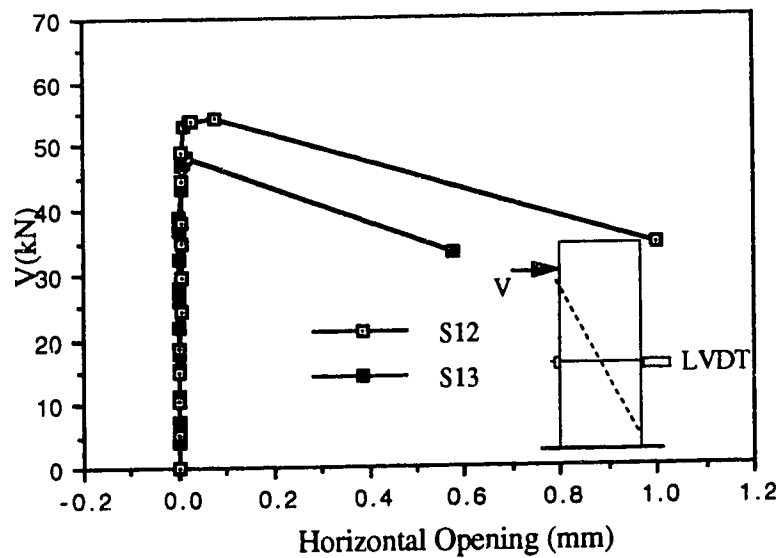
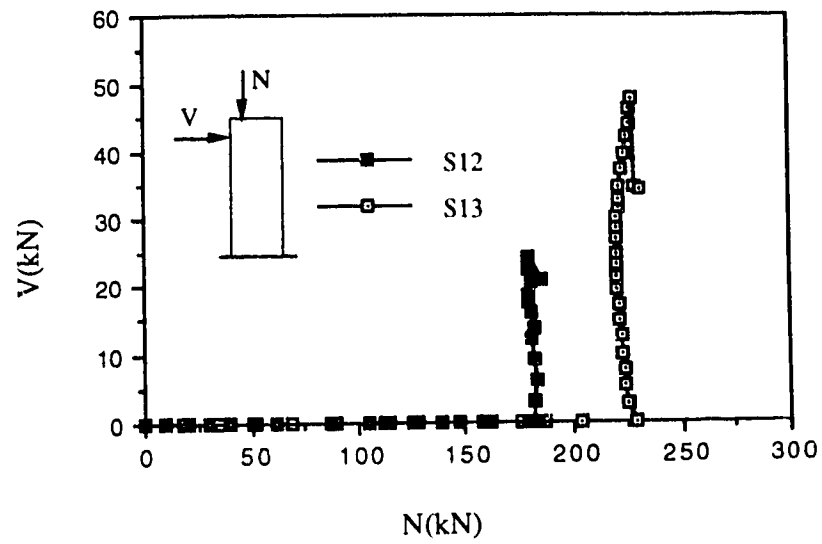
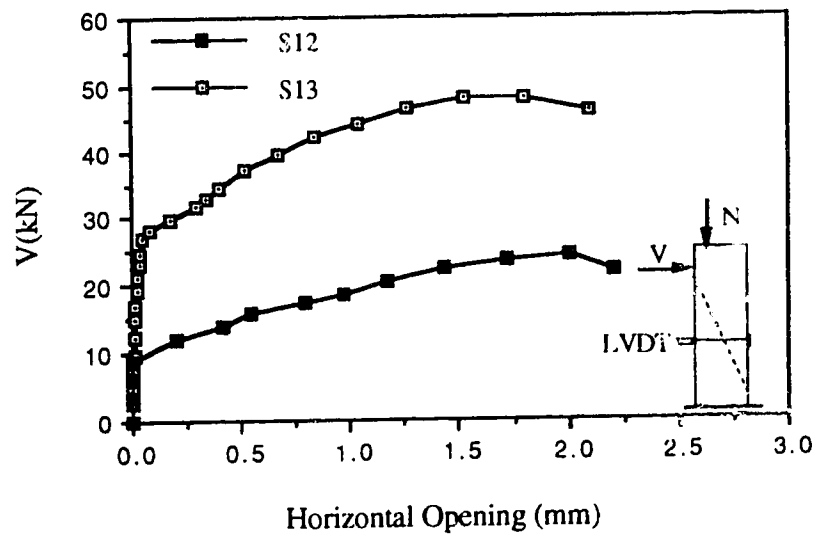


Figure 4.16 Load vs. horizontal relative movement of the two crack faces, S12 and S13

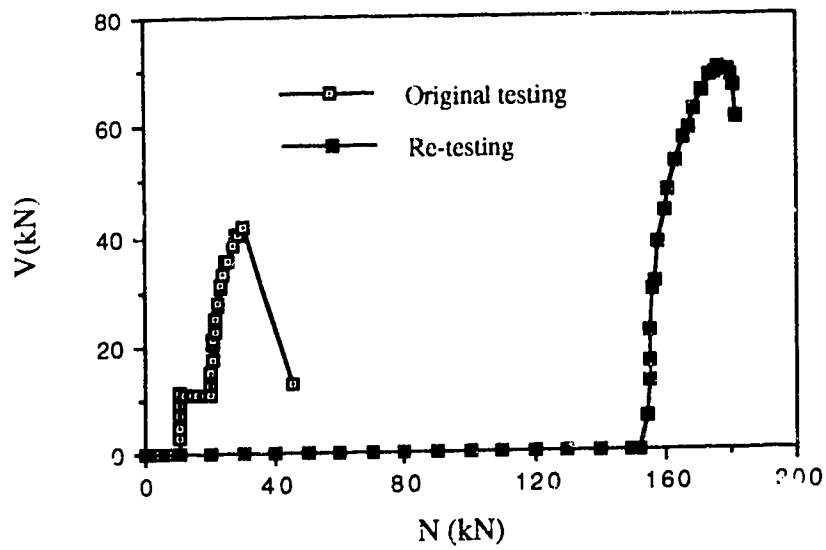


a) Load paths

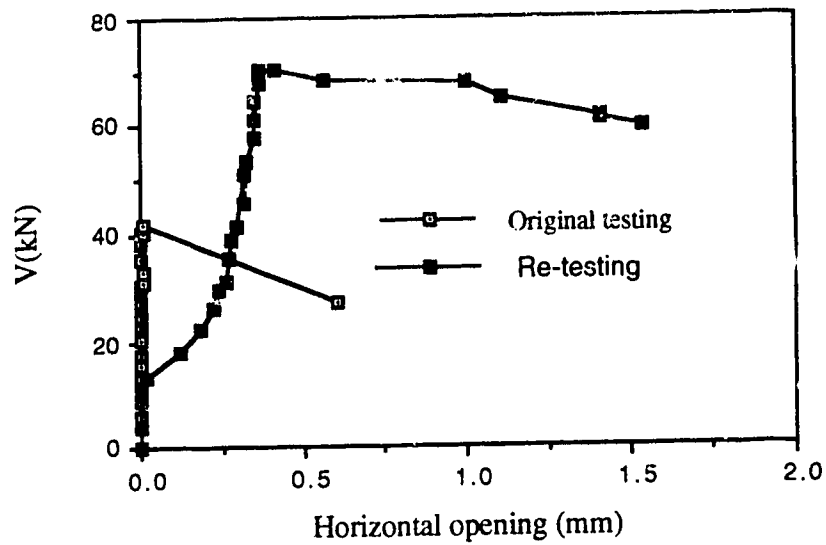


b) Load vs. horizontal opening of the crack

Figure 4.17 Re-testing of specimens S12 and S13



a) Load paths



b) Load vs. horizontal opening of the crack

Figure 4.18 Test result of specimen S14

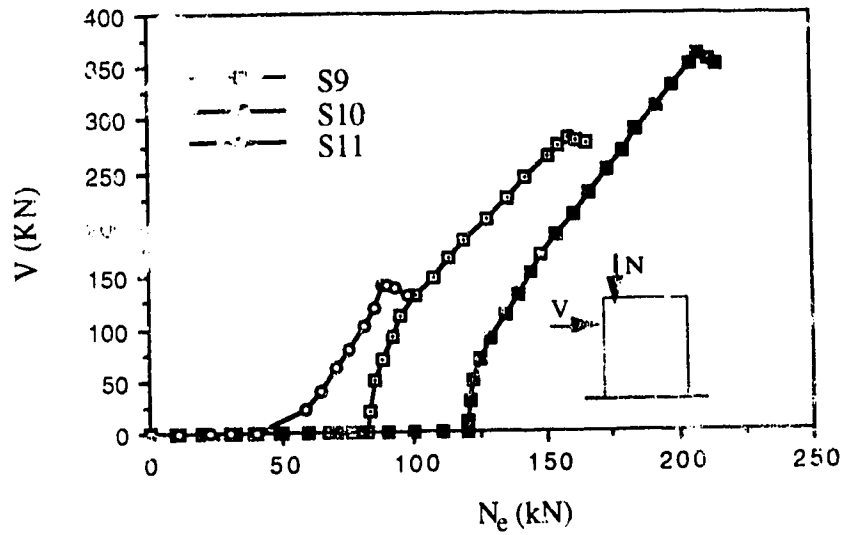


Figure 4.19 Load history, S9, S10 and S11

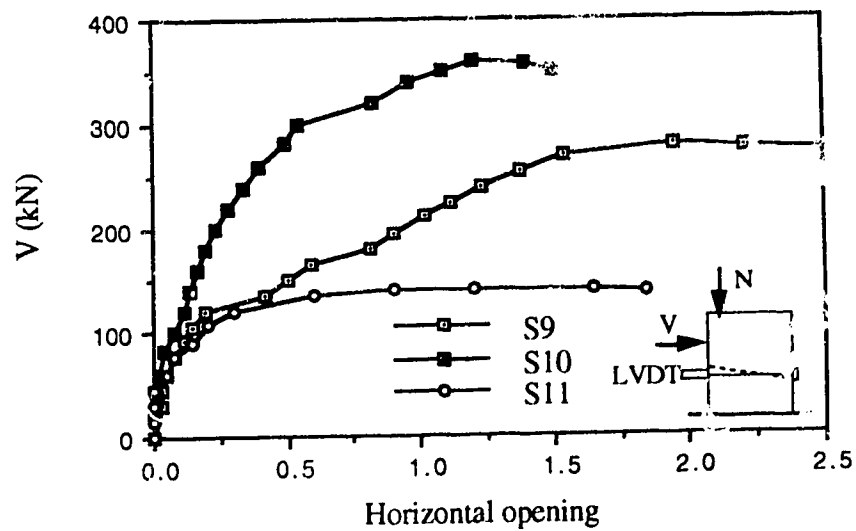
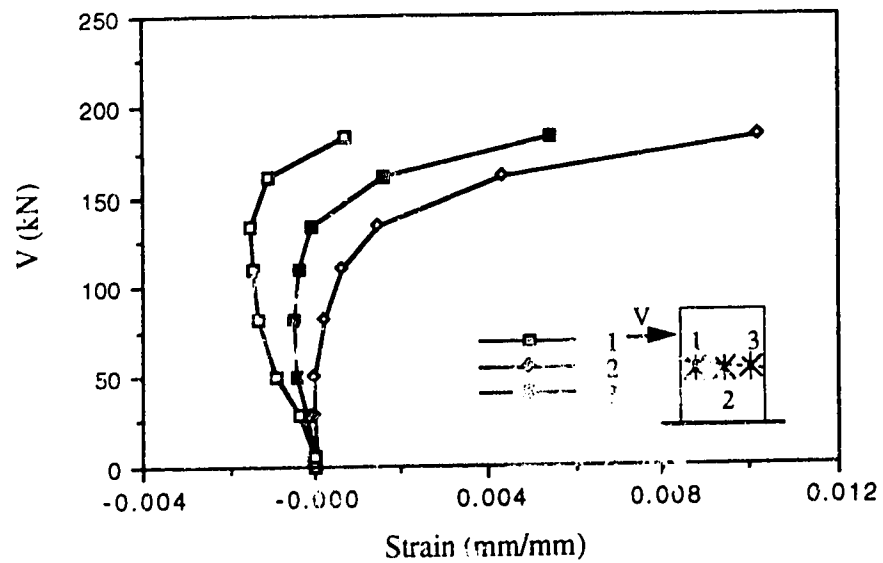
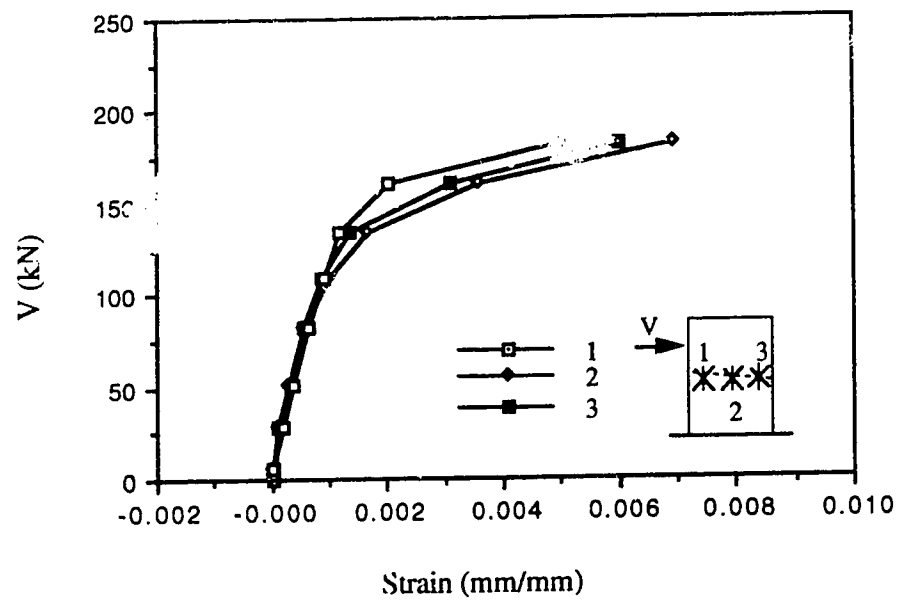


Figure 4.20 Load vs. horizontal relative of the two crack faces, S9, S10 and S11

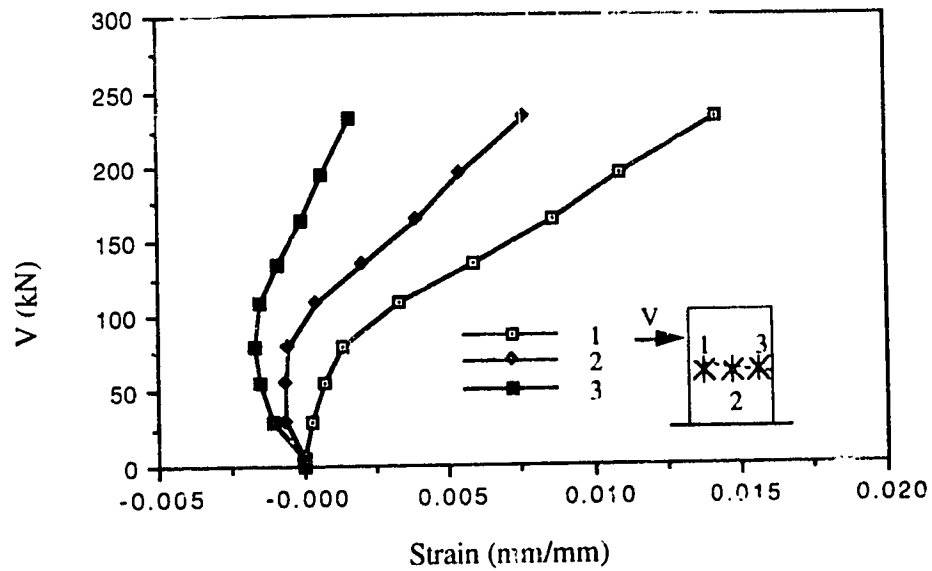


a) Strain perpendicular to the crack

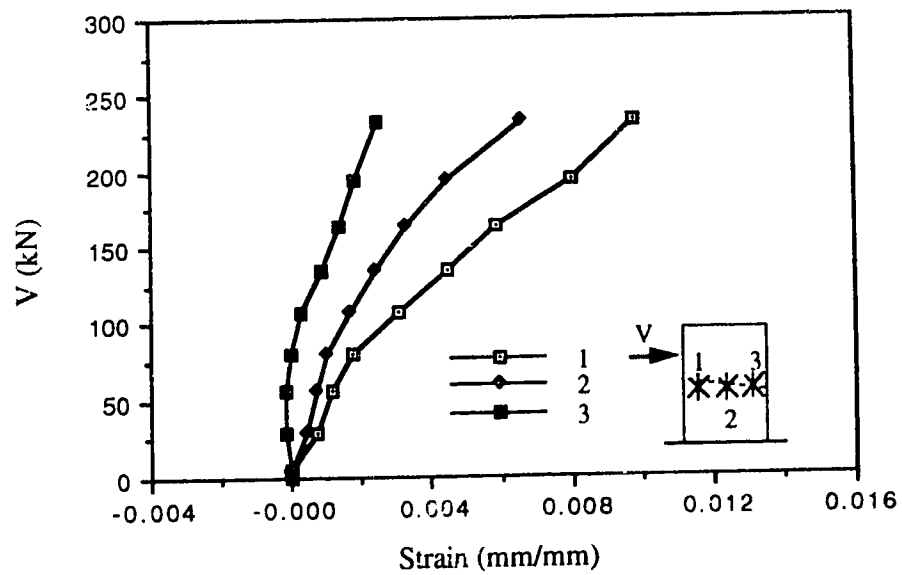


b) Strain parallel to the crack

Figure 4.21 Load vs. strains measured across the crack, S9

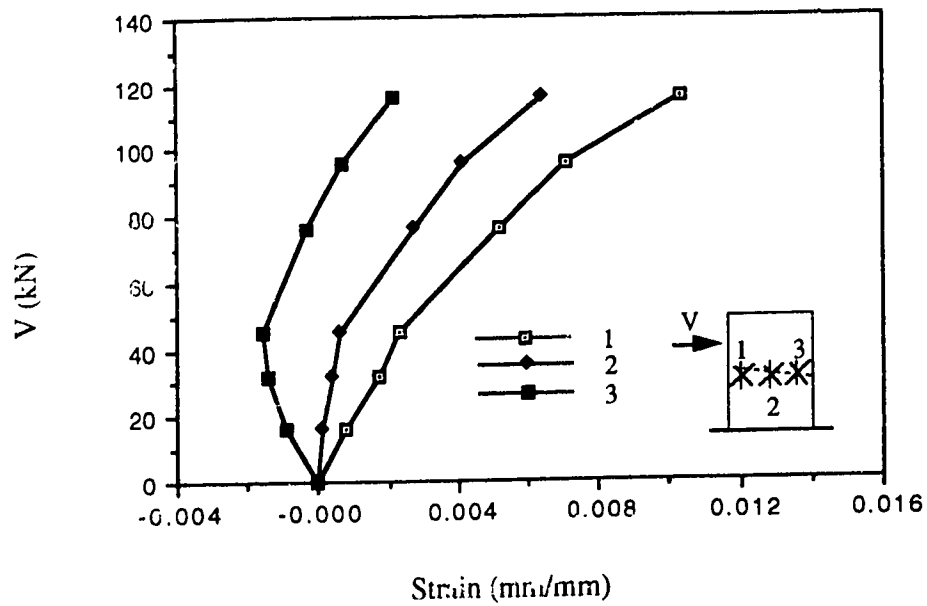


a) Strain perpendicular to the crack

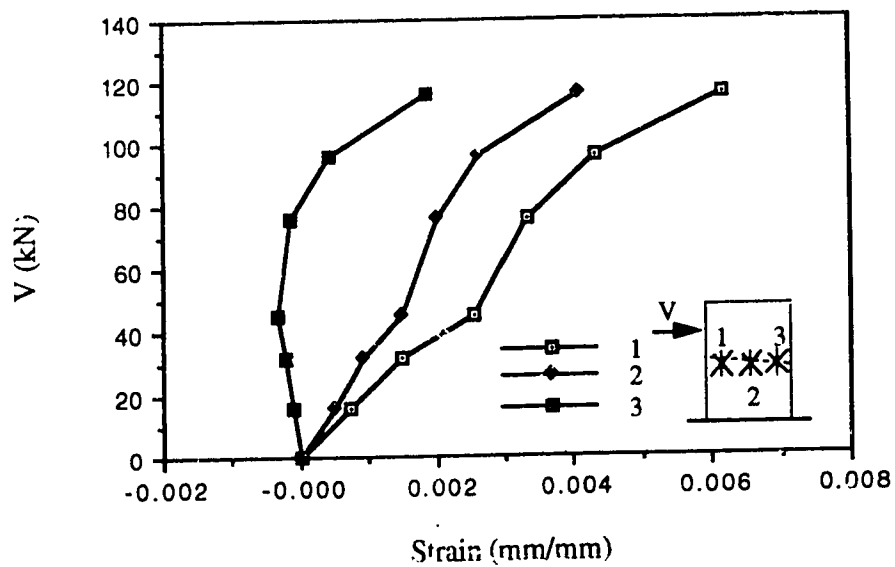


b) Strain parallel to the crack

Figure 4.22 Load vs. strains measured across the crack, S10



a) Strain perpendicular to the crack



b) Strain parallel to the crack

Figure 4.23 Load vs. strains measured across the crack, S11

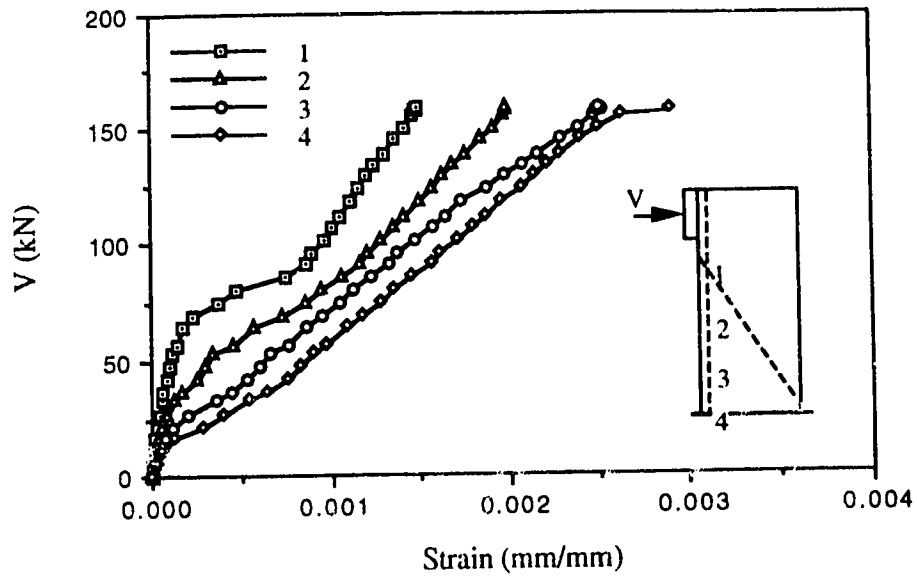


Figure 4.24 Strain in the longitudinal reinforcement, S16;

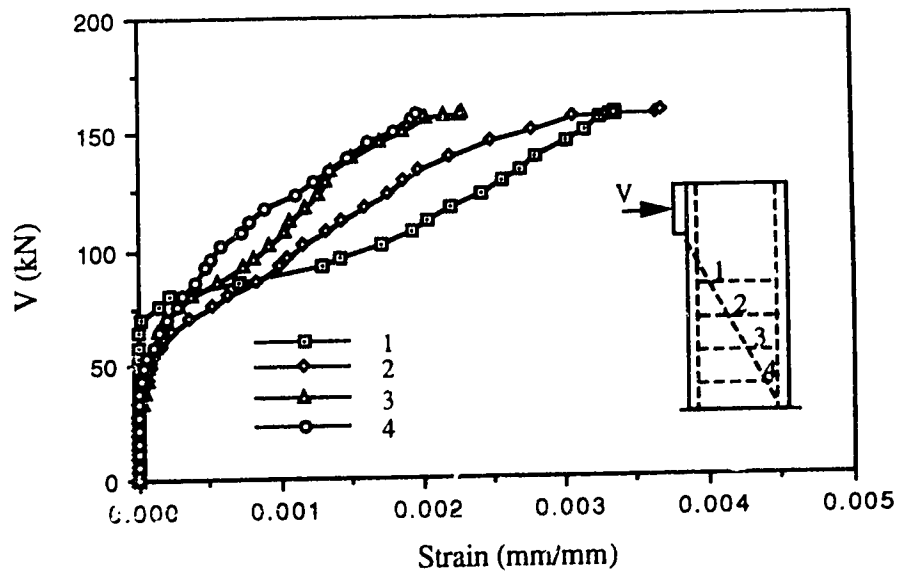


Figure 4.25 Strain in the stirrups, S16

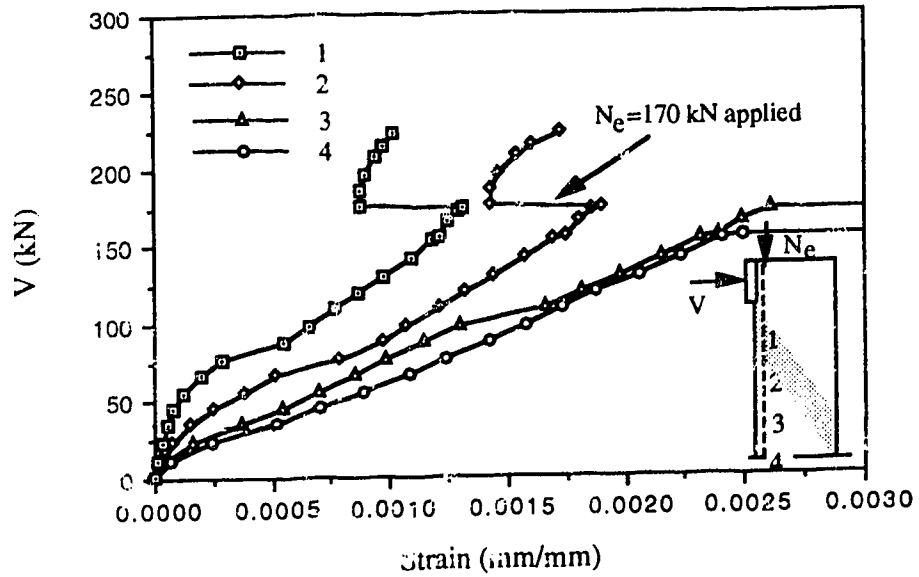


Figure 4.26 Strain in the longitudinal reinforcement, S15

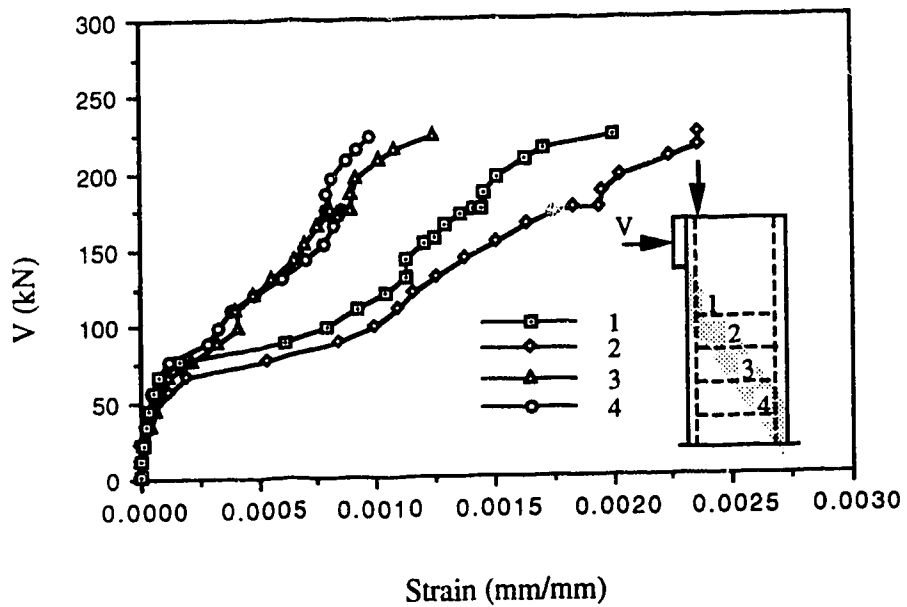


Figure 4.27 Strain in the stirrups, S15

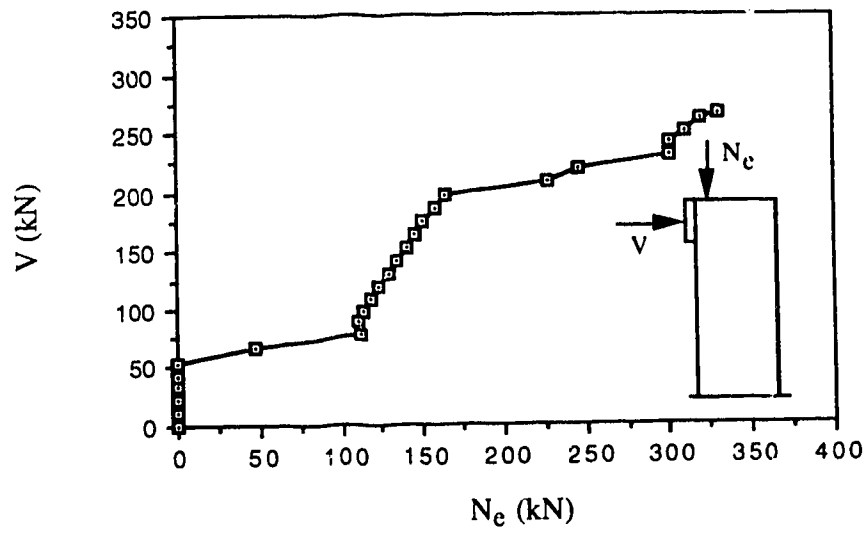


Figure 4.28 Load history, S17

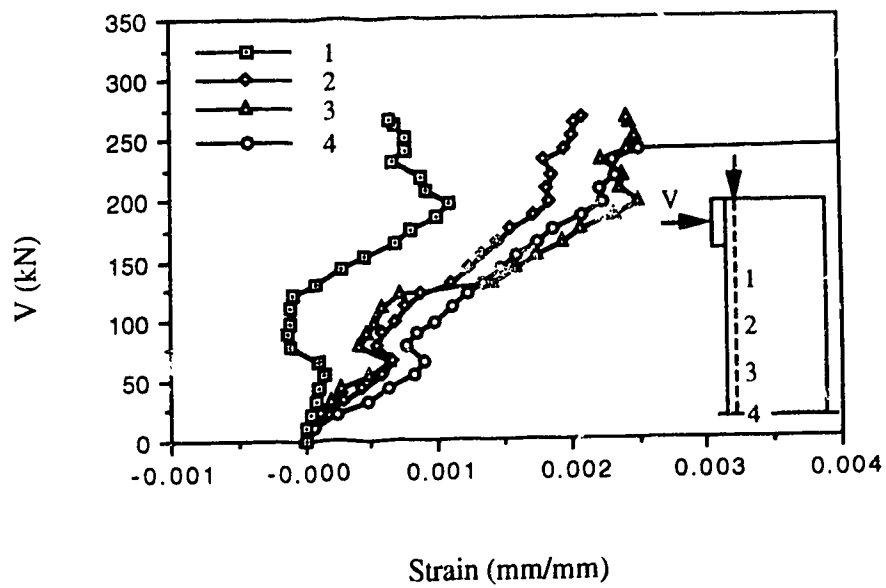


Figure 4.29 Strain in the longitudinal reinforcement, S17

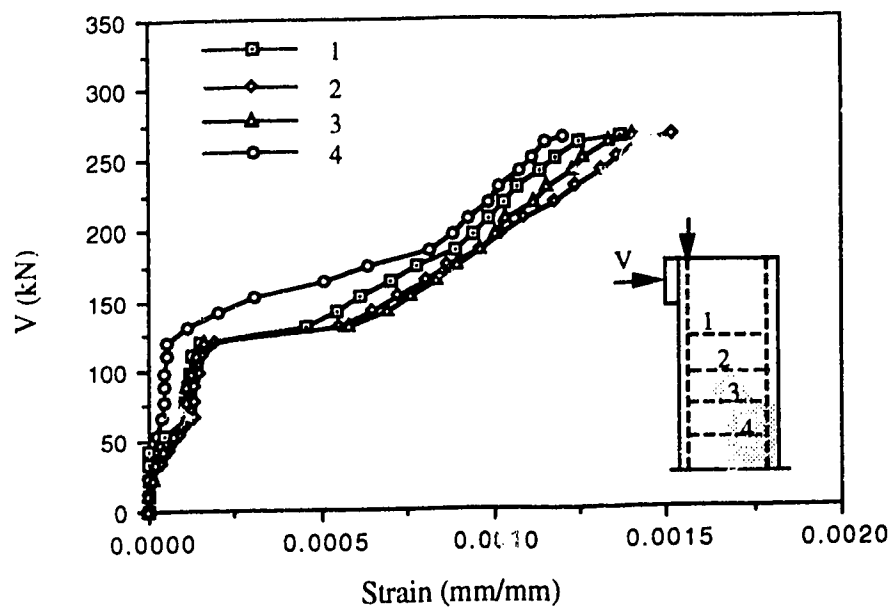


Figure 4.30 Strain in the stirrups, S17

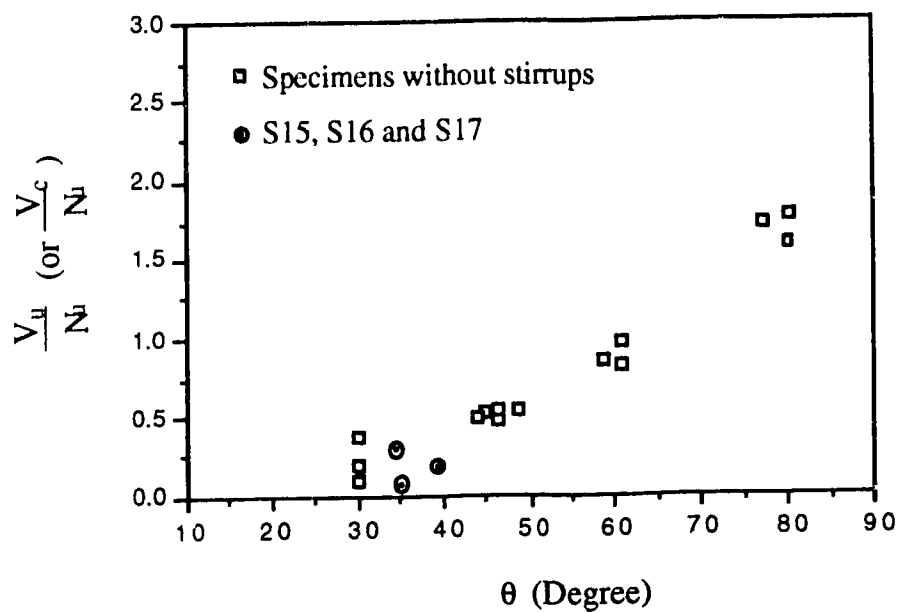


Figure 4.31 The relationship between $\frac{V_u}{N_u}$ and θ

5. THE SHEAR-FRICTION TRUSS MODEL

5.1 Introduction

This chapter deals with the development of the shear-friction truss model. This model is based on the dry friction law for rigid bodies and the traditional truss model for reinforced concrete beams. The contribution of the concrete to the shear strength is modelled using the shear-friction method while the shear contribution of the stirrups is represented using the truss model. By combining the two analogies a detailed computational approach is developed. The coefficient of shear-friction is calculated from the shear-friction tests presented in Chpt. 4.

The shear-friction truss model is used to analyze the well known test series by Bresler and Scordelis⁴⁻⁶ and very good results are achieved. The application of the model is extended into the calculations of shear strength of reinforced concrete beams with axial load, prestressed concrete beams and deep beams loaded indirectly.

5.2 The Internal Forces in a Cracked R/C Beam

The forces transferring shear and bending moment across an inclined crack are illustrated in Fig. 5.1a. N and V_s are the tensile forces in the longitudinal reinforcement and the stirrups respectively; V_d is the dowel force in the longitudinal reinforcement; f_c is the compressive stress distributed on the uncracked

compression zone and f_d is the compressive stress distributed on the crack plane. As observed from the shear-friction tests which are described in Chpt. 4, the two faces of an inclined crack experienced relative sliding and rotation. The stresses on the crack plane are caused by the relative movement between the two crack faces. The magnitude and the direction of the stresses on the crack plane change from point to point along the crack because the relative movement changes from point to point. At the uncracked compression zone the concrete is in high compression. The direction of the compressive force resultant is almost horizontal. This force is the major part of the force required to equilibrate the tensile force in the longitudinal tension reinforcement and the two act together to form the resisting moment. In the crack underneath the uncracked compression zone, two events occur simultaneously. The magnitude of stress decreases and its direction becomes more vertical as the point under consideration gets closer to the longitudinal tension steel. Figure 5.1b shows the resultant of f_c and f_d (F_c and F_d) together with the forces in the steels. In Fig. 5.1c F_c and F_d are expressed in their components in the horizontal and vertical direction. The vertical component of F_d , F_{dy} , is commonly referred to as the shear contribution of the aggregate interlock action. The vertical component of F_c , F_{cy} , is called the shear contribution of the uncracked compression zone. According to Fig. 5.1c the shear transferred across the inclined crack can be written as:

$$V = V_s + F_{cy} + F_{dy} + V_d \quad (5.1)$$

As shown in Fig. 5.1c, the points of action of the vertical force components are spread along the inclined crack. V_d is applied at the longitudinal reinforcement and F_{cy} is located at the uncracked compression zone. The point of action of V_s is in the lower portion of the crack but F_{dy} acts at the upper portion of the crack, both because of the non-uniform crack width. As a result the overall resultant of V_s , V_d , F_{cy} and F_{dy} is located around the midpoint of the inclined crack plane. For simplicity, the following assumption is made for the internal forces on the crack plane:

Assumption 1: The overall resultant of the shear resistance components, $(V_s + V_d + F_{cy} + F_{dy})$, is assumed to act at the midpoint of the inclined crack plane.

Thus the forces in Fig. 5.1c can be simplified as shown in Fig. 5.2, where V_c is the sum of F_{cy} , F_{dy} and V_d . V_c is commonly referred as to concrete contribution which is mainly attributed to the action of aggregate interlock along the inclined crack. C is the resultant of the longitudinal components of the compressions in the concrete, F_{cx} and F_{dx} , and is assumed to act in the compression zone. Thus Eqn. (5.1) becomes:

$$V = V_c + V_s \quad (5.2)$$

In Assumption 1 (as illustrated in Fig. 5.2), the shear resistance of the inclined crack, $(V_s + V_d + F_{cy} + F_{dy})$, is assumed acting at the midpoint of the inclined section. This is accomplished by moving the

points of action of V_s and V_d to the right and moving the points of action of F_{cy} and F_{dy} to the left. As a result both the concrete contribution, ($V_c = V_d + F_{cy} + F_{dy}$) and the steel contribution, V_s , are assumed to act at middle of the inclined interface. However the resultant of the horizontal forces, F_{cx} and F_{dx} , is assumed to act at the compression zone.

The shear-friction truss model developed in this chapter is based on the traditional truss model. According to the truss model, the section of a beam shown in Fig. 5.3 can be divided into three parts, each assumed to have a different function in resisting the applied load. The top element (part 1), including the concrete and the longitudinal compression steel, if any, is assumed to resist only the longitudinal compressive force. The bottom element (part 3), including only the longitudinal tension steel, is assumed to resist the longitudinal tensile force. The web (part 2) includes the stirrups and the web concrete, and, is assumed to be cracked with a series of inclined cracks at an angle θ to the longitudinal axis. The web resists the shear through diagonal compression in the concrete, tension in the stirrups and shear-friction across the cracks. The equilibrium equations for the truss system considering the concrete contribution are

$$V = V_c + V_s \quad (5.3),$$

$$C = N = 0.5N_v \quad (5.4),$$

and
$$N_v = V \cot \theta \quad (5.5)$$

The truss system shown in Fig. 5.3 has the same equilibrium equations as those for the traditional truss model except that in the traditional truss model the shear capacity is only from the stirrups.

5.3 Shear Friction Analogy

The shear force transferred across an interface of two rigid bodies, as shown in Fig. 5.4a, can be calculated by the dry friction law stated as following:

Dry Friction Law: The limiting static friction force is directly proportional to the magnitude of the normal force N , and is independent on the area in contact.

The dry friction law can be expressed in terms of forces as:

$$V = \mu_s N \quad (5.6)$$

where V is the maximum shear force transferred across the interface, N is the normal force on the interface and μ_s is the coefficient of static friction.

In Fig. 5.4a, the applied compressive force N is perpendicular to the friction interface while the shear force V is parallel to the friction interface. For the case of an inclined interface as shown in Fig. 5.5a, the applied longitudinal compression force N and the transverse tension force V can be transformed into the forces in the directions parallel and normal to the inclined surface, as shown in Fig. 5.6. They are given by Eqns. (5.7) and (5.8) respectively.

$$N_{\theta} = N \sin \theta - V \cos \theta \quad (5.7)$$

$$V_{\theta} = N \cos \theta + V \sin \theta \quad (5.8)$$

According to the dry friction law, the relationship between V_{θ} and N_{θ} is:

$$V_{\theta} = \mu_s N_{\theta} \quad (5.6)$$

Substituting Eqn. (5.7) and (5.8), Eqn. (5.6) is re-written as

$$V = \mu_{\theta} N \quad (5.9)$$

where μ_{θ} is referred to as the coefficient of friction of an inclined interface at angle θ and is expressed as:

$$\mu_{\theta} = \frac{\mu_s - \cot \theta}{1 + \mu_s \cot \theta} \quad (5.10)$$

The characteristics of the shear transferring mechanism in a cracked concrete beam without stirrups is very similar to that of dry friction. First, both cases have the same force actions on the interface. Figure 5.4b shows the internal forces at a cracked cross section of a concrete beam. The beam has the same free body diagram as that in the dry friction example, except that in the friction interface the normal compressive force is an external force while in the cracked plane of the reinforced concrete beam it is due to the tension in the reinforcement. In both cases the applied shear force is resisted by the shear stresses distributed on the portion of the interface in compression.

Figure 5.5 shows examples of inclined interfaces. Both the inclined dry friction interface and the inclined crack plane of the concrete beam have the same force actions. For equilibrium both horizontal and vertical forces are developed on the interface or on the crack plane to resist the applied load, except that in the dry friction interface the compression is due to the applied force N , while on the crack face of the beam is due to the tension in the reinforcement.

Second, both the dry friction force on the interface of rigid body and the concrete shear contribution in a concrete beam increase as the longitudinal compressive force on the interface increase. In dry friction, the shear force, V , is resisted by the friction on the interface and V is directly proportional to the magnitude of the normal force N . In a reinforced concrete beam, the shear force, V_c , is resisted by the aggregate interlock action on the crack plane, the shear force in the uncracked compression zone and the dowel action of the longitudinal reinforcement. According to the test results presented in Chpt. 4, the aggregate interlock action is the major contribution among the three actions which increased as N increased.

The aggregate interlock action is a friction action on the rough crack plane and, therefore, it increases as the compression force on the crack increases. The shear transferred by the uncracked compression zone increases as the area of the compression zone increases. The area of the compression zone increases as the compression on it increases. As a result, the shear transferred by

the uncracked compression zone increases as the compression force increases. The dowel action increases as the area of the longitudinal reinforcement increases. Since the longitudinal reinforcement in a beam is required to equilibrate the compression in the concrete, the dowel action increases as the compression force in the concrete increases.

Third, both the transverse shear transferred across an inclined crack by dry friction and the shear transferred across an inclined crack by the concrete contribution in a beam increase as θ increases. The relationship of V vs. N for dry friction is expressed by Eqn. (5.9) and (5.10). The manner in which V_c increased with θ is shown in Fig. 4.31 for the 17 test specimens.

Based on the above argument, the following assumption is made to describe the relationship between the concrete contribution, V_c , and the longitudinal compression force in the concrete, N .

Assumption 2: The shear contribution of the concrete, $V_c = F_{dy} + F_{cy} + V_d$, is directly proportional to the magnitude of the longitudinal compression on the concrete.

Assumption 2 is expressed as

$$V_c = \beta_\theta N \quad (5.11)$$

where β_θ is the equivalent coefficient of shear-friction across an inclined crack plane in concrete, N is the longitudinal compressive

force on the concrete. β_θ is a function of the angle of inclination of the crack plane under consideration.

5.4 The Equivalent Coefficient of Shear Friction of Concrete

According to the test results presented in Chpt. 4, the ratio of V_c/N_{\perp} , which is defined as the coefficient of shear-friction across an inclined crack plane of concrete in Sec. 5.3, increased as the angle of the inclined crack increased. The test results shown in Fig. 4.31 suggests that a similar formulation to Eqn. (5.10) can be used to express the relationship of V_c/N vs. θ , i.e.

$$\beta_\theta = \frac{V_c}{N} = \frac{\beta_0 - \cot\theta}{1 + \beta_0 \cot\theta} \quad (5.12)$$

where β_0 is referred, in this thesis, as to equivalent coefficient of shear-friction corresponding to $\theta=90^\circ$. β_0 is not a real coefficient of friction but rather it is the term defined by Eqn. (5.12). Figure 5.7 shows the test data from Chpt. 4 in the coordinate system of V_c/N and θ . The test data show that V_c/N increases as θ increases, varying from 0.17 for $\theta=30^\circ$ to 1.78 for $\theta=80^\circ$. In the same figure, curves of V_c/N vs. θ calculated using Eqn. (5.12) are also plotted. The figure indicates that for the specimens tested, β_0 is about 3.0. The mean value of V_c/N calculated from the test results using $\beta_0=3.0$ is 1.04 and the standard deviation is 0.23.

Tests have been carried out by Mattock^{21,22}, Paulay^{19,20} and others, using the pushoff or pull-off specimens of the general configuration shown in Fig. 2.12a. The tests indicate that the

coefficient of friction (V/N) is from 1.4 to 1.7. The ACI Code uses $\mu=1.4\lambda$ for concrete placed monolithically and $\mu=1.0\lambda$ for concrete placed against hardened concrete with the surface intentionally roughened, where λ relates to lightweight concrete. These numbers are very different from $\beta_o=3.0$. The explanations for this are given in the following paragraphs.

$\beta_o=3.0$ is calculated by fitting Eqn. (5.12) to the data of the 17 specimens. The actual angles of the inclined crack interface for the 17 tests were from 30° to 80° . As shown in Fig. 5.7, the curve of Eqn. (5.12) is very steep in the range from 80° to 90° , while the data points near $\theta=80^\circ$ is flatter. Hence, Equation (5.12) using $\beta_o=3.0$ may not be applicable for $\theta>80^\circ$. Thus, $\beta_o=3.0$ is not a coefficient of shear-friction for a crack interface with $\theta=90^\circ$. $\beta_o=3.0$ itself is not comparable with $\mu=1.4$ to 1.7 from the tests of pushoff specimens in which $\theta=90^\circ$. Actually, the value of $\beta_\theta=V/N$ for the two specimens with $\theta=80^\circ$ (S9 and S11) was 1.778 and 1.602 which were only a little larger than that from the pushoff tests.

As observed from the shear-friction tests described in Chpt. 4, it is not possible to form a crack with $\theta=90^\circ$ under shear forces. Thus in the Mattock and Paulay tests, the interfaces parallel to the load were precracked using a line load along the interface. As discussed in Sect. 2.5.2, the shear transfer mechanism of the pre-cracked interface in the push-off specimens is very different from that of the inclined crack in a reinforced concrete beam. The later has much stronger shear transfer mechanism than the former. For the specimens with monolithic interfaces tested by Mattock and Paulay,

the actual interfaces were a series of cracks at an angle with the applied shear forces. Considering the effect of the angle between the shear force and the crack (as described by Eqn. 5.9 and 5.10), μ_s is higher than $\mu_\theta = V/N$.

In the shear-friction tests presented in Chpt. 4, all the specimens had the same concrete strength and the same cross-section dimensions. The major variables were the angle of inclination of the crack, θ , and the confining force on the crack plane, N . However, according to the observations made during the tests, the failure of the shear transfer across the crack was associated with damage of the crack surface. In other words the failure is associated with a material failure of the crack surface. Therefore, the shear-friction capacity might be a function of the concrete strength and the area in contact. As the concrete strength and the area in contact increase, more and stronger projecting particles participate in shear-friction and as a result the capacity of the shear friction increases. Since the concrete strength and cross-section dimensions were not variables in the test series, their effects could not be mathematically determined from the test results.

Walraven²⁴ found in his study that the shear transferred by friction was directly proportional to $\sqrt{f'_c}$. The effect of cross-section dimensions on the shear contribution of concrete, V_c has been investigated experimentally by many researchers and has been written about in many text books. The shear contribution of concrete is a linear function of the cross-section dimensions (bd). By

adopting those research results, the coefficient of shear-friction in concrete may be assumed to be:

$$\beta_0 = \eta \sqrt{f'_c} bd \quad (5.13)$$

Substituting the values of β_0 , f'_c and bd from the tests, η is calculated to be 9.32×10^{-6} . The units in Eqn. (5.13) are mm^2 for bd , N for $\sqrt{f'_c}$, $1/\text{N}$ for η and non-dimensional for β_0 .

5.5 The Shear-Friction Truss Model

The shear-friction truss model is the combination of the shear-friction model based on Assumption 2 and the truss model based on Assumption 1. A free body diagram of the shear-friction truss model is illustrated in Fig. 5.3. The shear strength of the inclined crack plane of a reinforced concrete beam can be expressed as:

$$V = V_c + V_s \quad (5.14)$$

The first term on the right hand of Eqn. (5.14) is the concrete contribution which results from the action of shear-friction on the crack plane and is expressed as

$$V_c = \frac{\beta_0 - \cot\theta}{1 + \beta_0 \cot\theta} N \quad (5.15)$$

The second term is the contribution of the stirrups which are modelled as the tension ties in a truss. V_s is expressed as

$$V_s = \frac{A_v f_y d}{s \tan\theta} \quad (5.16)$$

The shear-friction truss model gives a very clear conceptual understanding of the shear resisting mechanism in a reinforced concrete beam. As in the traditional truss model, a reinforced concrete beam is divided into several components, each assumed to have a different function in resisting the applied load. The compression chord including the concrete and the longitudinal compression steel, if any, is assumed to resist the longitudinal compressive force. The tension chord, including the longitudinal tension steel, is assumed to resist the longitudinal tensile force. The diagonal compression struts consist of the concrete web which is cracked with a series of parallel cracks at an angle θ to the longitudinal axis. The stirrups act as the tension ties to transfer the transverse force from one diagonal compression strut to the adjacent one. In addition to the force transferred by the stirrups, shear-friction action between two adjacent diagonal struts is also assumed to transfer force between the diagonal compression struts. Figure 5.8 shows the force transferred across the crack between two struts. The force transferred by the shear-friction can be expressed either as the vertical force V_c acting midpoint of the crack (Fig. 5.8a) or as shear force V_{ci} parallel to the crack (Fig. 5.8b). The vertical force in Fig. 5.8a is induced by the longitudinal force N and is assumed calculated by Eqn. (5.15). In Sec. 5.1 it is explained that V_c and N do not act at the same point in the crack. In Fig. 5.8b part of the longitudinal compression in the crack plane is included in the shear force along the crack. As a result the longitudinal compression force,

C, is less than N and C acts at a point above that of the compression force N in Fig. 5.8a.

According to the shear-friction truss model model, the stirrups, or the transverse component of the reinforcement, transfer shear force directly by tension. The longitudinal reinforcement, or the longitudinal component of the reinforcement, has zero component in the direction of the transverse load but it indirectly transfers transverse load through the shear-friction action on the crack planes besides its function in resisting the flexural moment.

Figure 5.9 shows curves of V , V_c and V_s vs. θ . A non-dimensional coordinate, $V/(\frac{A_v f_y d}{s})$, is used for the vertical axis. As indicated by Eqn. (5.15), V_c increases as N increases. For a given section N, the force in longitudinal reinforcement at the critical inclined crack plane, is mainly due to bending moment. Generally, N is larger than $(\frac{A_v f_y d}{s})$. To discuss V_c , V_s and V as function of θ , N is taken equal to $2(\frac{A_v f_y d}{s})$ and $4(\frac{A_v f_y d}{s})$ respectively for illustration. The plots in Fig. 5.9 show how V_c , V_s and V change as the angle of inclination of the crack changes. The curves indicate that as θ increases, shear-friction on the crack plane becomes more efficient, and, as a result, V_c increases. But V_s decreases as θ increases because fewer stirrups are intercepted by a steep crack. As a result V , the sum of V_c and V_s , has a vertex with a minimum value. This value is the shear capacity of the beam and the corresponding θ is the critical angle of inclination. The inclined crack plane

corresponding to this θ is the weakest inclined crack plane on which the shear failure occurs. In a reinforced concrete beam, many cracks with various inclinations may be developed at the ultimate state, however, among all of these cracks only the crack with the inclination corresponding to the minimum V is the critical crack. This suggests shear failure will occur on a crack plane with a certain angle of inclination for a given beam.

The angle of inclination of the critical crack decreases as the horizontal force, N , increases. Figure 5.9 shows that θ is about 40° for $N=2(\frac{A_v f_y d}{s})$ and decreases to about 30° when N increases to $4(\frac{A_v f_y d}{s})$. This phenomenon is in agreement with the equilibrium of the truss analysis where a flatter strut corresponds to a larger force in the longitudinal tension chord.

The shear friction approach in the shear-friction truss model is different from the shear friction method developed by Crist²⁵ and the shear friction approach proposed in the ACI Code²⁶. In both the Crist and ACI shear friction methods, the goal of the shear transfer across a crack is to transfer a force parallel to the crack plane. Therefore, all the reinforcement is involved in fulfilling this goal. However, in a reinforced concrete beam the shear force is usually not parallel to the crack. In the shear-friction truss model, the goal of the shear transfer across a crack plane is to transfer transverse shear force which has a angle of $(90^\circ - \theta)$ to the crack plane. Figure 5.10 illustrates the applications of the three shear-friction models to

an inclined crack plane. According to Crist's shear-friction method the sole function of the shear reinforcement, including the vertical and the horizontal, is assumed to induce a normal compressive force on the crack plane and then to mobilize shear friction along the crack plane. In his shear-friction method, the component of the tensile force in the reinforcement parallel to the crack plane is neglected. The ACI shear-friction method is similar to Crist's shear-friction method but takes into account the component of the tensile force in the reinforcement parallel to the crack plane. In the shear-friction truss model, only the longitudinal reinforcement, or the horizontal component of the reinforcement, is assumed to be involved in the shear-friction action. The vertical reinforcement, or the vertical component of the reinforcement, is assumed to transfer the vertical shear force directly as the tension ties in a truss. For a reinforced concrete beam, if the reinforcement consists of vertical and horizontal reinforcement and the crack plane has an inclination of θ to the beam axis, the shear strength of the beam according to the three models is shown in Fig. 5.10 and expressed as follow:

$$V = \frac{A_v f_y d}{s} \left(\frac{1}{\tan \theta} \right) + \frac{A_h f_s d}{s_h} \left(\frac{\beta_0 - \cot \theta}{1 + \beta_0 \cot \theta} \right) \quad \text{SFTM} \quad (5.17)$$

$$V = \frac{A_v f_y d}{s} (\mu \cos^2 \theta) + \frac{A_h f_y d}{s_h} (\mu \sin^2 \theta) \quad \text{Crist's model} \quad (5.18)$$

$$V = \frac{A_v f_y d}{s} (\mu \cos \theta + \sin \theta) + \frac{A_h f_y d}{s_h} (\mu \sin \theta)$$

ACI shear-friction method (5.19)

In the above equations A_v is the area of vertical reinforcement within a horizontal distance s and A_h is the area of horizontal reinforcement within a vertical distance s_h . For the shear-friction truss model A_h includes all the horizontal reinforcement across the section under consideration and it has an average stress of $f_s \leq f_y$. For the other two shear-friction methods, A_h is only the horizontal shear reinforcement and it is assumed to yield at the failure. Equation (5.17) indicates that the shear contribution of the vertical reinforcement is equal to the force in the reinforcement intercepting the crack under consideration, which is not associated with the coefficient of shear-friction. In Eqns. (5.18) and (5.19) the contribution of the vertical reinforcement is associated with the coefficient of friction, which is not true because the vertical reinforcement acts as the vertical ties of truss. The Crist's shear-friction model and the ACI shear-friction method conflict with the well accepted truss models when applied in reinforced concrete beams.

5.6 The Computational Approach of Shear-Friction

Truss Model

According to the shear-friction truss model, the shear strength of a reinforced concrete beam can be expressed as:

$$\begin{aligned}
 V &= V_c + V_s \\
 &= \frac{\beta_0 - \cot\theta}{1 + \beta_0 \cot\theta} N + \frac{A_v f_y d}{s \tan\theta}
 \end{aligned}
 \tag{5.20}$$

Equation (5.20) indicates that as θ increases, shear-friction on the crack plane becomes more efficient, and, as a result V_c increases. But V_s decreases as θ increases because fewer stirrups are intercepted by a steep crack. As a result V , the sum of V_c and V_s , has a vertex with a minimum value. The value of θ corresponding to the vertex is the critical angle of inclination at which the inclined crack plane has the lowest shear transfer capacity and failure occurs at this crack. Thus the critical angle of inclination can be calculated by solving the derivative equation:

$$\frac{\partial V}{\partial \theta} = 0 \quad (5.21)$$

In Eqn. (5.20) N is the horizontal compression on the crack plane and is mainly due the bending moment, although the shear causes some additional force according to the truss model. Thus, N is assumed to be a function of the flexural moment at the section under consideration rather than the angle of the inclined crack plane. Substituting Eqn. (5.20) to Eqn. (5.21) gives:

$$\tan \theta = \frac{\beta_o}{\sqrt{(1+\beta_o^2) \frac{N}{(\frac{A_v f_y d}{s})} - 1}} \quad (5.22)$$

Equation (5.22) indicates that at a section with the compressive force N in concrete, if shear failure occurs, the critical angle of the crack is a function of the coefficient of shear-friction β_o and the ratio of N to $(\frac{A_v f_y d}{s})$ at the crack plane under consideration.

At shear failure, the vertical reinforcement usually yields and V_s is equal to $(\frac{A_v f_y d}{s \tan \theta})$ as expressed in Eqn. (5.20), however the horizontal reinforcement may not yet have yielded at sections in the shear span. Thus Eqns. (5.20) and (5.22) include three unknowns: V , N and θ . The shear strength can be calculated if either θ or N is known. Thus, either N or θ should be assumed in calculating the total shear strength. Usually θ is assumed in design.

By assuming θ , N is calculated from Eqn. (5.22) and V_c , V_s and V are calculated from Eqn. (5.20). This procedure involves solving two nonlinear equations. To simplify the procedure, a calculation chart is established in Fig. 5.11. Since the equivalent coefficient of shear-friction might not be a constant but a function of the concrete strength and the dimension of the beam section as expressed by Eqn. (5.13), the curves in the chart correspond to a range of values of β_o from 0 to 5. The curve with $\beta_o=0$ corresponds to the shear transferred by the stirrups only, which is calculated by the truss model. The difference between the curve with $\beta_o=0$ and the non-zero β_o curves is the concrete contribution. Thus, for a given β_o and θ , the total shear strength, the steel contribution and the concrete contribution can be determined from the chart. In Sec. 5.4 it was shown that $\beta_o=3.0$ gives best agreement with the tests reported in Chpt. 4.

Figure 5.11 shows that the contribution of reinforcement, V_s , decreases as θ increases because fewer vertical stirrups are intercepted by a steeper crack plane. The concrete contribution, V_c ,

is zero at a certain small θ since the inclined crack is too flat to mobilize shear friction.

5.7 Application of the SFTM to Tests by Bresler and Scordelis

The test series conducted by Bresler and Scordelis⁴⁻⁶ consisted of 34 simply supported reinforced concrete beams with one point load at the mid-span. Among the 34 beams, 7 were without stirrups and 27 were reinforced with stirrups. The objective of the tests was to investigate the behaviour and the strength of reinforced concrete beams in shear and the effects of bar cutoffs and bar size on the shear strength. The properties of the specimens and the test results were well defined and reported. Since the beams without stirrups cannot be modelled as a truss with vertical tension ties, only the 27 beams with stirrups are used in the analysis by the shear-friction truss model. Table 5.1 lists the properties and the test results of the 27 beams which are used in the analysis in this chapter. The crack patterns and failure modes are shown in Appendix C

For all the specimens, the cracks where shear failure occurred were well defined by their size. For most of specimens the failure cracks were close to straight overall and the angle of inclinations are well defined. For those specimens with an overall curved failure crack the angle of inclination is defined according to the truss model. In the truss model, the angle of the crack is used to calculate the number of the stirrups intercepting the crack. Thus the angle of the overall curved crack is defined as equal to the slope of the straight

line which links the two points where the critical crack intercepts the top and the bottom bars respectively, as shown in the crack patterns in Appendix C.

The predictions of the shear strengths of the test beams using the shear-friction truss model are listed in Table 5.2 together with the test results. The shear strengths are calculated using the calculation chart shown in Fig. 5.11. For a given angle of inclination, θ , and a given equivalent coefficient of shear friction, β_o , the corresponding value of $V/(\frac{A_v f_y d}{s})$ can be found in the chart and then the shear strength, V , can be calculated from the given $(\frac{A_v f_y d}{s})$.

The predictions using $\beta_o=3.0$ are listed in Table 5.2 and shown schematically in Fig. 5.12a. For the beams examined, the shear-friction truss model using $\beta_o=3.0$ safely estimates the shear strength for all but 3 beams. The mean V^t/V^{cal} ratio is 1.24 with a standard deviation of 0.25 and $v=0.202$. The ratio ranges from 0.79 to 1.80. The effects of the concrete strength and the dimension of the section are two of the factors causing the deviation. For the beams examined, $\sqrt{f'_c}$ and b were variables but d remained constant. Figure 5.12b shows that the V^t/V^{cal} ratio increases as the ratio of $\sqrt{f'_c}b$ for the beams to that for the shear-friction specimens increases.

As discussed in the previous section, the concrete strength and the dimension of the beam cross section may effect the equivalent coefficient of shear-friction in concrete but they were not studied in the shear-friction experimental program. In Eqn. (5.13) the equivalent coefficient of shear-friction is considered to be a linear

function of $\sqrt{f'_c}$ and bd . The prediction using Eqn. (5.13) is also listed in Table 5.2 and schematically shown in Fig. 5.13. The mean V^t/V^{cal} ratio is 1.00 with a standard deviation of 0.14 and $v=0.14$. The V^t/V^{cal} ratio ranges from 0.74 to 1.29.

Although the predictions of the shear-friction truss model using the coefficient given by Eqn. (5.13) gives a little better results than that by $\beta_o=3.0$, the number of the examined beams is limited and the specimens were not full scale practical beams. The effects of concrete strength and cross section dimension on the coefficient of shear-friction still need to be studied. Thus $\beta_o=3.0$ is recommended for design.

The test results are also compared to the failure shears predicted by the existing ACI method with $\phi=1$ using Eqn. (2.7). The results are shown in Table 5.3 and plotted in Fig. 5.14. For the beams examined, the ACI shear design procedure safely estimates all the beams. The mean V^t/V^{cal} ratio is 1.25 with a standard deviation of 0.17 and $v=0.136$. The ratios ranges from 1.0 to 1.6. The safe predictions of the ACI procedure is expected partly because the actual angles of inclination of the critical cracks, ranged from 18° to 36° for the examined beams, are flatter than 45° , and, as a result the ACI procedure must have underestimated the shear contribution of stirrups. This is why the ACI procedure underestimates the strengths of beams with small θ more than for beams with large θ , as shown in Fig. 5.14. However, the ACI procedure gives a reasonably good estimate.

Table 5.3 also lists the prediction using the variable angle truss model given by Eqn. (2.11). The plot of V^t/V^{cal} ratio against θ is shown in Fig. 5.15. The actual angle of inclination of the critical cracks are used in the variable truss model. As a result the shear contribution of the stirrups, V_s , is accurately estimated. However, neglecting the concrete contribution in the variable truss model leads to an underestimation of the overall shear strengths. The ratio of V^t/V^{cal} ranges from 0.99 to 2.46. The mean value is 1.58 with a standard deviation of 0.33 and $v=0.209$.

The last two columns in Table 5.3 shows the comparisons of the test results to the predication by the following equation:

$$V = \frac{1}{6} \sqrt{f_c'} bd + \frac{A_v f_y d}{s \tan \theta} \quad (5.24)$$

The first term in Eqn. (5.24) is the concrete contribution adopted from the ACI procedure and the second term is the stirrup contribution taken from the variable truss model. Since the variable truss model using the actual angle of inclination of the critical crack can accurately estimate the shear contribution of the stirrups, the comparisons between the test results and the predictions by Eqn. (5.24) can examine the concrete contribution term in Eqn. (5.24). The data in the last two columns in Table 5.3 shows that Eqn. (5.24) overestimates the shear strength. The mean ratio of V^t/V^{cal} is 0.87 with a standard deviation of 0.08 and $v=0.114$. The ratio ranges from 0.70 to 1.06. The results are plotted in Fig. 5.16.

The unsafe mean value of 0.87 by Eqn. (5.24) indicates that the ACI concrete contribution term overestimates the concrete shear contribution of reinforced concrete beams with stirrups unless θ is taken as 45° . The over-estimation of concrete contribution is expected because the ACI concrete contribution term is the ultimate shear force of concrete beams without stirrups. For normal slender beams without stirrups the failures were caused due to the cracking in the concrete. The shear strength is mainly from the tension in the concrete. However, for the beams reinforced with stirrups, the ultimate state is a post-cracking state at which the concrete contribution is due to the shear-friction on the concrete plane. For a slender beam a flatter critical crack is usually expected and the shear contribution from the tension in concrete exceeds that due to the shear-friction. If no stirrups are provided the beam fails immediately after the critical crack develops, as observed in the shear-friction tests of the specimens with $\theta=30^\circ$. Thus the ACI concrete contribution developed from the concrete beams without stirrups overestimates the concrete contribution of beams with stirrups at failure if the observed θ is used to compute V_s . However the ACI steel contribution based on the 45° truss model underestimates the contribution from the stirrups. The over-estimation of the shear carried by the concrete offsets the underestimation of the shear carried by the stirrups and as a result the ACI procedure gives a reasonable good estimation of the overall shear strength.

Although the ACI procedure can predict the shear strength of a reinforced concrete beam with acceptable safety and accuracy, it does not give a clear conceptual understanding of the concrete contribution. The shear-friction truss model can predict the shear strength accurately and also gives a very clear understanding of the mechanism of shear contributions both from the concrete and the stirrups.

5.8 Design Procedure and Example

The shear-friction truss model can be used to design the stirrups of reinforced concrete beams by selecting a reasonable angle for the struts. As shown by the plots in Fig. 5.9, the minimum shear strength is relatively insensitive to θ as θ varies from 25° to 45° . As the selected angle of θ decreases the amount of stirrups required to resist a certain applied shear force decreases. However, according to Eqn. (5.5), the resulting longitudinal reinforcement required to resist the resulting longitudinal tension increases. This is usually an economical trade off.

Consistent with the CSA design code, the shear contribution from the concrete is factored by ϕ_c and the shear contribution of the stirrups is factored by ϕ_s . ϕ_c is equal to 0.6 and ϕ_s is equal to 0.85. Thus the shear-friction truss model for the design is:

$$V_f \leq V_c + V_s = \phi_c \frac{\beta_0 - \cot\theta}{1 + \beta_0 \cot\theta} N + \phi_s \frac{A_v f_y d_v}{s \tan\theta} \quad (5.25)$$

where V_f is the factored load. For a given θ , V_f , V_c and V_s can be calculated as a function of $\frac{A_v f_y d_v}{s}$ by solving the two nonlinear equation Eqn. (5.21) and (5.25). For simplification, a design chart is presented in Fig 5.17. By substituting the value of ϕ_c , ϕ_s and the recommended value of $\beta_o=3.0$ and solving Eqn. (5.21) and (5.25) the curve of $\frac{V_f}{\phi_s (\frac{A_v f_y d_v}{s})}$ vs. θ shown in Fig. 5.17 is obtained. This can be used as a design chart.

The procedure for the design of the stirrups in a reinforced concrete beam is described as follows.

1. Compute V_f , select trial b and d .

2. Choose value of θ : The value of θ can be chosen by the designer from 25° to 45° . As θ is made smaller, f_2 , the diagonal compressive stress due to the applied shear, becomes larger and as a result the web concrete may crush before the stirrups yield. Thus θ is limited by Eqn. (5.26).

$$V_f \leq \phi_c f'_{ce} b d_v \sin \theta \cos \theta \quad (5.26)$$

where f'_{ce} is the effective strength of the concrete which will be discussed in Chpt. 7.

3. Design of stirrups: Determine the value of κ for the selected θ from the design chart in Fig. 5.20, where $\kappa = V_f / \frac{\phi_s A_v f_y d_v}{s}$ and comes from Eqn. (5.25). The required spacing of the stirrups is:

$$s = \frac{\kappa \phi_s A_v f_y d_v}{V_f} \quad (5.27)$$

4. Design of the longitudinal reinforcement: The longitudinal reinforcement is designed for the tensile force given by Eqn. (5.28) or Eqn. (5.29) whichever is larger.

$$N = \frac{M_f}{jd} + 0.5 V_f \cot \theta \quad (5.28)$$

$$N = V_c / \left(\phi_c \frac{\beta_o \cot \theta}{1 + \beta_o \cot \theta} \right) \quad (5.29)$$

Equation (5.28) is the force in the longitudinal reinforcement caused by bending moment and the diagonal compression in the beam web. N in Eqn. (5.29) is the force required to mobilize the shear-friction. In the normal case Eqn. (5.28) governs.

The shear-friction truss model is used to design the stirrups for the beam used in Example 4.1 and Example 4.4 of the CPCA Handbook⁵⁹ to demonstrate the Simplified Method and the General Method of stirrup design in the 1984 CSA A23.3 Code respectively. The dimensions of the cross section of the beam are $b=450$ mm, $d=755$ mm and $d_v=680$. The concrete strength is 25 MPa and the strength of the No.10 U stirrups is 400 MPa. The factored shear at a distance d from the support is $V_f=642$ kN.

The CSA Simplified Method is the same method used by the ACI Code except for the load and material factors. This method is demonstrated in Example 4.1 in the CPCA Handbook. The spacing of the stirrups required is:

$$s = \frac{\phi_s A_v f_y d}{V_f - 0.2\lambda\phi_c\sqrt{f'_c} bd} = \frac{0.85 \times 200 \times 400 \times 755}{642000 - 0.2 \times 1.0 \times 0.6 \times \sqrt{25} \times 450 \times 755} = 117 \text{ mm}$$

The force in the longitudinal reinforcement is:

$$A_s = \frac{M_f}{jd \times \phi_s f_y}$$

The longitudinal bars must be extended a distance d past where they are needed for flexure.

The CSA General Method is a variable angle truss model. This method is demonstrated in Example 4.4 in the CSA Handbook for the same beam but $V_f=607$ kN, the shear at distance 1000 mm from the support, is used. For comparison with the design carried out using the Simplified Method, $V_f=642$ kN is used here. In Example 4.4 $\theta=34.2^\circ$. The spacing of the stirrups required according to the General Method is:

$$s = \frac{\phi_s A_v f_y d_v}{V_f \tan \theta} = \frac{0.85 \times 200 \times 400 \times 680}{642000 \times \tan 34.2} = 106 \text{ mm}$$

The longitudinal reinforcement required is

$$N = \frac{M_f}{jd \times \phi_s f_y} + \frac{472 \text{ kN}}{\phi_s f_y}$$

but not more than $N = \frac{M_{f \max}}{jd \phi_s f_y}$.

The same $\theta=34.2^\circ$ is chosen for the shear-friction truss model. From the design chart in Fig. 5.20, the value of κ corresponding to $\theta=34.2^\circ$ is 1.90. Thus the spacing of the stirrups required according to the shear-friction truss model is:

$$s = \frac{\kappa \phi_s A_v f_y d_v}{V_f} = \frac{1.9 \times 0.85 \times 200 \times 400 \times 680}{642000} = 136 \text{ mm}$$

The longitudinal reinforcement required is

$$N = \frac{M_f}{j d \times \phi_s f_y} + \frac{472 \text{ kN}}{\phi_s f_y}$$

but not more than $N = \frac{M_{f \max}}{j d \phi_s f_y}$.

The above calculations indicate that if $\theta = 34.2^\circ$ the General Method uses more stirrups and more longitudinal reinforcement than that by the Simplified Method. The shear-friction truss model uses less stirrups but more longitudinal reinforcement.

In the above example $\theta = 34.2^\circ$ is used. For further evaluation of the shear-friction truss model, $\theta = 45^\circ, 40^\circ, 35^\circ, 30^\circ, 25^\circ$ and 20° are used in the CSA General Method and the shear-friction truss model. Table 5.4 shows the results together with those calculated by the Simplified Method. The comparison results indicate that the shear-friction truss model requires less stirrups than that designed by the CSA General Method but needs the same longitudinal reinforcement. Compared to the CSA Simplified Method, the shear-friction truss model requires less stirrups but more longitudinal reinforcement. By considering the extended steel d required by the Simplified Method, the relative increase in the longitudinal reinforcement required by the shear-friction truss model may be reduced. If the increase in the longitudinal reinforcement and decrease in the stirrups is an economic trade off, the design of shear using the shear-

friction truss model is about as economical as the CSA Simplified Method but more economical than the CSA General Method.

5.9 Extension of the Application of SFTM

The shear-friction truss model is developed from a general inclined cracked plane to calculate the capacity of shear transfer across the crack. Theoretically, the model is applicable to any reinforced concrete members with force transfer mechanisms across inclined cracks. In this section, attempts are made to extend the shear-friction truss model to the cases of reinforced concrete beams with axial load, prestressed concrete beams and deep beams loaded indirectly. Only theoretical derivations are involved in this part of work.

5.9.1 Beam with External Axial Load

Researchers²⁶ have found that external axial force has a significant effect on the shear strength of reinforced concrete beams. However, the mechanism of the effects of axial force on the shear strength has not been explained very well by the researchers.

In the shear-friction truss model, the effect of the axial force on the shear strength can be explained. According to the shear-friction truss model, the concrete contribution, V_c , is directly proportional to the compressive force on the crack plane under consideration. Axial force affects the concrete contribution by changing the compressive force on the crack plane. Figure 5.18 shows the forces in two

cracked beams. Assume the two beams have the same configuration, the tensile force in the reinforcement in the beam with axial load N_e is:

$$N_s = N - 0.5 N_e \quad (5.30)$$

where N is the tensile force in the reinforcement in the beam without axial load under the same transverse load. Thus the compressive force on the concrete is

$$C = N + 0.5 N_e \quad (5.31)$$

From the shear-friction truss model the concrete contribution of the beam with external axial force is

$$V_c^e = \beta_\theta (N + 0.5 N_e) \quad (5.32)$$

Equation (5.32) can be rewritten as

$$V_c^e = \beta_\theta N \left(1 + \frac{0.5 N_e}{N}\right) \quad (5.32a)$$

or

$$V_c^e = V_c \left(1 + \frac{0.5 N_e}{N}\right) \quad (5.32b)$$

where V_c is the concrete contribution of a beam without axial force. Equation (5.32b) indicates that a compression axial force increases the shear strength of the beam while a tensile axial force decreases the shear strength. Equation (5.32b) has a similar formulation to the CSA code equation for calculating the shear strength of reinforced concrete beams with axial compression:

$$V_c^e = V_c \left(1 + \frac{3 N_c}{A_g f_c'} \right) \quad \text{CSA Eqn. (11.9) (5.33)}$$

where A_g is the area of the beam cross section. Equation (5.33) can be rewritten as

$$V_c^e = V_c \left(1 + \frac{0.5 N_c}{A_g f_c' / 6} \right) \quad (5.33a)$$

A comparison between the Eqn. (5.32b) and (5.33) is not practical since V_c from both methods is different, however it is helpful to understand the behaviour of the model. By considering $(A_g f_c' / 6)$ as a measure of the compression in the concrete, in both Eqn. (5.32b) and (5.33a), V_c^e is directly proportional to the ratio of axial force to the compression in the concrete. The compression on the concrete, N , in Eqn. (5.32b) is equivalent to $(A_g f_c' / 6)$ in Eqn (5.33a).

5.9.2 Prestressed Concrete Beams

Similar to reinforced concrete beams with axial compressive load, the shear strength of prestressed concrete beams is larger than that of normal reinforced concrete beams. For a prestressed concrete beam, if shear failure governs, the longitudinal reinforcement usually has not yet yielded and the force in the longitudinal reinforcement at failure is larger than that of the same beam without prestressing. As a result prestressed concrete beams have larger shear strength than normal reinforced concrete beams do. Figure 5.19 shows the forces in a cracked prestressed beam and a normal reinforced concrete beam. The compression in the concrete is

$$C = N + N_p \quad (5.34)$$

where N is the tension in the longitudinal reinforcement in the beam without prestressing and N_p is the effective prestressing force. From the shear-friction truss model the concrete contribution to the shear strength of a prestressed concrete beam is

$$V_c^p = \beta_\theta (N + N_p) \quad (5.35)$$

Equation (5.35) can be rewritten as

$$V_c^p = \beta_\theta N \left(1 + \frac{N_p}{N}\right) \quad (5.35a)$$

$$V_c^p = V_c \left(1 + \frac{N_p}{N}\right) \quad (5.35b)$$

where V_c is the concrete contribution of a reinforced concrete beam with the same configuration and material properties except prestressing.

5.9.3 Deep Beams Loaded Indirectly

As discussed in Sect. 2.3.4, reinforced concrete beams loaded at the top and supported at bottom act as a strut-and-tie model. The transverse load is directly transferred to the supports by the compression in the struts. No shear transfer across cracks is involved in the strut-and-tie model. The shear strength is expressed by Eqn. (2.15).

However for deep beams loaded indirectly, a direct strut linking the load points and the supports is not possible and a shear transfer

mechanism across the cracks is required. As shown in Fig. 5.20, the load is applied to web of the beam under the critical crack through the loading bars or to the cross beams and is then transferred to the compression struts above the crack through the stirrups and the shear-friction in the crack. Therefore the shear strength of a reinforced concrete deep beams loaded indirectly is:

$$V = V_c + V_s \leq V_{top} \quad (5.36)$$

where V_c and V_s are the shear contributions by the shear-friction and the transverse stirrups in the crack under consideration, respectively, and V_{top} is the shear strength of the same deep beam loaded at the top which is given by Eqn. (2.14). V_c and V_s are the same shear transfer mechanisms across an inclined crack as in slender beams. Thus the shear strength of reinforced concrete deep beams loaded indirectly can be expressed as

$$V = V_c + V_s = \frac{\beta_0 - \cot\theta}{1 + \beta_0 \cot\theta} N + \frac{A_v f_y d}{s \tan\theta} \leq V_{top} \quad (5.37)$$

In deep beams, the critical cracks are usually defined by the shear span of the beams, rather than that calculated by Eqn. (5.21). The critical cracks usually start from the edge or the supports to the top of the load introduction bars or cross beams, as shown in Fig. 5.23. In this case $\cot\theta$ is approximately equal to the shear span ratio. Thus Eqn. (5.37) becomes

$$V = V_c + V_s = \frac{\beta_0 - a/d}{1 + \beta_0 a/d} N + \frac{A_v f_y a}{s} \leq V_{top} \quad (5.38)$$

Ref. 60 reported the tests of deep beams loaded at bottom through loading bars. The tests indicated that for deep beams loaded at bottom, if enough stirrups are provided, the failure is usually caused by the diagonal crushing of the concrete web and the same shear strength as the deep beams loaded at the top can be reached. The stirrups can be designed according to Eqn. (5.38).

5.10 Summary

In summary, this chapter has dealt with the development of the shear-friction truss model as a design tool for the shear strength of reinforced concrete beams. In this model the function of the stirrups is represented by the variable angle truss model and the contribution of the concrete is modelled by shear-friction. In a reinforced concrete beam the stirrups act to transfer the shear directly as do the tension ties in a truss. At the same time the longitudinal reinforcement transfers the shear indirectly by inducing confinement on the crack plane which mobilizes shear-friction. The application of the shear-friction truss model to the test beams shows that the model gives predications with acceptable safety and accuracy. The design example indicates that the shear-friction truss model usually requires less stirrups than beams designed by the CSA Simplified Method or by the CSA General Method but needs more longitudinal reinforcement than required by the CSA Simplified Method. Part of the increase in longitudinal reinforcement is offset by the extended steel d required by the Simplified Method.

It is found that the CSA Simplified Method and the ACI shear design procedure underestimate the shear contribution from stirrups because they use a conservative angle of 45° for the truss model. At the same time the CSA Simplified Method and the ACI procedure overestimate the shear contribution from the concrete by using the shear strength of concrete beams without stirrups as the concrete contribution of beams with stirrups. The underestimation of the stirrup contribution and overestimation of the concrete contribution offset, and as a result, the code procedure can give good predictions of the shear strengths of reinforced concrete beams. However the code procedure does not give a clear understanding of the shear transfer mechanism across an inclined crack.

Further research is needed to improve the shear-friction truss model in the following aspects.

1. The effects of the concrete strength and the cross section on the coefficient of shear-friction of concrete needs to be studied experimentally.

2. The width of crack is not a prime variable in the shear-friction tests. However, according to the aggregate interlock tests by other researchers, the shear transfer decreases as crack width increases. On the other hand the tension in the reinforcement at the crack in a reinforced concrete beam increases as the crack width increases. Therefore two events occur simultaneously as the crack width increases. The aggregate interlock action decreases as the crack width increases and the shear-friction increases because the

compression in the crack plane increases. Therefore in a reinforced concrete beam the critical crack seldom starts from the edges of the support where the force in the reinforcement is the lowest. Crack width has very a complicated effect on the shear-friction in the crack and further research on this issue is worthwhile

3. In the shear-friction truss model procedure, as expressed by Eqns. (5.20) and (5.21), three unknowns are included in the two equations. For the shear design of reinforced concrete beams, an angle of inclination can be chosen from 15 to 40 degrees and the stirrups can be designed according to the chart in Fig. 5.17. However, for predicting the shear strength of an existing beam either the angle of the critical crack or the compression force on the critical crack plane is needed. Further studies to develop the procedure calculating the critical crack inclination and the compressive force on the critical crack would be useful.

4. Theoretically, the shear-friction truss model deals with the force transfer mechanism across an inclined crack. Therefore the model can be applied to calculate the shear strengths of reinforced concrete members in which shear failure is caused due to the loss of the force transfer mechanism across an inclined crack, such as beams with axial load, prestressed concrete beams and deep beams loaded at the bottom. Further work is needed to examine test results using the shear-friction truss model.

Table 5.1 The properties of the test beams by Scordelis⁴⁻⁶

Specimen No.	b	d	a/d	f'_c	Long. reinf.			Stirrups			Test Result	
					No.	A_s	f_y	A_v	s	f_y	V^t	θ
A - 1	307	466	3.92	24.1	4 - #9	2628	555	64.5	210	325	234	18
A - 2	305	464	4.93	24.3	5 - #9	3285	555	64.5	210	325	245	22
A - 3	307	466	6.91	35.0	6 - #9	3943	552	64.5	210	325	234	20
B - 1	231	461	3.95	24.8	4 - #9	2628	555	64.5	191	325	222	19
B - 2	229	466	4.91	23.2	4 - #9	2628	555	64.5	191	325	200	18
B - 3	229	461	6.95	38.8	5 - #9	3285	552	64.5	191	325	178	32
C - 1	156	464	3.95	29.6	2 - #9	1314	555	64.5	210	325	156	24
C - 2	152	464	4.93	23.8	4 - #9	2628	555	64.5	210	325	162	18
C - 3	155	459	6.98	35.0	4 - #9	2628	552	64.5	210	325	136	23
XB - 1	231	458	4.0	24.5	4 - #9	2585	665	65.4	191	339	200	20
CA - 1	307	459	3.98	26.7	4 - #9	2585	665	65.4	210	339	165	30
CB - 1	229	458	3.98	24.8	4 - #9	2585	665	65.4	191	339	176	24
CC - 1	152	459	3.98	27.2	2 - #9	1293	665	65.4	210	339	110	18
RA - 1	305	458	3.98	24.9	6 - #7	2323	656	65.4	210	339	200	25
RB - 1	229	459	3.98	24.6	6 - #7	2323	656	65.4	191	339	200	25
RC - 1	155	459	3.98	29.2	3 - #7	1161	656	65.4	210	339	137	27
CRA-1	305	460	3.98	25.1	6 - #7	2347	697	65.8	210	342	167	36
CRB-1	229	457	4.01	23.7	6 - #7	2347	697	65.8	191	342	172	28
CRC-1	155	458	4.0	24.4	3 - #7	1174	697	65.8	210	342	118	32
1WCRA-1	305	457	4.01	26.3	6 - #7	2347	697	65.8	156	342	214	26
1WCRB-1	229	459	3.99	23.2	6 - #7	2347	697	65.8	141	342	204	28
1WCRC-1	152	459	3.98	26.8	3 - #7	1174	697	65.8	162	342	144	29
1WCA-1	304	463	3.95	25.2	4 - #9	2675	663	65.8	146	342	220	29
1WCB-1	231	460	3.97	26.5	4 - #9	2675	663	65.8	141	342	202	30
1WCC-1	155	460	3.97	24.9	2 - #9	1338	663	65.8	162	342	142	24
2WCA-1	305	461	3.96	26.3	4 - #9	2675	663	65.8	156	342	241	25
3WCA-1	305	460	3.97	26.3	4 - #9	2675	663	65.8	162	342	207	24

- Note: 1. The units are mm for length, kN for force and MPa for stress.
 2. The stirrup spacing for W-beams are variable and the numbers in the table are the average spacing.

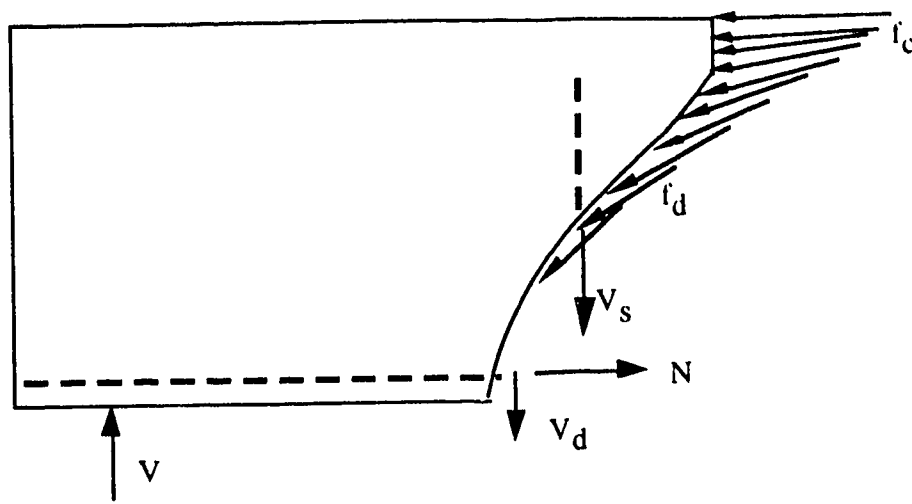
Table 5.3 The strengths predicted by ACI procedure and CSA general method

Specimen No.	V^t	θ^{**}	ACI Procedure: $V = V_c + V_s$				Variable angle truss Model		Eqn. (5.34)	
			V_c	V_s	V^{cal}	V^t/V^{cal}	V^{cal}	V^t/V^{cal}	V^{cal}	V^t/V^{cal}
A - 1	234	18	117.1	46.7	163.8	1.43	143.7	1.62	260.8	0.90
A - 2	245	22	116.1	46.5	162.6	1.50	115.1	2.13	231.2	1.06
A - 3	234	20	141.3	46.7	188.0	1.24	128.3	1.82	269.6	0.87
B - 1	222	19	88.4	50.8	139.2	1.60	147.6	1.51	235.9	0.94
B - 2	200	18	85.4	51.3	136.7	1.46	157.9	1.27	243.3	0.82
B - 3	178	32	109.2	50.8	160.0	1.11	81.2	2.19	190.4	0.93
C - 1	156	24	65.1	46.4	111.6	1.40	104.3	1.49	169.4	0.92
C - 2	162	18	57.5	46.5	104.0	1.56	143.2	1.13	200.7	0.81
C - 3	136	23	70.1	46.0	116.1	1.17	108.3	1.25	178.4	0.76
XB - 1	200	20	87.4	53.3	140.7	1.42	146.5	1.37	233.9	0.86
CA - 1	165	30	121.5	48.6	170.1	0.97	84.2	1.96	205.8	0.80
CB - 1	176	24	86.9	53.4	140.2	1.25	119.9	1.47	206.8	0.85
CC - 1	110	18	60.8	48.6	109.4	1.01	91.4	1.20	152.2	0.72
RA - 1	200	25	116.2	48.6	164.8	1.21	104.1	1.92	220.3	0.91
RB - 1	200	25	86.7	53.4	140.2	1.43	114.6	1.75	201.3	0.99
RC - 1	137	27	64.0	48.6	112.6	1.22	95.3	1.43	159.3	0.86
CRA-1	167	36	117.0	49.4	166.4	1.01	68.1	2.46	185.1	0.90
CRB-1	172	28	84.7	54.1	138.7	1.24	101.7	1.70	186.3	0.92
CRC-1	118	32	58.4	49.3	107.7	1.10	78.8	1.50	137.2	0.86
1WCRA-1	214	26	119.1	70.5	189.5	1.13	144.5	1.48	263.5	0.81
1WCRB-1	204	28	84.2	73.2	157.4	1.29	137.7	1.48	221.9	0.92
1WCRC-1	144	29	60.4	63.9	124.3	1.16	115.4	1.25	175.7	0.82
1WCA-1	220	29	117.9	71.4	189.2	1.16	128.8	1.71	246.6	0.89
1WCB-1	202	30	91.1	73.3	164.5	1.23	127.0	1.59	218.1	0.93
1WCC-1	142	24	59.3	64.0	123.3	1.15	143.8	0.99	203.1	0.70
2WCA-1	241	25	120.1	71.1	191.2	1.26	152.5	1.58	272.6	0.89
3WCA-1	207	24	119.8	64.0	183.8	1.13	143.8	1.44	263.6	0.79
* All the forces are in KN						$\bar{X}=1.25$ $\sigma=0.17$ $v=0.136$	$\bar{X}=1.58$ $\sigma=0.33$ $v=0.209$		$\bar{X}=0.87$ $\sigma=0.08$ $v=0.092$	
** See figures in Appendix C										

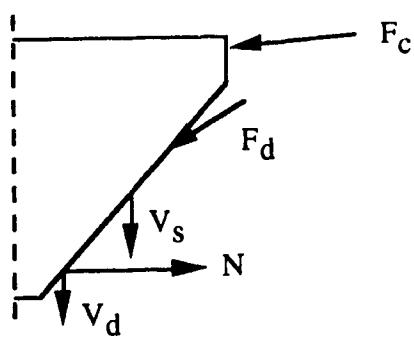
Table 5.4 The Comparisons of the CSA Simplified Method, the CSA General Method and the shear-friction truss model in the design of stirrups

θ	The shear-friction truss model		The CSA General Method		The CSA Simplified Method	
	Spacing of the stirrups (mm)	Longitudinal reinforcement	Spacing of the stirrups (mm)	Longitudinal reinforcement	Spacing of the stirrups (mm)	Longitudinal reinforcement
20°	208	$\frac{M_f}{jd\phi_s f_y} + \frac{882 \text{ kN}}{\phi_s f_y}$	197	$\frac{M_f}{jd\phi_s f_y} + \frac{882 \text{ kN}}{\phi_s f_y}$	117	$\frac{M_f}{jd\phi_s f_y} + \text{Extend steel}$
25°	181	$\frac{M_f}{jd\phi_s f_y} + \frac{688 \text{ kN}}{\phi_s f_y}$	154	$\frac{M_f}{jd\phi_s f_y} + \frac{688 \text{ kN}}{\phi_s f_y}$		
30°	158	$\frac{M_f}{jd\phi_s f_y} + \frac{556 \text{ kN}}{\phi_s f_y}$	125	$\frac{M_f}{jd\phi_s f_y} + \frac{556 \text{ kN}}{\phi_s f_y}$		
35°	136	$\frac{M_f}{jd\phi_s f_y} + \frac{458 \text{ kN}}{\phi_s f_y}$	103	$\frac{M_f}{jd\phi_s f_y} + \frac{458 \text{ kN}}{\phi_s f_y}$		
40°	120	$\frac{M_f}{jd\phi_s f_y} + \frac{383 \text{ kN}}{\phi_s f_y}$	86	$\frac{M_f}{jd\phi_s f_y} + \frac{383 \text{ kN}}{\phi_s f_y}$		
45°	107	$\frac{M_f}{jd\phi_s f_y} + \frac{321 \text{ kN}}{\phi_s f_y}$	72	$\frac{M_f}{jd\phi_s f_y} + \frac{321 \text{ kN}}{\phi_s f_y}$		

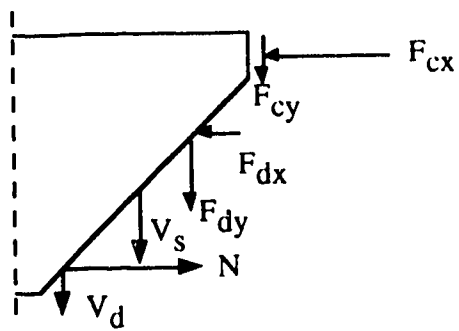
Note: The area and strength of the stirrups used in this example are $A_v=200 \text{ mm}^2$ and $f_y=400 \text{ MPa}$.



(a)



(b)



(c)

Figure 5.1 Internal forces in a cracked beam

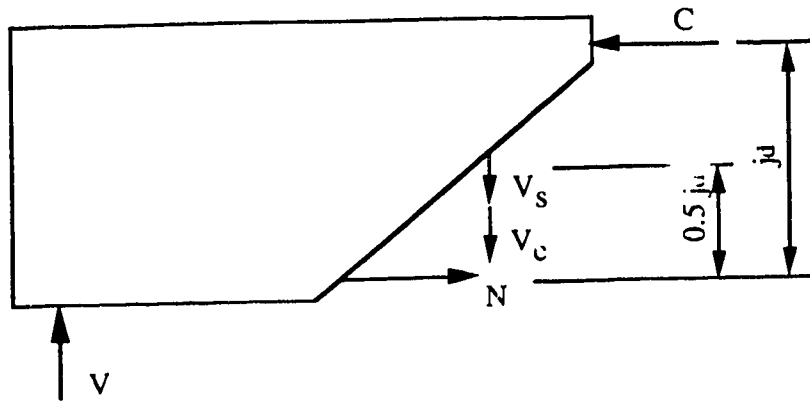


Figure 5.2 The simplified internal forces in the crack plane

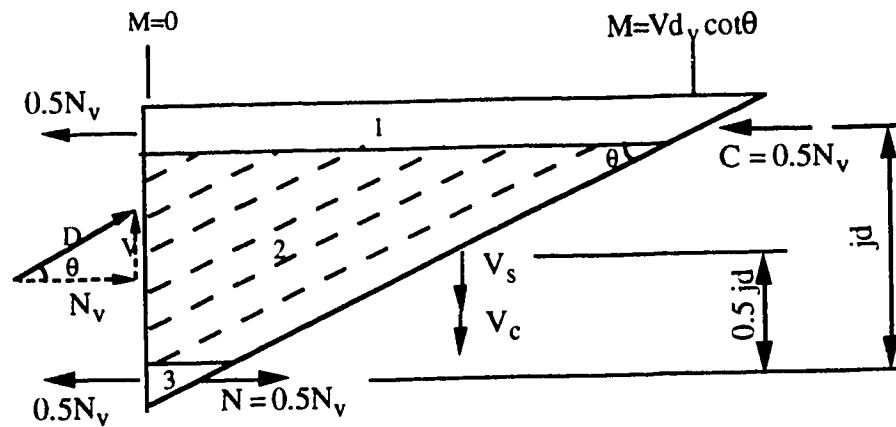
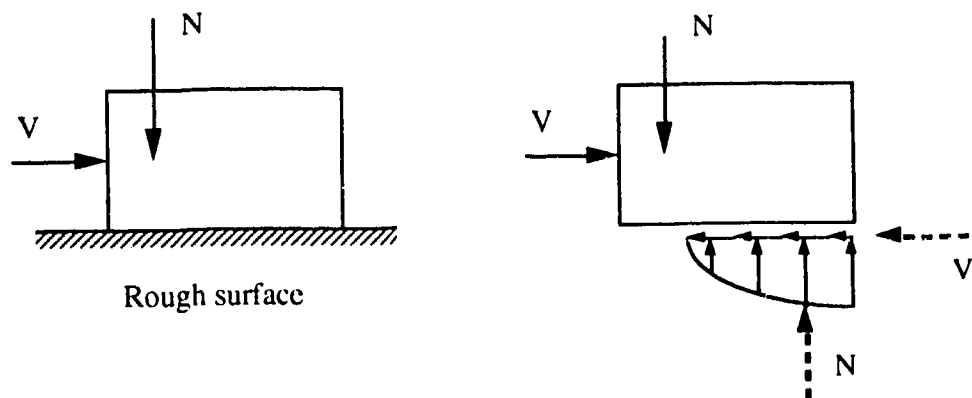
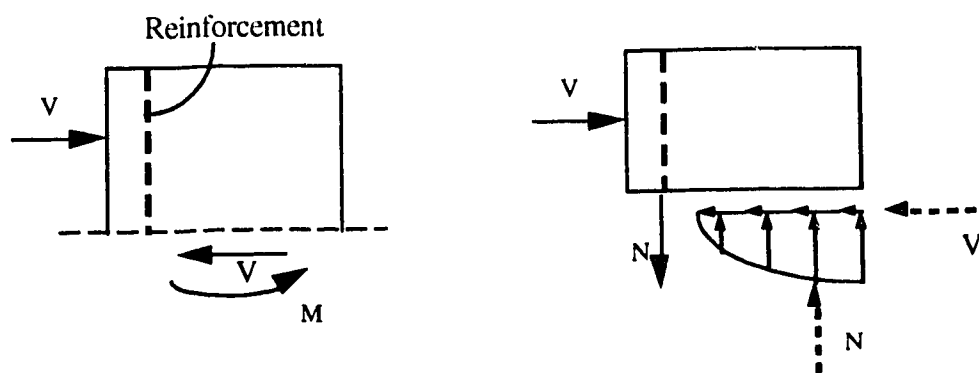


Figure 5.3 A truss system account for the concrete contribution

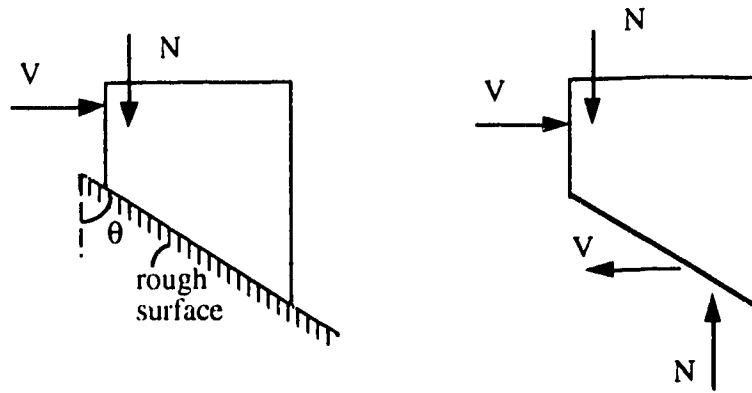


a) Dry friction on a rigid body

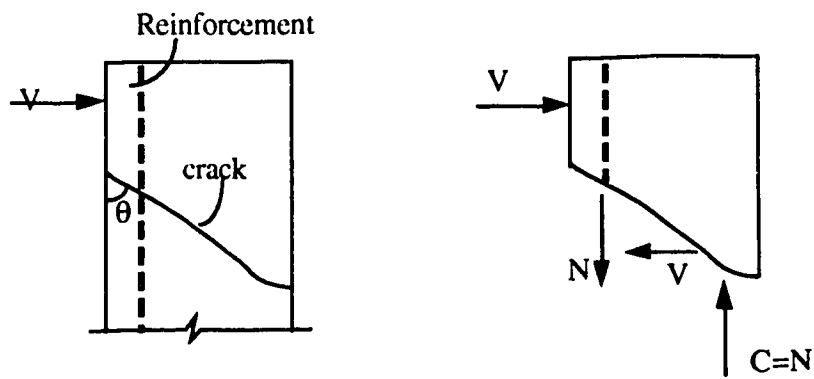


b) Forces in a reinforced concrete beam

Figure 5.4 Dry friction analogy for the cross section of a reinforced concrete beam ;

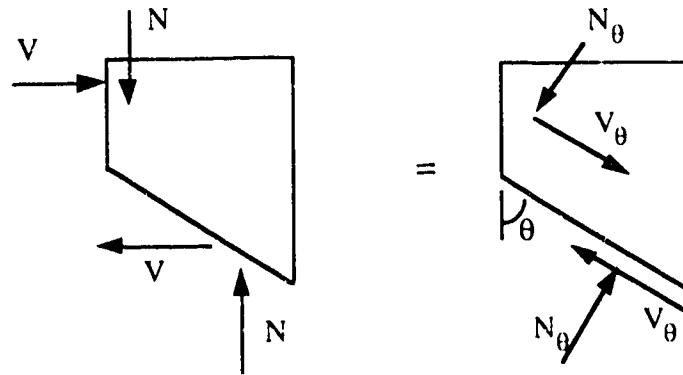


a) Dry friction on a rigid body



b) Forces in a reinforced concrete beam

Figure 5.5 Dry friction analogy in an inclined section of a reinforced concrete beam;



$$N_{\theta} = N \sin \theta - V \cos \theta \quad V_{\theta} = N \cos \theta + V \sin \theta$$

Figure 5.6 Force transformation

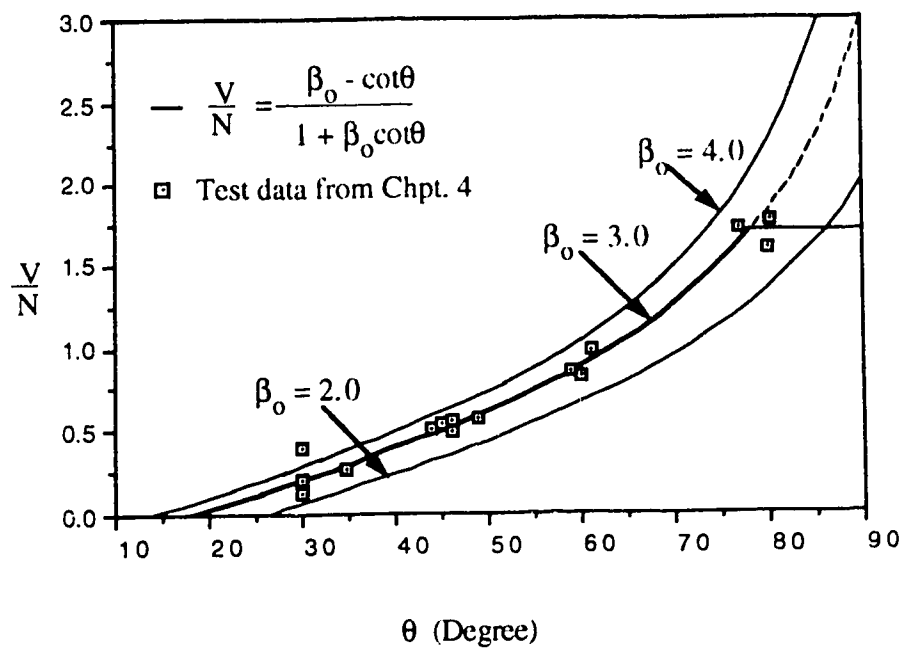
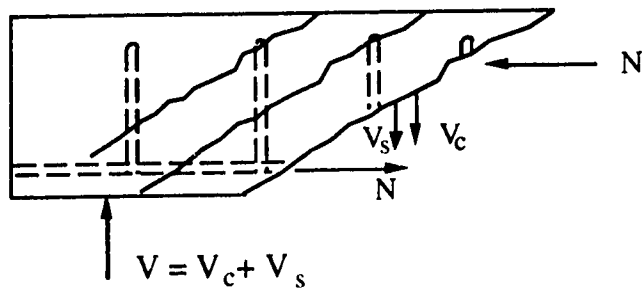
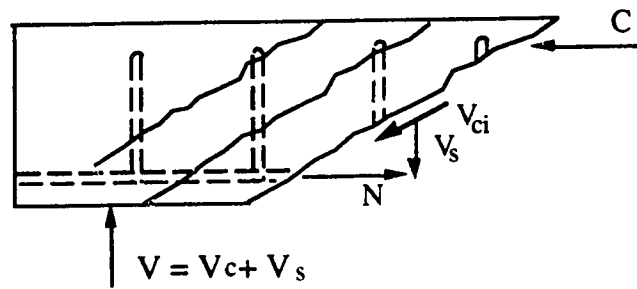


Figure 5.7 Analysis of the coefficient of shear-friction

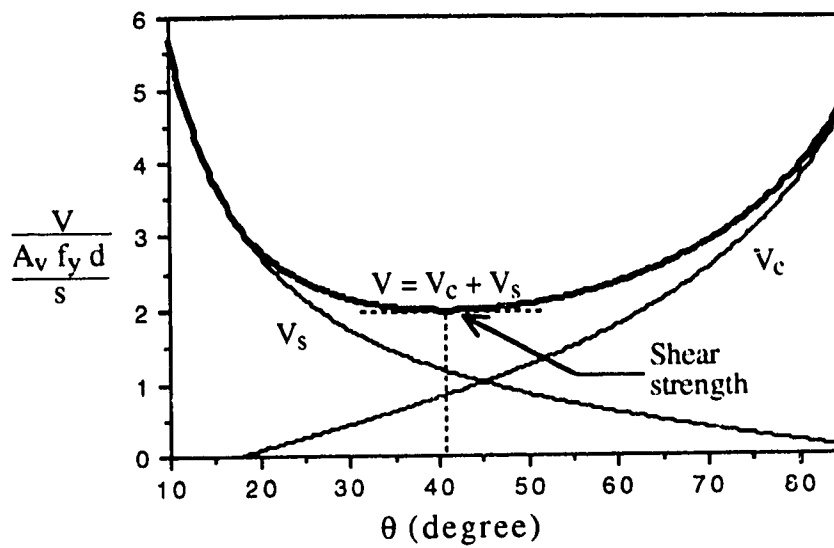


a) V_c as transverse force

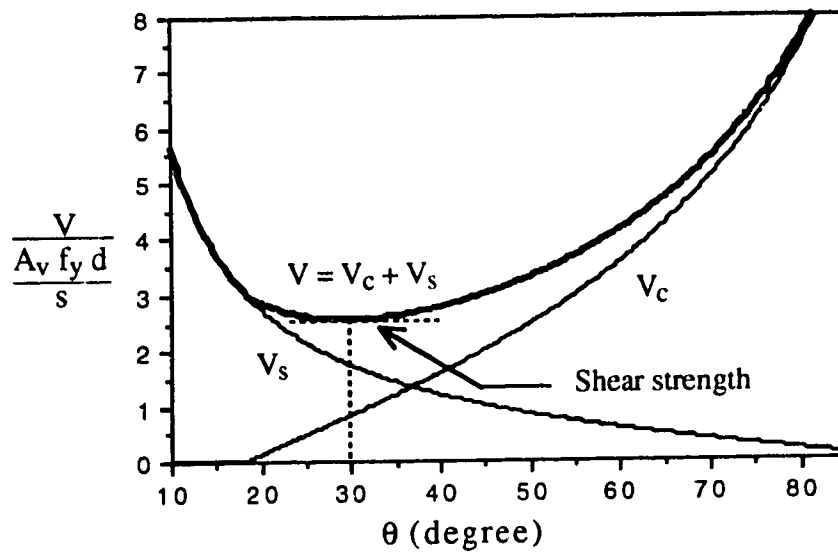


a) V_{ci} as shear force parallel to the crack

Figure 5.8 Force transfer across the crack between two diagonal struts

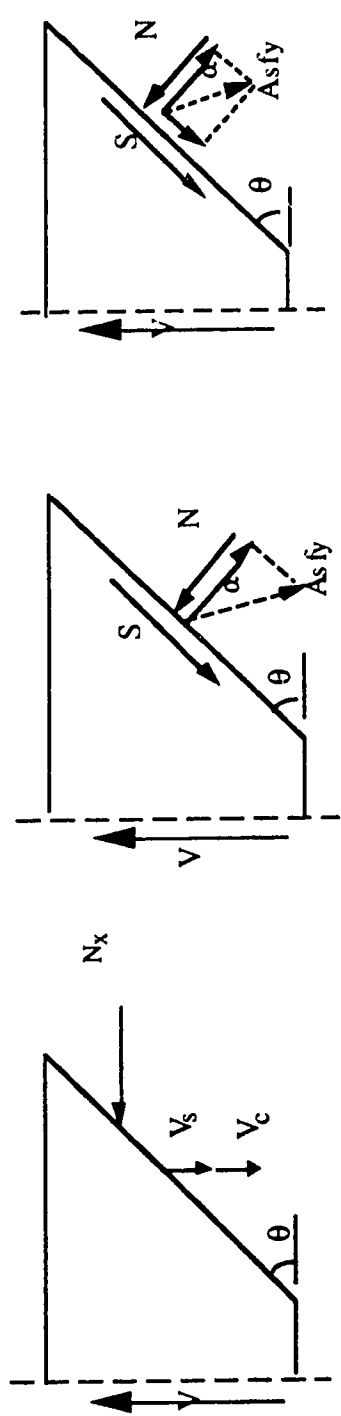


a) Shear strength for $N = 2 \frac{A_v f_y d}{s}$



a) Shear strength for $N = 4 \frac{A_v f_y d}{s}$

Figure 5.9 Shear strength vs. angle of inclination



$$V = V_c + V_s$$

$$V_c = \beta \frac{N_x}{\theta}$$

$$V_s = \frac{A_v f_y d}{s \tan \theta}$$

a) Shear-friction truss model

$$V = S \sin \theta$$

$$S = \mu N$$

b) Crist's shear-friction model

$$V = S \sin \theta$$

$$S = \mu N + N \tan \alpha$$

c) The ACI shear-friction model

Figure 5.10 The differences between the shear-friction truss model, Crist's shear-friction model and ACI's shear-friction method

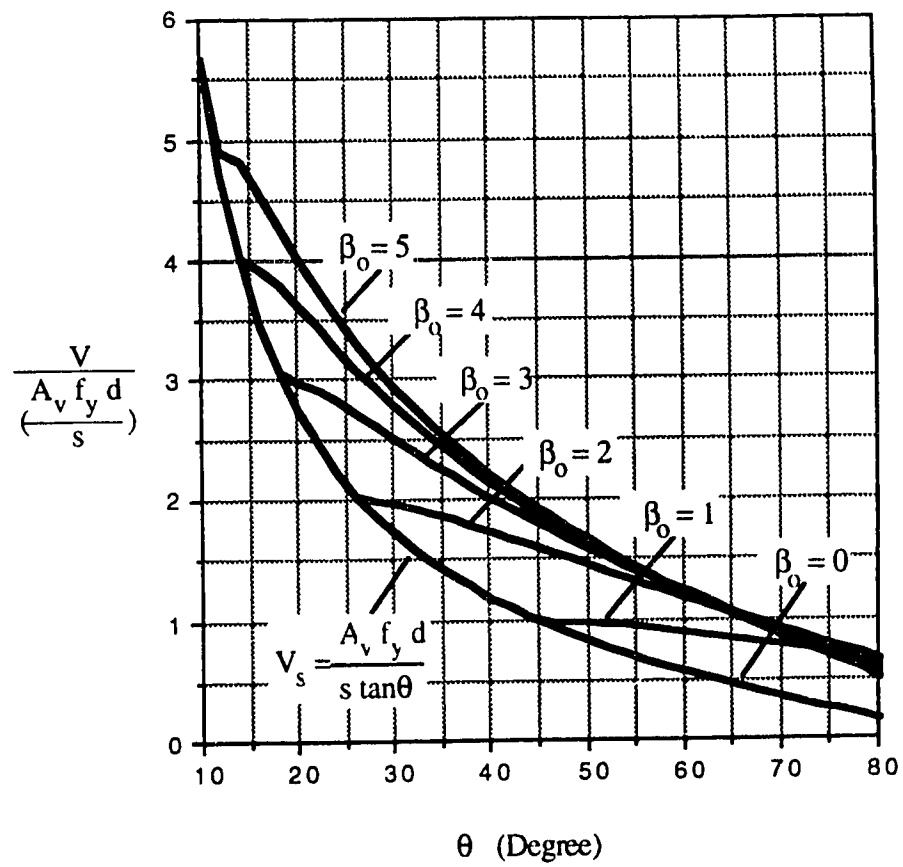
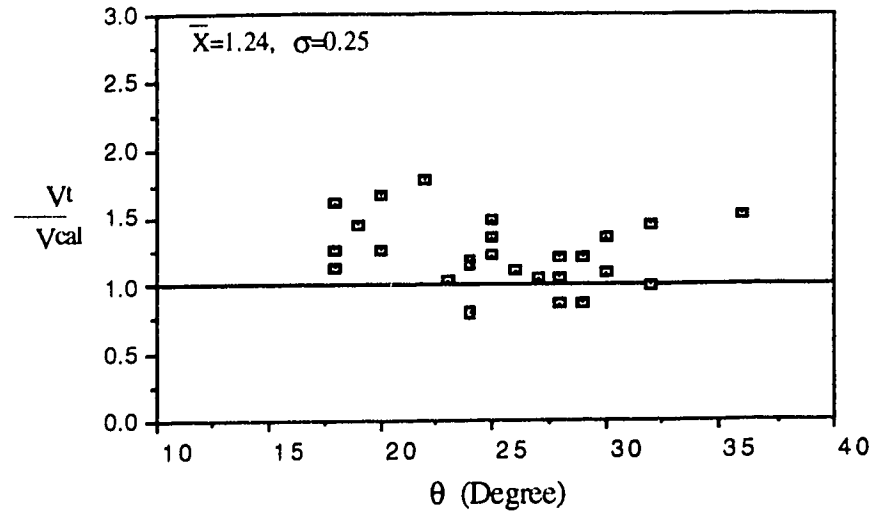
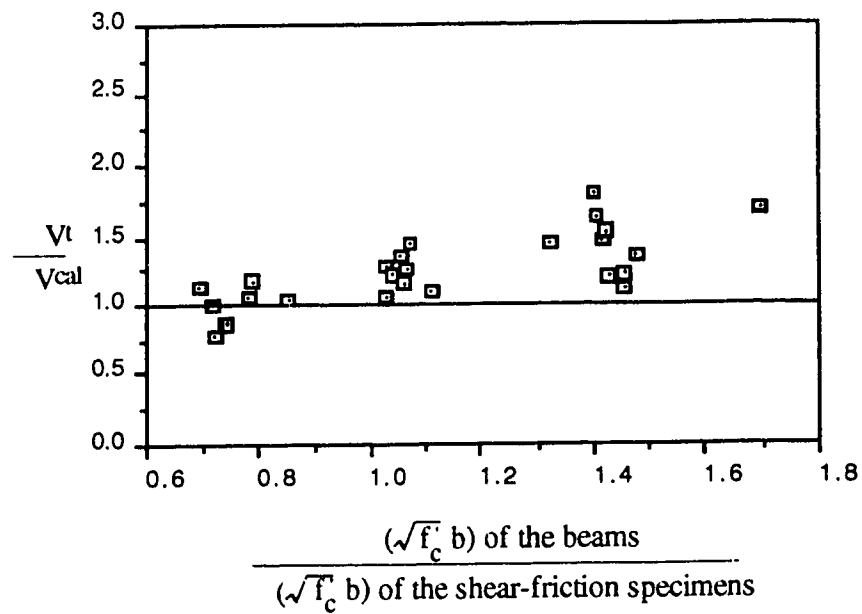


Figure 5.11 Relationship between $\frac{V}{\frac{A_v f_y d}{s}}$ and θ



a) The predicted by SFTM using $\beta_0=3.0$



b) The effect of concrete strength and beam width

Figure 5.12 Shear strength predicted by SFTM using $\beta_0=3.0$

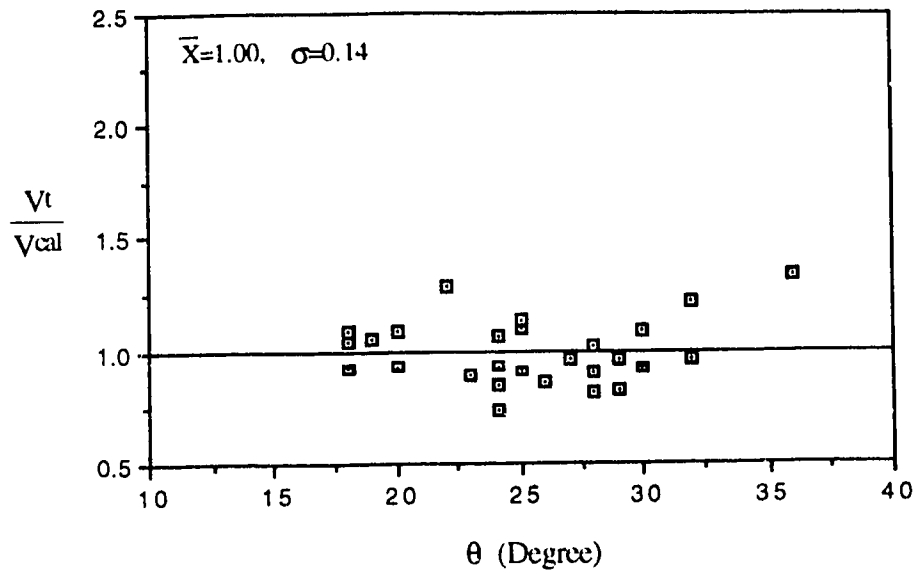


Figure 5.13 The prediction by SFTM using Eqn. (5.13)

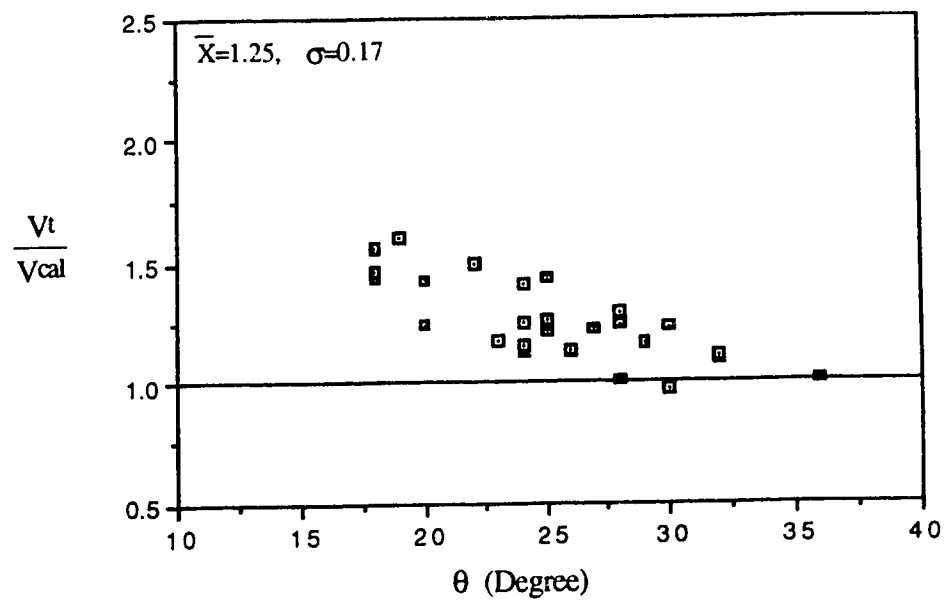


Figure 5.14 The prediction by the ACI procedure

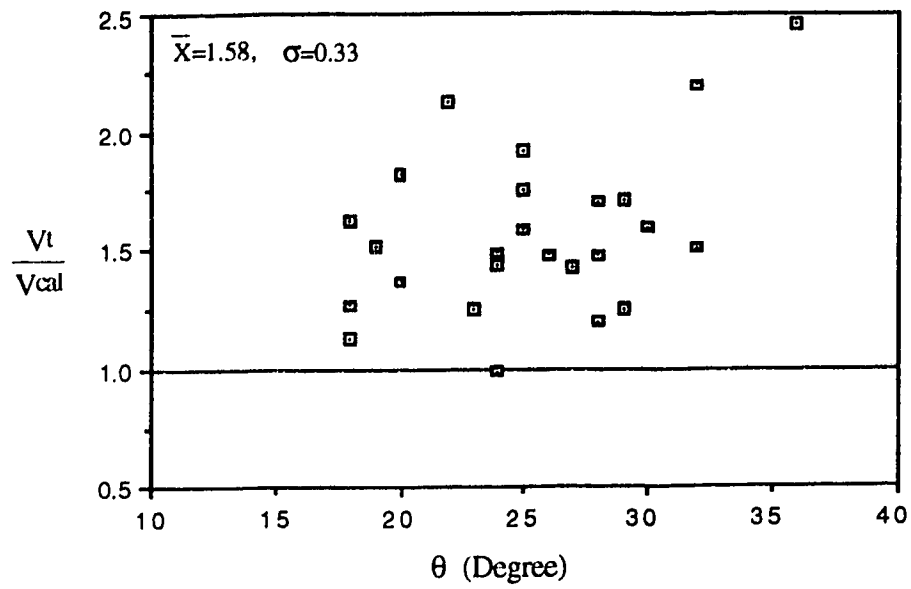


Figure 5.15 The prediction of variable angle truss model

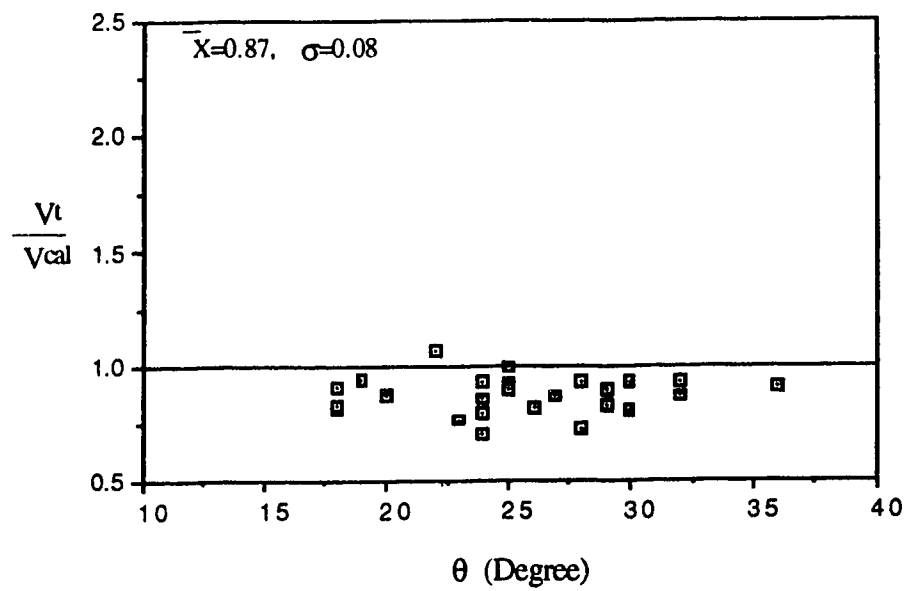


Figure 5.16 The prediction of Equation (5.24)

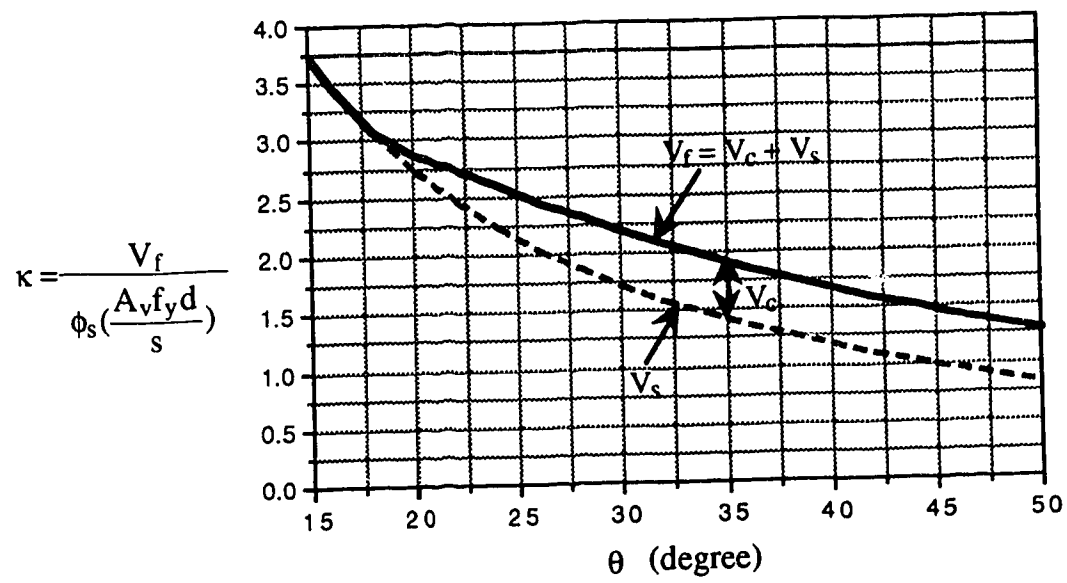
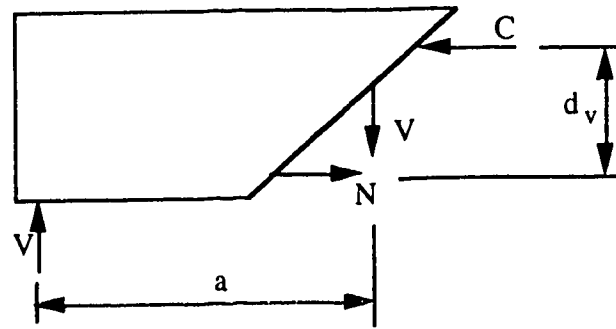
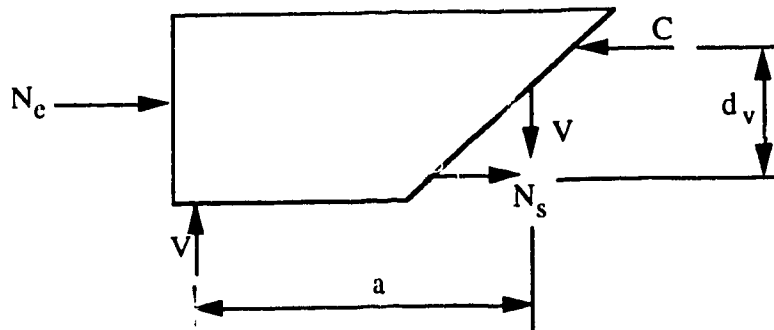


Figure 5.17 Design chart



$$Va = N d_v$$

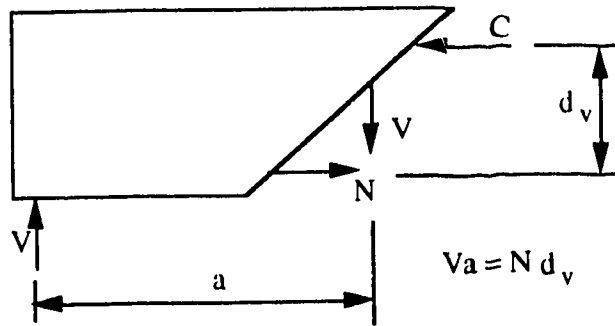
a) Beam without external axial force



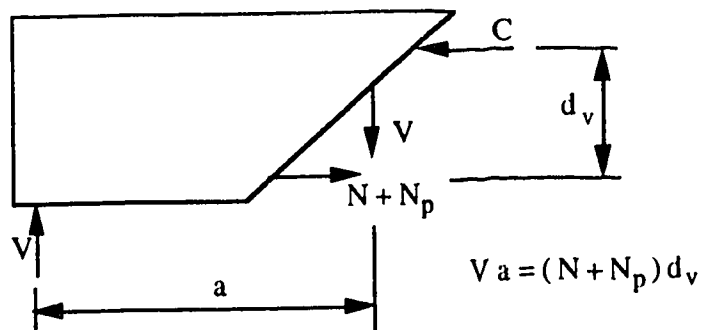
$$Va = N_s d_v + 0.5 N_e d_v$$

b) Beam with external axial load

Figure 5.18 Forces in a beam with external axial force



a) Normal reinforced concrete beam



b) Prestressed concrete beam

Figure 5.19 Forces in a prestressed concrete beam;

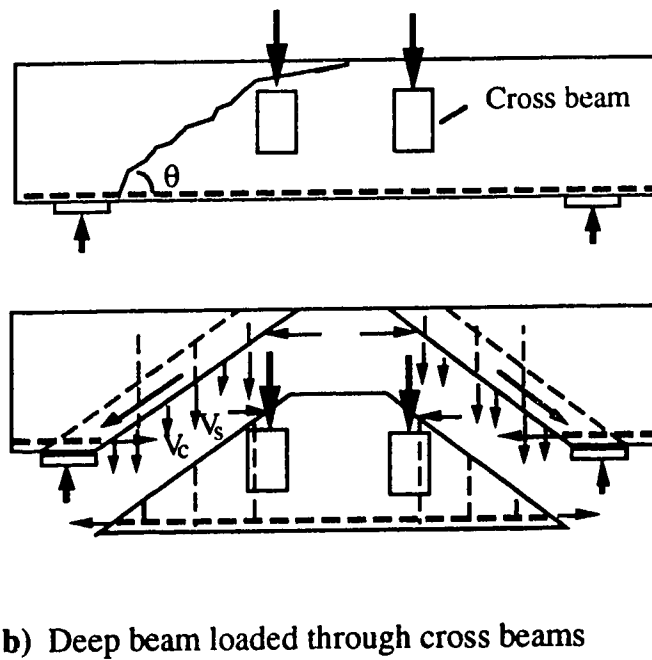
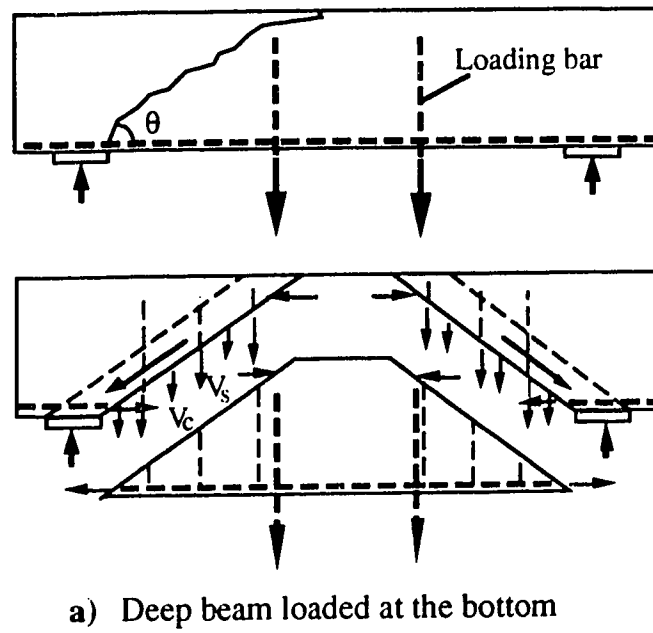


Figure 5.20 Shear transfer mechanism in deep beams loaded indirectly

6. RESULTS OF TESTS ON CONCRETE SOFTENING

6.1 Presentation of Test Data

To investigate the mechanics of concrete softening under transverse tension, a total 40 reinforced concrete panels were axially loaded until they crushed with a variety of different transverse tensions.

The following sections present the test results for each group of specimens to illustrate the behavior of the specimens under longitudinal compression and transverse tension. These results consist of the loading histories (N vs. T), plots of longitudinal compression (N/bhf_c') vs. average transverse tensile strains (ϵ_t) and longitudinal compressive strains (ϵ_c) respectively, the loads and the deformations at the ultimate state and the failure modes. The major test data for each specimens are listed in Table 6.1 and photographs of the specimens at failure are given in Appendix B.

The longitudinal compressive and the transverse tensile loads were measured by two individual load cells. In this chapter N is the total longitudinal compressive force applied to the concrete panels while T is the transverse tensile force applied to each loading bar. Eight loading bars were placed in each specimen. However, the total transverse tensile force was less than $8T$ in some of the specimens since less tension was applied to the two bars at the loading and supporting respectively. Transverse tensile strains were measured by LVDT's mounted to the two edges of the panel, and by Demec

gauges with targets on both the concrete and the reinforcement across the entire width of the specimens (see Chpt. 3). Except for the Demec gauges on the reinforcement which were only mounted on one side, all the deformations and the strains discussed in this chapter are the average of the two readings taken on both faces of the specimens.

For all the specimens tested, the deformations measured by the LVDT's and by the Demec gauges are in good agreement. Figure 6.1 shows examples of the average tensile strains across the entire width of the panel measured both by the LVDT's and Demec gauges at the same heights. Figure 6.1a shows that the LVDT's had approximately equal measurements to those by the Demec gauges on the concrete. The strains measured by the Demec gauges mounted on the reinforcement were a little larger than those by the LVDT's (Fig.6.1b). This is because the tensile strains were introduced to the concrete through the reinforcement. The bonding between the concrete and the reinforcement was not fully developed near the edges of the panels and, as a result, the reinforcement had larger tensile strains than the concrete. The fact that the deformations measured by the three methods are in good agreement inspired confidence in the accuracy of the data. In the following sections, the average transverse deformations are based on the LVDT's readings since the LVDT readings covered the entire range of load applied in the tests.

On each specimen five LVDT's were arranged on each face of the specimen, at a spacing of 80 mm. Figure 6.2 shows examples of the

readings at the five heights. In most cases the readings were quite uniformly distributed (as shown in Fig.6.2b) or had dispersions as shown in Fig. 6.2a. In order to be consistent with the test results reported by other researchers⁴⁷ and the truss model in which the entire web of a beam is assumed uniformly strained, the average of the five LVDT readings are used in the analysis.

6.2 Group I: General Study of the Reduction of Compressive Strength of Concrete due to Transverse Tension

Eighteen specimens (#1 to #18) were included in this group. The concrete strength was from 20.6 MPa to 26.8 MPa. The reinforcement through which the transverse tensile strain was introduced to the concrete was 10M deformed bars with a yield strength of 350 MPa. The specimens were loaded to failure by crushing with various levels of transverse tensile strains to investigate the general behavior of concrete softening. In the course of the tests, both the longitudinal compressive and the transverse tensile strain were monotonically increased from zero to failure. An approximately constant ratio of longitudinal compressive stress to transverse tensile strain was followed in the course of each test. These ratios were different from specimen to specimen so that different transverse strains were reached at the ultimate state.

Three plain concrete panels (#5, #12 and #17) were tested under uniaxial compression only. The strengths of these panels were compared with the concrete cylinder strength to investigate the shape effect of the panels. Specimen #4, a reinforced panel, was also

tested under uniaxial longitudinal compression to investigate the effect of transverse restraint by the reinforcement.

In specimens #1 to #3 and #6, equal tensile force was applied to all the eight loading bars. However, local bearing crushing was observed at the loading and supporting ends of specimens #1, #2, and #6, (See Fig. 6.3a). To prevent the specimens from local bearing crushing, less tension was applied to the top and bottom bars in the tests of the following specimens. This was accomplished by locking the four jacks linked to these two bars after the bars yielded ($\epsilon_t=0.0025$) while the rest of the loading bars were continuously pulled to the designed transverse tensile strain. Thus, in the following loading stages, the loading and supporting ends had less transverse tensile strain than the central part of the panel and bearing failure was avoided.

All the panels in this group, except specimens #4, #5, #12, and #17 which were uniaxially loaded until crushing, had similar general behaviors but different ultimate loads due to different transverse tensile strains. The first crack formed between $T=12$ to 20 kN, compared to the yield capacity of the reinforcement $T=35$ kN. The initial crack was usually located near the mid-width of the panel along the longitudinal direction, with a length of about half to the entire height of the panel. As the transverse tension force increased, the number and the width of the cracks also increased. The second and the following cracks usually formed after the reinforcement yielded. The cracks near the edges of the panel were curved in some of the panels tested with the jacks at the loading and supporting

ends loaded (See Fig. 6.3b). For the specimens tested under uniaxial compression, no cracks were observed before failure. A splitting crack occurred in the plane of panel #12 at the ultimate state.

The cracking of the concrete was governed by the transverse tension. The longitudinal compression had no measurable effect on the cracking of the concrete. The reason was that the Poisson ratio effect was small compared to the strains caused by the transverse tensile forces. On the other hand, however, the transverse tension reduced the longitudinal compressive strength and stiffness of the concrete significantly.

Figure 6.4 shows the test results of panel #1 to #4. As shown in Fig. 6.4a, the reinforcement of panels #1 to #3 were pulled to the post yield stage, while in #4 transverse tension was not applied. Fig. 6.4b shows plots of N/bhf_c' vs. the average transverse tensile strains. For the three transversely tensioned panels, the major part of the tensile strains were developed after the yield of the reinforcement. The strain in panel #4 near failure was due to the Poisson ratio of the concrete. Due to the transverse tension, the three transversely tensioned panels had ultimate strengths lower than the concrete cylinder strengths. The reduction of the strengths increased as the transverse tensile strain increased. Panel #4 had a strength higher than the cylinder strength due to the transverse restraint of the reinforcement. Panels #3 and #4 failed due to crushing of concrete across the entire section at the loading end, with $N_u/bhf_c' = 0.982$ and 1.149 respectively. The failures of panels #1 and #2 were characterized by local bearing crushing, with $N_u/bhf_c' = 0.769$ and

0.714 respectively. Figure 6.4c shows plots of N/bhf_c' vs. the longitudinal compression strains for the four specimens. The plots indicate that at the same longitudinal compressive stress the compression strain increased as the transverse tension strain increased. In other words, the transverse tension reduced the stiffness of the concrete in the longitudinal direction.

The test results of panels #5 to #8 are shown in Fig. 6.5. Fig. 6.5a shows the loading histories and Fig. 6.5b is the plots of N/bhf_c' vs. the average transverse tensile strain. Panel #8 experienced the largest transverse tension strain ($\epsilon_t=0.0143$) and, as a result, had the lowest ultimate compressive strength ($N_u/bhf_c'=0.550$) among the four panels. The plain concrete panel (#5) was uniaxially loaded and the compressive strength was approximately equal to the concrete cylinder strength ($N_u/bhf_c'=1.016$). The transverse tension strains of #6 and #7 were between those of #5 and #8 and the ultimate strengths were also between that of #5 and #8. Figure 6.5c shows plots of N/bhf_c' vs. the longitudinal compression strain. The plots indicates that the transverse tension reduced the stiffness of the concrete in the longitudinal direction. Panels #5, #7 and #8 reached failure due to concrete crushing across a large part or the entire section of the panels. Panel #6 failed because of local bearing crushing underneath a loading plate. The reduction of the ultimate strengths was approximately proportional to the transverse tensile strain.

Figure 6.6 shows the test results of specimens #9 to #12. The transverse tensile strains of the three transversely tensioned

specimens were ranged from 0.014 to 0.018. Panels #9 to #11 failed due to concrete crushing along the major cracks. The ratios of N_u/bhf_c' were 0.553, 0.504 and 0.476 respectively. Specimen #12 was a plain panel and tested under uniaxially longitudinal compression. The failure was caused due to the splitting of the concrete near the middle of the supported end and crushing of the corners at $N_u/bhf_c' = 0.949$. The ultimate capacity of the four specimens decreased as the transverse tensile strain increased (Fig. 6.6b). As with the previously tested specimens, the the transverse tension reduced the stiffness of the concrete in the longitudinal direction, (See Fig. 6.6c).

The test results of the last six specimens of Group I are shown in Fig. 6.7. Specimens #13 and #14 experienced the largest transverse tensile strains in Group I ($\epsilon_t = 0.0212$ and 0.0217 respectively). Both of them failed due to concrete crushing along the major cracks at $N_u/bhf_c' = 0.550$ and 0.440 respectively. During failure shearing was observed across the cracks where the concrete crushed. Specimens #15 and #16 were transversely tensioned to smaller strains than the rest of the specimens in Group I ($\epsilon_t = 0.0044$ and 0.0083 respectively). Both specimens failed due to concrete crushing of the lower half panel, at load ratios of $N_u/bhf_c' = 0.935$ and 0.750 respectively. Specimen #17 was a plain concrete panel tested under uniaxial compression. It failed due to splitting at mid-thickness and crushing over the entire width of the supporting end at $N_u/bhf_c' = 0.975$.

6.2.1 Relationship between Softening and Transverse Strain and Stress

Tension forces in the reinforcement caused two consequences in the concrete: transverse tensile strain and tensile stress. Collins⁴⁷ attributes the concrete softening to the transverse tensile strain computed using a gauge length which includes the cracks. Kollegger and Mehlhorn⁵⁷ suggest that the effective strength of concrete under transverse tension is more accurately described as a function of tensile transverse tensile stress than a function of tensile strain. For reinforced concrete, the largest tensile stress in the concrete is the cracking stress. After cracking the stress in the concrete is released by unloading to the reinforcement at the crack. To distinguish the real factor that softens the concrete, specimen #18 was transversely tensioned to a stress stage just before the initial crack occurred so that a large tensile stress was developed in the concrete of the entire panel while only very small strain existed in the concrete. According to the specimens previously tested, the initial cracks occurred at $T=12$ kN to 20 kN. Specimen #18 was transversely pulled to $T=15$ kN without any crack and was then loaded with longitudinal compression to failure. No crack formed in the entire test and the transverse tensile strain was unmeasurable. The specimen failed due to the crushing of the major part of the section at $N_u/bhf_c'=1.051$. Although the transverse tensile stress was near the maximum tensile stress the concrete could resist (cracking strength), no measurable reduction of compressive strength was observed.

Transverse tensile stress in the concrete itself did not soften the concrete.

The plots of N/bhf_c' vs. the longitudinal strains for specimen #13 to #18 were shown in Fig. 6.7c. As observed in the previous tests, the transverse tensile strain reduced the longitudinal stiffness.

The ultimate compressive strengths (N_u/bhf_c') for all 18 specimens were plotted against the ultimate average transverse tensile strain in Fig. 6.8. The test results show that the transverse tension reduces the compressive strength of the concrete. The largest reduction was 56%. To study the mechanisms of concrete softening and provide more test data to develop the relationship between N_u/bhf_c' and ϵ_{tu} , specimens of Group II and III were designed and tested.

6.3 Specimen Group II: Study of the Mechanism of Concrete Softening;

Fifteen specimens (#19 to #33) were included in Group II. The specimens had the same dimensions except the yield strength of the reinforcement was 423 MPa and concrete cylinder strength was from 33.7 MPa to 35.7 MPa. Specimens #19 to #22 were tested to study the effect of the load history on concrete softening. The longitudinal compression and the transverse tension were increased alternately rather than simultaneously. Specimens #23 to #29 were tested under repeated transverse tension. The tensile stress in the transverse reinforcement was cycled from zero to either a pre-yield

stress or a post-yield stress. As a result, a different number and pattern of cracks occurred under the same transverse tensile strain due to different cycles, and different transverse tensile strains might occur under the same transverse tensile stress. The purpose of this group of tests was to determine the real factor which reduced the concrete strength among transverse tensile stress, transverse tensile strain and cracking. Specimens #30 to #33 were cast with 5 mm deep and 10 mm wide grooves on both sides to result in different crack slopes to investigate their effects on concrete softening. The grooves are shown in Fig. 3.18.

The test results of specimens #19 to #22 are shown in Fig. 6.9. Fig. 6.9a shows the loading histories, Fig. 6.9b presents plots of N/bhf_c' vs. the average tensile strains and Fig. 6.9c presents plots of N/bhf_c' vs. longitudinal compressive strains. Specimen #19 was first loaded transversely to $\epsilon_t=0.009$ and then loaded longitudinally to failure. Cracks formed as a result of the application of transverse tension and did not change in the course of applying the axial compression N . The specimen failed due to crushing of the concrete at $\epsilon_t=0.01094$ and $N_u/bhf_c'=0.80$. Specimen #20 was first loaded longitudinally to the designated stress ($N_u/bhf_c'=0.81$) which was approximately the ultimate strength of #19 and then transversely pulled to failure. The failure occurred at $\epsilon_t=0.00943$ due to crushing of the concrete. The most significant observation in the test of #20 was that the concrete crushing in the longitudinal direction as directly caused by the increase of transverse tension, rather than an increase of longitudinal compression.

The close compressive strengths and transverse tensile strains at the ultimate state of panels #19 and #20 indicated that the load history had no effect on the ultimate strengths in the two specimens. However, the load history had an effect on the stiffness of the specimens (see Fig. 6.9c). Specimen #20 had a larger stiffness before the ultimate state than #19.

Specimens #21 and #22 were tested in a similar way as #19 and #20 but the load paths were in two steps. The load histories are shown in Fig. 6.9a and the changes of the strains vs. the longitudinal compressive stress are shown in Fig. 6.9b and 6.9c. Both specimens experienced similar behaviors to #19 and #20. Cracks formed in the concrete as a result of transverse tension applied. Specimen #21 was pulled to a large transverse tensile strain ($\epsilon_t=0.03883$), and as a result, the failure was very soft and no obvious crushing of concrete was observed at failure. The panel failed at $N_u/bhf_c'=0.411$ when no additional longitudinal load could be applied. Specimen #22 reached failure at $N_u/bhf_c'=0.51$ due to concrete crushing near the major cracks. Specimen #21 had a lower compressive strength than specimen #22 because it had larger transverse tensile strain. The load history had no obvious effect on the ultimate strengths of the two panels.

The application of the transverse tension caused two effects on the longitudinal deformation: reduction of the stiffness of concrete and an instant increase of compressive strain. As shown in Fig. 6.9c the specimens with larger transverse tensile strain had larger

compressive strain at the same compressive stress level. This was the softening effect caused by the transverse tension. Under a constant sustained longitudinal compression, the application of the transverse tension usually resulted in a significant increase in the longitudinal compressive strain (see the plateaus of the curves for Specimens #20 and 21 in Fig. 6.9c). The amount of the compressive strain increase was proportional to the amount of the sustained compressive stress. Thus no compressive strain was observed during the application of transverse tension at $N=0$ in the tests of #19 and #22. The instant increase of compressive strain was because the softening due to transverse tension concentrated at the sustained compressive stress level.

Specimens #23 to #29 were tested under longitudinal compression and cyclic transverse tension. As in the previous specimens, the concrete cracked and the cracks increased in number and size as a result of the transverse tension. The longitudinal compression had no measurable effect on the cracking. If the transverse tension reached a post-yield stage of the reinforcement, it usually caused a large transverse permanent tensile strain in the concrete after the tensile stress in the reinforcement was released (see Figs 6.10b to 6.12b). The larger transverse tensile strain usually corresponded to a plateau in the curves of N/bhf_c' vs. ϵ_c due to the softened stiffness (see Figs. 6.10c to 6.12c).

Figs. 6.10 and 6.11 show the test results of specimens #23 to #26. These four specimens were subjected to cyclic transverse tension but with different cycles and stress levels. The

reinforcement was pulled to either a pre-yield or a post-yield stress and then released to zero stress under approximately the same longitudinal load. Several cycles of the "pull-and release" transverse tensile force were applied until the average transverse tensile strain in the concrete reached the designated amount. The panels were then loaded longitudinally to failure under zero transverse tensile force ($T=0$). Specimen #23 was subjected to two cycles of the repeated tension before $\epsilon_t=0.01164$ was developed in the concrete. The panel failed at $N_u/bhf_c'=0.688$ due to crushing of the concrete. Specimen #24 experienced 4 cycles of repeated tension and a total transverse tensile strain of $\epsilon_t=0.04321$ was developed in the concrete. The panel failed at $N_u/bhf_c'=0.390$ when no additional compressive force could be applied. The failure was very soft and no crushing of concrete was observed. Specimens #25 and #26 experienced one and two cycles of repeated transverse tension to develop the transverse tensile strain of $\epsilon_t=0.00262$ and 0.01450 respectively. Specimen #25 reached failure at $N_u/bhf_c'=0.702$ due to local crushing at the upper left corner. Specimen 26 failed at $N_u/bhf_c'=0.596$ due to crushing of concrete across the loading end.

The test results of specimens #27 to #29 are shown in Fig. 6.12. Specimen #29 was a plain concrete panel tested under uniaxial longitudinal compression while #27 and 28 experienced repeated transverse tensile stress similar to specimens #23 to 26 except that #27 and #28 were loaded longitudinally to failure under a sustained tensile force, rather than zero force. They failed at $N_u/bhf_c'=0.656$ and 0.694 respectively due to crushing of the concrete. The plain

concrete panel (#29) reached failure at $N_u/bhf_c'=1.003$ due to crushing of the upper left corner.

The test results of specimens #23 to #29 indicated that among transverse tensile stress, strain and cracking, transverse tensile stress had no direct effect on the reduction of the compressive strength. The ultimate compressive force decreased as the average gross transverse tensile strain increased. Specimens #27 and #28 experienced non-zero transverse tensile force at the ultimate state, and as a result, the concrete between cracks had non-zero tensile stress. However specimens #27 and #28 had higher compressive strengths than the specimens (#24 and #26) with zero transverse tensile stress but larger average transverse tensile strain. Specimen #18 had a tensile stress approximately equal to the tensile strength of the concrete but it displayed no measurable softening in the concrete since only very small tensile strains and no cracking were developed in the concrete.

The test results of specimens S23 to S29 also indicates that the number and the width of the cracks were proportional to the gross transverse tensile strain. Actually, gross transverse tensile strain is a measure of cracks in the concrete. The larger the gross transverse tensile strain developed in the concrete, the more cracks formed in the concrete and the more the concrete was softened.

Specimen #30 to #33 were tested to study the effect of the crack pattern on the concrete softening. The location and the slope of the crack were defined by the grooves in the specimen surface. As

shown in Fig. 6.13a and 6.14a, the specimens were pulled transversely to develop the designated transverse tensile strains in the concrete and then loaded longitudinally to failure. Like the specimens previously tested, the concrete cracked as a result of the transverse tension. However, the initial crack usually formed within the groove(s) and this crack was the critical crack at failure. The cracks increased in number and width as the transverse tension increased. The later cracks might intercept the cracks in the inclined grooves (#30 and #32). Near failure, shearing was observed across the inclined cracks and crushing occurred where the inclined cracks intercepted the longitudinal cracks, (see the photos in Appendix B).

Figure 6.13 shows the test results of specimen #30 and #31. Specimen #30 had an inclined groove 18° to the longitudinal axial while in #31 the groove was in the longitudinal direction. Both specimens were pulled transversely to a transverse tensile strain approximately equal to 0.009, under an axial load of $N/bhf_c' = 0.13$. The specimens were then loaded longitudinally to failure. Specimen #30 failed at $N_u/bhf_c' = 0.674$ due to crushing of the concrete where the inclined crack intercepted other longitudinal cracks. The failure was combined with shearing across the inclined crack. Specimen #31 failed at $N_u/bhf_c' = 0.732$ due to crushing of the concrete at the upper right part of the specimen. Although both specimens had approximately equal transverse tensile strains at the ultimate state, #31 had a higher strength than #30.

The test results of specimens #32 and 33 are shown in Fig. 6.14. Both specimens had two grooves on each face to define cracks. In

specimen #32 the two grooves were inclined, compared with #33 in which the grooves were longitudinal. The inclination of the inclined grooves was 10° . The specimens were pulled transversely to tensile strains of 0.00437 and 0.00671 respectively under $N/bhf_c' = 0.15$, and then loaded longitudinally to failure. Specimen #32 failed at $N_u/bhf_c' = 0.701$ due to crushing of the concrete near the grooves within which the major cracks were developed, combined with shearing across these cracks (see photos in Appendix B). Specimen #33 failed at $N_u/bhf_c' = 0.636$ due to concrete crushing at the two upper corners.

6.4 Group III: Study of the Concrete Softening due to Non-uniform Stresses

Seven specimens (#34 to #40) were included in Group III. The specimens was tested to investigate concrete softening due to a non-uniform distribution of the compression stresses. The non-uniform distributions of stress were produced by one center force P and two side forces nP as shown in Fig. 3.19. Thus the total longitudinal compressive force in the concrete was $N = P + 2nP$. Four configurations of stress distributions, ($n=0.25$, $n=0.5$, $n=0.75$ and $n=1$) were tested. The specimens were tested with either uniaxial compression or under compression and transverse tension.

Figure 6.15 shows the test results for the specimens #40, #35, #34 and #36, with the non-uniform loading configuration factor n equal to 1.0, 0.75, 0.5 and 0.25 respectively. The specimens were loaded to failure under uniaxial longitudinal compression. Specimen

#35 failed at $N_u/bhf_c' = 0.981$ due to crushing of the concrete across the entire cross section. Specimens #34 and #36 reached failure at $N_u/bhf_c' = 0.858$ and 0.731 respectively by splitting of the concrete along the mid-width of the panel. The splitting was combined by local crushing underneath the center loading plates. Specimen #40 failed at $N_u/bhf_c' = 1.036$ due to crushing of the concrete at an upper corner. The specimens with lower loading configuration factor, n , had higher total compressive load (N_u) but lower center force (P_u) than the specimens with higher n . In other words, the specimens with more uniform stress distributions had higher average compressive strengths but lower peak stresses than the specimens with more non-uniformly distributed stresses.

The test results of #37 to #39 are shown in Fig. 6.16. The specimens were loaded with both the transverse tension and non-uniform compression. As shown in Figs. 6.16a and 6.16b, the specimens were pulled transversely to a designated transverse tensile strain and then loaded longitudinally to failure. As in the previous tests, the cracking is a result of the transverse tension. The nonuniform longitudinal compressive stress had no measurable effect on the cracking of the concrete. All three specimens failed due to crushing of the entire cross section. Specimens #37 and #38, with $n=0.5$ and 0.75 respectively, had approximately equal transverse tensile strains at failure ($\epsilon_t = 0.0079$ and 0.0081 respectively), however #37 failed at $N_u/bhf_c' = 0.703$ compared to $N_u/bhf_c' = 0.838$ for #38. Panel #39 had the same compressive stress configuration as #37 ($n=0.5$) but a higher transverse tensile strain at failure

($\epsilon_t=0.015$), as a result, #39 failed at a lower failure load ($N_u/bhf'_c=0.622$).

The results of the 7 specimens indicated that the non-uniform compressive stress reduced the average strength of the concrete but increased the peak strength. The reduction of the concrete strength increased as non-uniform configuration factor n increased. The panels with $n \leq 0.5$ and uniaxial compression usually failed due to splitting of the concrete. The three panels (#27 to #29) with both non-uniform compressive stress distribution and transverse tension had strength lower than the specimens with non-uniform compressive stress only. As indicated by the test results of panels #34, #37 and #39 which had the same n ($n=0.5$) but different transverse tensile strains ($\epsilon_t=0, 0.0079$ and 0.0150 respectively), the strength decreased as ϵ_t increased. Thus for the panels with both non-uniform compressive stress and transverse tension at the same time, the reductions of concrete strength due to the non-uniform compressive stress and transverse tension appeared to be superimposable. Since only three specimens were tested with both the transverse tension and non-uniform longitudinal compression, there were inadequate test data to determine the portions of strength reduction caused by transverse tension and non-uniform distribution of compression. The data points for these three tests in Fig. 6.17 (solid points at $\epsilon_{tu}>0$) fall in or near the top of the data points for uniformly loaded panels.

6.5 Summary of Test Results

1. The concrete compressive strength and stiffness were softened under the transverse tension. The effective compressive strength of concrete decreased as the average transverse tensile strain increased (Fig. 6.17).

2. The concrete was softened by the average transverse tensile strain or cracks, rather than the transverse tensile stress in the concrete. The larger the average tensile strain was, the more the concrete cracked and the more the concrete was softened.

3. For the specimens with cracks in directions other than longitudinal, failure usually resulted from crushing of the concrete where the cracks intercepted each other. The crushing usually combined with shearing along these cracks.

4. The loading history or load path taken to get to a given combination of longitudinal stress and transverse strain had no effect on the effective compressive strength of the concrete. However it might change the relationship between the compressive stress and compressive strain of the concrete.

5. The non-uniform distribution of the compressive stress (strain) also reduced the compressive strength of the concrete. As the compressive stress and strain got more non-uniformly distributed, the average strength decreased while the peak strength increased. This reduction was to some extent superposable with the reduction due to transverse tension.

Table 6.1 Major results of tests on concrete softening;

Specimen No.	f'_c MPa	Transverse Tension				Longitudinal Compression		
		T_u^{**} kN	ΣT_u kN	Δu mm	ϵ_{tu}	N_u kN	$\frac{N_u}{bhf'_c}$	Failure* Model
#1	20.6	35.1	280.6	3.860	0.00919	465.6	0.769	B.C
#2	21.0	37.7	296.2	3.041	0.00724	440.7	0.714	B.C
#3	22.3	33.5	271.0	2.152	0.00512	643.8	0.982	C
#4	22.6	0.00	0.000	0.145	0.00035	763.5	1.149	C
#5	23.0	0.00	0.000	0.240	0.00057	687.2	1.016	C
#6	23.6	32.4	264.4	1.391	0.00331	603.6	0.870	B.C
#7	24.1	34.1	274.6	2.535	0.00604	626.1	0.884	C
#8	24.5	38.0	298.0	6.006	0.01430	396.0	0.550	C
#9	24.9	36.5	259.0	5.720	0.01362	405.3	0.553	C
#10	25.1	38.0	298.0	7.215	0.01718	372.0	0.504	C
#11	25.7	39.6	307.6	7.524	0.01791	359.4	0.476	C
#12	26.0	0.00	0.000	0.410	0.00098	725.4	0.949	B.C
#13	26.2	40.0	310.0	8.907	0.02121	423.9	0.550	C
#14	26.4	41.3	317.8	9.106	0.02168	341.7	0.440	C
#15	26.5	32.6	265.6	1.861	0.00443	728.1	0.935	C
#16	26.8	36.2	287.2	3.515	0.00837	591.3	0.750	C
#17	26.8	0.00	0.000	0.133	0.00032	690.0	0.975	C
#18	26.8	14.5	116.0	0.450	0.00107	828.1	1.051	C
#19	33.7	41.8	335.4	4.593	0.01094	792.9	0.800	C
#20	33.9	45.1	355.2	3.961	0.00943	809.2	0.812	C

* B.C: Local bearing crushing

C: Crushing of Concrete across major part of the panel

S.F: Soft failure occurred when no additional longitudinal load could be applied.

No concrete crush was observed in this failure mode.

** Per transverse bar except top and bottom bars

Table 6.1 Continued

Specimen No.***	f'_c MPa	Transverse Tension				Longitudinal Compression			
		T_u^{**} kN	ΣT_u kN	Δu mm	ϵ_{tu}	N_u kN	$\frac{N_u}{bhf'_c}$	n	Failure* Moedel
#21	34.0	51.4	393.0	14.210	0.03383	410.7	0.411	1	C
#22	34.0	51.5	393.6	11.405	0.02715	509.4	0.510	1	S.F
#23	34.3	0.0	0.000	4.887	0.01164	693.6	0.688	1	C
#24	34.5	0.0	0.000	18.148	0.04321	396.0	0.390	1	S.F
#25	35.0	0.0	0.000	1.101	0.00262	722.4	0.702	1	B.C
#26	35.1	0.0	0.000	6.510	0.01450	615.0	0.596	1	C
#27	35.2	43.6	261.6	4.385	0.01044	678.9	0.656	1	C
#28	35.3	42.9	257.4	6.150	0.01464	720.6	0.694	1	C
#29	35.3	0.0	0.000	0.200	0.00048	1041.0	1.003	1	B.C
#30	35.4	39.9	324.0	4.120	0.00981	701.1	0.674	1	C
#31	35.5	37.4	309.0	4.153	0.00989	763.5	0.732	1	C
#32	35.7	36.7	304.8	1.834	0.00437	735.3	0.701	1	C
#33	35.7	40.0	324.6	2.820	0.00671	667.2	0.636	1	B.C
#34	36.0	0.00	0.000	0.000	0.00000	907.7	0.858	0.50	C
#35	36.0	0.00	0.000	0.000	0.00000	1038.2	0.981	0.75	C
#36	36.0	0.00	0.000	0.000	0.00000	774.0	0.731	0.25	B.C
#37	36.0	41.0	248.6	3.301	0.00786	744.6	0.703	0.50	C
#38	36.0	45.3	265.8	3.385	0.00806	866.9	0.838	0.75	C
#39	36.0	57.6	315.0	6.300	0.01500	659.2	0.622	0.50	C
#40	36.0	0.00	0.000	0.000	0.00000	1096.2	1.036	1	B.C

* B.C: Local bearing crushing

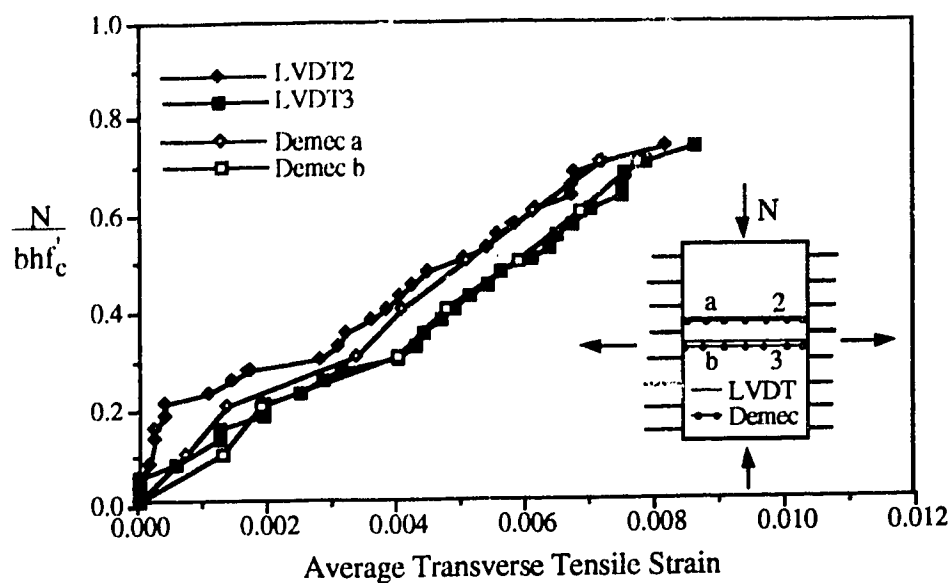
C: Crushing of Concrete across major part of the panel

S.F: Soft failure occurred when no additional longitudinal load could be applied.

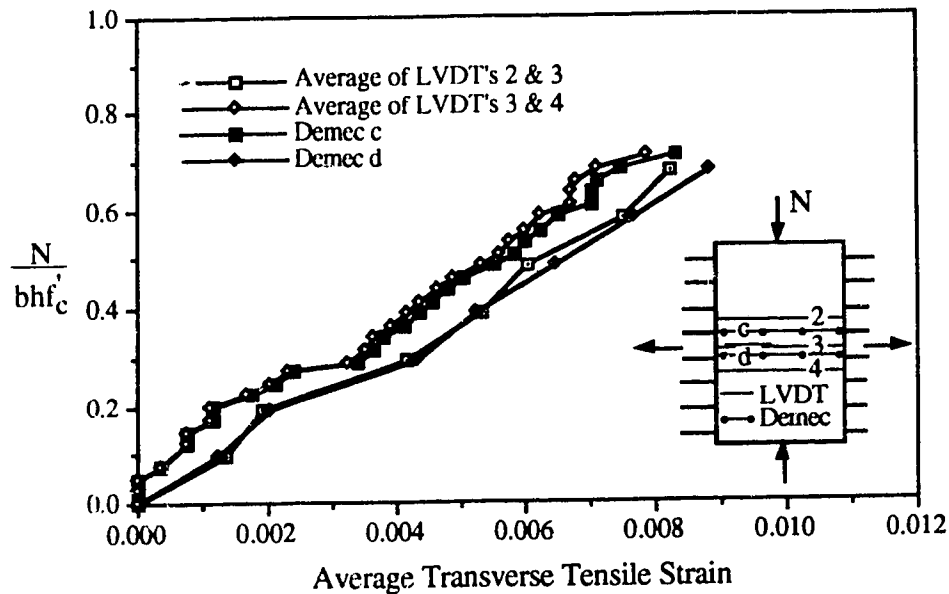
No concrete crushing was observed in this failure mode.

** Per transverse bar except top and bottom bars.

*** Specimens #37 to #39 were shorter and had six transverse bars.
Specimens #30 to #33 had grooves.

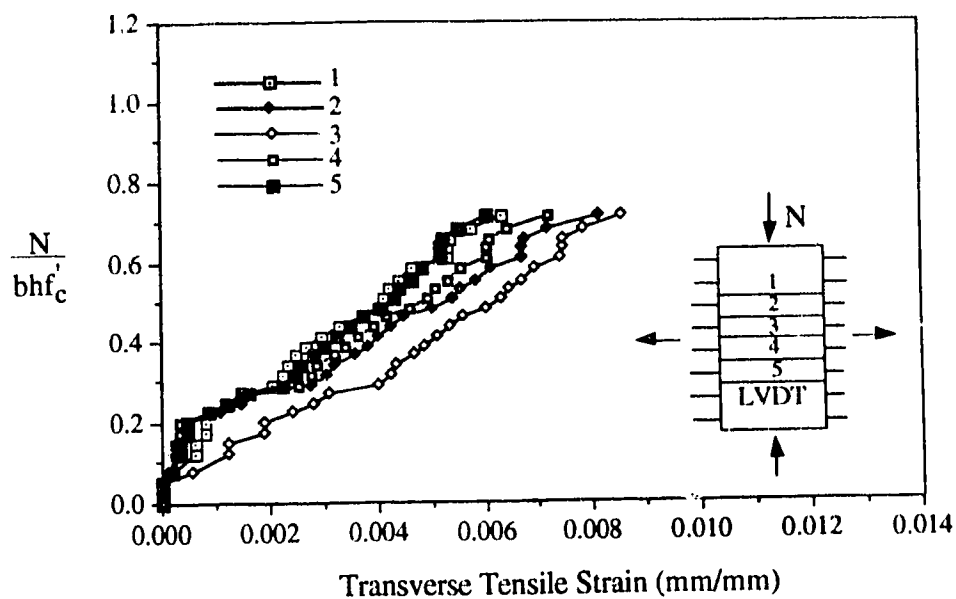


a) Comparison between the readings of the demec gauges on the concrete surface and the LVDT's

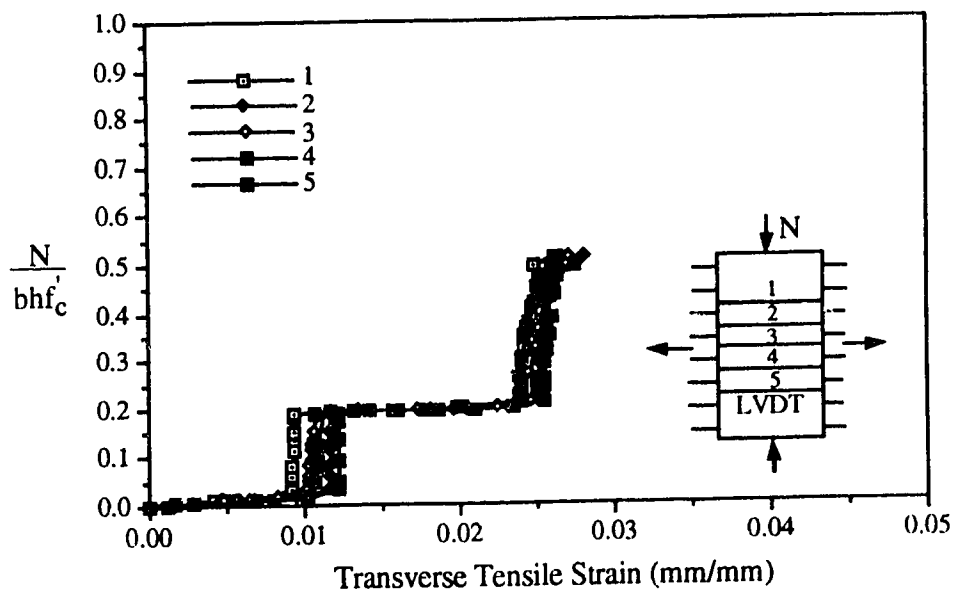


b) Comparison between the readings of the demec gauges on the steel and the LVDT's

Figure 6.1 Examples of transverse deformations measured by the demec gauges and LVDT's, (specimen #2)

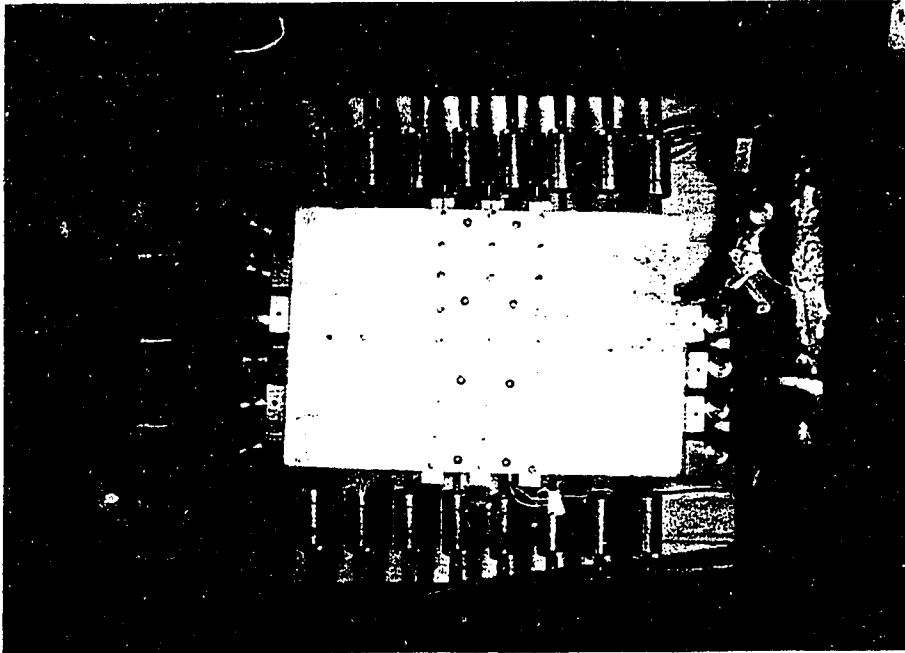


a) Specimen #2

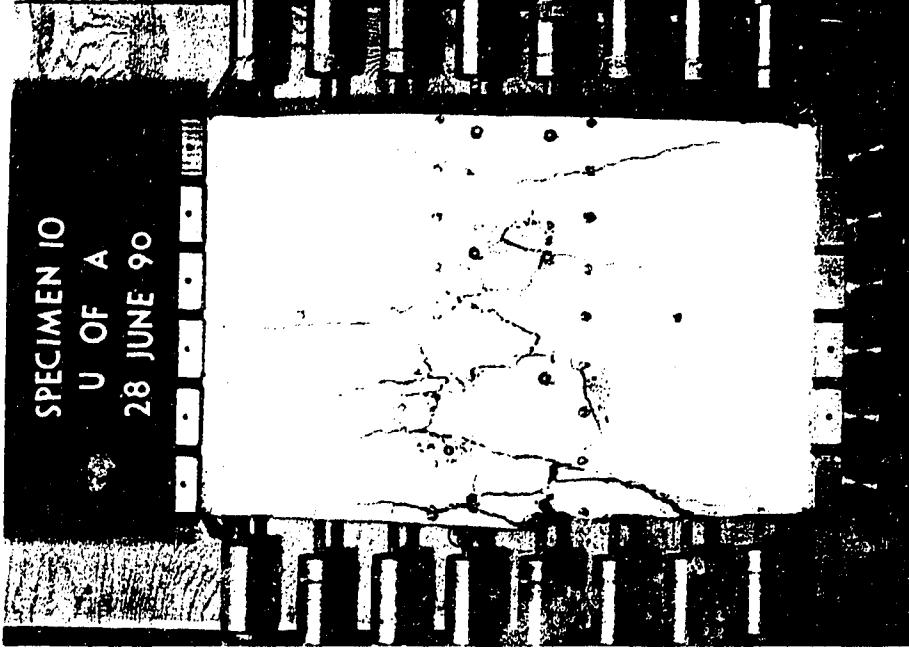


b) Specimen #22

Figure 6.2 Examples of LVDT readings at different heights

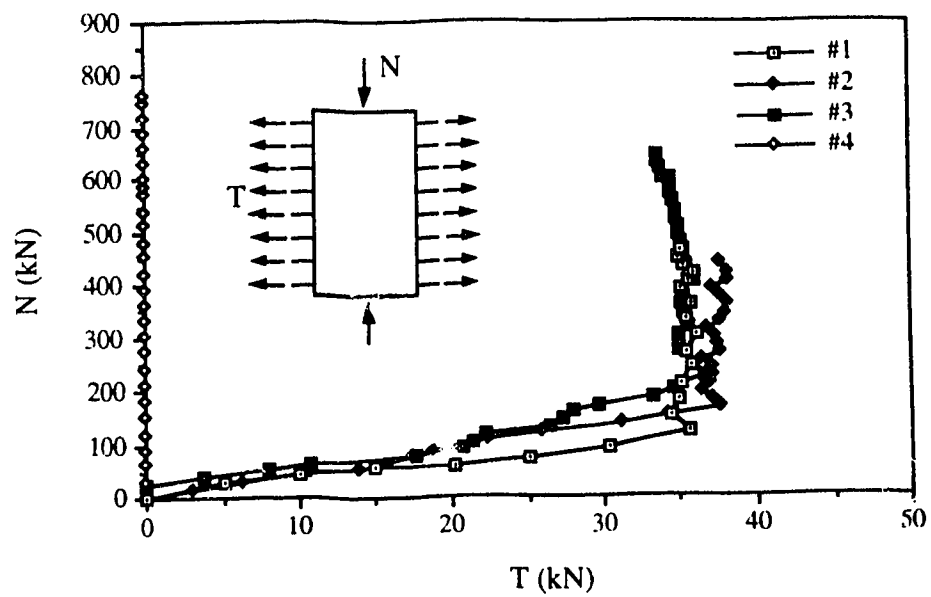


a) Specimen #1

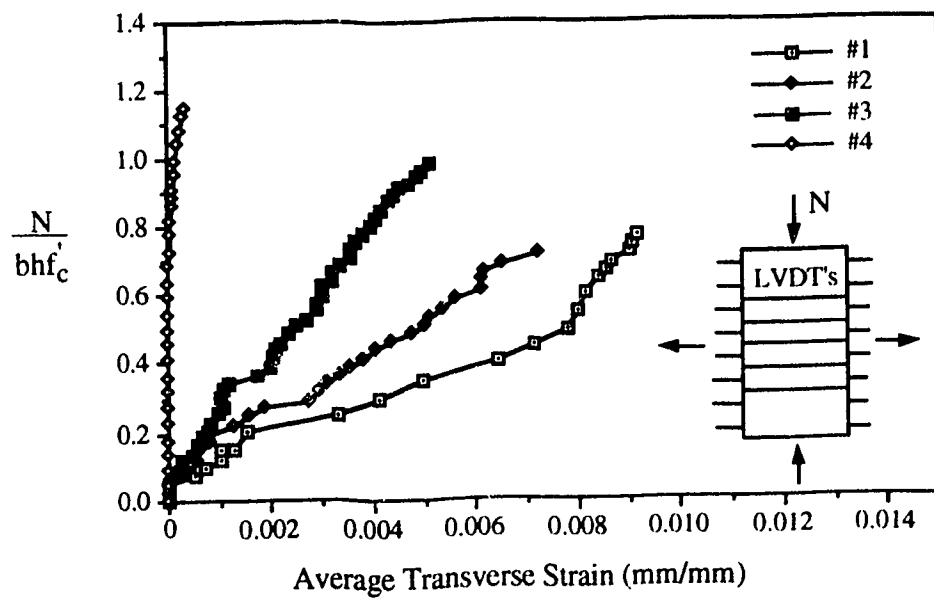


b) Specimen #10

Fig. 6.3 Photos of Specimens #1 and #10 after Failure

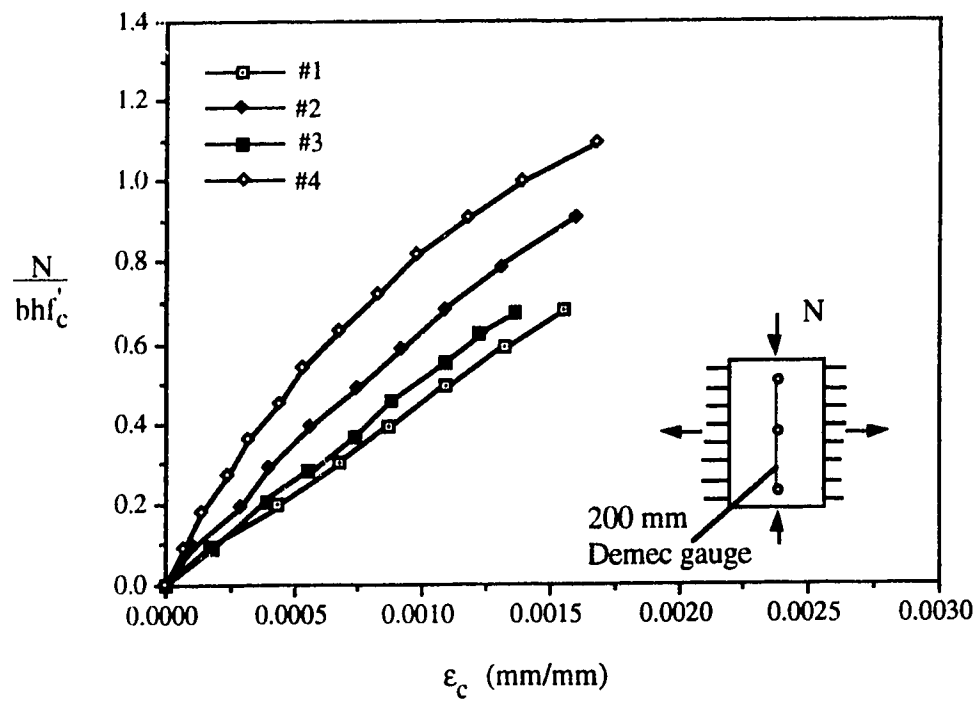


a) Load history



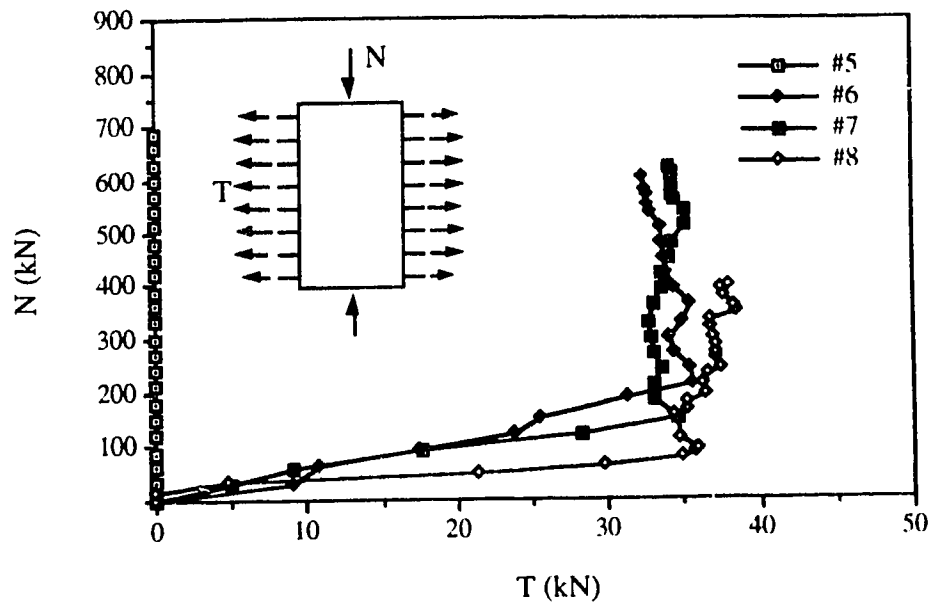
b) Compressive stress vs. transverse strain

Figure 6.4 Test results, specimens #1 to #4

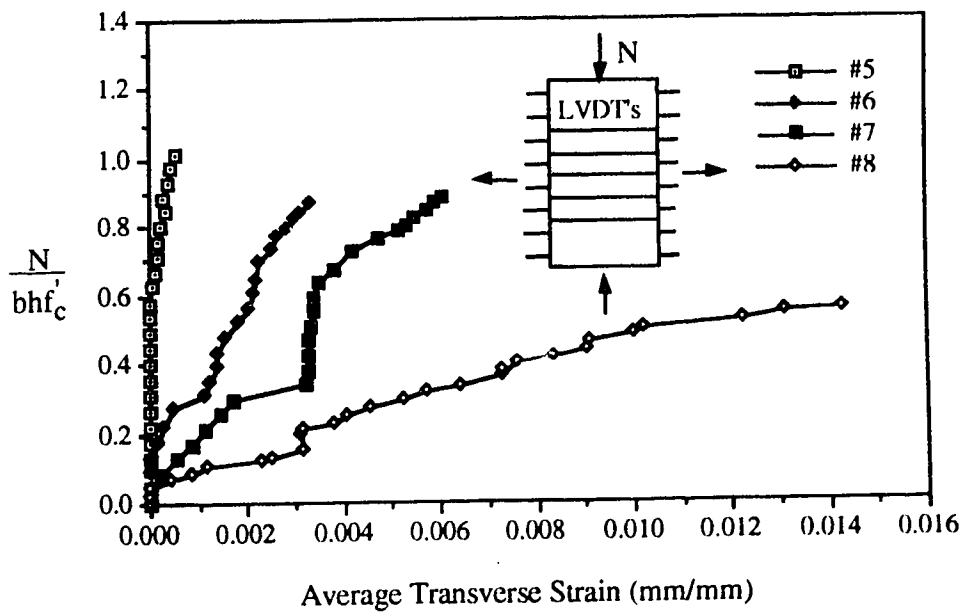


c) Load vs. vertical compressive strain

Figure 6.4 Test results, specimens #1 to #4

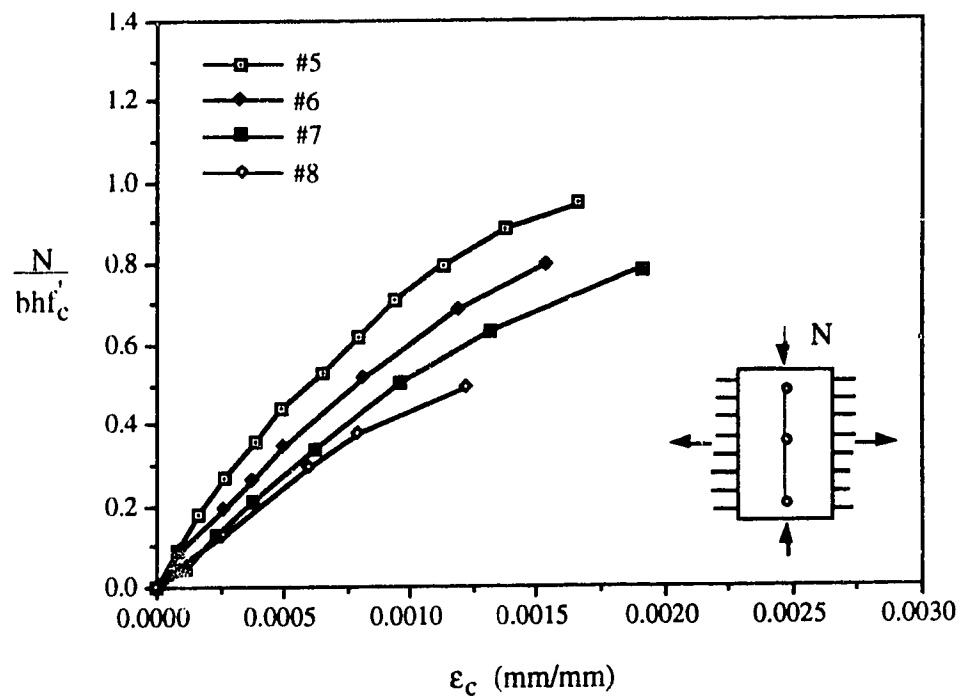


a) Load history



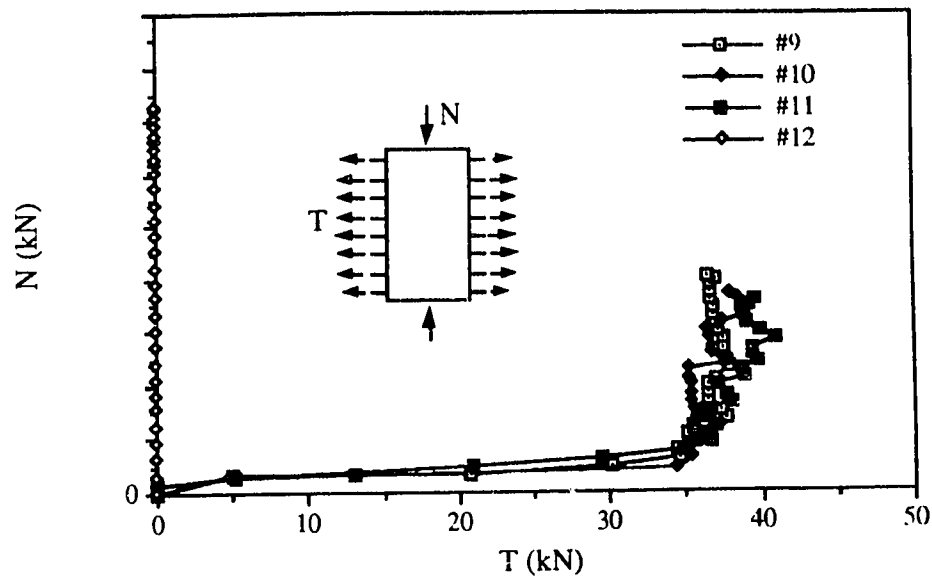
b) Compressive stress vs. transverse strain

Figure 6.5 Test results, specimens #5 to #8

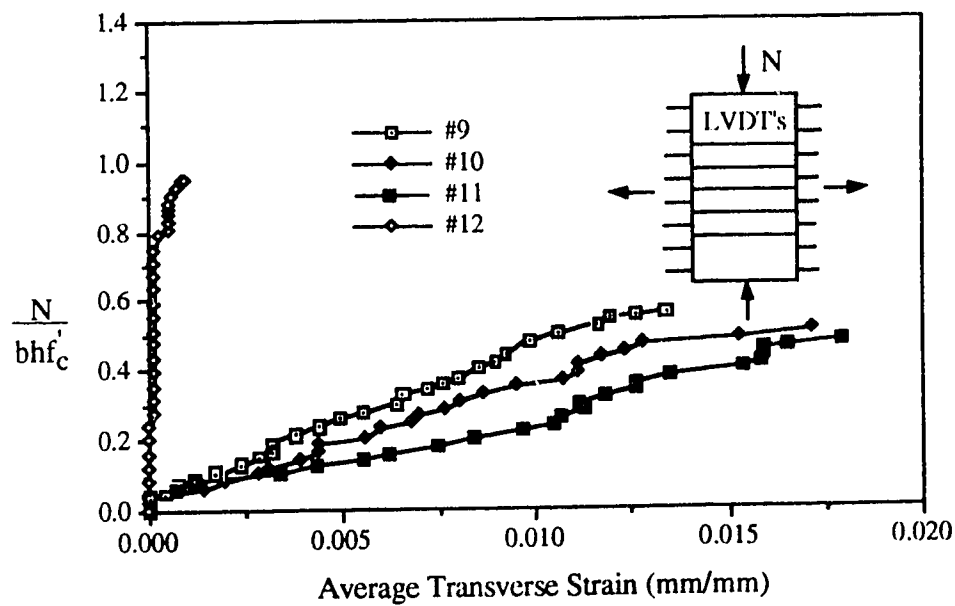


c) Load vs. vertical compressive strain

Figure 6.5 Test results, specimens #5 to #8

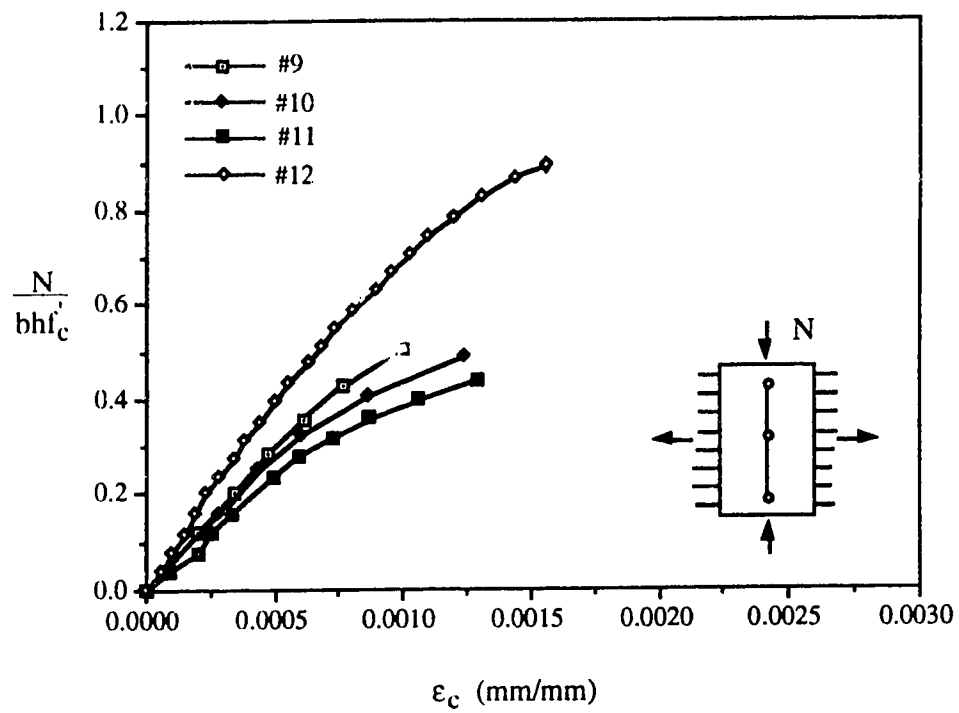


a) Load history



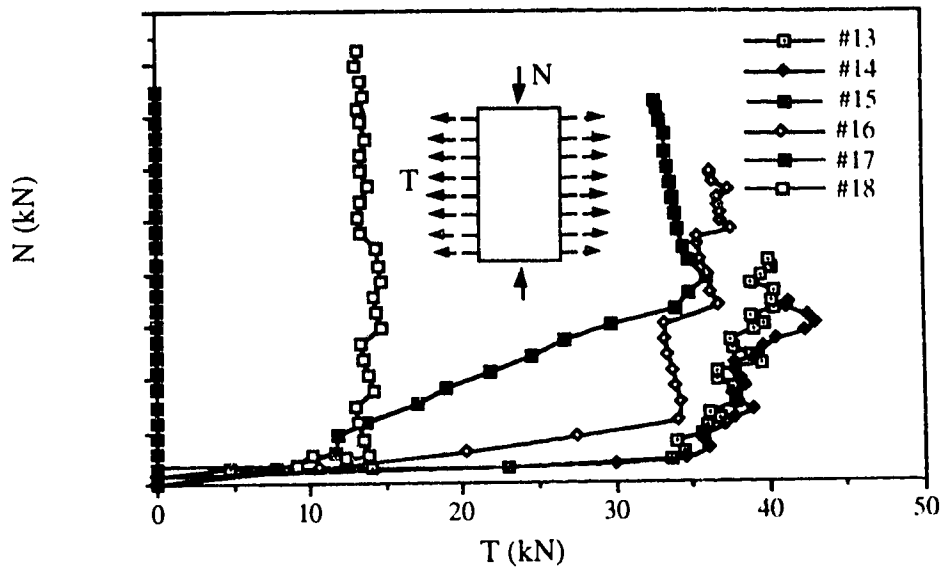
b) Compressive stress vs. transverse strain

Figure 6.6 Test results, specimens #9 to #12

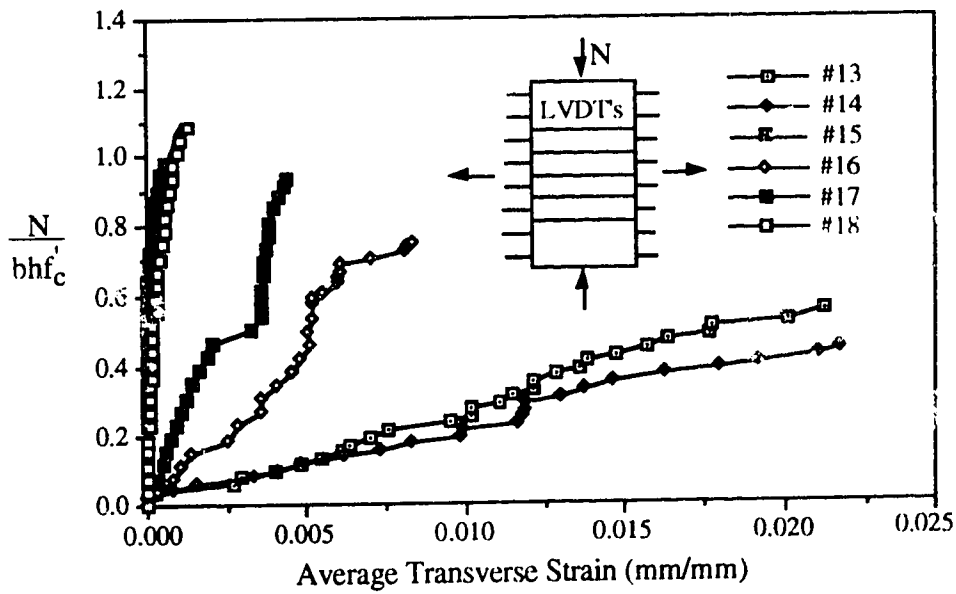


c) Load vs. vertical compressive strain

Figure 6.6 Test results, specimens #9 to #12

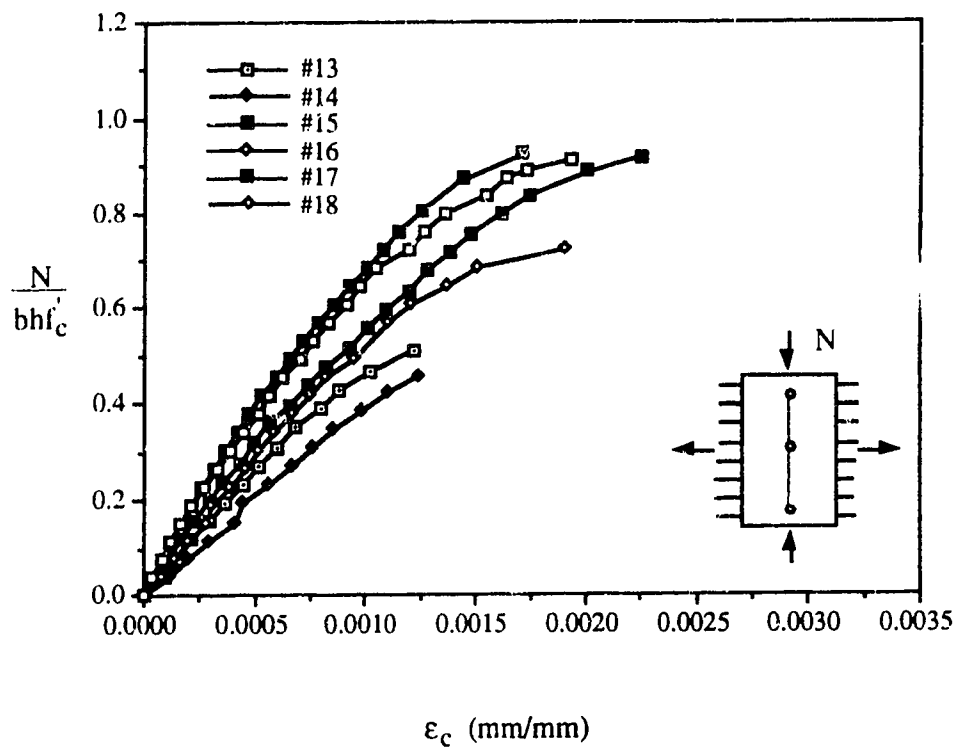


a) Load history



b) Compressive stress vs. transverse strain

Figure 6.7 Test results, specimens #13 to #18



c) Load vs. vertical compressive strain

Figure 6.7 Test results, specimens #13 to #18

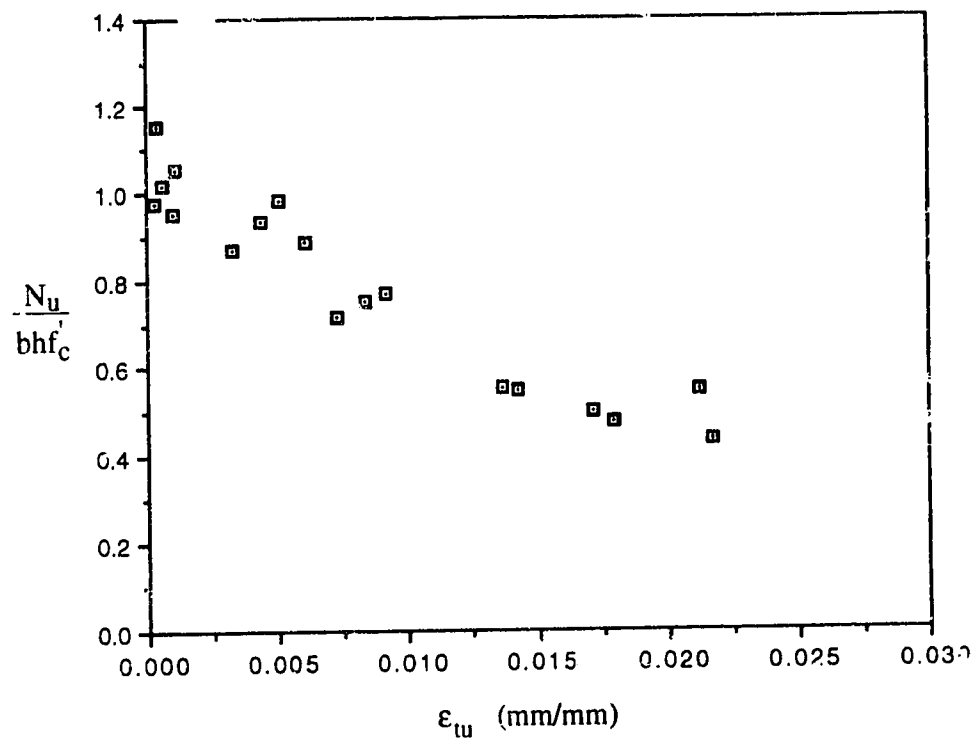
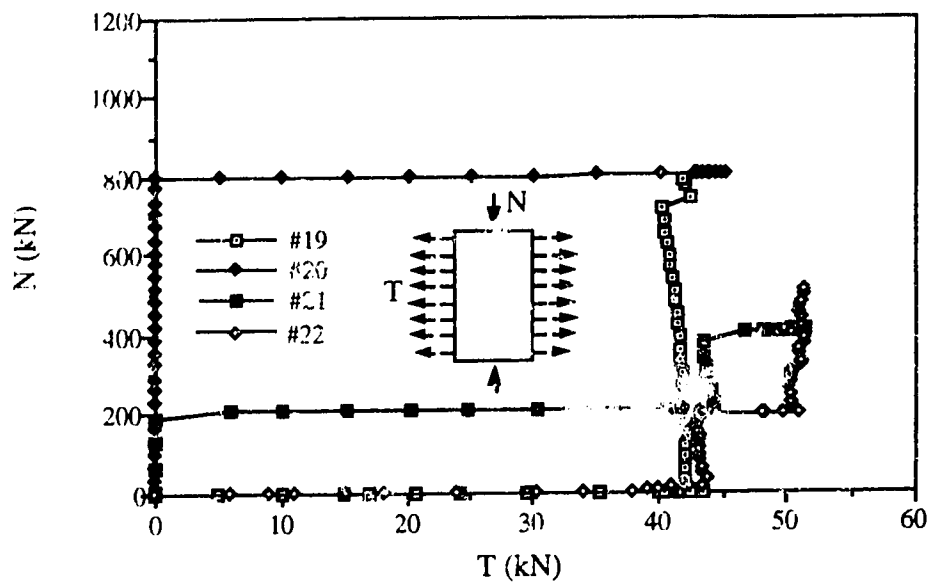
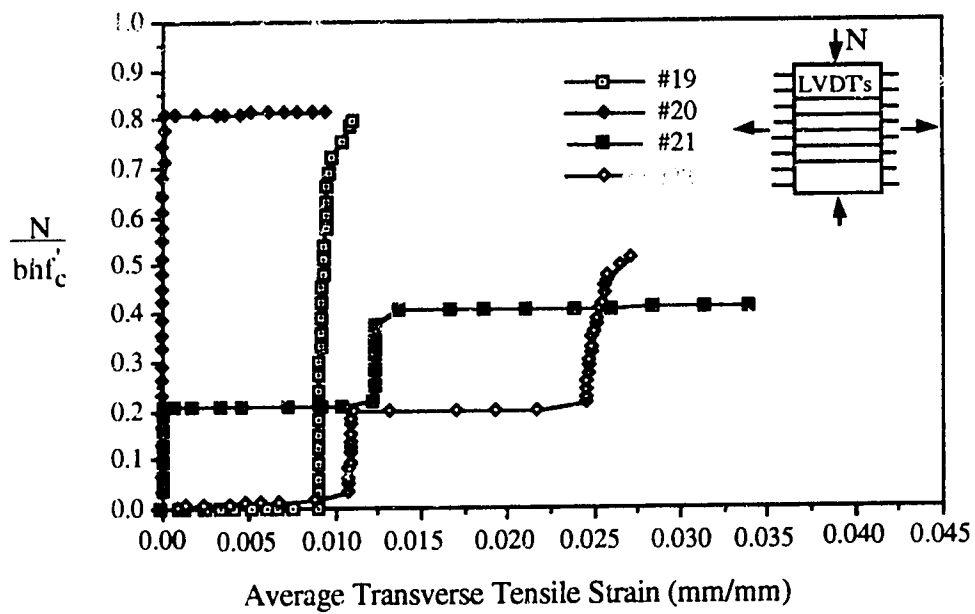


Figure 6.8 The effective compressive strengths for specimens of Group I

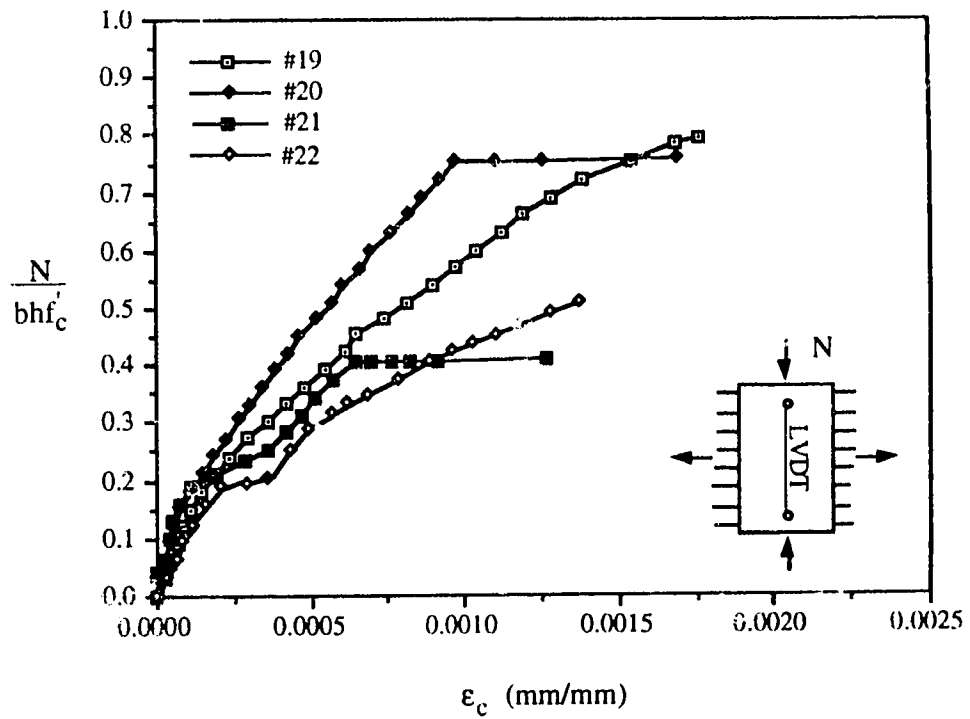


a) Load history



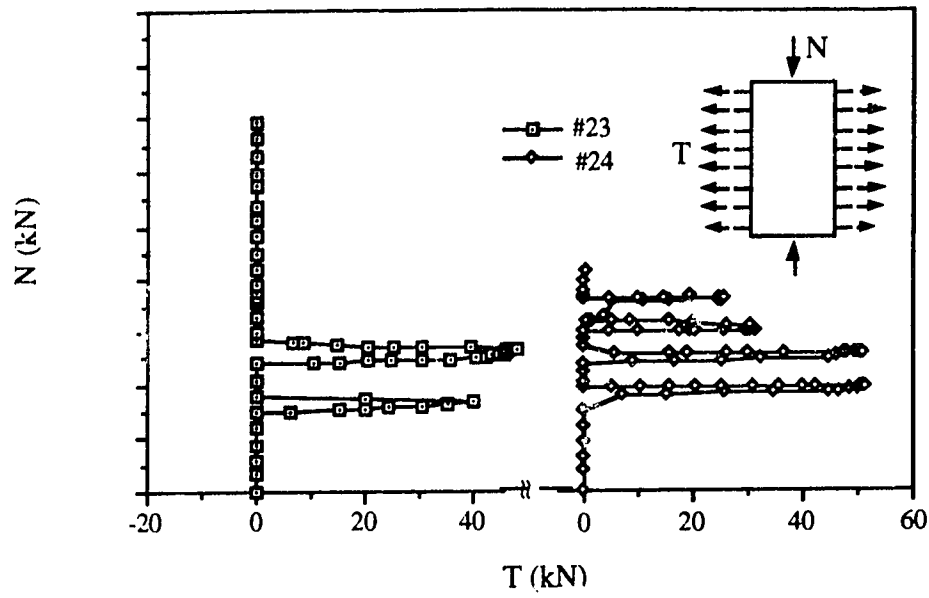
b) Load vs. transverse tensile strain

Figure 6.9 Test results, specimens #19 to #22

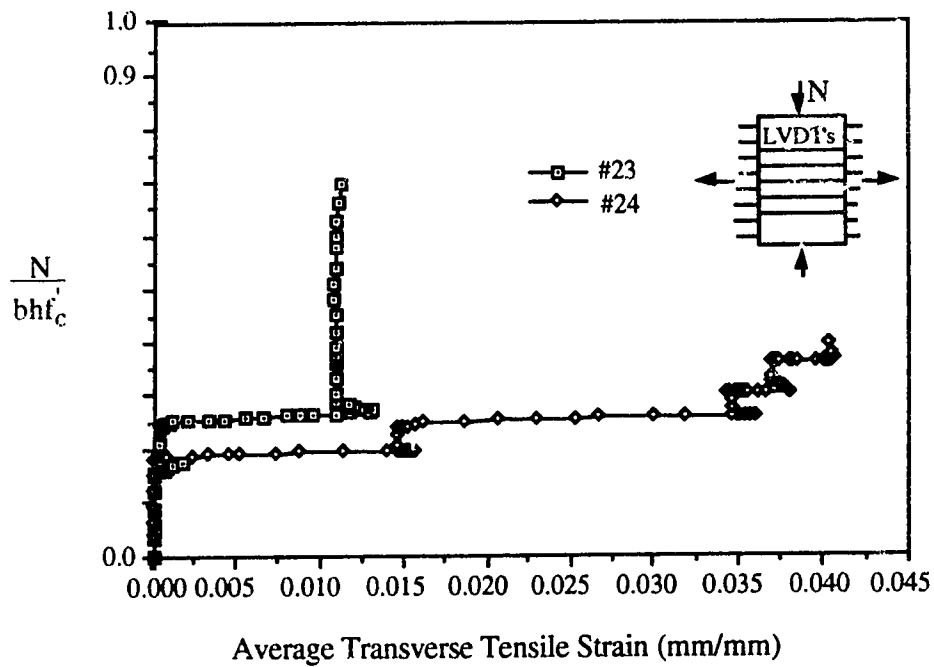


c) Load vs. vertical compressive strain

Figure 6.9 Test results, specimens #19 to #22

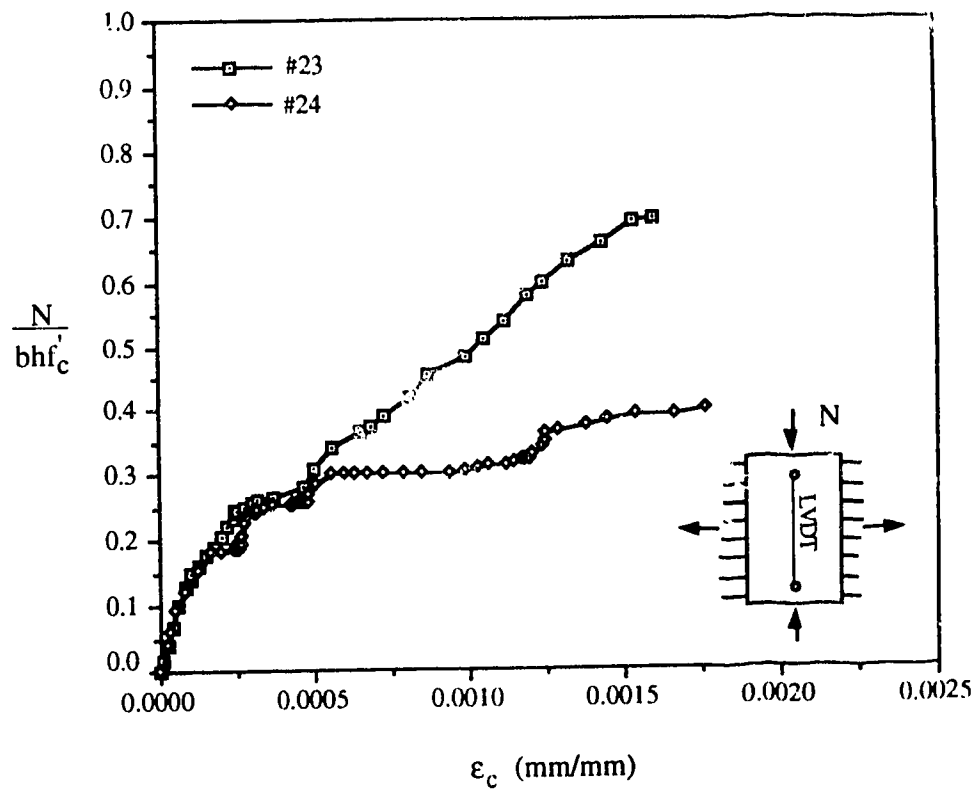


a) Load history



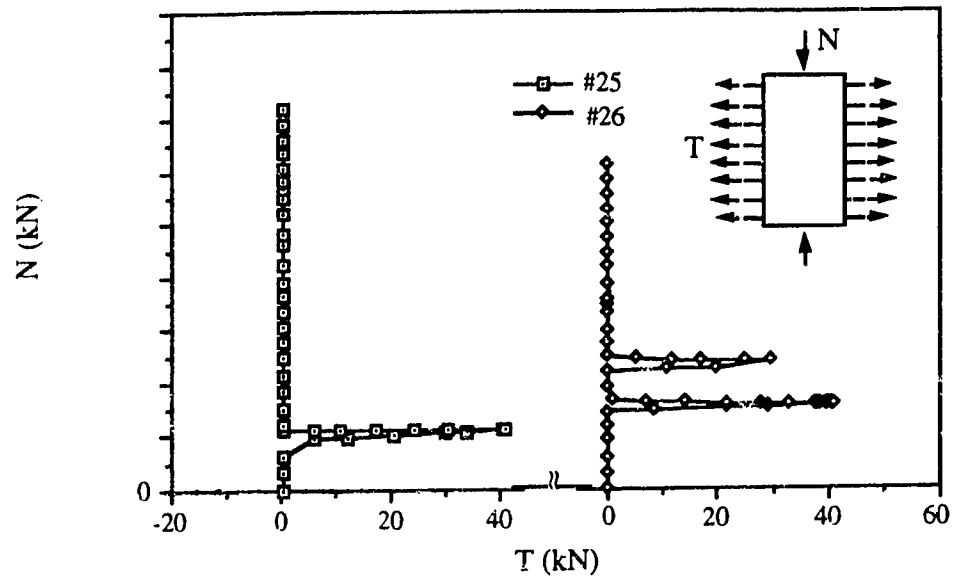
b) Load vs. transverse tensile strain

Figure 6.10 Test results, specimens #23 and #24

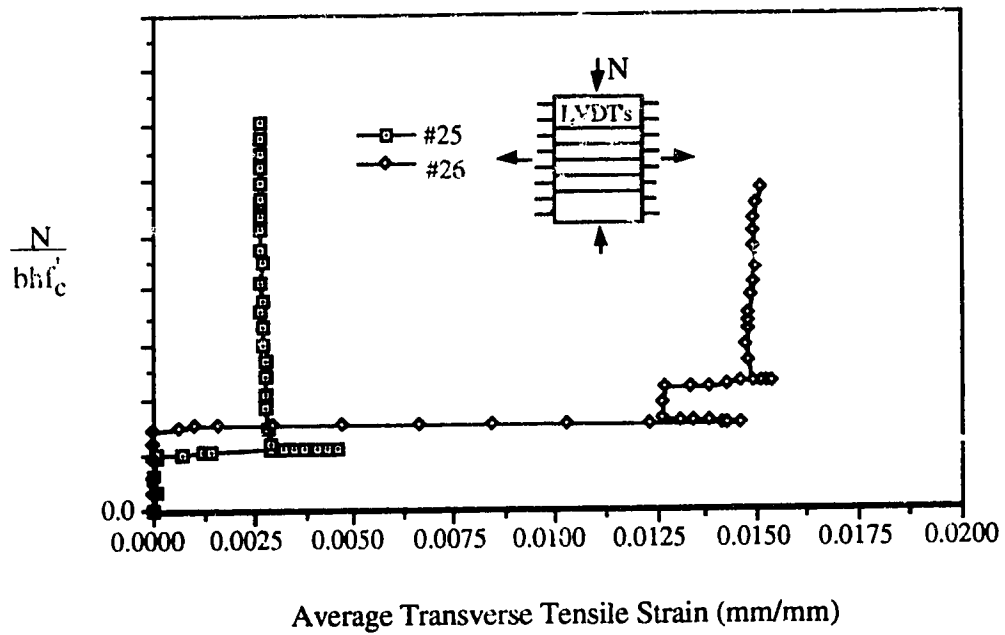


c) Load vs. vertical compressive strain

Figure 6.10 Test results, specimens #23 and #24

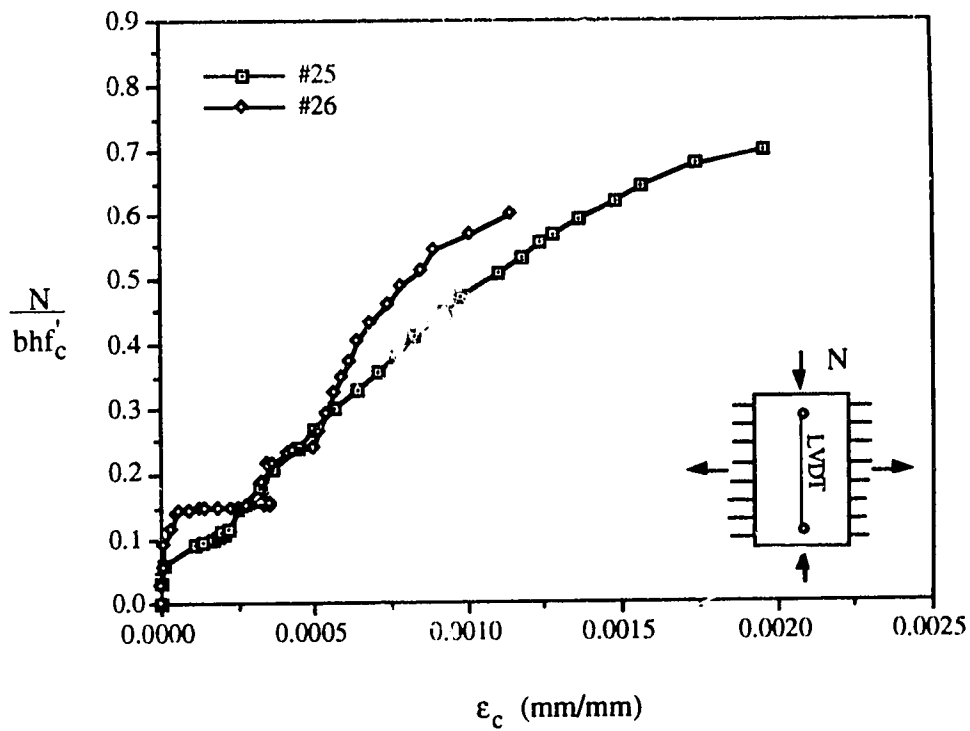


a) Load history



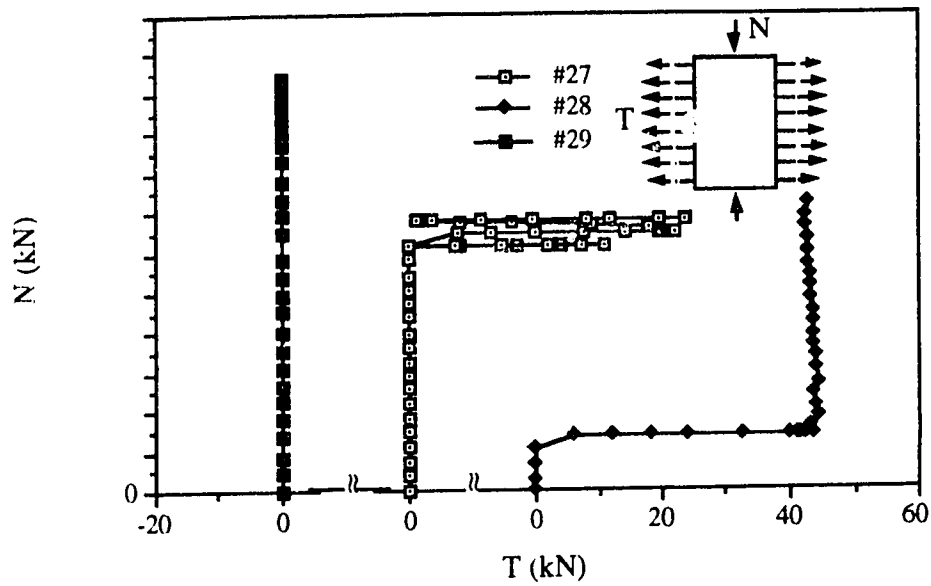
b) Load vs. transverse tensile strain

Figure 6.11 Test results, specimens #25 and #26

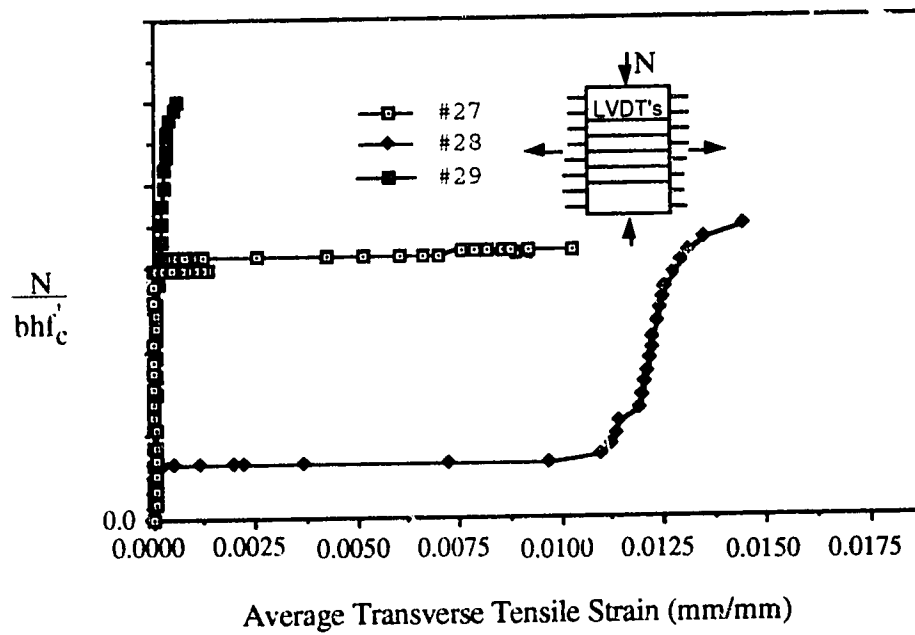


c) Load vs. vertical compressive strain

Figure 6.11 Test results, specimens #25 and #26

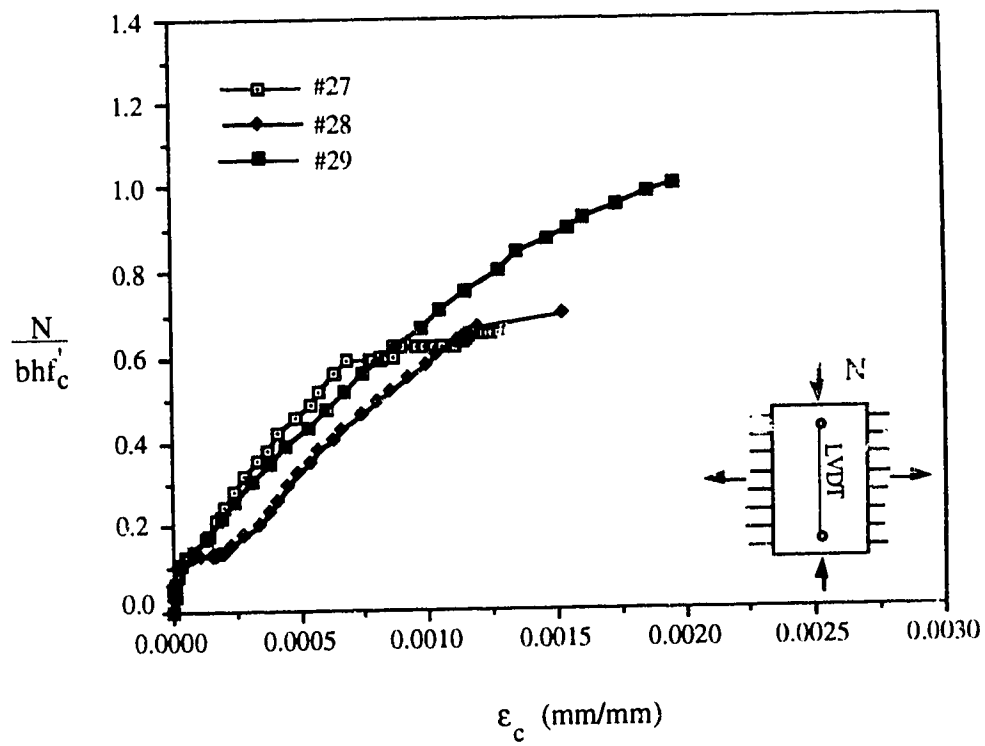


a) Load history



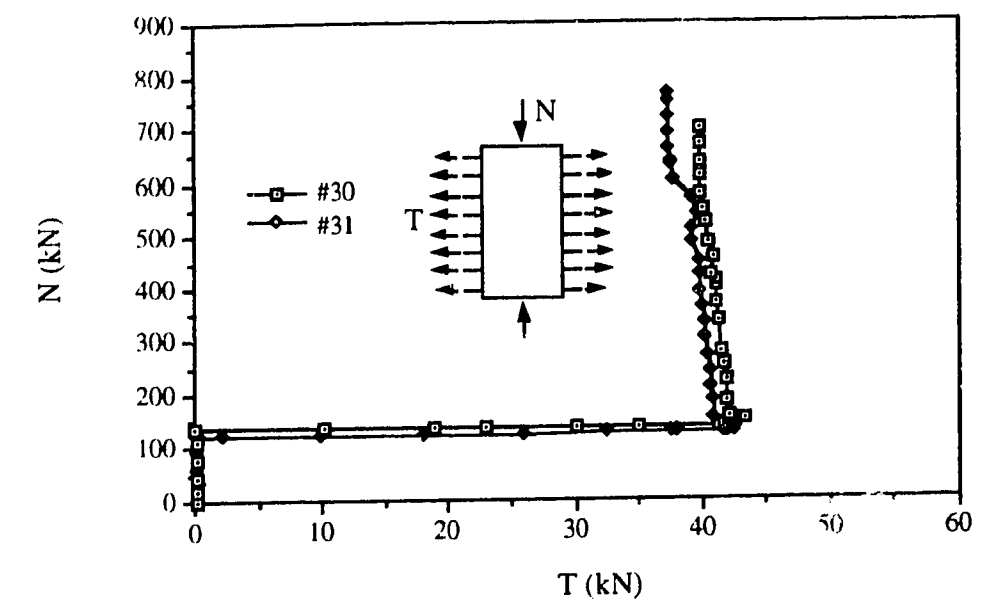
b) Load vs. transverse tensile strain

Figure 6.12 Test results, specimens #27 to #29

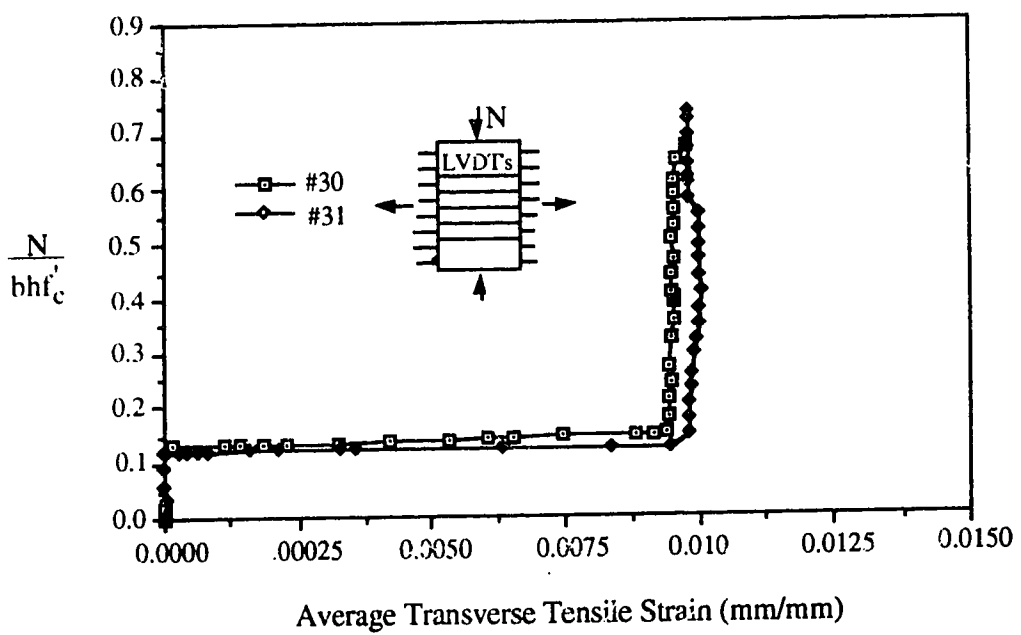


c) Load vs. vertical compressive strain

Figure 6.12 Test results, specimens #27 to #29

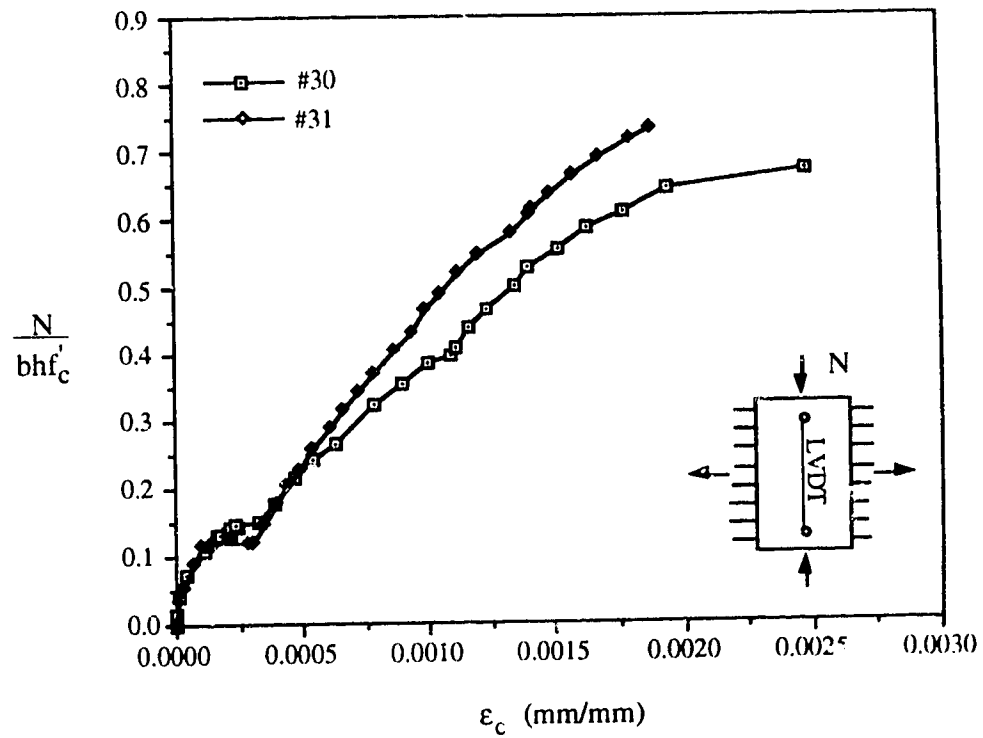


a) Load history



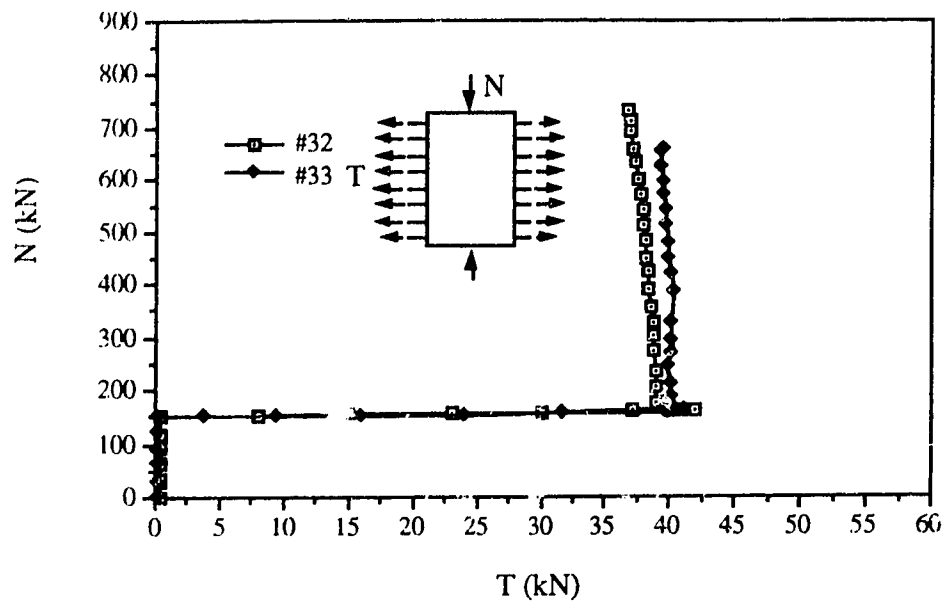
b) Load vs. transverse tensile strain

Figure 6.13 Test results, specimens #30 and #31

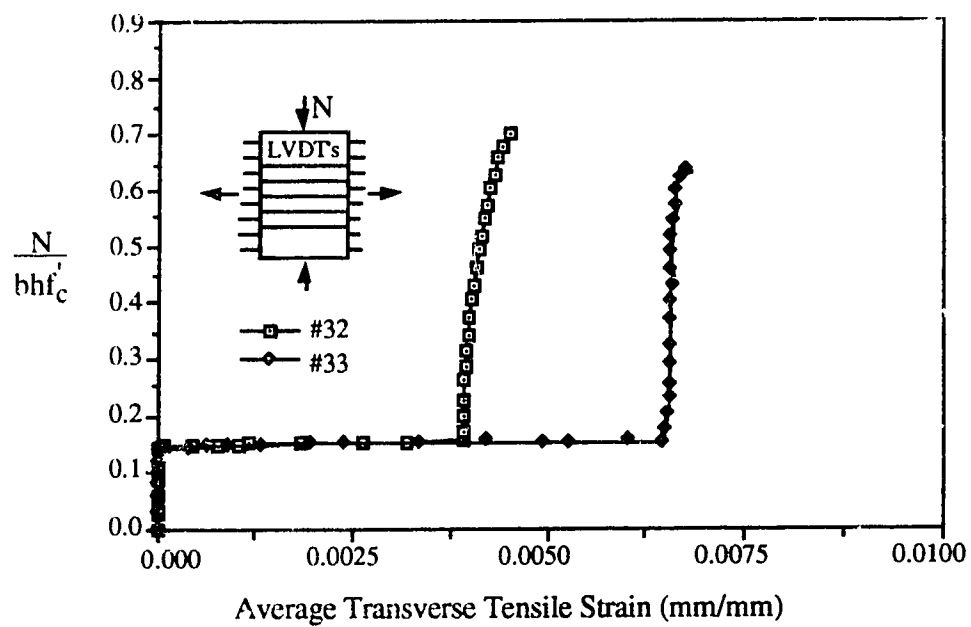


c) Load vs. vertical compressive strain

Figure 6.13 Test results, specimens #30 and #31

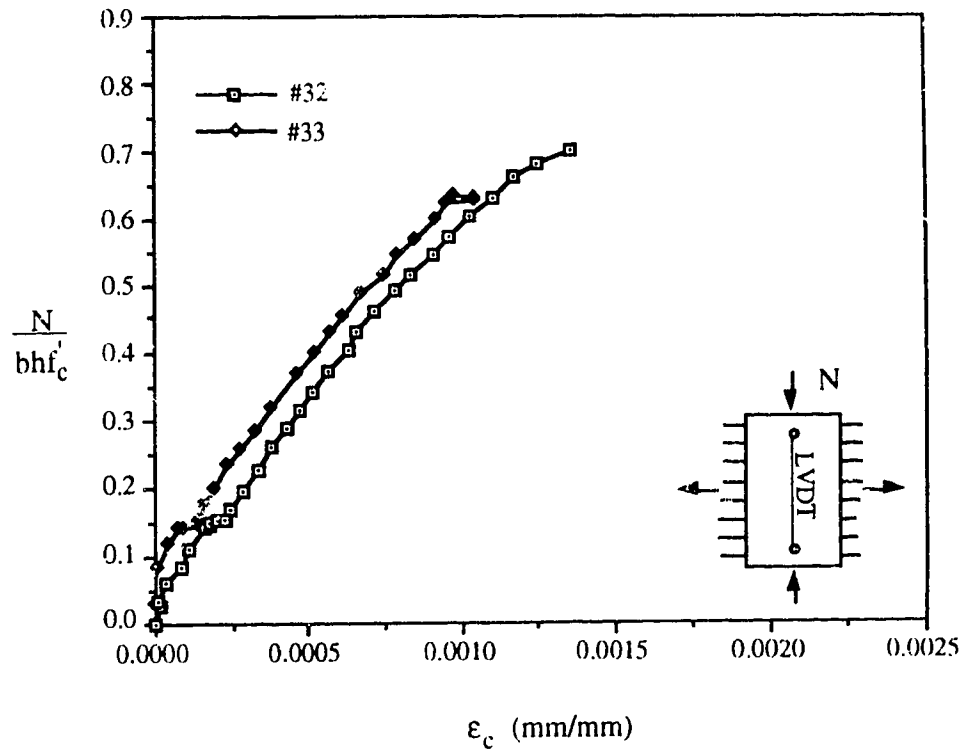


a) Load history



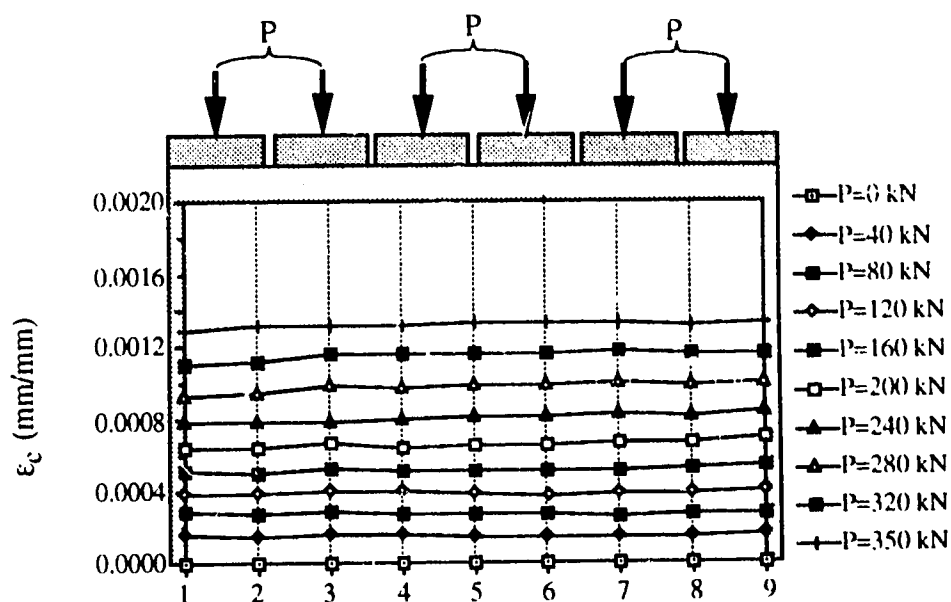
b) Load vs. transverse tensile strain

Figure 6.14 Test results, specimens #32 and #33

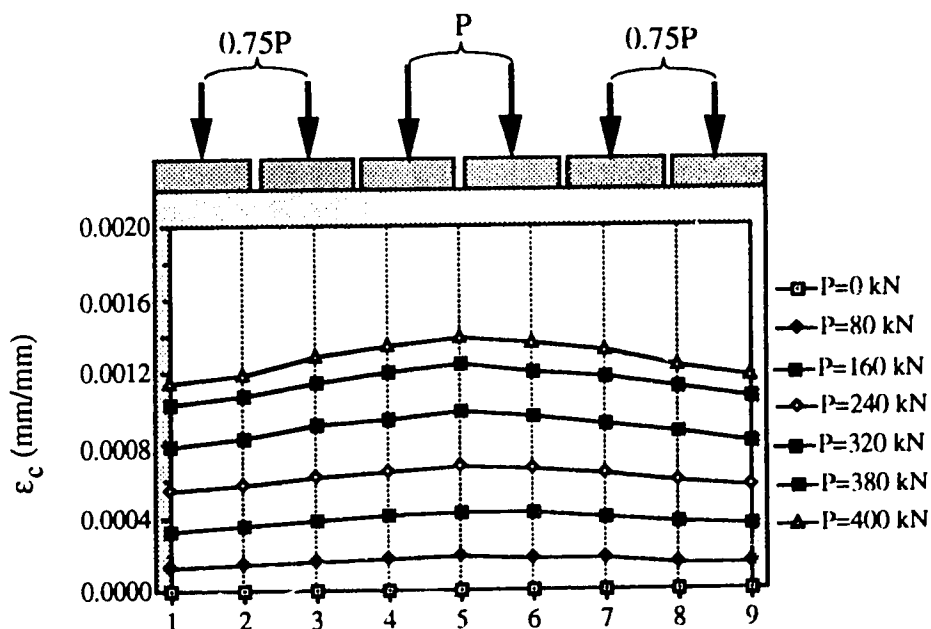


c) Load vs. vertical compressive strain

Figure 6.14 Test results, specimens #32 and #33

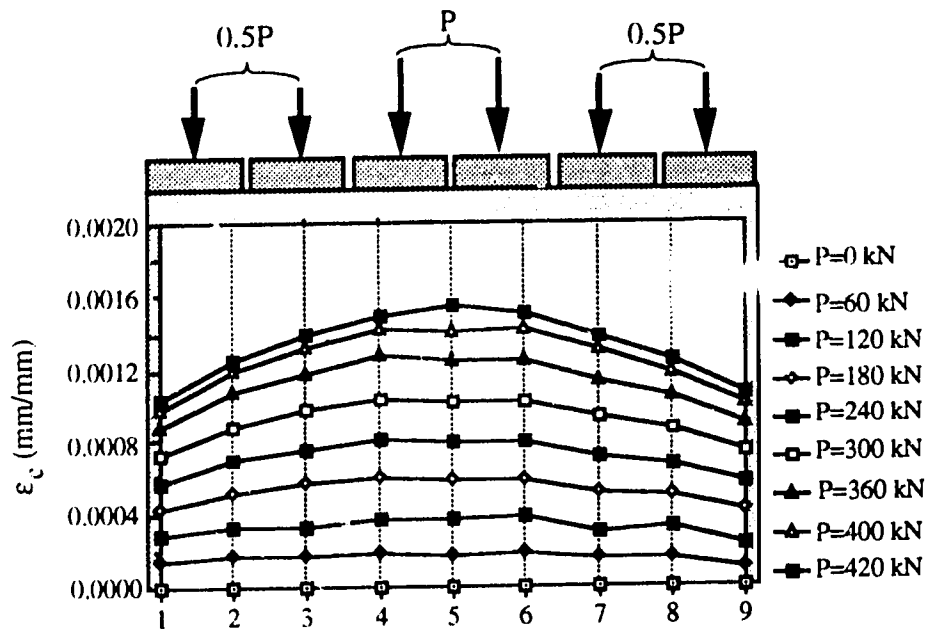


a) Longitudinal compressive strain distribution, #40
($n=1.0$, $P_u=365.4$ kN)

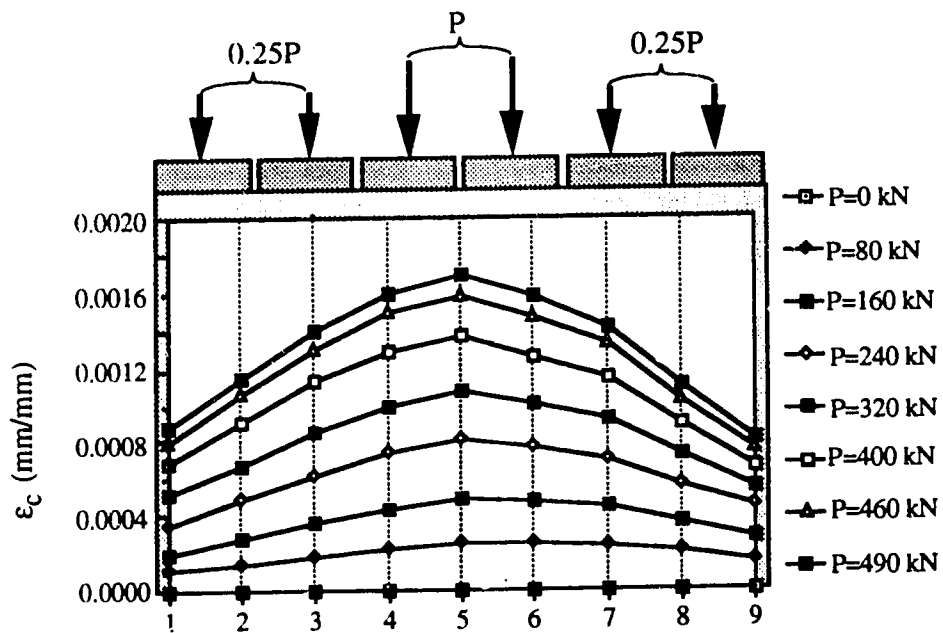


b) Longitudinal compressive strain distribution, #35
($n=0.75$, $P_u=415.0$ kN)

Figure 6.15 Test results, specimens #34 to 36 and #40

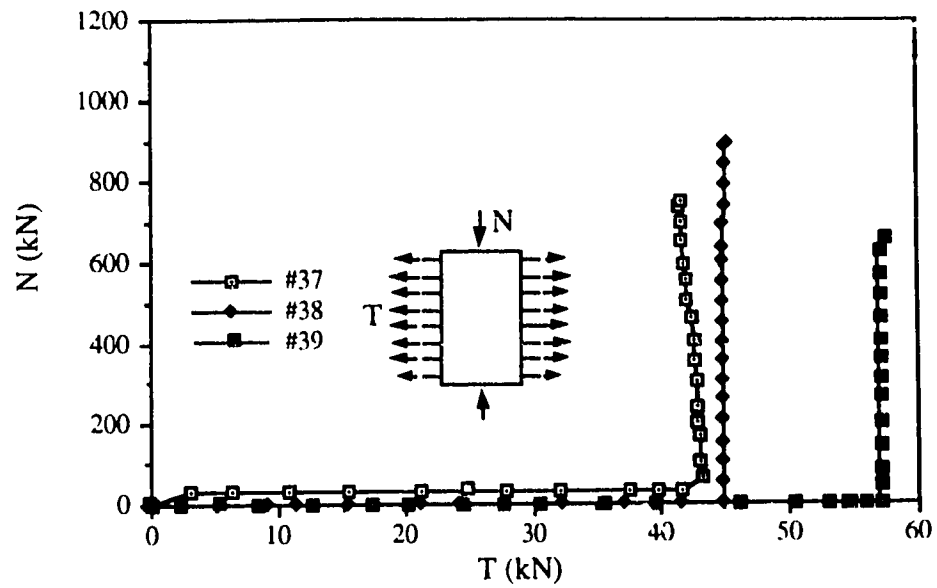


c) Longitudinal compressive strain distribution, #34
($n=0.5$, $P_u=453.9$ kN)

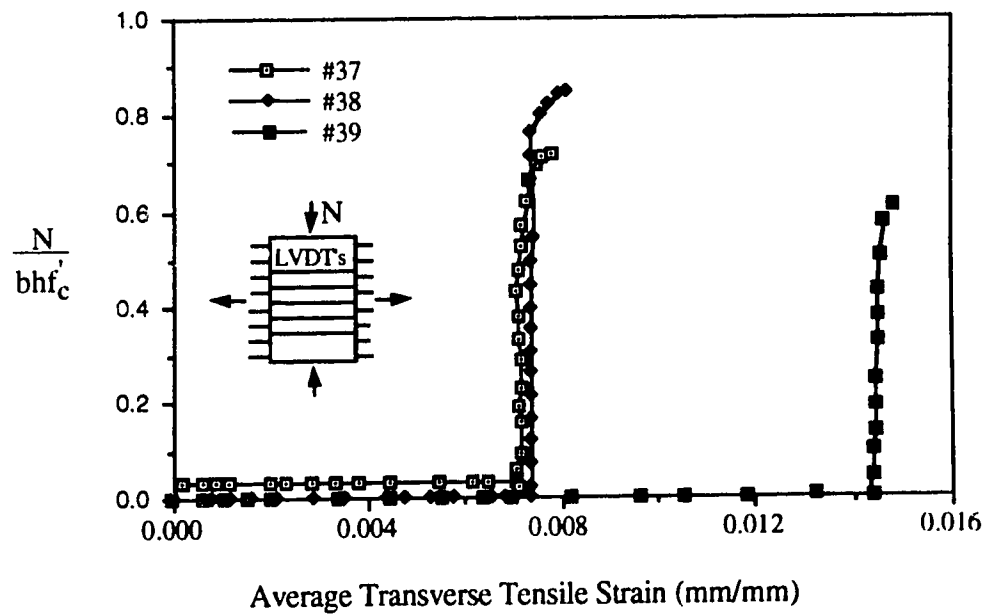


d) Longitudinal compressive strain distribution, #36
($n=0.25$, $P_u=516.0$ kN))

Figure 6.15 Test results, specimens #34 to 36 and #40



a) Load history



b) Load vs. transverse tensile strain

Figure 6.16 Test results, specimens #37 to #39

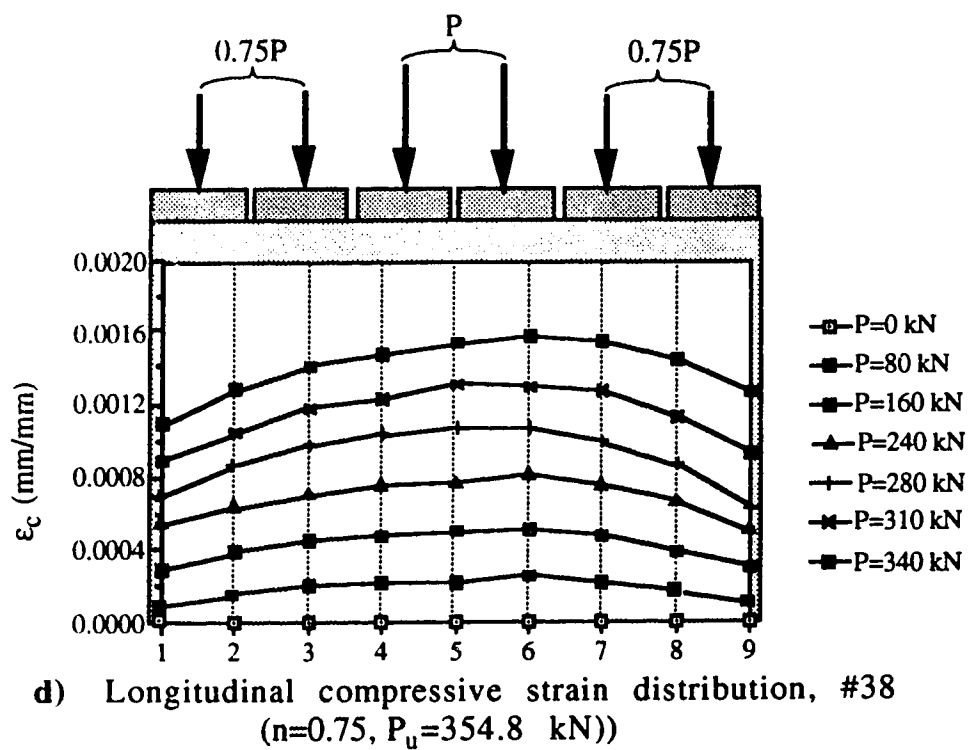
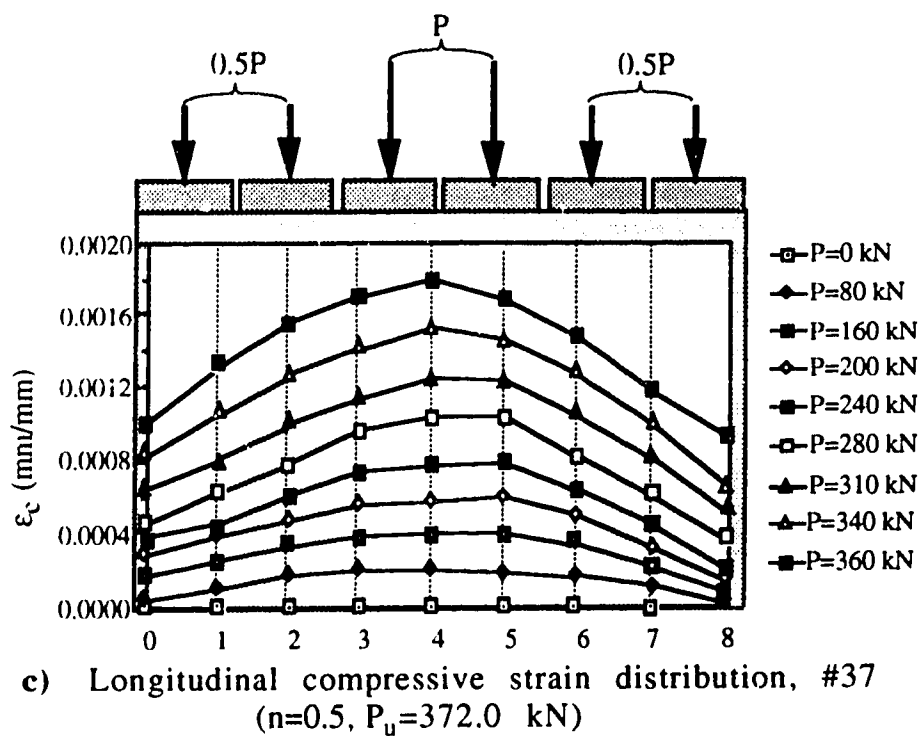
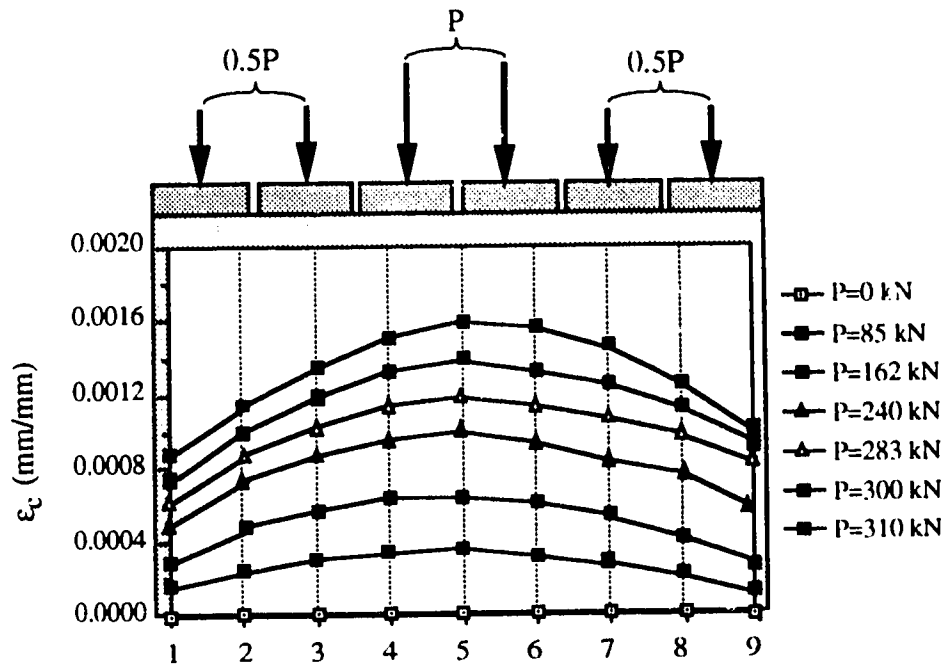


Figure 6.16 Test results, specimens #37 to 39



e) Longitudinal compressive strain distribution, #39
($n=0.5$, $P_u=329.6$ kN)

Figure 6.16 Test results, specimens #37 to 39

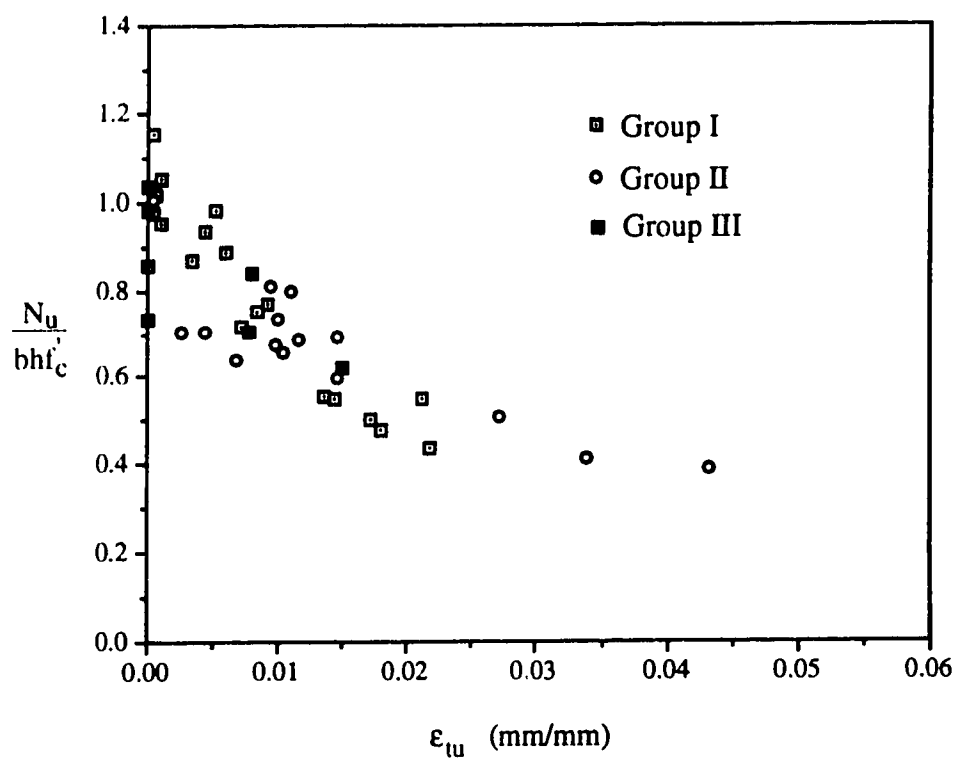


Figure 6.17 The effective compressive strengths for the test specimens

7 THE MECHANISM OF CONCRETE SOFTENING AND THE EFFECTIVE STRENGTH OF CONCRETE

In this chapter, the mechanisms of concrete softening due to transverse tension and non-uniformly distributed compressive strains are discussed. An empirical equation is developed to calculate the effective compressive strength of concrete due to transverse tension and a constant efficiency factor is proposed for design. The proposed effective strength of concrete is compared with the work by other researchers and the equation used in the current CSA Code².

7.1 Factors Affecting Concrete Softening

The test results of the 40 concrete panels indicated that the concrete was significantly softened by transverse tension. The effective strength of the concrete was reduced as the average gross transverse tensile strain increased. The maximum reduction of the concrete strength was as large as 60%. The load paths had no effect on the reduction of concrete strength.

The concrete softening is generally attributed to transverse tension. However, transverse tension causes three consequences in the concrete: transverse tensile stress, transverse tensile strain and cracking of concrete. Collins^{46,47} describes the effective strength of softened concrete as a function of gross transverse tensile strain, while Kollegger and Mehlhorn⁵⁷ attribute the concrete softening to transverse tensile stress. It is important to determine the factor

which causes the concrete softening in the study of softening mechanism.

The results of the tests show that the effective strength of concrete was not directly related to transverse tensile stresses in the concrete. In the cracked panels, the transverse tensile stress in the concrete varied from location to location due to the cracks. The peak tensile stress would be expected to occur halfway between two cracks. As the applied transverse tension increased, the peak tensile stress reached the cracking strength of the concrete and a new crack occurred and, as a result, the tensile stress in the concrete at this location decreased to zero. The stress halfway between the new pair of cracks then became the new peak stress in the concrete and it increased to the cracking strength of the concrete and then decreased to zero as the applied transverse tension increased. Therefore, the peak transverse tensile stress in the concrete cycled, increasing and decreasing as the applied transverse tension increased. However, as the applied transverse tensile strain increased, the effective strength of the concrete decreased monotonously (Fig. 6.17). No obvious relationship was discovered between the effective strength of the concrete and the transverse tensile stress in the concrete. In panels #24 and #26 the transverse tensile force was unloaded to zero after the desired permanent gross transverse tensile strain had developed in the panels. Thus at the ultimate state, no tensile stress existed in the concrete in these panels. However, these two panels had lower ultimate strengths than panels #27 and #28 which had larger transverse tensile stresses but smaller transverse tensile strains at

the ultimate state. In Panel #18 the tensile stress was near the maximum stress the concrete could carry without cracking but it caused no strength reduction because no cracks had developed in the concrete. All this evidence suggests that the tensile stress in the concrete had no direct effect on the effective strength of the concrete. As a result, the transverse tensile stress in the concrete is excluded from the three possible factors which cause the concrete softening.

The tests also indicated that the tensile stress in the reinforcement had no effect on the effective compressive strength of the concrete. As presented in Chpt. 6, in all the specimens except for #4, #5, #12, #17 and #18, the major portion of the transverse tensile strain was developed after the reinforcement yielded. As a result the tensile stress in the reinforcement was around ϵ_y . However, the effective compressive strength of the concrete varied from $0.98f'_c$ to $0.39f'_c$ as ϵ_t increased from 0.005 to 0.043. In panels #24 and #26 the tensile stress in the reinforcement was approximately zero at failure but they had lower effective strengths than panels #27 and #28 which had post yield stresses in the reinforcement. In #18 the tensile stress in the reinforcement was about 150 MPa but no softening was detected since no crack formed in the concrete.

In the tests of panels #23 to #29, the transverse tensions were applied with different cycles and different stresses in order to create different numbers of cracks under approximately the same gross transverse tensile strain to distinguish between the effects of the cracks and the gross transverse tensile strain on the concrete

softening. However, it was found that the number and the width of the cracks were proportional to the gross transverse tensile strain (see the crack patterns of the specimens at failure in Appendix B). At low strain stages, the number of the cracks increased as the gross transverse tensile strain increased. At high strain stages, the crack pattern became relatively stable and the number of cracks increased at a slower rate but, as a result, the width of the cracks increased at fast rate. The gross transverse tensile strain is a measure of the number and width of the cracks in the concrete since the major portion of the gross tensile strain after the cracking of the concrete was caused by the widening of the cracks. As will be discussed in Sec. 7.4, the number and the width of the cracks in concrete were the real factors which softened the concrete. The concrete softening due to transverse tension can be described as a function of the gross transverse tensile strain. The larger the gross transverse tensile strain developed in the concrete, the more the concrete cracked and the worse the concrete was softened. This behavior was demonstrated by the test results shown in Fig. 6.17 which indicates that the effective strength of concrete decreased as the ultimate gross tensile strain increased.

7.2 The Effective Strength of Concrete

As observed in the tests, the compressive strength of reinforced concrete with transverse tension is lower than the specified compressive strength of concrete. Commonly, the reduced strength of concrete is referred to as the effective strength of concrete. The effective strength of concrete is expressed as:

$$f'_{ce} = v f'_c \quad (7.1)$$

where v is the efficiency factor.

According to the discussion in the previous section, the effective strength of concrete could be expressed as a function of the gross transverse tensile strain which is computed using a gauge length that includes the cracks in the concrete. A formulation was sought to model the relationship between the efficiency factor and the gross transverse tensile strain. It was found that the relationship between the strength and the transverse tensile stress in plain concrete subjected to combined tension and compression is similar to that between the effective compressive strength and the gross transverse tensile strain in reinforced concrete. In the case of plain concrete, the ratio of the reduced strength to the specified strength is expressed as³⁰:

$$\frac{f'_{ce}}{f'_c} = \frac{1}{1 + k t} \quad (7.2)$$

where k is the ratio of principal tensile stress to principal compressive stress and t is the ratio of the uniaxial ultimate compressive strength to the uniaxial ultimate tensile strength. The results of the forty tests shown in Fig. 6.17 suggest that a similar formulation to Eqn. (7.2) can be used to model the relation between v and ϵ_t , i.e:

$$v = \frac{1}{1 + c \epsilon_t} \quad (7.3)$$

where c is a constant which can be determined by fitting the equation to the test results.

Since Eqn. (7.3) is only concerned with the concrete softening due to transverse tension, the test data of the six panels (#34 to #39) in which non-uniform compressive forces were applied is not used in determining c . By fitting Eqn. (7.3) to the test results of the thirty-four panels (#1 to #33 and #40), c is found equal to 42:

$$v = \frac{1}{1 + 42 \epsilon_t} \quad (7.3a)$$

The predictions of the efficiency factor of the thirty-four panels using Eqn. (7.3a) are shown in Table 7.1 and Fig. 7.1. The mean v^t/v^{cal} ratio is 1.001 with a standard deviation of 0.110 and $v=0.110$. The ratio ranges from 0.779 to 1.193. Among the thirty-four panels examined, sixteen had a predicted v^{cal} larger than the v^t from the tests.

An empirical equation should have a certain safety. A larger constant ($\mu=60$) was tried to achieve a better safety index. The results are also shown in Fig. 7.1 and Table 7.1. For the thirty-four tested panels, the mean v^t/v^{cal} ratio is 1.113 with a standard deviation of 0.137 and $v=0.123$. The ratio ranges from 0.812 to 1.401. As shown in Fig. 7.1, only three test points are obviously below the curve. The three panels were #25, #32 and #33. Panels #25 and #33 had local bearing failure and #32 was pre-weakened by the grooves in the surface of the concrete.

According to the above analysis, Eqn. (7.3) using $c=60$ is recommended for calculating the efficiency of concrete under transverse tension:

$$v = \frac{1}{1 + 60 \epsilon_t} \quad (7.3b)$$

From their experimental tests on uniformly sheared reinforced concrete panels, Collins and Vecchio⁴⁷ found that the principal compressive strength decreased as the ratio of the average principal tensile strain, ϵ_t , to the average principal compressive strain, ϵ_d , increased (see Fig. 7.2). The lowest effective strength was only about $0.2f'_c$. Based on the test results they developed the following equation to express the effective strength of concrete:

$$\frac{f'_{ce}}{f'_c} = \frac{1}{0.85 + 0.27 \epsilon_t / \epsilon_d} \quad (7.4)$$

The stresses and strains in the principal directions used to derive the above equation were calculated based on the compression field theory they developed. Eqn. (7.4) was modified in the Modified Compression Field Theory³ as:

$$\frac{f'_{ce}}{f'_c} = \frac{1}{0.8 + 0.34 \epsilon_t / \epsilon_o} \quad (7.5)$$

Eqn. (7.5) with $\epsilon_o = 0.002$ is used in the CSA Code². The predictions of effective strength of the thirty-four tested specimens by Eqn. (7.5) using $\epsilon_o = 0.002$ are also shown in Table 7.1 and Fig. 7.1. It is found that Eqn. (7.5) underestimated the effective strength for most of the specimens. The mean v^l/v^{cal} ratio is 1.671 with a standard deviation of 0.556 and $v = 0.333$. The ratio ranges from 0.874 to 3.177.

In their tests, Schafer and Kollegger et al.^{57,58} also found that the Collins and Vecchio's equations underestimated the effective strength

of the concrete. They reviewed the experiments by Vecchio and Collins and reported that the majority of the panels failed due to yielding of one or both sets of reinforcement or load introduction problems. The specimens in which one or both layers of steel yielded prior to failure were shown with open symbols in Fig. 7.2. Kollegger et al. claim only three panels experienced a compressive failure of the concrete.

In the Collins and Vecchio tests, the load was generally applied to the concrete panels as shear forces. The reinforcement participated in transferring the applied shear stresses into principal tensile and compressive stresses. If the reinforcement yielded, the force transferring system in the panel failed and no additional shear forces could be applied and as a result, failure of the panel was reached. At failure the concrete might not yet have crushed. This type of failure is similar to the shear failure in reinforced concrete beams caused by the yielding of the stirrups. The strength is not governed by the concrete strength but by the steel strength. Therefore the effective strengths of the concrete were underestimated by Collins and Vecchio's tests. The tests presented in this thesis were different from the Collins and Vecchio experiments. In our tests, the load carrying mechanisms in the longitudinal and transverse directions were two individual systems. The yielding of the transverse reinforcement did not cause the failure of the compression resistance in the longitudinal direction. It only acted to reduce the concrete strength by introducing transverse tensile strains and cracks to the concrete. The failure in the longitudinal

direction was eventually caused by the crushing of concrete. For this reason it is believed that Eqn. (7.3b) better represents the capacity of softening concrete than Eqn. (7.5)

7.3 Proposal for the Design of Reinforced Concrete Beams

In Sec. 7.2, Eqn. (7.3b) is recommended to calculate the effective strength of concrete with transverse tension. In applying Eqn. (7.3b) a known transverse tensile strain is required. For a reinforced concrete beam the calculation of the transverse tensile strain (principal tensile strain) may involve tedious work. A simple method to calculate it is needed in applying Eqn. (7.3b).

Collins and Mitchell⁴⁵ and the CSA Code² use the Mohr's circle relationship to calculate the principal strain in the concrete web:

$$\epsilon_t = \epsilon_h + \frac{\epsilon_h - \epsilon_d}{\tan^2 \theta} \quad (7.6)$$

where ϵ_d is the diagonal compressive strain which is taken equal to the strain at maximum stress (-0.002) and ϵ_h is the strain in the direction of beam axis. Due to the strain gradient caused by bending moment, the CSA Code suggests that ϵ_h be taken as the strain at the mid-height of the cross section and in lieu of computing ϵ_h the designer can take it equal to 0.002. Thus Eqn. (7.6) can be rewritten as:

$$\epsilon_t = 0.002 + \frac{0.004}{\tan^2 \theta} \quad (7.6a)$$

A question may be raised that, if the longitudinal strain at the mid-height of the cross section is equal to 0.002, the strain in the tension reinforcement must be two or more times 0.002 and the flexural reinforcement must have yielded before the web concrete crushes. At this time the beam would be very close to flexural failure. If a beam failed due to diagonal crushing of the web concrete, it should not have failed in flexure and the strain in the tension reinforcement should not be larger than the yielding strain. Therefore the average longitudinal strain across the cross section is much less than 0.002 because of the strain gradient. Eqn. (7.6a) over-calculates the transverse tensile strain and, as a result, the effective strength of the concrete is underestimated. In more recent design rules, ϵ_h is computed at the level of the tension steel. Eqn. (7.5) is still used to compute the effective concrete strength.

The gradient of the longitudinal strain makes it difficult to determine ϵ_h for Eqn. (7.6). In using Eqn. (7.6) to calculate the principal tensile strain for the compression field in the shear span of a beam, Collins and Mitchell actually make two assumptions. First, ϵ_t is a function of the average longitudinal strain, ϵ_h . Second, the assumed uniform strain, ϵ_h , is equal to the strain at the mid-height of the beam which is equal to 0.002.

However, the principal tensile strain can also be expressed as a function of the vertical strain, ϵ_v . It is more acceptable to assume ϵ_v uniform over the shear span of a beam. In the sense of average strain, ϵ_v is equal to the strain in the vertical stirrups which is

assumed uniform over the shear span. The value of the strain in the stirrups at failure can also be reasonably estimated. According to the Mohr's circle, ϵ_t can be expressed as:

$$\epsilon_t = \epsilon_v + (\epsilon_v - \epsilon_d) \tan^2 \theta \quad (7.7)$$

At the ultimate state at which the failure is caused by the diagonal crushing of concrete, the diagonal compressive strain ϵ_d will be assumed equal to (-0.002). As discussed in Chpt. 2 and Chpt. 5, if shear failure of a reinforced concrete beam is governed by the diagonal crushing of web concrete, all the stirrups have not yet yielded. Thus the strain ϵ_v in the stirrups is less than the yield strain of the steel, i.e.

$$\epsilon_v \leq 0.002 \quad (7.8)$$

Substituting $\epsilon_d = (-0.002)$ and $\epsilon_v \leq 0.002$ into Eqn. (7.7) gives

$$\epsilon_t \leq 0.002 + 0.004 \tan^2 \theta \quad (7.9)$$

In the design of reinforced concrete beams using the truss model, the designer is free to choose θ from 15° to 65° . However, in most cases the critical inclined cracks in slender beams is from 15° to 35° (see the crack patterns of the test beams by Scordelis in Appendix C). For deep beams θ is a function of the geometry and generally not less than 45° . By conservatively taking $\theta = 40^\circ$ for slender beams, Eqn. (7.9) becomes

$$\epsilon_t \leq 0.00482 \quad (7.10)$$

Substituting $\epsilon_t=0.00482$ into Eqn. (7.3b) a conservative efficiency factor is calculated:

$$v = \frac{1}{1 + 60 \times 0.00482} = 0.775 \quad (7.11)$$

A conservative efficiency factor ($v=0.75$) is proposed to calculate the effective strength of concrete in shear design of slender beams:

$$f'_{ce} = 0.75 f'_c \quad (7.12)$$

Compared to Collins and Mitchell's equations (Eqns. (7.5) and (7.6a)), Eqn. (7.12) gives larger effective strength of concrete. The reason is that the Collins and Vecchio tests underestimated the effective compressive strength and the Collins and Mitchell method (Eqn. 7.6) overestimates the principal tensile stress ϵ_t . According to the Mohr's circle shown in Fig. 7.3, the relationship between ϵ_v and ϵ_h is:

$$\epsilon_v = \frac{(\epsilon_h - \epsilon_d)}{\tan^2 \theta} + \epsilon_d \quad (7.13)$$

If taking $\epsilon_h=0.002$ and $\epsilon_d=-0.002$ Eqn. (7.13) becomes:

$$\epsilon_v = \frac{0.004}{\tan^2 \theta} - 0.002 \quad (7.13a)$$

Eqn. (7.13a) indicates that for $\theta < 45^\circ$, ϵ_v is larger than 0.002 at which the stirrups start to yield, if ϵ_h is assumed equal to 0.002. For most common cases θ is around 30° . At this angle ϵ_v is equal to 0.01 which is about 5 times the yield strain of the steel. Thus, ϵ_t is overestimated by assuming $\epsilon_h=0.002$.

If θ is selected equal to 30° , the effective strength is predicted equal to $0.31f'_c$ by Collins and Mitchell's equations. The effective strength expressed by Eqn. (7.12) is between those proposed by Thurlimann⁴¹ ($0.6f'_c$) and by Schlaich⁸ ($0.8f'_c$). The efficiency factors proposed by other researchers are listed in Table 2.1 in Chpt 2.

If Eqn. (7.12) is used in the design of shear strength of slender reinforced concrete beams using the shear-friction truss model, the design equations described in Chpt. 5 become:

$$V_f \leq V_c + V_s \leq 0.75 \phi_c f'_c b d_v \sin\theta \cos\theta \quad (7.14)$$

where
$$V_c = \phi_c \frac{\beta_0 - \cot\theta}{1 + \beta_0 \cot\theta} N \quad (7.15)$$

and
$$V_s = \phi_s \frac{A_v f_y d_v}{s \tan\theta} \quad (7.16)$$

7.4 The Mechanism of Concrete Softening due to Transverse Tension

Two models were discovered from the tests to explain the mechanisms of concrete softening due to transverse tension. They are referred to in this chapter as the "shearing softening model" and the "buckling softening model".

7.4.1 The Shearing Softening Mechanism

In most of the specimens, the cracks caused by the transverse tension were, overall or locally, not parallel to each other. Some cracks even intercepted others. The failure in these specimens was usually caused by the combined shearing across the inclined cracks and crushing of the concrete near the sheared cracks. Specimen #30 and #32 were typical examples. In these two panels the inclined cracks were defined by the grooves on the concrete surface. Near the failure, clear shearing was observed across these inclined cracks. The crushing of concrete which caused the failure of the specimens occurred near the locations where the inclined cracks intercepted the other vertical cracks (see the photos of the specimens #9, #10, #19, #20, #22, #30 and #32 after failure in Appendix B). The mechanism of this type of softening is referred to as shearing softening and is illustrated in Fig. 7.4.

The two panels shown in Fig. 7.4 illustrate the two typical crack patterns: divergent cracks and intersecting cracks. The panels are subjected to a uniform compressive stress σ_d at the two ends. Free body diagrams of the shaded elements between the two cracks are shown under the two panels. Since the element shown in Fig. 7.4b is a special case of that in Fig. 7.4a ($\Delta_2=0$), only the case shown in Fig. 7.4a is discussed.

As shown in the free body diagram, uniform compressive stresses σ_{d1} and σ_{d2} act on the two horizontal borders of the element respectively. Before shearing occurs along the cracks, σ_{d1} and σ_{d2} are

assumed equal to the applied compressive stress, σ_d . Because the lengths of the two horizontal borders are not equal, shear stresses must exist on the surfaces of the cracks which form the two side borders of the element. As the applied load increases, the compressive and the shear stresses acting on the element increase. At the same time, as the transverse tension increases, the cracks widen and the maximum shear stress the cracks can carry is reduced. As a result, shearing across the cracks may occur before the applied compressive stress reaches the specified compressive strength of the concrete. The portion of the force carried by the shear stresses on the crack surfaces is then released to the bottom border of the element, making the compressive stresses on the bottom border of the specimen, σ_{d2} , larger than applied compressive stress, σ_d . Failure is caused when σ_{d2} reaches f_c' and the concrete crushes. At failure the applied compressive stress σ_d which is defined as the effective compressive strength of the concrete is less than f_c' .

In Fig. 7.4 only one shearing softening element was shown in the panel. In the practical case, several shearing softening elements may form and the failure of the concrete is caused when one or more of them fail. In panel #30 three shearing elements failed and in #32 two of them failed (see Appendix B).

According to the shearing softening model, the number and the width of the cracks are the real factors causing the concrete softening. As the number of cracks increases, more cracks are involved in forming the shearing softening elements. As the width of

the cracks increase, the contact between the crack surfaces decreases and, as a result, the shearing strength of the cracks decreases. Therefore the concrete softening due to transverse tension increases as the number and width of the cracks increases. Since the gross transverse tensile strain is a measure of the number and width of cracks, the effective strength of concrete with transverse tension decreases as the gross transverse tensile strain increases.

Figure 7.5 is a photograph from Ref. 3 which shows the shear span of a reinforced concrete beam after failure. The failure of the shear span was caused due to the diagonal crushing of the concrete. As shown in the photo, crushing of the concrete was located at the narrow ends of the diagonal struts which were divided by the cracks. The crushing was combined with shearing across the cracks. As a result the concrete was softened by the cracks due to the transverse tension.

7.4.2 The Buckling Softening Mechanism

When very large gross transverse tensile strain is developed in the concrete, the buckling softening mechanism is involved in the failure of concrete. For the tested specimens buckling softening occurred when $\epsilon_t > 0.03$. As discussed previously, the number and the width of the cracks in the concrete are proportional to the gross transverse tensile strain. Due to a large gross tensile strain, closely spaced cracks develop in the concrete. These closely spaced cracks divide the concrete into a number of prisms which are subjected to compressive stress. These prisms tend to be eccentrically loaded

because of the irregularity of the cracks. Also due to the large gross tensile strain, the cracks have large width and, as a result, the contact between the crack surfaces which provide the transverse bracing for the prisms is decreased. As the compressive stress in the concrete increases, buckling of the prisms may occur before the stress in the concrete reaches the specified compressive strength. Since the failure is caused by large deformations in the prisms, the concrete might not be obviously crushed at the ultimate state. Failures of specimens #21 and #24 belong to this type of softening mechanism (see photographs in Appendix B).

As described by the two softening models discussed above, cracks in the concrete are the real factor causing concrete softening. It is difficult to describe the cracking phenomena (crack pattern, crack number and crack width) mathematically. However, the gross transverse tensile strain is an approximate measure of the cracks. The gross tensile strain increases as the number and width of the cracks in the concrete increases. Therefore, the effective strength of the concrete can be expressed as a function of gross transverse tensile strain.

7.4.3 The Difference between the Concrete Softening of Plain Concrete and Reinforced Concrete

The mechanism of softening in reinforced concrete under transverse tension is different from the strength reduction of plain concrete subjected to combined tension and compression, although in both cases the strengths of the concrete are reduced because of the

presence of combined tension and compression. For the plain concrete element shown in Fig 7.6a, failure is often caused when the transverse tensile stress exceeds the concrete cracking strength. The presence of the longitudinal compressive stress reduces the cracking strength of the concrete. For the reinforced concrete element shown in Fig. 7.6b, cracking of the concrete does not bring the element to failure instantly but softens the concrete as more cracks are developed in the concrete. The failure is eventually caused by crushing of the concrete.

The interaction diagram developed by Kupfer, Hilsdorf and Rusch²⁸ is well accepted to describe the strength of plain concrete under biaxial stresses. The interaction diagram was based on the tests of plain concrete plates subjected to biaxial stresses which were introduced to the concrete through steel brush bearing platens. As most of the tests conducted by other researchers²⁸⁻³¹, the stresses in the two principal directions (σ_1 and σ_2) in the Kupfer et al. tests were applied through a single loading pump and the ratio of the stresses in the two directions was maintained constant throughout a test. As a result, failure of the element in either direction could cause loss of load in the loading system. In most of the tension-compression combinations, the strength predicted by the interaction diagram is actually controlled by the cracking strength of the concrete rather than the compressive strength of the concrete.

In plain concrete, longitudinal compression reduces the transverse tensile strength. The reduction of the tensile strength of the concrete is caused by the Poisson's ratio of concrete. The average

Poisson's ratio for concrete is about 0.2 and, near the crushing of the concrete, it may be larger than 0.2 due to the microcracks in the concrete. The transverse tensile strain caused by Poisson's ratio increases the total tensile strain in the concrete and, as a result, reduces the concrete tensile strength. However, transverse tension does not cause a significant reduction on the compressive strength of concrete. Transverse cracking failure occurs in plain concrete before a sufficient transverse tensile strain is developed in the concrete to soften its compressive strength. In the Kupfer et al. tests, most elements with combined tension and compression failed due to the concrete cracking. Only the specimens with $\sigma_2/\sigma_1 = -1/0.052$ failed due to combined crushing and cracking and the strength was very close to the strength of uniaxial compression. In the tests conducted by the writer, the tensile stress in specimen #18 was near the cracking stress of the concrete, but no strength reduction was detected, because no cracks had developed in the concrete.

Transverse tension can cause large reduction on the compressive strength in reinforced concrete, because large transverse tensile strains can be developed in the concrete after cracking due to the existence of reinforcement. The tests by the writer show that the reduction of the compressive strength due to transverse tension may as large as 60%. Due to the presence of reinforcement, cracking of the concrete does not represent failure of the reinforced concrete. As more cracks are developed in the concrete, it is softened and its compressive strength is reduced. The failure is eventually caused by crushing of the concrete or buckling of the concrete prisms formed

by the cracks. As found in the tests by the writer, the transverse tensile stresses in the concrete caused the concrete cracking but had no effect on the effective compressive strength of the concrete.

The above arguments suggest that it is incorrect to use the biaxial strength interaction diagram of plain concrete to calculate the concrete compressive strength in reinforced concrete members with combined tension and compression. Thus, the use of the Kupfer et al. interaction diagram in non-linear finite element analyses of reinforced concrete on a smeared crack basis may underestimate the compressive strength of the concrete in the case of biaxial tension and compression. The effective strength expressed by Eqn. (7.3b) or (7.12) should be used in a global analysis to calculate the compressive strength of the concrete with reinforcement.

7.5 Softening due to Non-uniform Compressive Strain

For reinforced concrete slender beams, the truss models assume that the shear span is uniformly strained in the diagonal direction (see Fig. 7.7a). In this case, softening of concrete is caused by transverse tension. The effective strength expressed by Eqn. (7.12) is proposed for the design. In deep reinforced concrete beams shown in Fig. 7.7b, the applied force is directly carried by the isolated strut. The stirrups do not introduce high tensile strain to the concrete struts as they do in slender beams. Softening of the concrete due to transverse tension in a deep beam as shown in Fig. 7.7b is much less important and, for the reasons presented in the rest of this section, will be neglected.

The diagonal compressive strain in the shear span of such a beam is not uniformly distributed. This has two effects. First, the relatively unstressed concrete adjacent to the strut allows a redistribution of load from the highly stressed concrete strut which has the effect of delaying the crushing of the strut. This effect is governed by the dimensioning of the strut-and-tie model. Second, the non-uniform diagonal compressive strains in the concrete cause some concrete softening. The softening of concrete due to non-uniform compressive strain is studied in this section.

Six specimens (#34 to #39) were tested to model the concrete struts in deep beams. Three of them were tested with non-uniform longitudinal compressive forces only. The other three were tested with both non-uniform longitudinal compressive forces and transverse tension. The test results indicated that the non-uniform compressive strain reduced the average strength of concrete but increased the apparent peak strength. The reduction increased as non-uniformity of the compression increased. Since only three specimens were involved in each case, the test data were not adequate to give quantitative analysis. In the remainder of this section, the mechanism of concrete softening due to non-uniform compression is discussed.

The mechanism of concrete softening caused by the non-uniform distribution of compressive strain is illustrated in Fig. 7.8. The concrete element is assumed to subject a non-uniform compressive strain (Fig. 7.7b or 7.8a). As the load increases, the compressive

strains in the concrete increase. Eventually the strain in the middle of the element reaches ϵ_0 before the strains in the rest of the element. The strain ϵ_0 corresponds to the maximum stress (f_c') in the stress-strain curve of the concrete shown in Fig. 7.8b. After this has occurred the stresses in the concrete where $\epsilon_d > \epsilon_0$ start to decrease as the applied load increases, while the stresses in the rest of the element still increase. As a result, the total compressive force in the element is still able to increase as the applied load increases. Fig. 7.8c shows the stress distribution after the strain in the middle of the element exceeds ϵ_0 . The total compressive force in the concrete is:

$$N = \int_0^d \sigma_d(x) dx = \int_0^d f(\epsilon_d(x)) dx \quad (7.17)$$

According to the stress-strain curve in Fig. 7.8b, N expressed by Eqn. (7.17) has a maximum limit when ϵ_d reaches a certain strain. The panel fails when N reaches its maximum. Due to the non-uniform distribution, the average stress in the concrete at failure, f_{ce}' , is less than the specified compressive strength f_c' (see Fig. 7.8c). The average stress in the concrete at failure is defined as the effective strength of the concrete. Therefore, in the concrete subjected to non-uniform compressive strain, the concrete is softened by the compressive stresses corresponding to the descending portion in the stress-strain curve of concrete.

Figure 7.9 illustrates the internal force paths in the concrete. The applied forces have a non-uniform distribution in which the

center forces are larger than the side forces. Before the compressive strain in the concrete exceeds ϵ_0 , the internal compressive stress in the concrete has a distribution as shown in Fig. 7.9a. The internal force paths in the concrete are approximately parallel to the axis of the panel, since the applied forces have a similar configuration to that of the internal compressive stresses. After the compressive strain exceeds ϵ_0 , the internal compressive stresses are redistributed as shown in Fig. 7.9b. However the distribution of the applied forces does not change. As load increases, the forces in the middle of the loading end increase, while the internal compressive stresses in the middle of the panel decrease. Thus, part of the forces applied to the center of the panel must be carried by the concrete where $\epsilon_d < \epsilon_0$. As a result, inclined internal force paths must form in the concrete, and transverse tension is caused along the center line of the element and splitting is caused. The splitting of the concrete may also reduce the concrete strength. In the three panels without transverse tension (#34, #35 and #36), vertical splitting cracks were observed midway along the width of the panel at the failure (see photographs in Appendix B).

7.6 Summary

1. The softening of reinforced concrete due to transverse tension is caused by the number and width of the cracks in the concrete. Two types of softening mechanisms, the "shearing softening" mechanism and the "buckling softening" mechanism are involved in the concrete softening. The gross or average transverse tensile strain

which includes the cracks is a measure of the cracks in the concrete and the effective compressive strength of concrete can be described as a function of the average transverse tensile strain.

2. The shearing softening mechanism is caused by divergent cracks. Shear stresses on the crack surfaces are required by equilibrium if the cracks diverge in a compression field. Redistribution of the compressive stresses in the concrete is caused when the cracks are no longer able to carry the shear stresses. As a result the concrete in the narrow spaces where the divergent cracks are closest together has higher compressive stresses than the rest of the concrete. The softening of concrete is caused when the compressive stress in these locations reaches the specified strength of concrete.

3. When very large gross transverse tensile strains develop in the concrete ($\epsilon_t > 0.03$ for the tested specimens), closely spaced cracks form in the concrete. The cracks divide the concrete into a number of prisms. The softening of the concrete in this case may be caused by buckling of the prisms before the compressive stress in the concrete reaches the specified strength of concrete. At failure, obvious crushing of concrete may not be observed.

4. The equation for effective strength of concrete with transverse tension developed by Collins and Vecchio⁴⁶ and that used in the current CSA Code² both underestimate the strength of concrete. These equations were based on tests of concrete panels,

most of which failed due to other causes than crushing of the concrete.

5. The effective strength of concrete subjected to transverse tension is a function of the gross transverse tensile strain as expressed by the empirical equation Eqn. (7.3b). Equation (7.9), derived from a truss model rather than a plane section model predicts much smaller transverse strain than Collins and Vecchio's Eqn. (7.6). As a result, an efficiency factor with a constant value of 0.75 can be used in the design of slender beams using the truss model or the shear-friction truss model.

6. Non-uniform compressive strains also cause concrete softening. Because of the non-uniform distribution of the compressive strains, stresses in some portion of the concrete may reach the descending portion of the stress-strain curve of concrete while others are still increasing. As a result the effective strength of the concrete which is defined as the average strength across the section will be less than the specified concrete strength. Furthermore, the splitting stresses due to the redistribution of compressive stresses also reduce the strength.

Table 7.1 Comparison of measured and computed effective strength of concrete

Specimen No.	ϵ_{tu}	v^t	Eqn. (7.3a)		Eqn. (7.3b) (Proposed)		Eqn. (7.5) (By Collins)	
			v^{cal}	v^t/v^{cal}	v^{cal}	v^t/v^{cal}	v^{cal}	v^t/v^{cal}
#1	0.00919	0.769	0.722	1.066	0.645	1.193	0.423	1.817
#2	0.00724	0.714	0.767	0.931	0.697	1.024	0.492	1.450
#3	0.00512	0.982	0.823	1.193	0.765	1.284	0.599	1.640
#4	0.00035	1.149	0.986	1.166	0.979	1.173	1.000	1.149
#5	0.00057	1.016	0.977	1.040	0.967	1.051	1.000	1.016
#6	0.00331	0.870	0.878	0.991	0.834	1.043	0.734	1.186
#7	0.00604	0.884	0.798	1.108	0.734	1.204	0.547	1.615
#8	0.01430	0.550	0.625	0.880	0.538	1.022	0.310	1.777
#9	0.01362	0.553	0.636	0.869	0.550	1.005	0.321	1.723
#10	0.01718	0.504	0.581	0.868	0.492	1.024	0.269	1.875
#11	0.01791	0.476	0.571	0.834	0.482	0.988	0.260	1.830
#12	0.00098	0.949	0.960	0.988	0.944	1.005	1.000	0.949
#13	0.02121	0.550	0.529	1.040	0.440	1.250	0.227	2.423
#14	0.02168	0.440	0.523	0.841	0.435	1.012	0.223	1.974
#15	0.00443	0.935	0.843	1.109	0.790	1.184	0.644	1.452
#16	0.00837	0.750	0.740	1.014	0.666	1.127	0.450	1.667
#17	0.00032	0.975	0.987	0.988	0.981	0.994	1.000	0.975
#18	0.00107	1.051	0.957	1.098	0.940	1.118	1.000	1.051
#19	0.01094	0.800	0.685	1.168	0.604	1.325	0.376	2.128
#20	0.00943	0.812	0.716	1.134	0.639	1.271	0.416	1.951
#21	0.03383	0.411	0.413	0.995	0.330	1.245	0.153	2.693
#22	0.02715	0.510	0.467	1.092	0.380	1.341	0.185	2.762
#23	0.01164	0.688	0.672	1.024	0.589	1.168	0.360	1.912
#24	0.04321	0.390	0.355	1.098	0.278	1.401	0.123	3.177

Table 7.1 Continued

Specimen No.	ϵ_{tu}	v^t	Eqn. (7.3a)		Eqn. (7.3b) (Proposed)		Eqn. (7.5) (By Collins)	
			v^{cal}	v^t/v^{cal}	v^{cal}	v^t/v^{cal}	v^{cal}	v^t/v^{cal}
#25	0.00262	0.702	0.901	0.779	0.864	0.812	0.803	0.874
#26	0.01450	0.596	0.622	0.959	0.535	1.115	0.306	1.946
#27	0.01044	0.656	0.695	0.944	0.615	1.067	0.388	1.689
#28	0.01464	0.694	0.619	1.121	0.532	1.304	0.304	2.282
#29	0.00048	1.003	0.980	1.023	0.972	1.032	1.000	1.003
#30	0.00981	0.674	0.708	0.952	0.629	1.071	0.405	1.663
#31	0.00989	0.732	0.707	1.036	0.628	1.166	0.403	1.816
#32	0.00437	0.701	0.845	0.830	0.792	0.885	0.648	1.082
#33	0.00671	0.636	0.780	0.815	0.713	0.892	0.515	1.234
#40	0.00000	1.036	1.000	1.036	1.000	1.036	1.000	1.036
			$\bar{X}=1.001$		$\bar{X}=1.113$		$\bar{X}=1.671$	
			$\sigma=0.110$		$\sigma=0.137$		$\sigma=0.556$	
			$v=0.110$		$v=0.123$		$v=0.333$	
#34	0.00000	0.858	1.000	0.858	1.000	0.858	1.000	0.858
#35	0.00000	0.981	1.000	0.981	1.000	0.981	1.000	0.981
#36	0.00000	0.731	1.000	0.731	1.000	0.731	1.000	0.731
#37	0.00786	0.703	0.752	0.935	0.680	1.035	0.468	1.502
#38	0.00806	0.838	0.747	1.122	0.674	1.243	0.461	1.819
#39	0.01500	0.622	0.613	1.014	0.526	1.182	0.299	2.084

$$* v = \frac{f'_{ce}}{f'_c}$$

** Panels #34 to #39 were loaded with non-uniform compressive stress and their results are not included in the statistical analyses

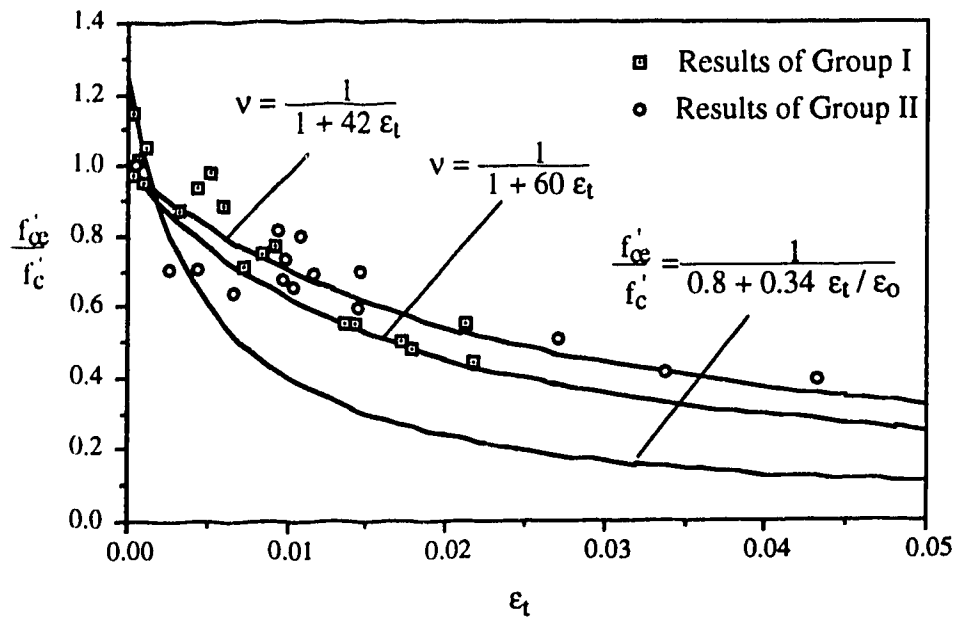


Figure 7.1 The relationship between $\frac{f'_{ce}}{f'_c}$ and ϵ_t

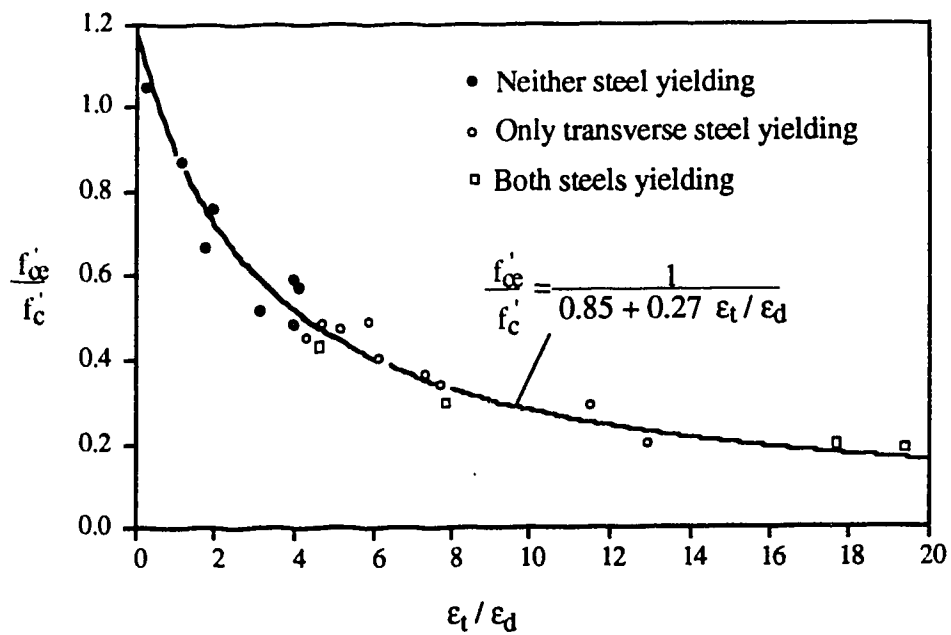


Figure 7.2 Collins and Vecchio's test results;

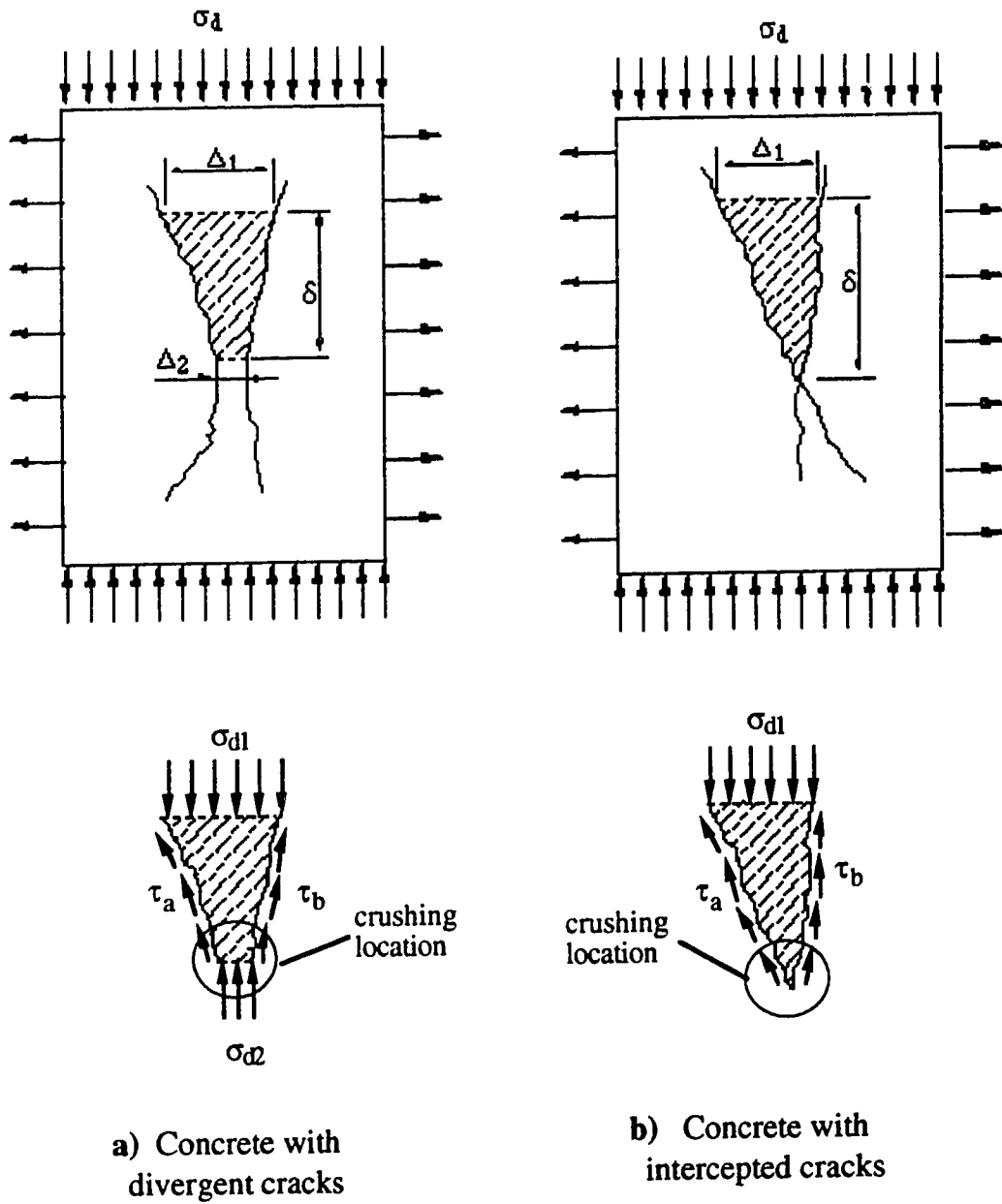


Figure 7.4 Concrete softening due to divergent cracks



Fig. 7.5 Diagonal crushing in a R.C. beam;

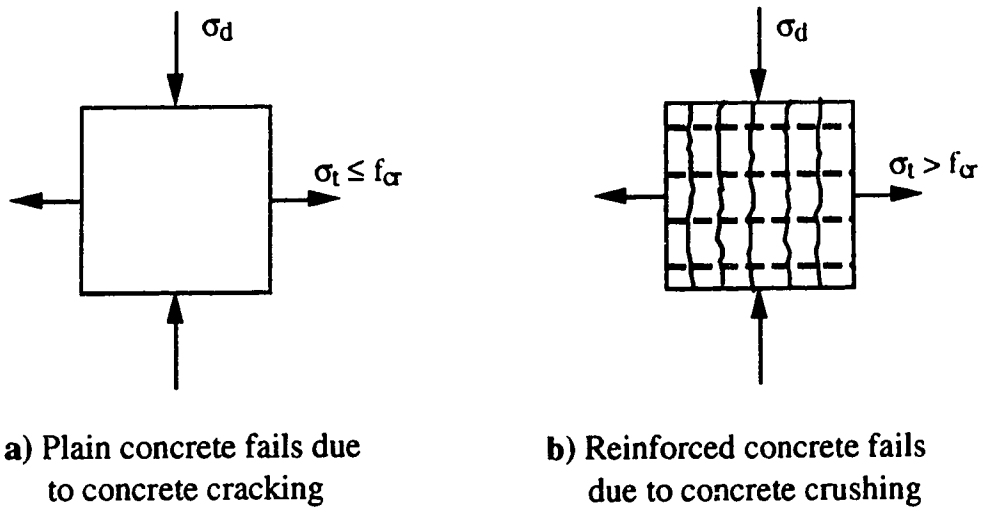
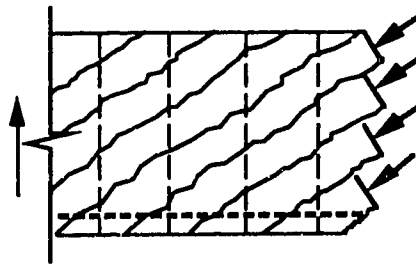
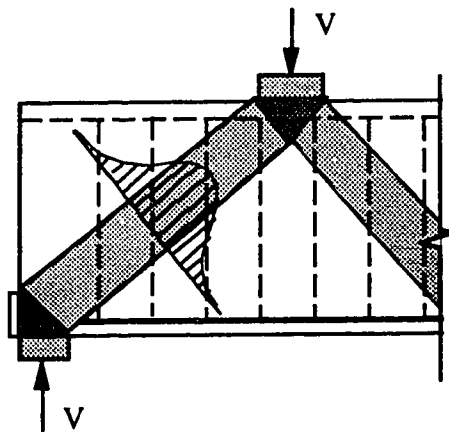


Fig. 7.6 Comparison of plain concrete and reinforced concrete;

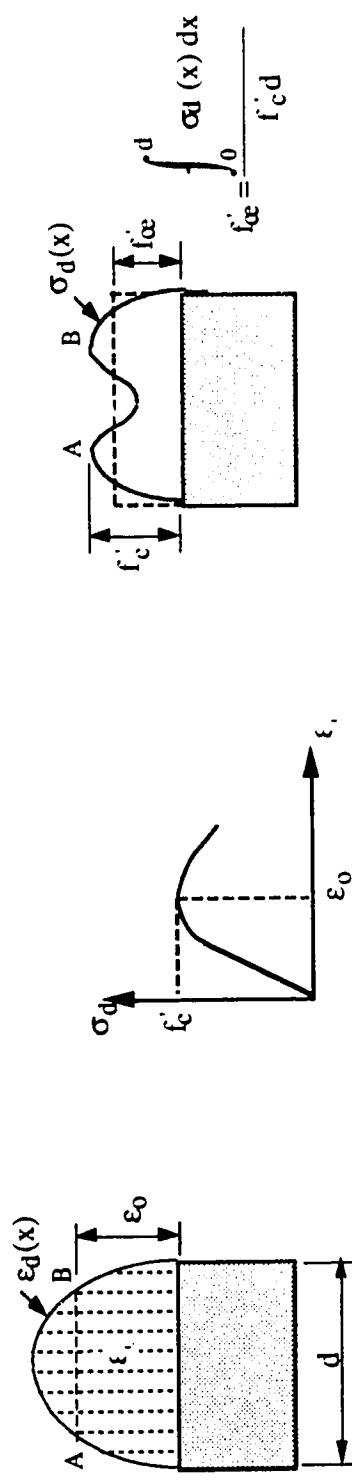


a) Slender beam: uniform diagonal strains



b) Deep beam: non-uniform diagonal strains

Figure 7.7 Comparison of diagonal strains distributions between slender and deep beams

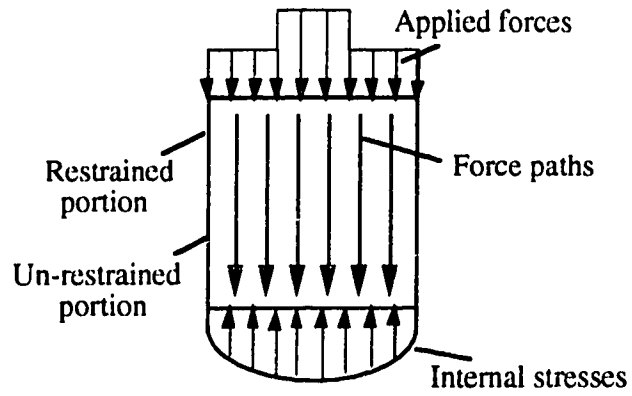


c) The compressive stress in the concrete

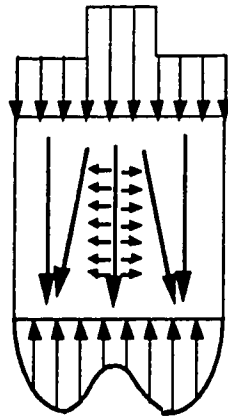
b) The stress-strain curve

a) The compressive strain in the concrete

Figure 7.8 The mechanism of concrete softening due to non-uniform compressive strain



a) Approximately vertical stress paths when $\epsilon_d < \epsilon_o$



a) Inclined stress paths when $\epsilon_d < \epsilon_o$

Figure 7.9 Compressive force paths in non-uniformly stressed concrete

8. SUMMARY AND CONCLUSIONS

8.1 Experimental Observations

Tests were conducted to investigate the shear-friction across inclined cracks and the concrete softening due to transverse tension. A total of 57 specimens was involved in two test series.

8.1.1 Tests on Shear-friction

Seventeen tests were carried out on concrete cantilevers. The designed angles of the inclined cracks studied were 30° , 45° , 60° and 90° . Five types of inclined interfaces were studied: interfaces with both longitudinal reinforcement and stirrups, interfaces with longitudinal reinforcement only, interfaces with longitudinal reinforcement having reduced dowel action, interfaces without any reinforcement and interfaces precracked in the compression zone. All the specimens failed due to either the loss of the shear transfer across the failure cracks (shear-friction failure) or diagonal crushing of the concrete (diagonal strut failure of the truss). The following observations were made from the tests:

- The ratio of the shear transferred by shear-friction across the inclined cracks to the longitudinal compression force on the crack face (V_u/N_u) increased as the angle of inclination of the failure crack, θ , increased. The ratio of (V_u/N_u) for the seventeen specimens varied from 0.114 to 1.778. If V_u and N_u

are transformed to forces parallel and perpendicular to the failure crack using the dry friction law, the equivalent coefficient of shear-friction calculated from the tests was 3.0. Reasons why the equivalent shear-friction coefficient is larger than the normal coefficient of friction are given in Sec. 2.5.2 and Sec. 5.4.

- For the inclined interfaces with $\theta=30^\circ$, the shear causing the interface cracking was larger than the strength of shear-friction across the crack interface. For many slender reinforced concrete beams the inclination of the failure cracks is 30° or less. This suggests that using the inclined cracking load to define the shear contribution of the concrete may overestimate the shear strength of beams if V_s is based on the actual angle θ .
- The principal shear contribution of the longitudinal reinforcement was its ability to hold the two faces of the crack together and induce an axial compressive force and hence a shear friction across the crack, rather than the shear stress in the cross section of the reinforcement. Reduction of the dowel action of the longitudinal reinforcement reduced the failure shear force by decreasing the shear friction across the crack due to the greater unbonded length of reinforcement crossing the crack.
- The uncracked compression zone contributes to the shear resistance of reinforced concrete beams more because it is under compression than because it is uncracked. The

compression zone may crack due to the extension of the crack from the tension zone. However it is still under compression. The compression induces the shear friction to resist the shear.

- For the specimens with stirrups, the shear force was resisted by both the tension in the stirrups intercepted by the failure crack and the shear-friction across the failure crack. The stirrups participated in resisting the shear by direct tension across the inclined cracks. The longitudinal reinforcement and the external longitudinal force, if any, induce the confining force on the failure crack surfaces and mobilize the shear friction across the crack.

8.1.2 Tests on Concrete Softening

Forty tests were conducted on reinforced concrete panels with longitudinal compression and transverse tension. The panels were loaded to crushing under various transverse tensile strains. Different load histories were used in the tests. In six panels, non-uniform distributed compressive forces were applied to study their effect on the concrete softening. The panels failed either due to crushing of the concrete or inability to carry additional load because of large deformations. The test observations are summarized in the following:

- The concrete compressive strength decreased under the transverse tension. The effective compressive strength of concrete decreased as the gross transverse tensile strain increased. The transverse tensile stress in the concrete and

reinforcement had no direct effect on the effective strength of the concrete. The maximum reduction in the concrete compressive strength was 60%.

- For the specimens with divergent cracks, shearing across the cracks was observed before failure. The failure usually resulted from the crushing of concrete near the sheared cracks. For specimens with very large gross transverse tensile strain ($\epsilon_t > 0.03$), failure was caused by large deformation and no obvious crushing of concrete was observed at failure.
- A nonuniform distribution of compressive strain also reduced the compressive strength of the concrete. As the compressive stress and strain were distributed more non-uniformly, the average strength decreased while the apparent peak strength increased.

8.2 Conclusions (the Shear-friction Truss Model)

Chapter 5 deals with the development of the shear-friction truss model as a design tool for the shear strength of reinforced concrete beams. In this model the function of the stirrups is represented by the truss model and the concrete contribution is modelled by shear-friction. Both the stirrup contribution represented by the truss model and the concrete contribution modelled by the shear-friction method are a function of the angle of the inclined cracks. As θ increases, V_s decreases since fewer stirrups are intercepted by a steep crack, while V_c increases, because the shear-friction becomes

more efficient. As a result, a plot of the sum of V_s and V_c versus θ has a vertex with a minimum value. The angle θ corresponding to the vertex is the critical angle of inclination at which the inclined crack plane has the lowest shear transfer capacity and failure occurs at this crack.

In the shear-friction truss model, the concrete contribution, V_c , is assumed directly proportional to the magnitude of the longitudinal compression on the concrete. Hence, in a reinforced concrete beam the longitudinal reinforcement transfers the shear indirectly by inducing compression on the crack plane which mobilizes shear-friction, while the stirrups act to transfer the shear directly as the tension ties in a truss. The application of the shear-friction truss model to twenty-seven beams tested by Scordelis⁴⁻⁶ shows that the model gives shear strength predications with acceptable safety and accuracy. The design example indicates that the shear-friction truss model usually requires fewer stirrups than that the CSA Simplified Method but may need more longitudinal reinforcement. Compared with the CSA General Method the shear-friction truss model uses the same longitudinal reinforcement but less stirrups.

It is found that the CSA Simplified Method and the ACI shear design procedure underestimate the shear contribution from stirrups because they use a conservative angle of 45° for the truss model. At the same time the CSA Simplified Method and the ACI procedure overestimate the shear contribution from the concrete by using the shear strength of concrete beams without stirrups as the concrete contribution of beams with stirrups. The underestimation of the

stirrup contribution and overestimation of the concrete contribution offset each other, and as a result, the CSA Simplified Method and the ACI procedure can give reasonable predictions to shear strengths of reinforced concrete beams. However, they do not give a clear understanding of the shear transfer mechanism across an inclined crack.

8.3 Conclusions (the Effective Strength of Concrete under Transverse Tension)

According to the 40 tests on reinforced concrete panels, the effective compressive strength of concrete with transverse tension decreased as the gross transverse tensile strain increased. The reduction of the concrete strength is caused by the number and width of the cracks in the compressed concrete. The gross transverse tensile strain is a measure of the cracks in the concrete and the effective compressive strength of the concrete can be described as a function of the gross transverse tensile strain (Eqn. (7.3b)).

The loading history followed to get to a given combination of longitudinal stress and transverse strain had no effect on the effective compressive strength of concrete. However it might change the relationship between the compressive stress and compressive strain of the concrete.

Two types of softening mechanisms, the "shearing softening" mechanism and the "buckling softening" mechanism are involved in the concrete softening. The shearing softening mechanism is caused by divergent cracks. Required by equilibrium, shear stresses exist in

the surfaces of the divergent cracks. Redistribution of the compressive stresses in the concrete is caused when the cracks no longer can carry the shear stresses. As a result the concrete in the spaces between the divergent cracks has higher compressive stresses than the rest of the concrete. The softening of concrete is caused when the compressive stress in these locations reaches the concrete specified strength.

When very large gross transverse tensile strains develop in the concrete ($\epsilon_t > 0.03$ for the tested specimens), closely spaced cracks form in the concrete. These cracks divide the concrete into a number of prisms. The softening of the concrete in this case is caused by the buckling of the prisms before the stress in the concrete reaches the concrete cylinder strength. At failure, crushing of concrete may not be observed.

The expression for the effective strength of concrete with transverse tension developed by Collins and Vecchio⁴⁶ and included in the General Method of the current CSA Code² underestimate the strength of concrete in the test panels. The reason is that the equation was based on tests of concrete panels, most of which failed by mechanisms not involving failure in the principal compression direction.

The strength softening in reinforced concrete due to transverse tension is mechanically different from the strength reduction of plain concrete with combined tensile and compressive stresses. In the later case failure is defined by first cracking and the longitudinal

compressive stress reduces the transverse tensile strength. It is a mistake to use the interaction diagram of plain concrete to calculate the compressive strength of reinforced concrete with cracks due to transverse tension.

8.3.1 The Effective Strength of Concrete in Beam Webs

Collins and Mitchell⁴⁵ derived their expression for the principal strain in a beam web on a plane section analysis. A new equation for the principal tensile strain has been derived based on the strains in a compression field web which gives much lower principal tensile strains and hence higher effective compressive strengths. On the basis of this, an efficiency factor with a constant value of 0.75 can be used in the design of slender beams using the truss model or the shear-friction truss model.

REFERENCES

1. ACI Committee 318, "Building code requirements for reinforced concrete, (ACI 318-89), American Concrete Institute, Detroit, Michigan, 1989
2. Canadian Standards Association, "Design of concrete structures for buildings, (CAN3-A23.3-M84)", Canadian Standards Association, Rexdale, Ontario, 1984
3. Vecchio, F.J. and Collins, M.P., "The Modified Compression Field Theory for reinforced concrete elements subjected to shear", American Concrete Institute Journal, Vol. 83, No. 2, March-April 1986, pp 219-231
4. Bresler, B., and Scordelis, A.C., "Shear strength of reinforced concrete beams", Series 100, Issue 13, Institute of Engineering Research, University of California, Berkeley, California, 1961
5. Bresler, B., and Scordelis, A.C., "Shear strength of reinforced concrete beams - series II", Report No. 64-2, Structural Engineering Laboratory, University of California, Berkeley, California, 1964
6. Bresler, B., and Scordelis, A.C., "Shear strength of reinforced concrete beams - series III", Report No. 65-10, Structural Engineering Laboratory, University of California, Berkeley, California, 1966
7. MacGregor, James G. and Hanson, J.M., "Proposed changes in shear provisions for reinforced and prestressed concrete beam", American Concrete Institute Journal, Vol. 66, No. 4, April 1969, pp 276-288
8. Schlaich, J., Schafer, K., and Jennewein, M., "Toward a consistent design of structural concrete", Journal of the Prestressed Concrete Institute, Vol. 32, No. 3, May-June 1987, pp 74-150
9. Ritter, W., "Die bauweise hennebique", Schweizerische Bauzeitung, Februaury 1899, pp 59-61

10. Mörsch, E., "Concrete-steel construction", English translation by E.P. Goodrich, McGraw-Hill Book Company, New York, 1909, pp 386
11. MacGregor, James G., "Reinforced concrete, mechanism and design", Prentice Hall, 1988, pp 169-217, 679-717
12. Rogowsky, D.M. and MacGregor, J.G. "The design of reinforced concrete deep beams", *Concrete international: Design and Construction*, No. 8, 1985
13. Kong, F.K., "Reinforced concrete deep beams", *Reinforced concrete deep beams*, Edited by Kong, F.K., Van Nostrand Reinhold, New York, 1990, pp 1-20
14. Manual, R.F. "Failure of deep beams", *Shear in reinforced concrete*, ACI-ASCE Publication SP42, American Concrete Institute, Detroit, 1974, pp 425-440
15. Kotsovos, M.D., "Strength and behaviour of deep beams", *Reinforced concrete deep beams*, Edited by Kong, F.K., Van Nostrand Reinhold, New York, 1990, pp 21-57
16. Cook, W.D., and Mitchell, D., "Studies of disturbed regions near discontinuous in reinforced concrete members", *American Concrete Institute Journal*, March-April 1988, pp 2106-216
17. Mitchell, D. and Collins, M.P. "Diagonal compression field theory-A rational model for structural concrete in pure torsion", *American Concrete Institute Journal*, Vol. 71, Aug. 1974, pp 396-408
18. Collins, M.P., "Towards a rational theory for RC members in shear", *Journal of the Structural Division, American Society of Civil Engineers*, Vol. 104, April 1978, pp 649-666
19. Paulay, T. and Loeber, P.J., "Shear transfer by aggregate interlock", *Shear in reinforced concrete*, ACI-ASCE Publication SP42, American Concrete Institute, Detroit, 1974, pp 1-16

20. Fenwick, R.C. and Paulay, T., "Mechanisms of shear transfer in concrete beams", Proceedings, ASCE, Vol. 94, No. ST10, Oct. 1968, pp 2235-2350
21. Hofbeck, J.A., Ibrahim, I.A. and Mattock, A.H., "Shear transfer in reinforced concrete", American Concrete Institute Journal, Vol. 66, No. 2, 1969, pp 119-128
22. Mattock, A.H., "Shear transfer in concrete having reinforcement at an angle to the shear plane", *Shear in reinforced concrete*, ACI-ASCE Publication SP42, American Concrete Institute, Detroit, 1974, pp 17-42
23. Taylor, H.P.J., "The fundamental behavior of reinforced concrete beams with bending and shear", *Shear in reinforced concrete*, ACI-ASCE Publication SP42, American Concrete Institute, Detroit, 1974, pp 43-77
24. Walraven, J.C., "Fundamental analysis of aggregate interlock". Journal of the Structural Division, American Society of Engineers, Vol. 107, No. ST11, Nov. 1981, pp 2245-2270
25. Crist, R.A., "Static and dynamic shear behaviour of uniformly loaded reinforced concrete deep beams", Ph.D. Thesis, University of New Mexico, 1971
26. ACI-ASCE Committee 426, "The shear strength of reinforced concrete members", Proceedings ASCE, Journal of the Structural Division, Vol. 99, No. ST6, June 1973, pp 1091-1187
27. Mattock, A.H. and Hawkins, N.M., "Research on shear transfer in reinforced concrete", Journal of the Prestressed Concrete Institute, Vol. 17, No. 2, March-April 1972, pp 55-75
28. Kupfer, H.B., Kilsdorf, H.K. and Rusch, H., "Behavior of concrete under biaxial Stresses", American Concrete Institute Journal, Vol. 66, No. 8, August, 1969, pp 656-666

29. Kupfer, H.B. and Gersle, K.H., "Behaviour of concrete under biaxial stresses", ASCE, EM, Vol. 99, 1973, pp 853-866
30. Tasuji, M.E., Slate, F.O. and Nilson, A.H., " Stress-strain response and fracture of concrete in bi-axial loading", American Concrete Institute Journal, Vol. 75, 1978, pp 306-312
31. Mchenry, J.K., "Strength of combined tension and compression stresses", American Concrete Institute Journal, Vol. 54, 1958, pp 829-839
32. Mattock, A.H. and Kaar, P.H., "Precast-prestressed concrete bridge 4. shear tests of continuous girders", Journal of the Research and Development Laboratories, Portland Cement and Association, Vol. 3, No.1, Jan., 1961, pp 19-46
33. Leonhardt, F. and Walther, R., "The stuttgart shear tests", Cement and Concrete Association, Library Translation No.. 111, 1964
34. Taylor, R., "Some aspects of the problem of shear in reinforced concrete beams", Civil Engineering and Public Works Review, Vol. 58, May, 1963, pp 629-632
35. Bennett, E.W. and Balasooriya, B.M.A., "Shear strength of prestressed beams with thin webs failing in inclined compression", American Concrete Institute Journal, Vol. 68, Mar. 1971, pp 204-212
36. Placas, A., and Regan, P.E., "Shear failure of reinforced concrete beams", American Concrete Institute Journal, Vol. 68, Oct. 1971, pp 763-773
37. Lyngberg, B.S. "Ultimate shear resistance of partially prestressed reinforced concrete I-beam", American Concrete Institute Journal, Vol. 73, Apr. 1976, pp 214-222
38. Nielsen, M.P. and Brastrup, M.W., "Plastic shear strength of reinforced concrete beams", Bygningsstatistiske Meddeleser, Vol. 46, No.3, Denmark, 1975 pp 61-69

39. Nielson, M.P., et al., "Concrete plasticity-beam shear-shear in joints-punching shear", Special publication Udgivet of Dansk Selskab for Bygningstatik, Lyngby, Denmark, Oct. 1978
40. Exner, H., "On the effectiveness factor in plastic analysis of concrete", IABSE Colloquium on Plasticity in Reinforced Concrete, Copenhagen, Denmark, Final Report, V-29, 1979, pp 35-42
41. Thurlimann, B., "Shear strength of reinforced and prestressed concrete--CEB approach", Concrete Design: U.S. and European Practices, ACI-CEB-PCI-FIP Symposium, ACI Publication SP-59, 1979, pp 93-144
42. Campbell, T.I., Batchelor, B.D. and Chitnuyanondh, L., "Web crushing in concrete girders with prestressing ducts in the web", Journal of Prestressed Concrete Institute, Vol. 24, No. 5, Sept./Oct. 1979, pp 70-88
43. Campbell, T.I. Chitnuyanondh, L. and Batchelor, B.D., "Rigid plastic theory v. truss analogy method for calculating the shear strength of reinforced concrete beams", Magazine of Concrete Research, Vol. 32, No. 10, Mar. 1980, pp 39-44
44. Batchelor, B.D., George, H.K. and Campbell, T.I., "Effectiveness factor for reinforced concrete beams", Journal of Structural Engineering, ASCE, 1986, pp 1464-1477
45. Collins, M.P. and Mitchell, D., "Shear and torsion design of prestressed and non-prestressed concrete beams", Journal of the Prestressed Concrete Institute, Vol. 25, No. 5, Sept.-Oct. 1980, pp 32-100
46. Vecchio, F., and Collins, M.P., "Stress-strain characteristics of reinforced concrete in pure shear", IABSE Colloquium, Advanced Mechanics of Reinforced Concrete, Delft Final Report, International Association of Bridge and Structural Engineering, Zurich, Switzerland, 1981, pp 221-225

47. Vecchio, F. and Collins, M.P., "The response of reinforced concrete to in-plane shear and normal stresses", Publication No. 82-03, Department of Civil Engineering, University of Toronto, 1982
48. Marti, P., "Basic tools of reinforced concrete beam design", American Concrete Institute Journal, Jan./Feb. 1985, pp 46-56
49. Lou, M.C. and Marti, P., "Staggered shear design of concrete beams: Large-scale tests", Canadian Journal of Civil Engineering, Vol. 14, 1987, pp 257-267
50. Marti, P., "Truss models in detailing", Concrete International, December 1985, pp 66-73
51. Hsu, T.C., Mau, S.T. and Chen, B., "Theory of shear transfer of reinforced concrete", American Concrete Institute Journal, Vol. 84, No. 2, 1987, Mar.-Apr., pp 149-160
52. Hsu, T.T.C and Mo, Y.L., "Softening of concrete in torsional members-theory and tests", American Concrete Institute Journal, Vol. 82, No. 3, 1985, May.-June., pp 290-303
53. Hsu, T.T.C., Mau, S.T. and Chen, B., "Theory of shear transfer strength of reinforced concrete", American Concrete Institute Journal, Vol. 84, No. 2, Mar./Apr. 1987, pp 149-160
54. Hsu, T.T.C and Mo, Y.L., "Softening truss model theory for shear and torsion", American Concrete Institute Journal, Vol. 85, No. 6, Nov./Dec. 1988, pp 624-635
55. Hsu, T.C., "Unified theory of reinforced concrete", CRC Press, Boca Raton, 1993, pp 193-255
56. Rogowsky, D.M. and MacGregor, J.G., "Shear strength of deep reinforced concrete continuous beams", Structural Engineering Report No. 110, University of Alberta, 1983

57. Kollegger, J. and Mehlhorn, G., "Experimental investigations into the compressive strength of reinforced concrete subjected to transverse tension", Deutscher Ausschuss für Stahlbeton, Heft 413, Berlin 1990
58. Schafer, K., Schelling, G. and Kuchler, T., "Biaxial compression and tension in reinforced concrete elements", Deutscher Ausschuss für Stahlbeton, Berlin, 1990
59. Canadian Portland Cement Association, "Concrete Design Handbook", 1985, pp 4.14 - 4.21
60. Aimian Chen, "Shear strength of restrained reinforced concrete deep beams loaded at the bottom", International Symposium on Concrete, Nanjing, China, 1986

APPENDIX A

PHOTOGRAPHS OF THE SHEAR-FRICTION SPECIMENS AFTER FAILURE

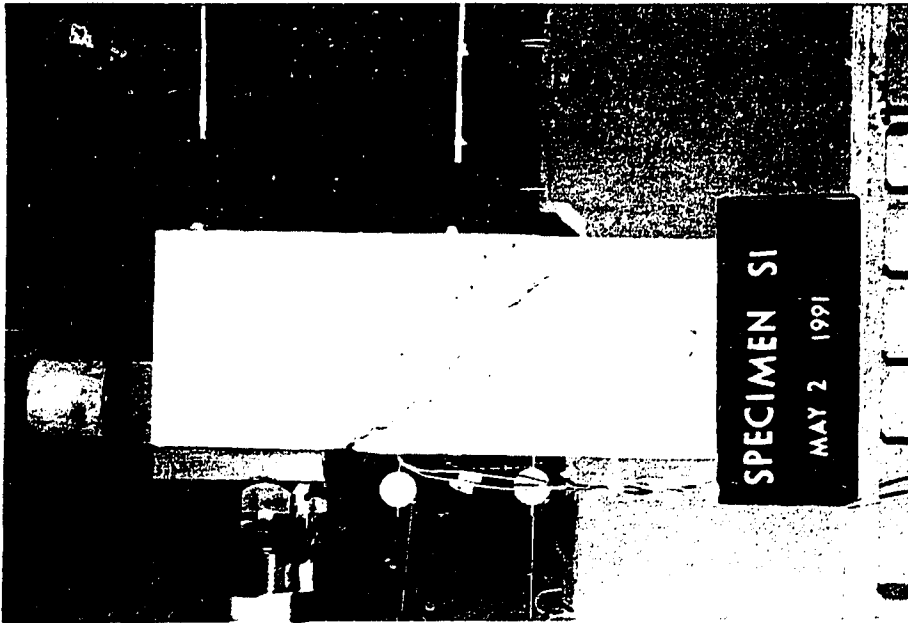


Figure A-1 Specimen S1

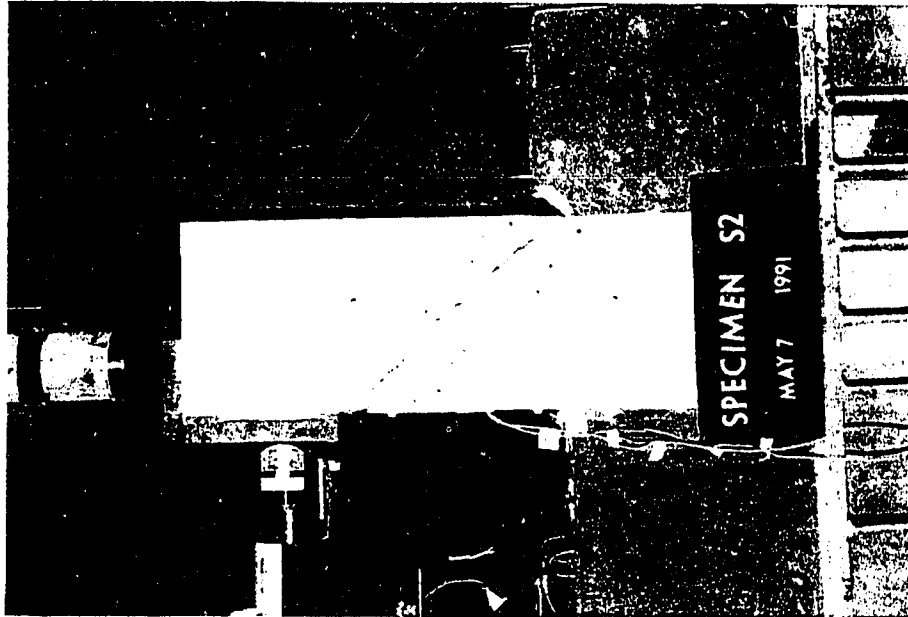
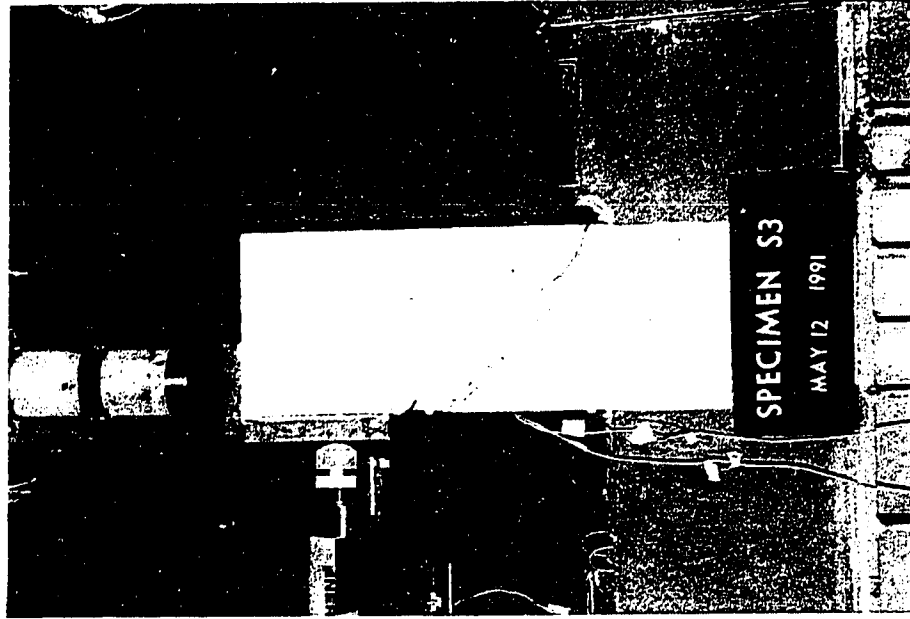
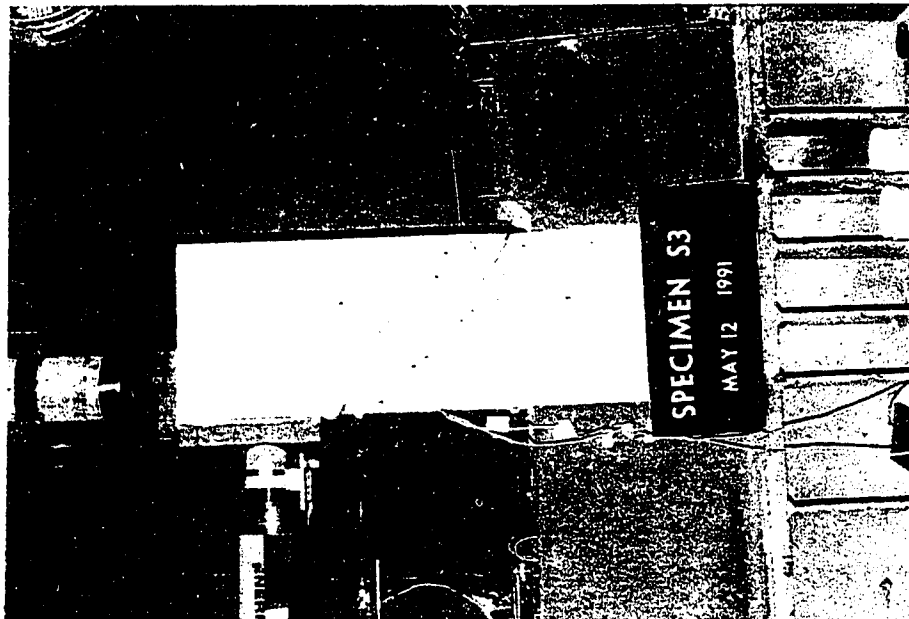


Figure A-2 Specimen S2



**Figure A-4 Specimen S3
after Failure**



**Figure A-3 Specimen S3
before Test (Precrack)**

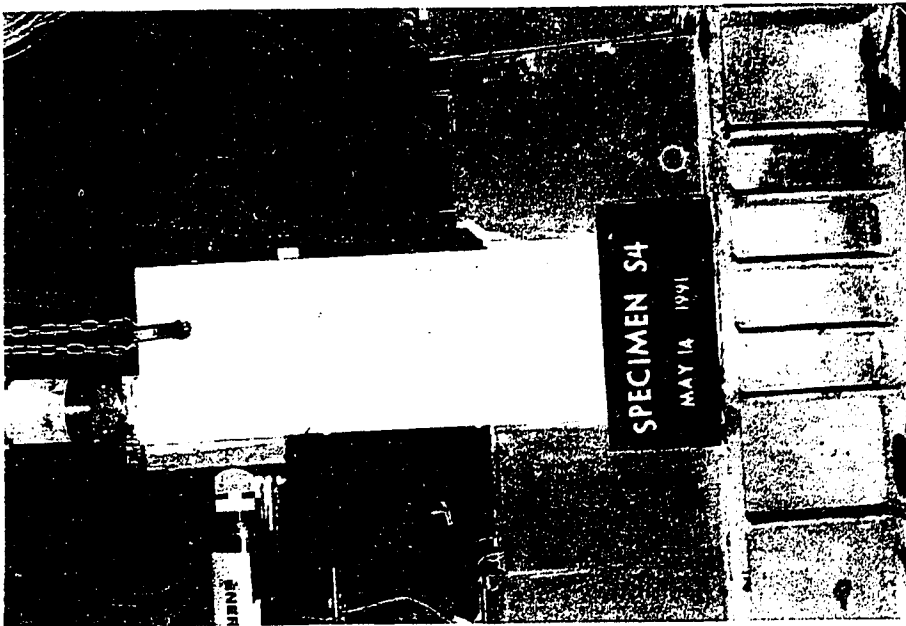


Figure A-5 Specimen S4

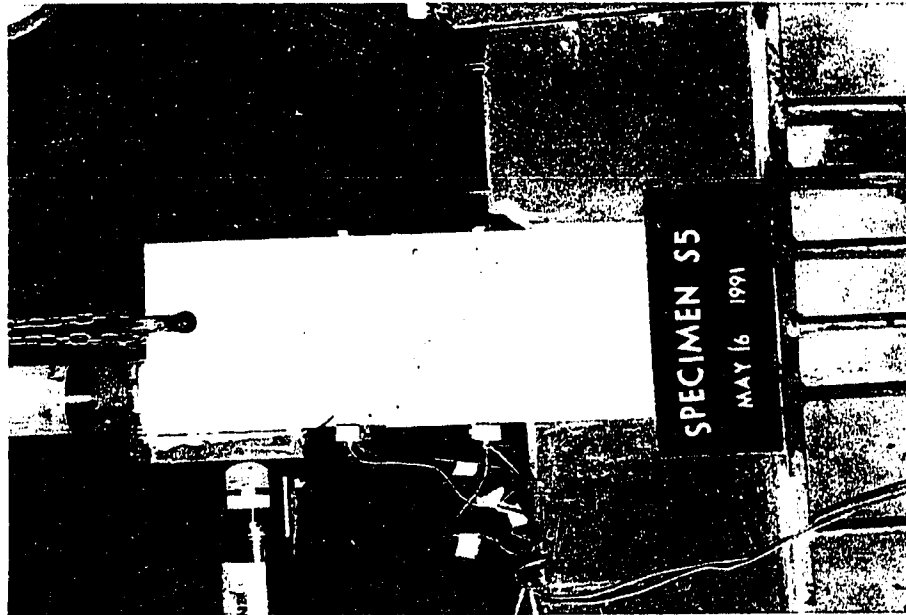
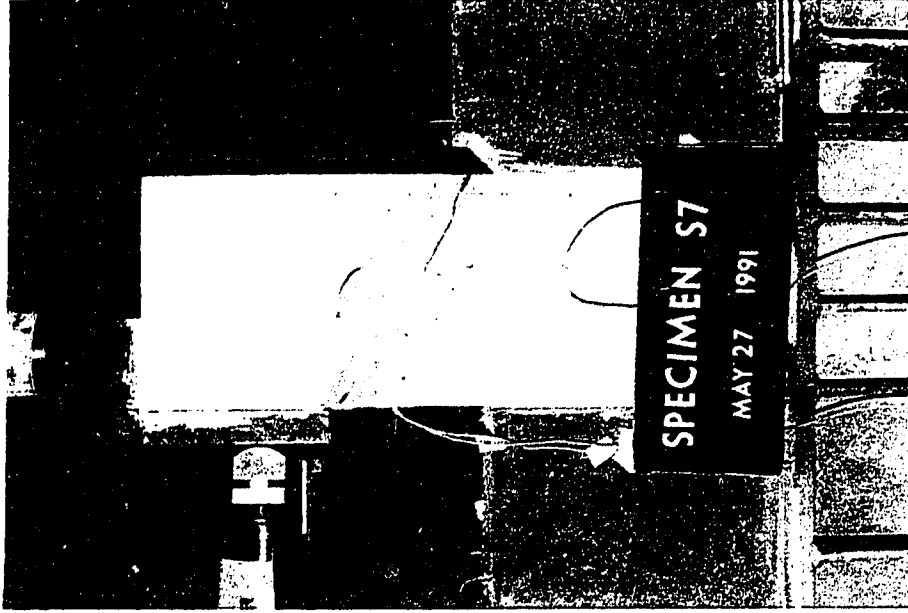
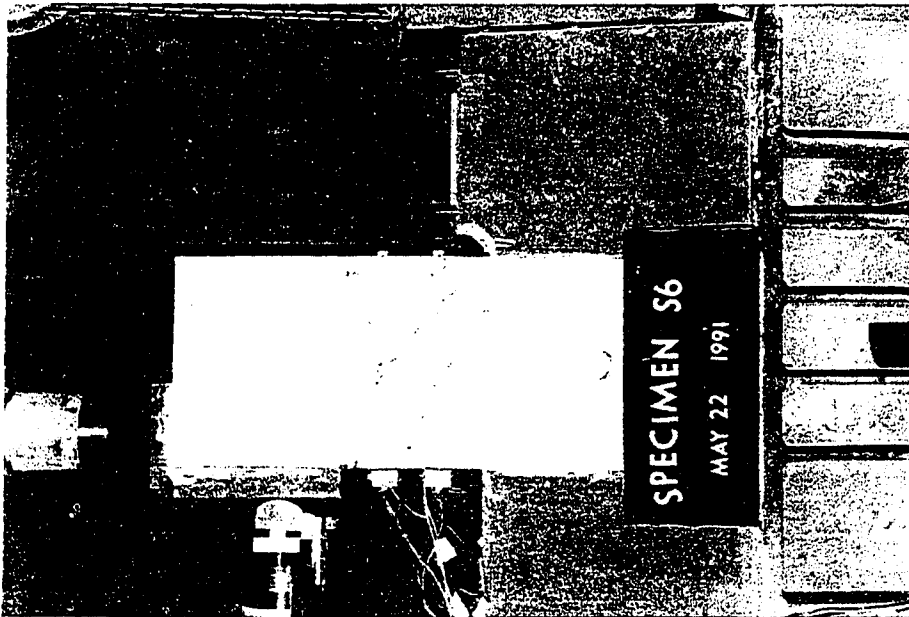


Figure A-6 Specimen S5



**Figure A-8 Specimen S7
before Test (Precrack)**



**Figure A-7 Specimen S6
before Test (Precrack)**

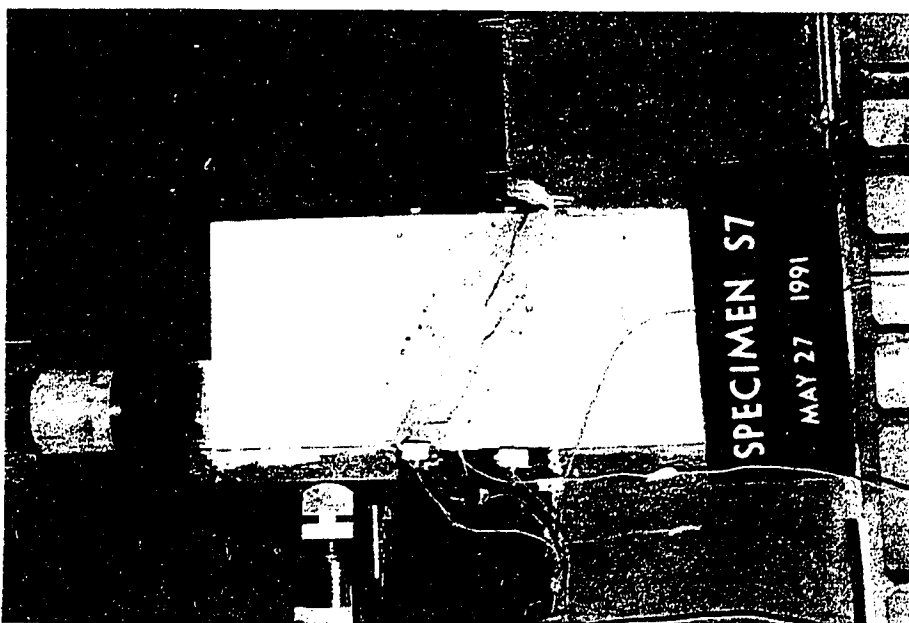


**Figure A-9 Specimen S7
after Failure**

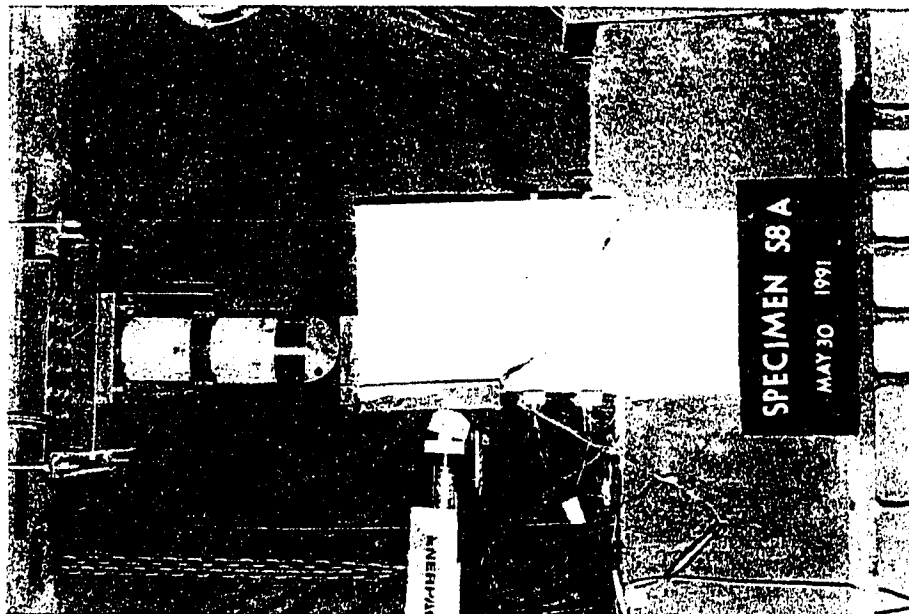
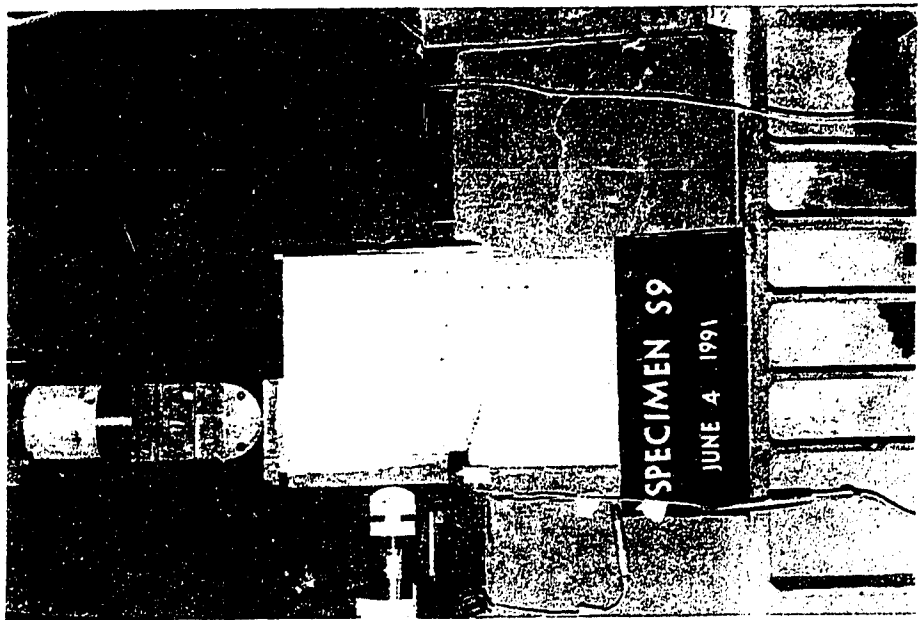
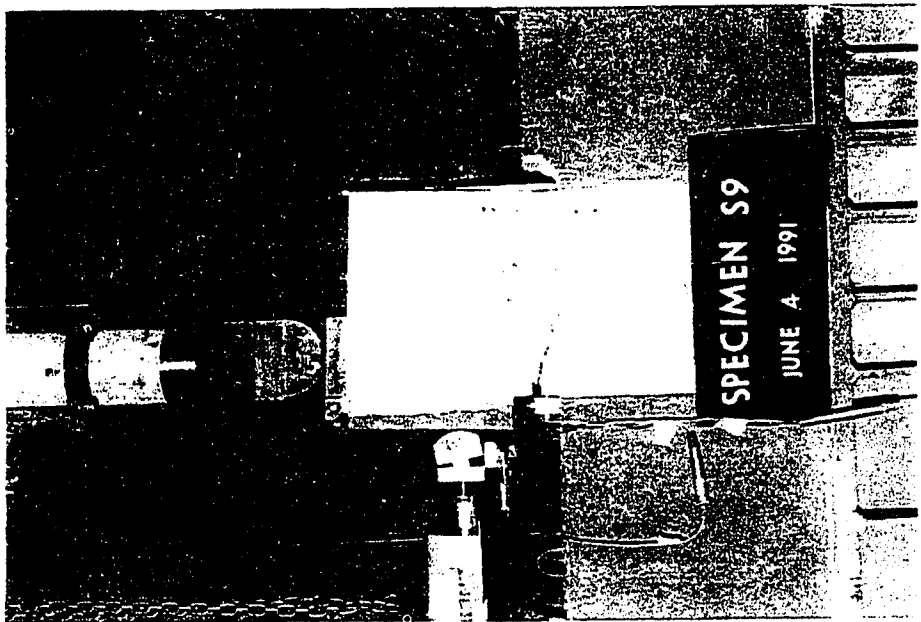


Figure A-10 Specimen S8



**Figure A-12 Specimen S9
(Retest)**



**Figure A-11 Specimen S9
(Initial Test)**

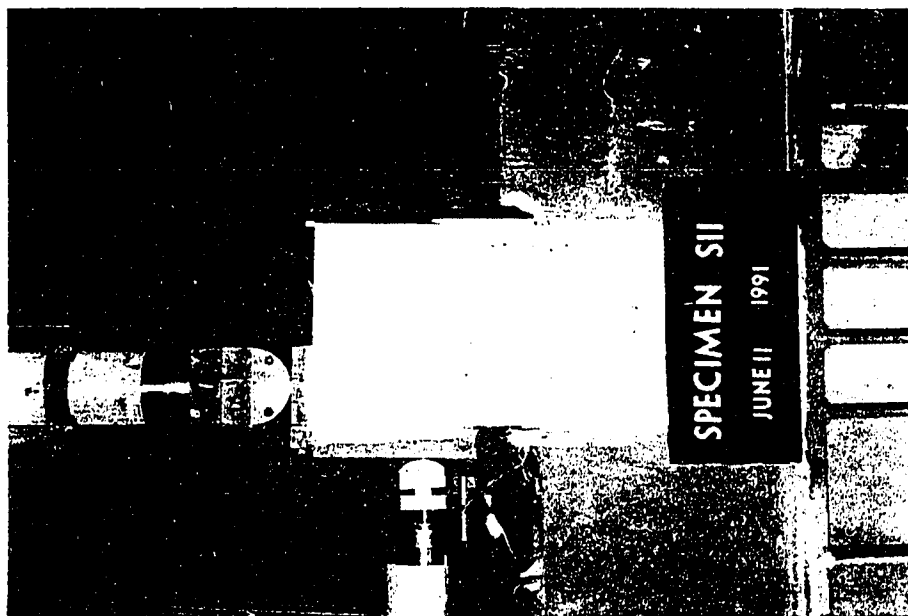


Figure A-14 Specimen S11

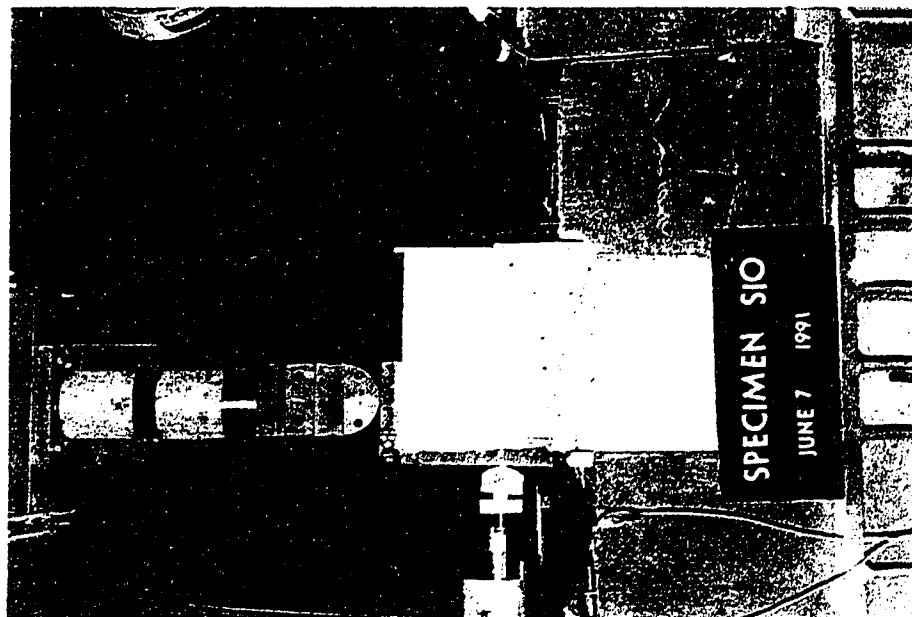


Figure A-13 Specimen S10

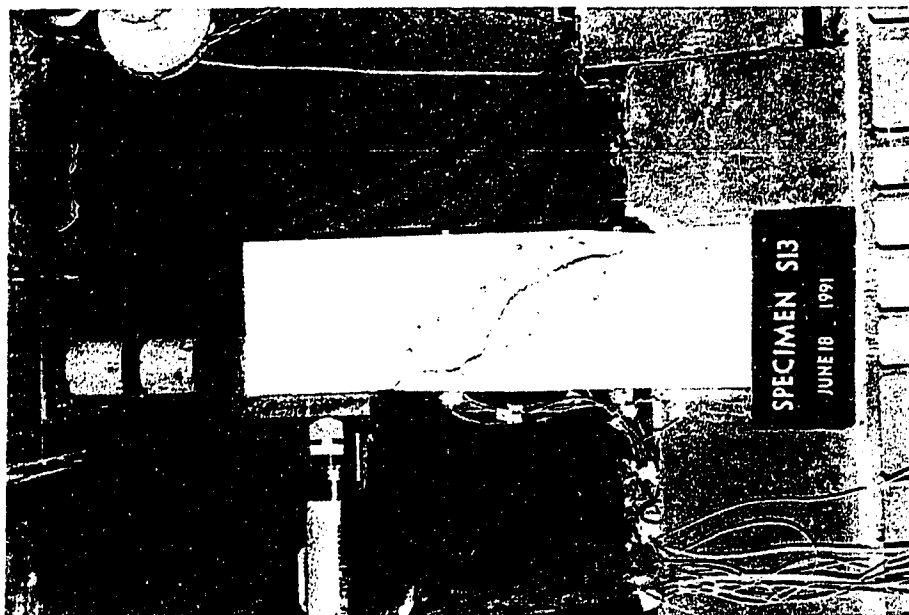


Figure A-16 Specimen S13

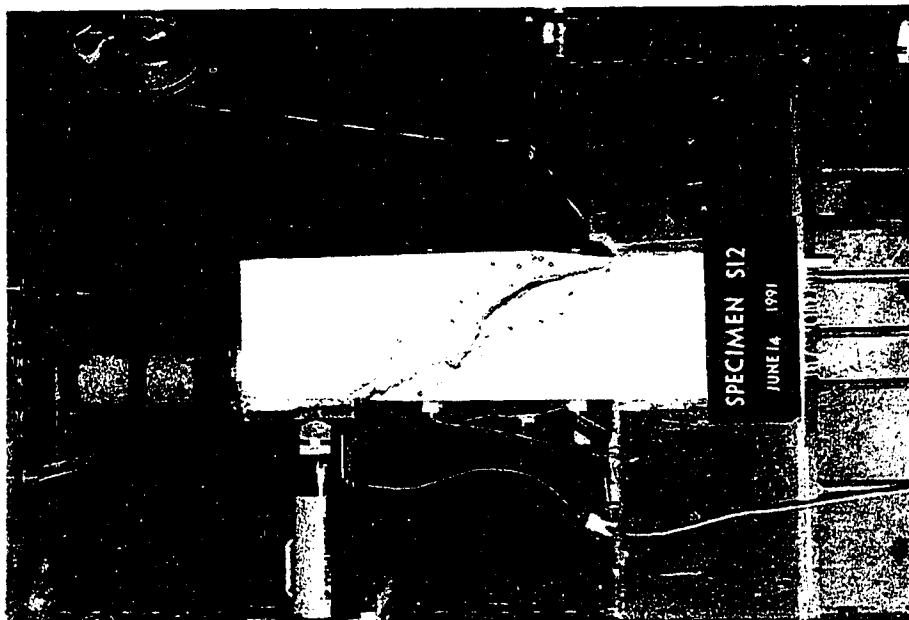


Figure A-15 Specimen S12

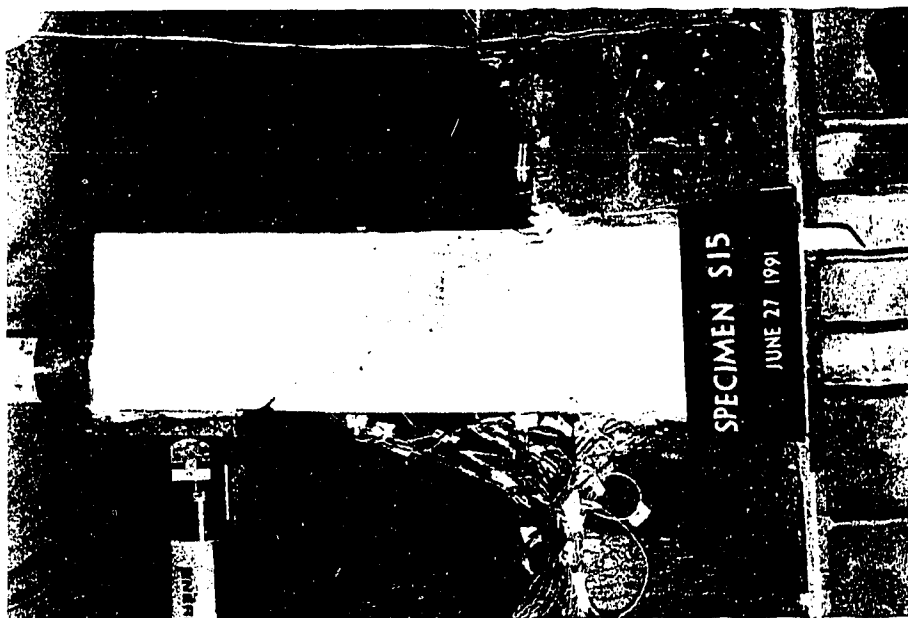


Figure A-18 Specimen S15

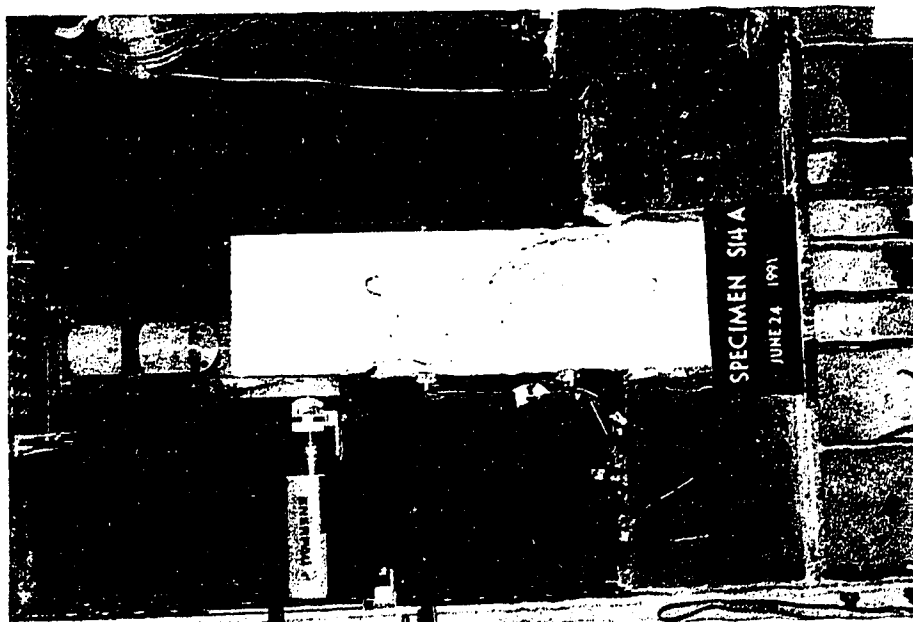


Figure A-17 Specimen S14

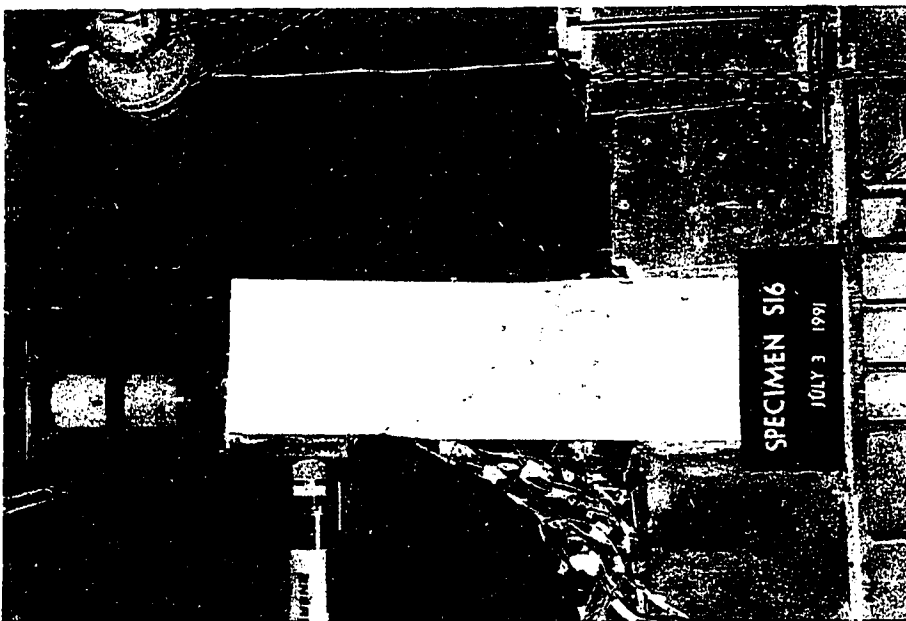


Figure A-19 Specimen S16

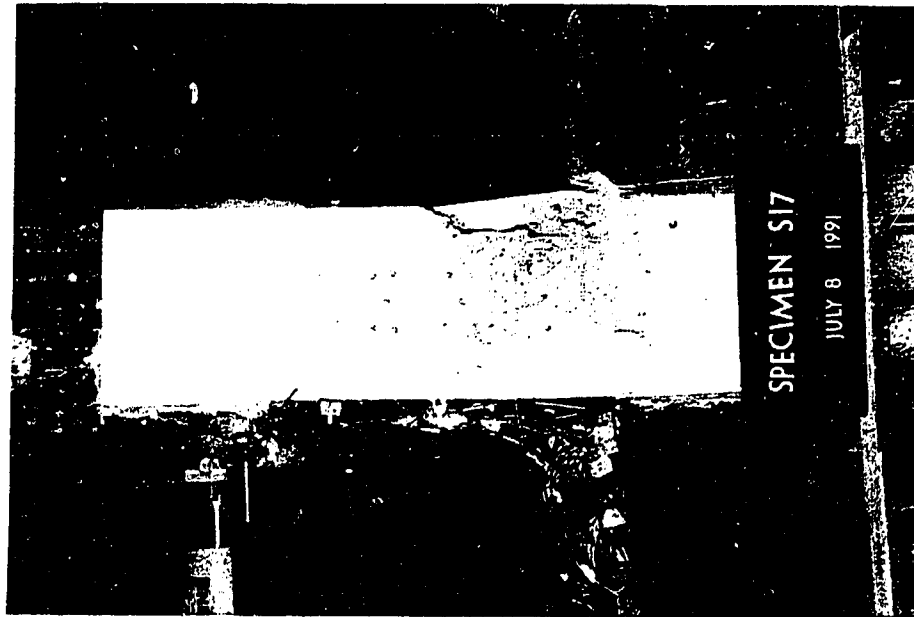
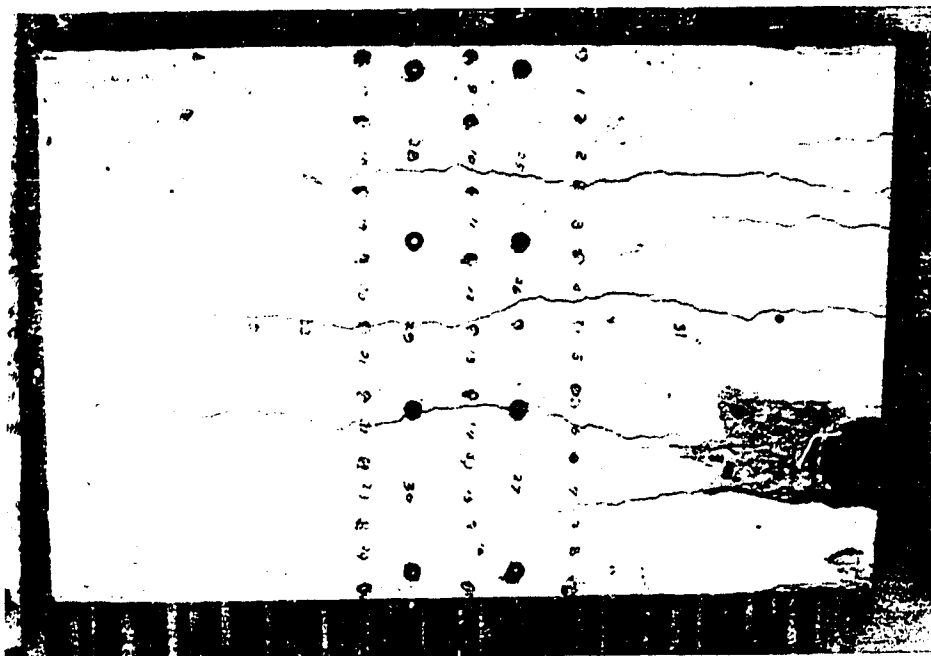


Figure A-20 Specimen S17

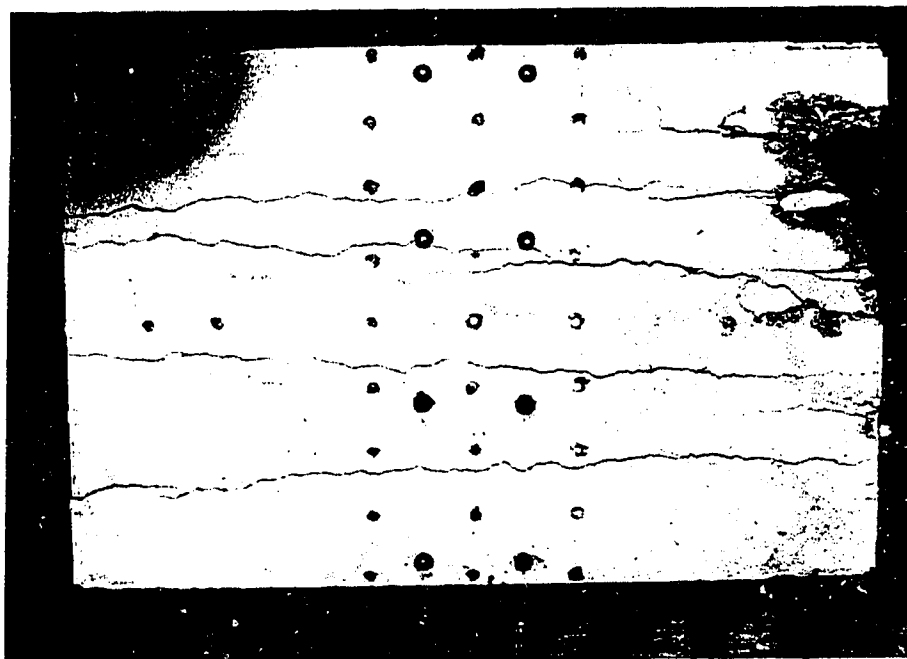
APPENDIX B

PHOTOGRAPHS OF THE SPECIMENS FOR CONCRETE SOFTENING TESTS



$$\frac{V_u}{bhf_c} = 0.714, \epsilon_t = 0.0072$$

Specimen #2

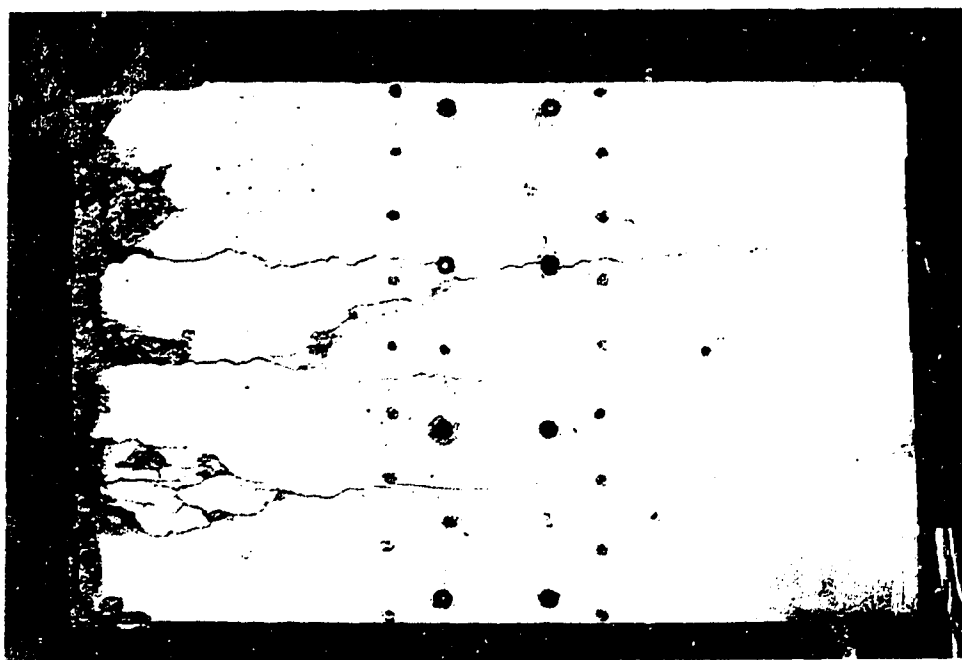


$$\frac{V_u}{bhf_c} = 0.769, \epsilon_t = 0.0092$$

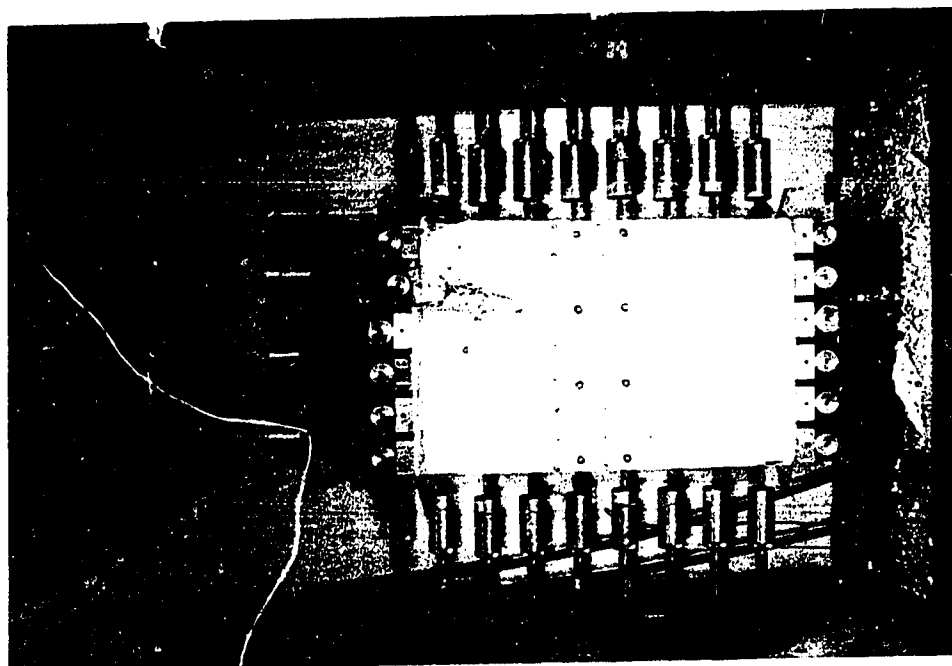
Specimen #1



$\frac{V_u}{bh f_c} = 1.149, \epsilon_t = 0.0003$
 Specimen #4

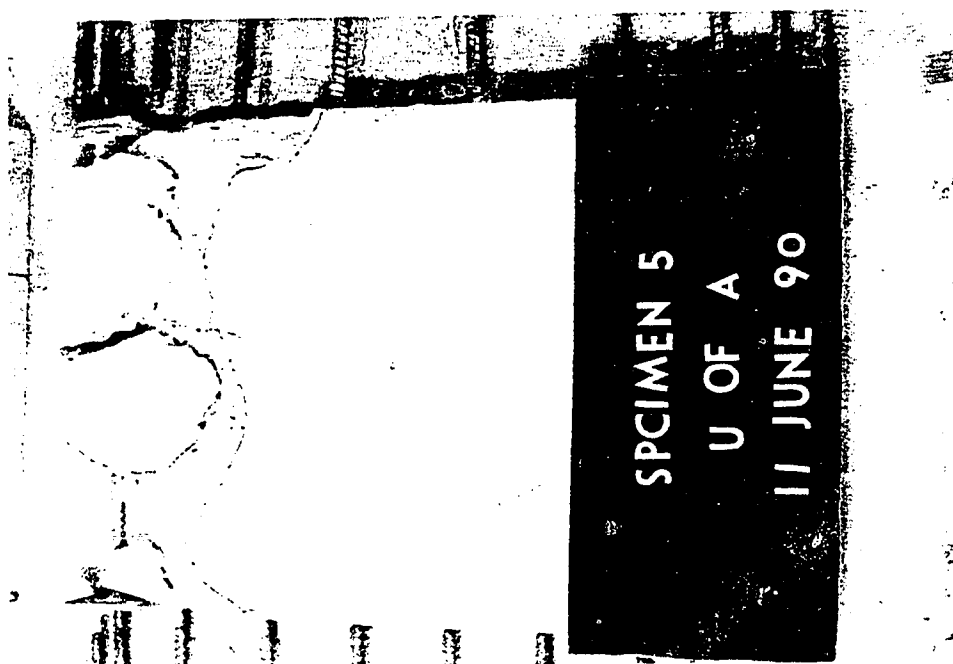


$\frac{V_u}{bh f_c} = 0.982, \epsilon_t = 0.0051$
 Specimen #3



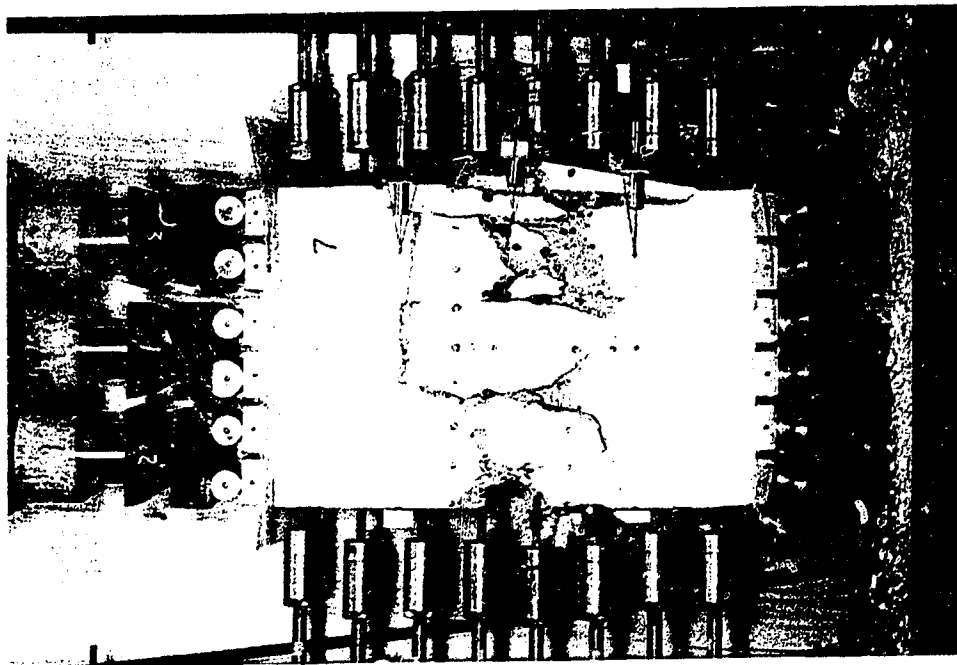
$$\frac{V_u}{bhf_c} = 0.87, \epsilon_t = 0.0053$$

Specimen #6

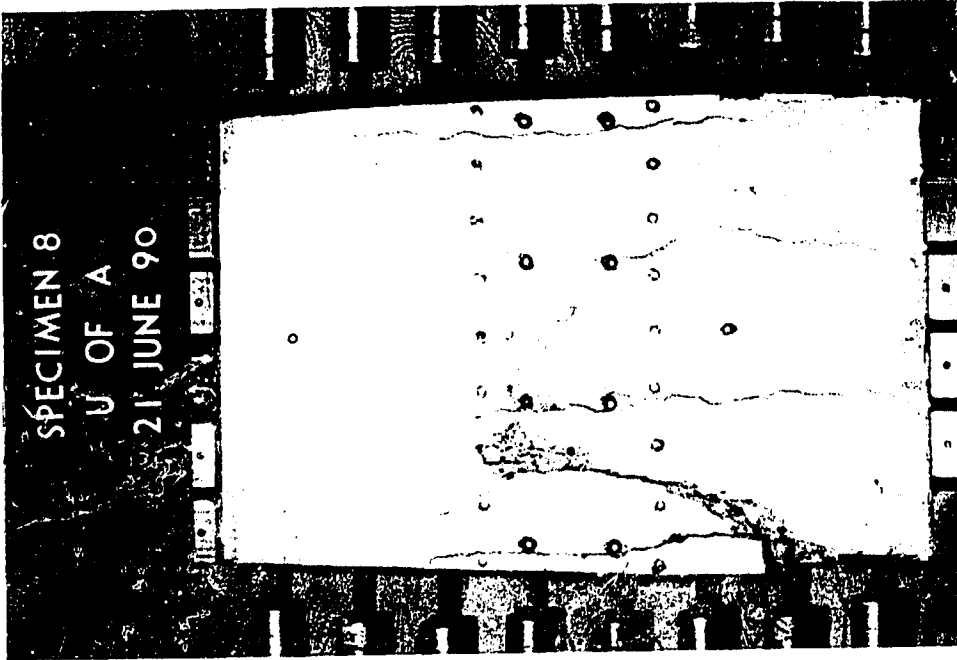


$$\frac{V_u}{bhf_c} = 1.106, \epsilon_t = 0.0006$$

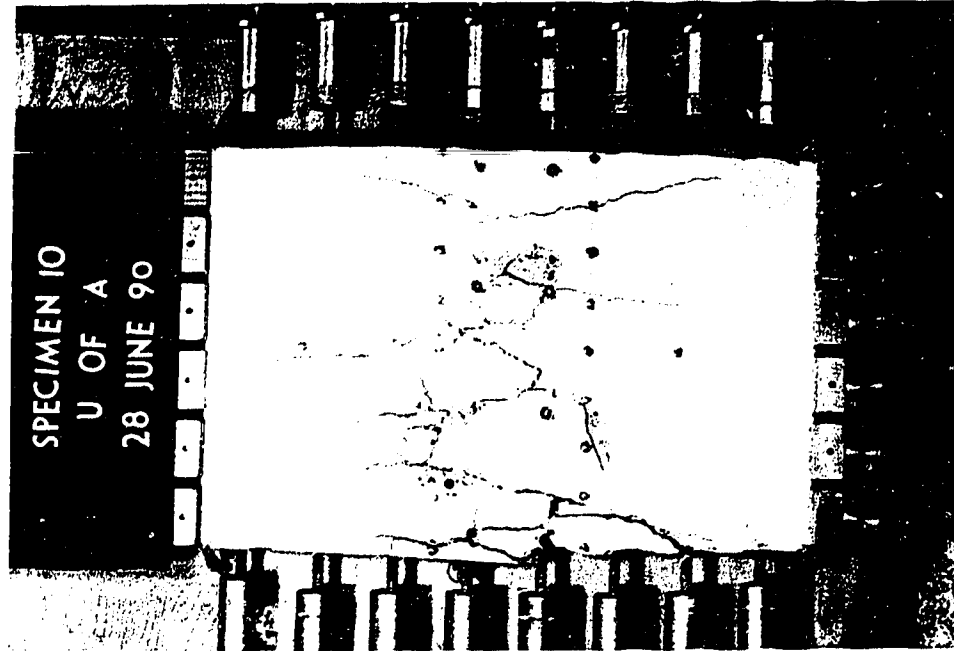
Specimen #5



$\frac{V_u}{b h f_c} = 0.884, \epsilon_t = 0.0060$
 Specimen #7

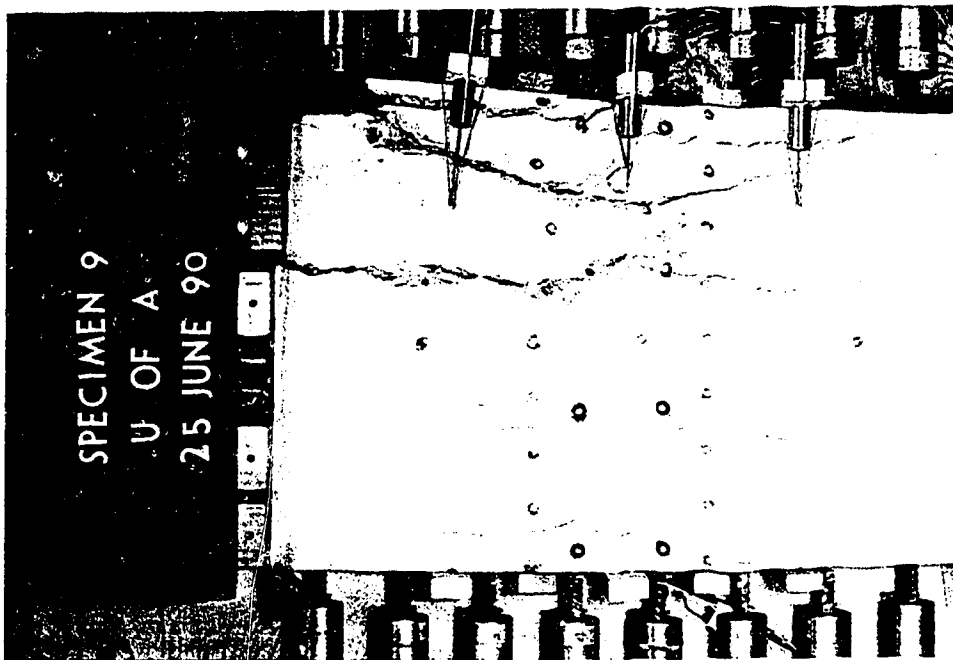


$\frac{V_u}{b h f_c} = 0.550, \epsilon_t = 0.0143$
 Specimen #8



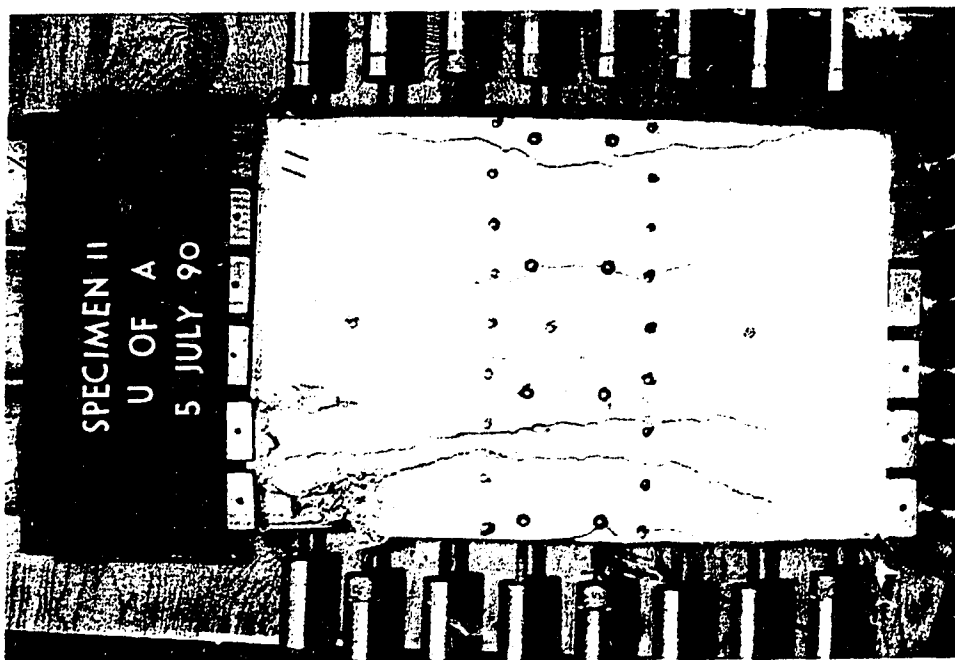
$$\frac{V_u}{b h f_c} = 0.504, \epsilon_t = 0.0172$$

Specimen #10



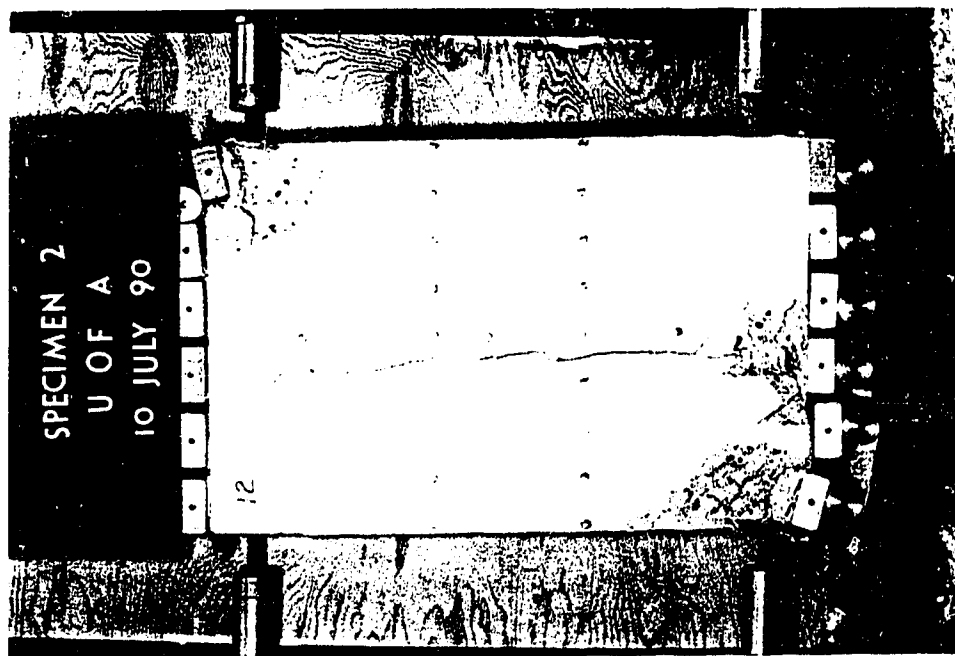
$$\frac{V_u}{b h f_c} = 0.553, \epsilon_t = 0.0136$$

Specimen #9



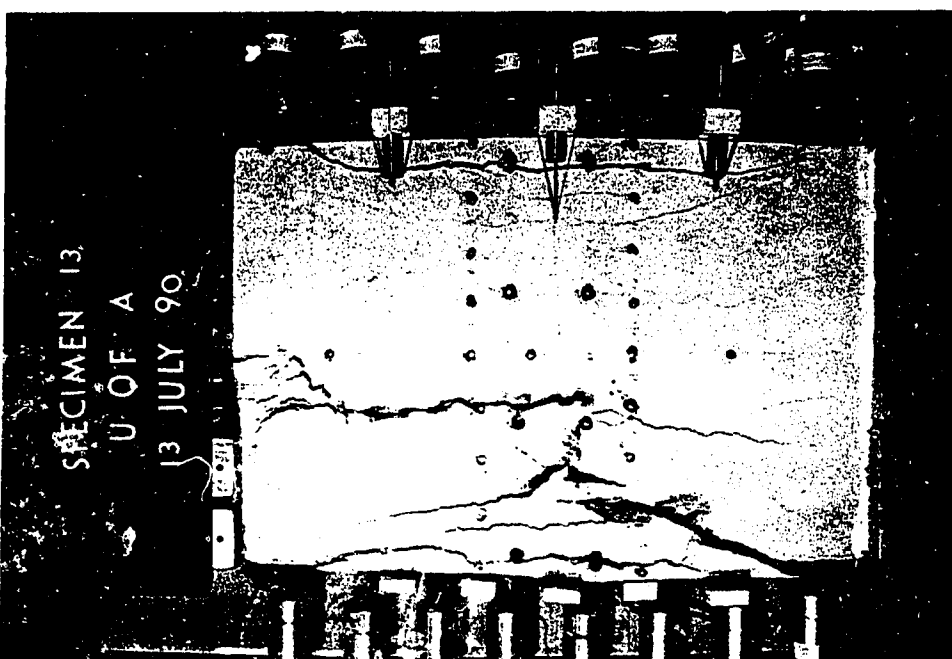
$$\frac{V_u}{b h f_c} = 0.476, \epsilon_t = 0.0179$$

Specimen #11



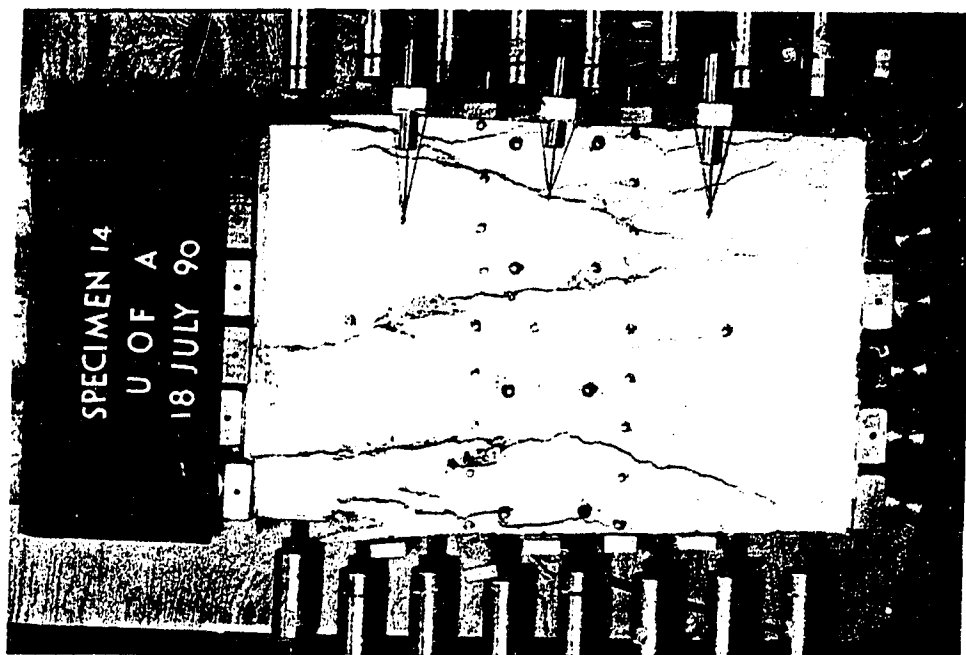
$$\frac{V_u}{b h f_c} = 0.949, \epsilon_t = 0.0010$$

Specimen #12



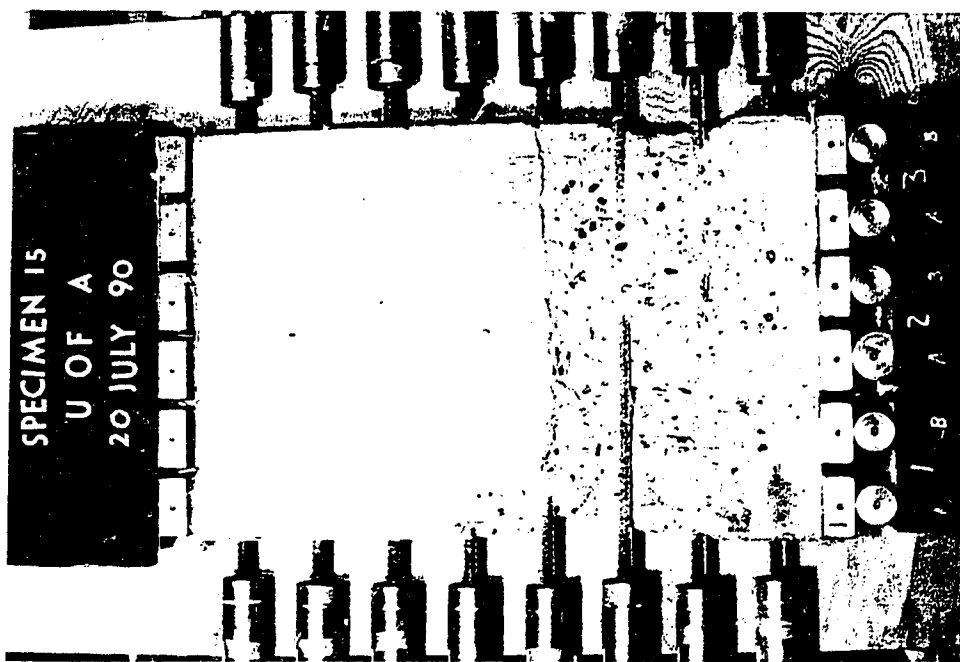
$$\frac{V_u}{bhf_c} = 0.550, \epsilon_t = 0.0212$$

Specimen #13



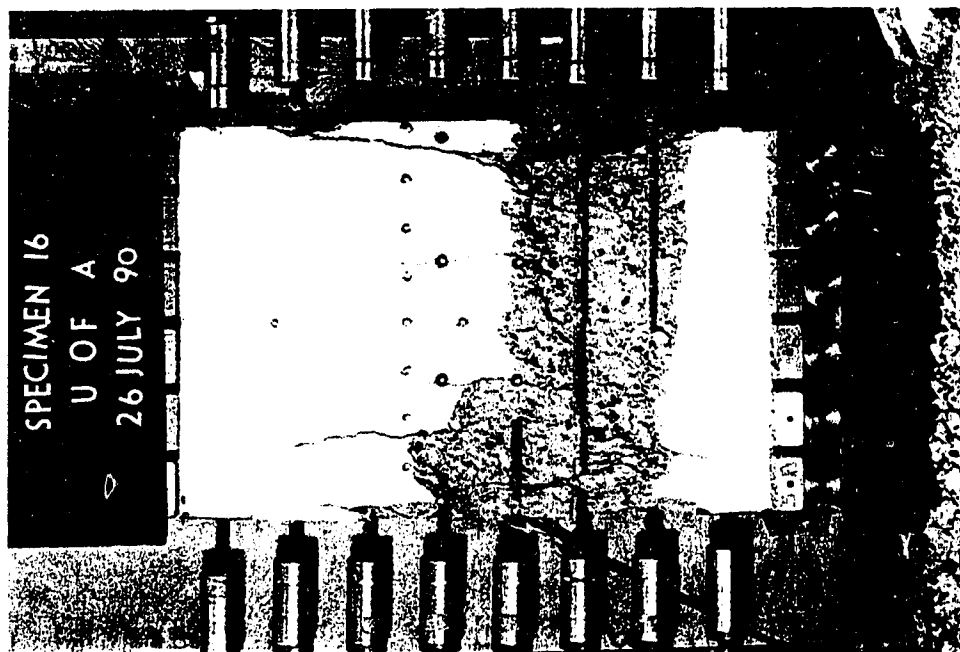
$$\frac{V_u}{bhf_c} = 0.440, \epsilon_t = 0.0217$$

Specimen #14



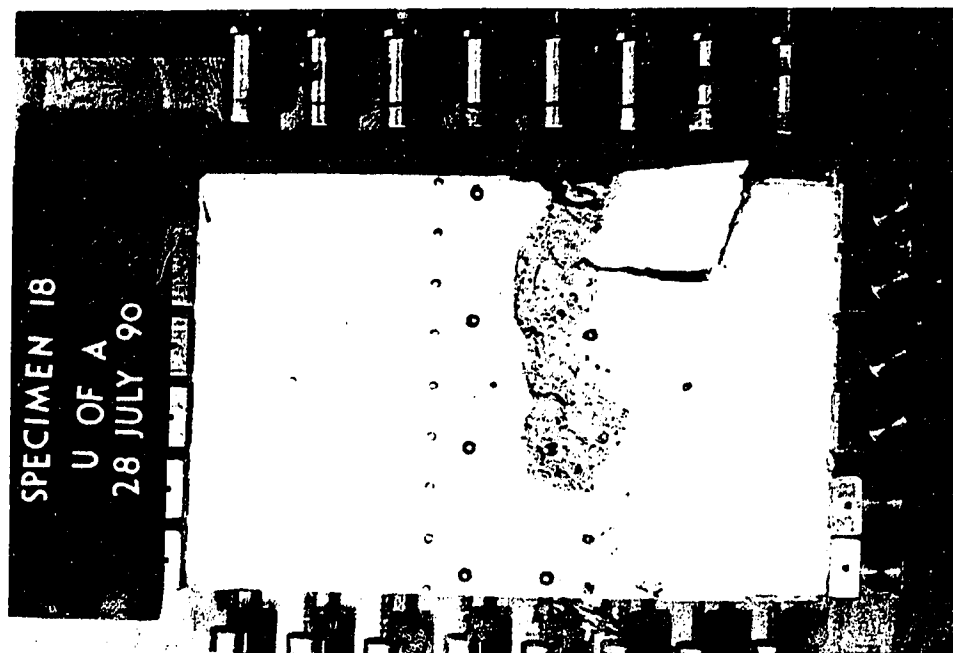
$$\frac{V_u}{bhf_c} = 0.935, \epsilon_t = 0.0044$$

Specimen #15



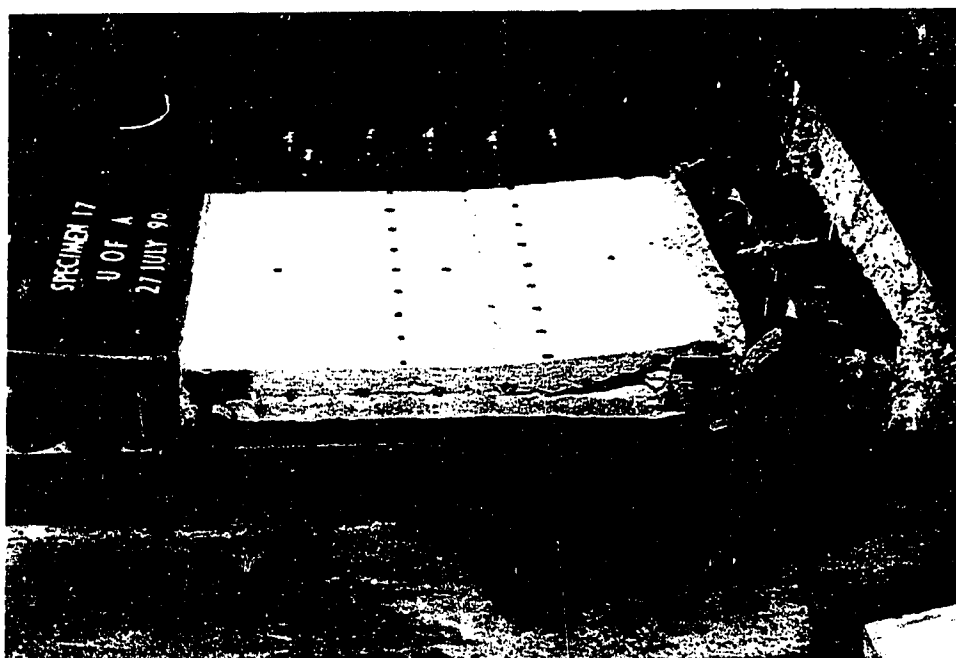
$$\frac{V_u}{bhf_c} = 0.750, \epsilon_t = 0.0084$$

Specimen #16



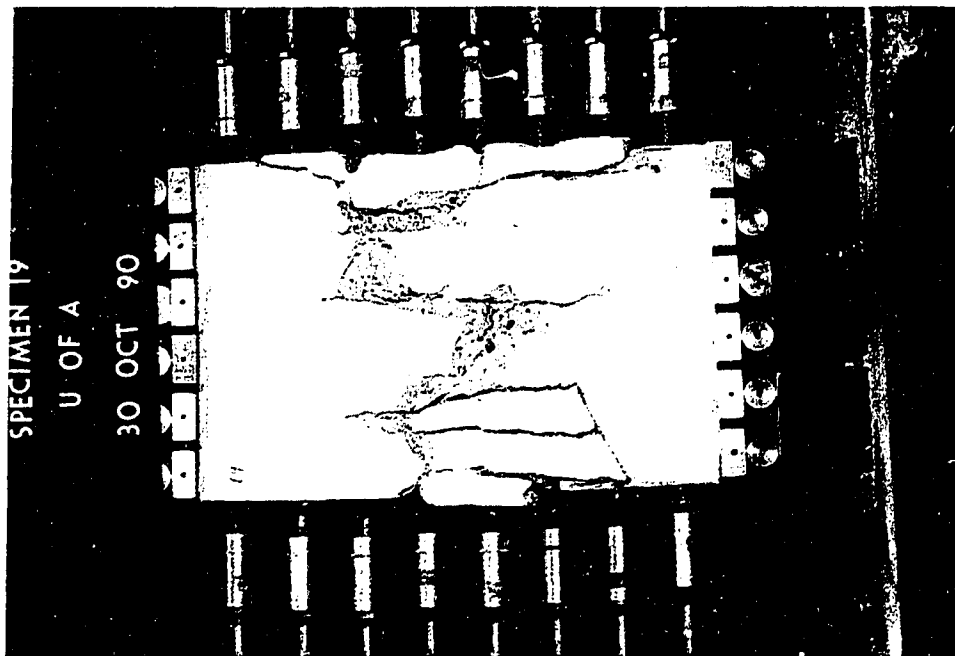
$$\frac{V_u}{bhf_c} = 1.051, \epsilon_t = 0.0011$$

Specimen #18



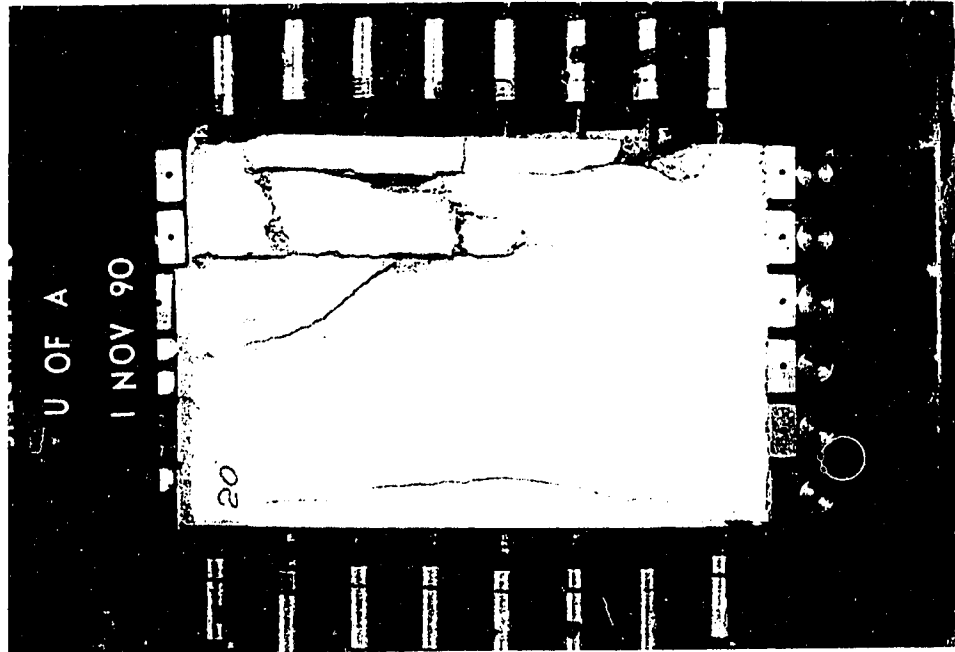
$$\frac{V_u}{bhf_c} = 0.975, \epsilon_t = 0.0003$$

Specimen #17



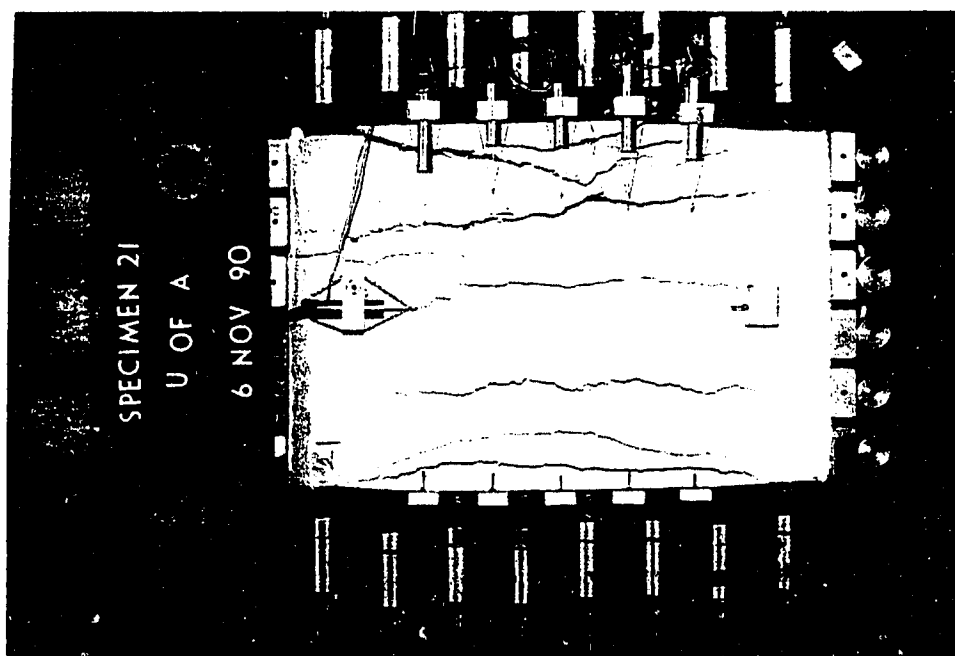
$$\frac{V_u}{bh f_c} = 0.800, \epsilon_t = 0.0109$$

Specimen #19



$$\frac{V_u}{bh f_c} = 0.812, \epsilon_t = 0.0094$$

Specimen #20



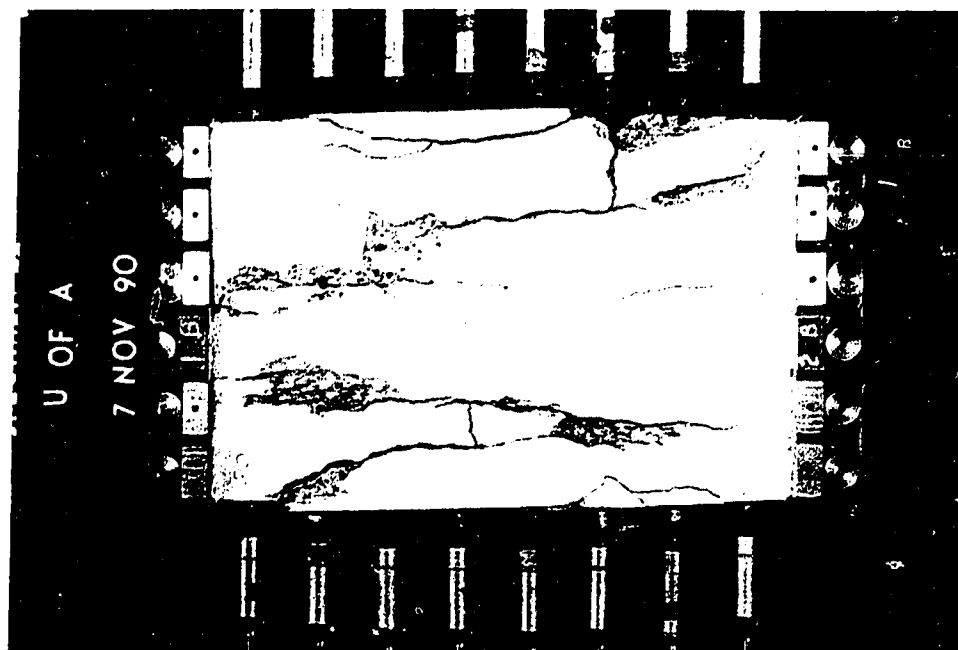
SPECIMEN 21

U OF A

6 NOV 90

$$\frac{V_u}{bhf_c} = 0.411, \epsilon_t = 0.0338$$

Specimen #21

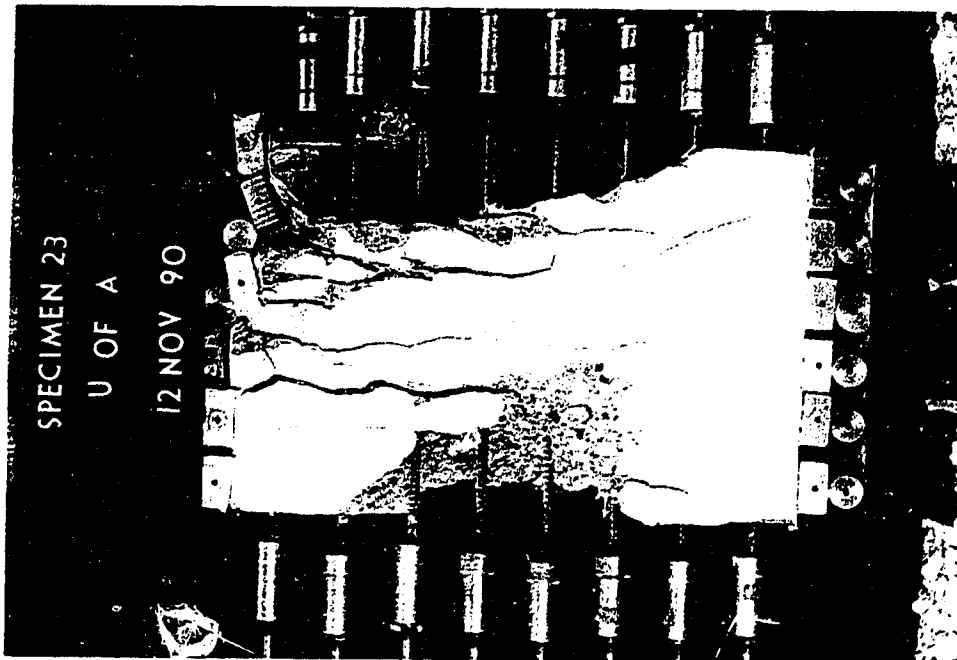


U OF A

7 NOV 90

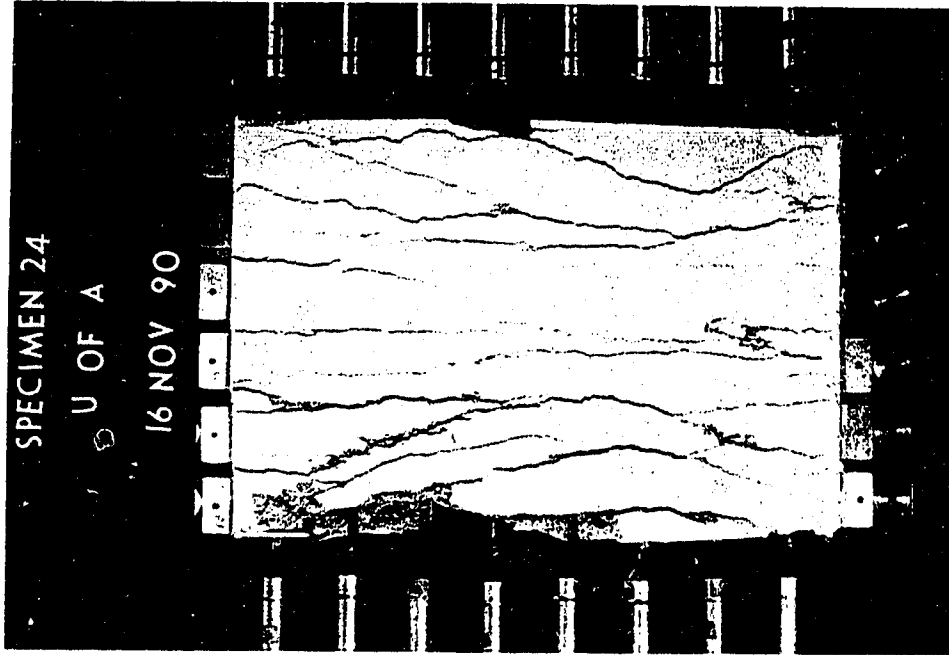
$$\frac{V_u}{bhf_c} = 0.510, \epsilon_t = 0.0272$$

Specimen #22



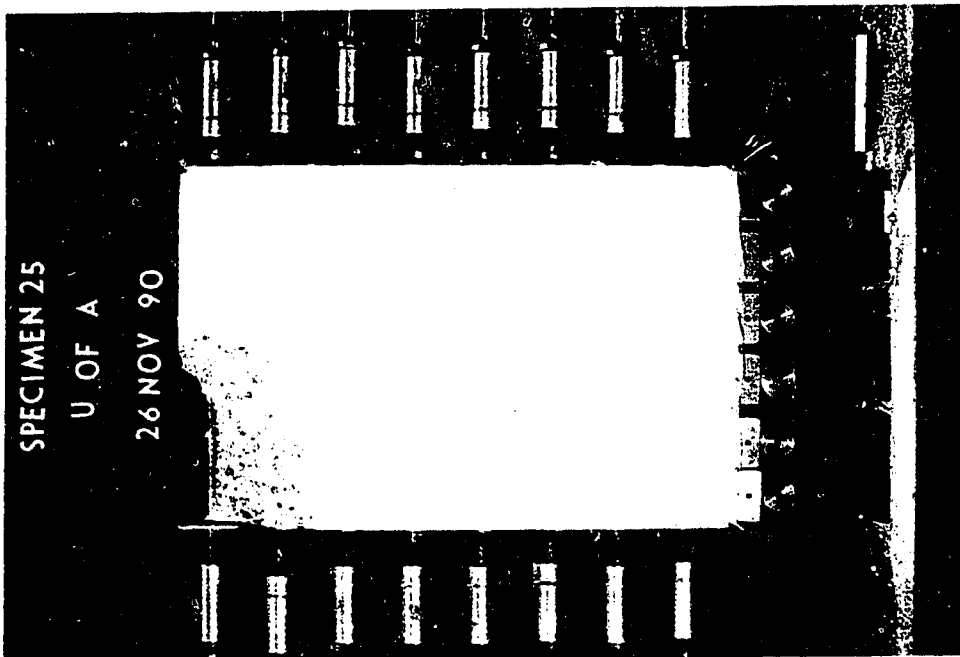
$$\frac{V_u}{bhf_c} = 0.688, \epsilon_t = 0.0116$$

Specimen #23



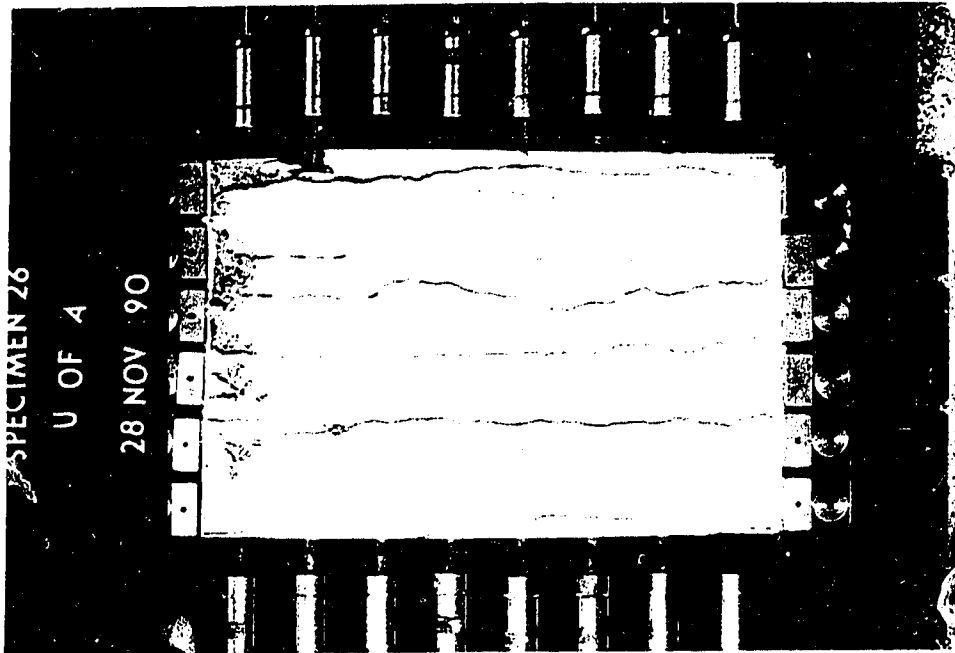
$$\frac{V_u}{bhf_c} = 0.390, \epsilon_t = 0.0432$$

Specimen #24



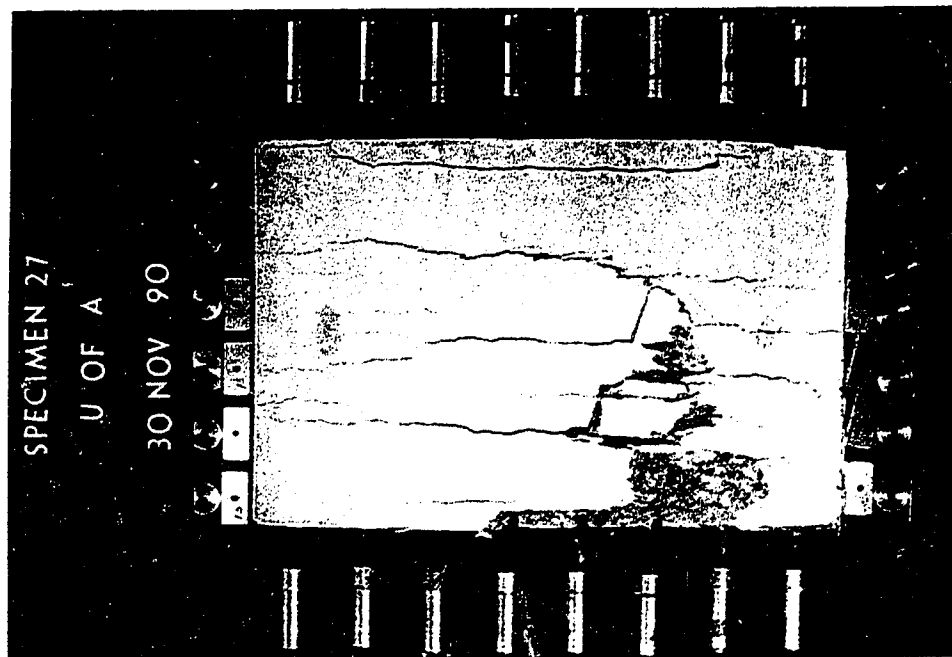
$$\frac{V_u}{bhf_c} = 0.702, \epsilon_t = 0.0026$$

Specimen #25



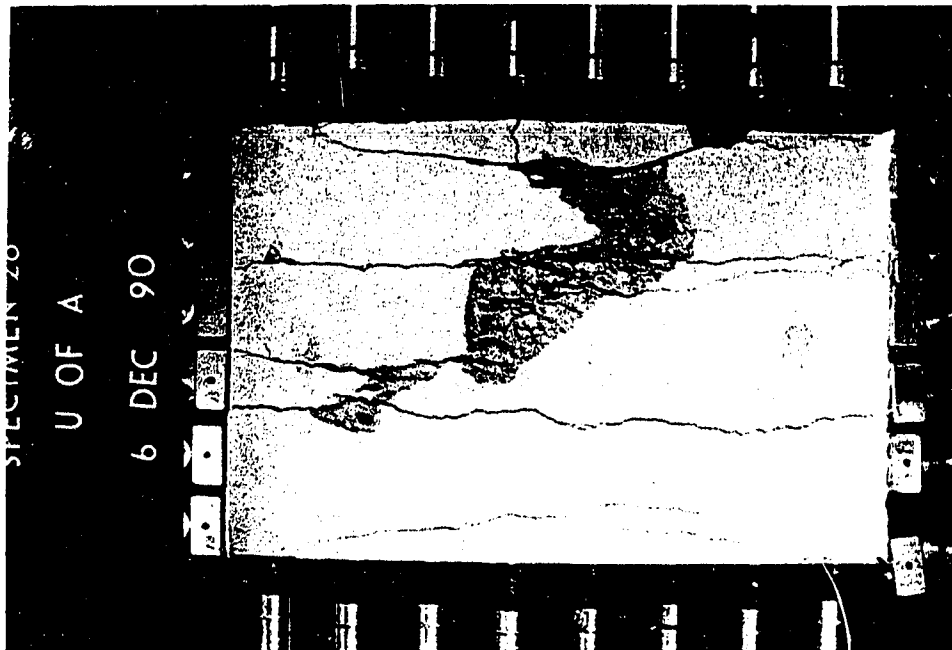
$$\frac{V_u}{bhf_c} = 0.596, \epsilon_t = 0.0145$$

Specimen #26



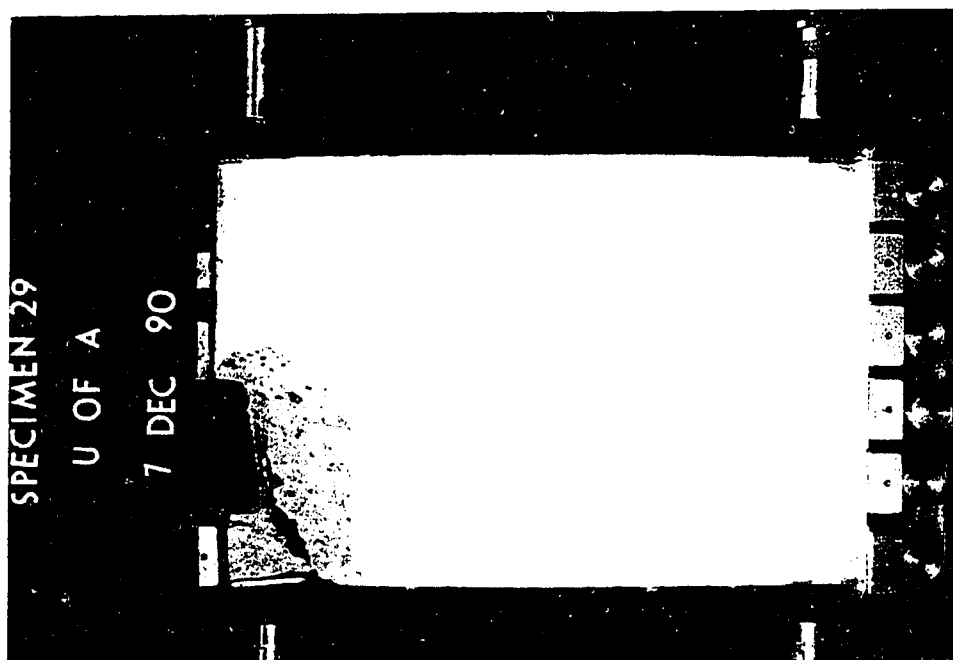
$$\frac{V_u}{bhf_c} = 0.656, \epsilon_t = 0.0104$$

Specimen #27



$$\frac{V_u}{bhf_c} = 0.694, \epsilon_t = 0.0146$$

Specimen #28



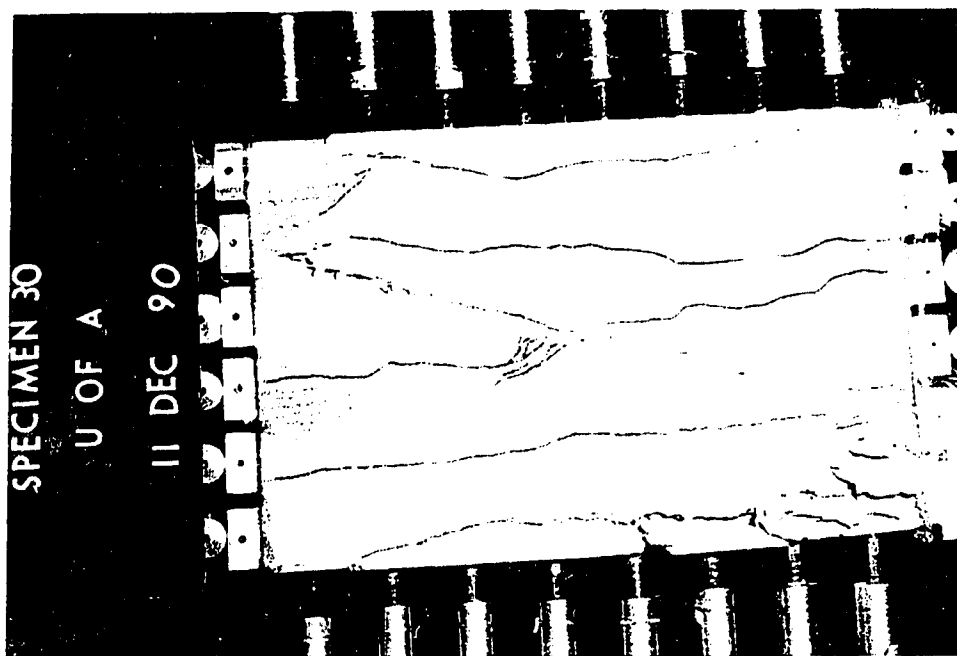
SPECIMEN 29

U OF A

7 DEC 90

$$\frac{V_u}{bhf_c} = 1.003, \epsilon_t = 0.0005$$

Specimen #29



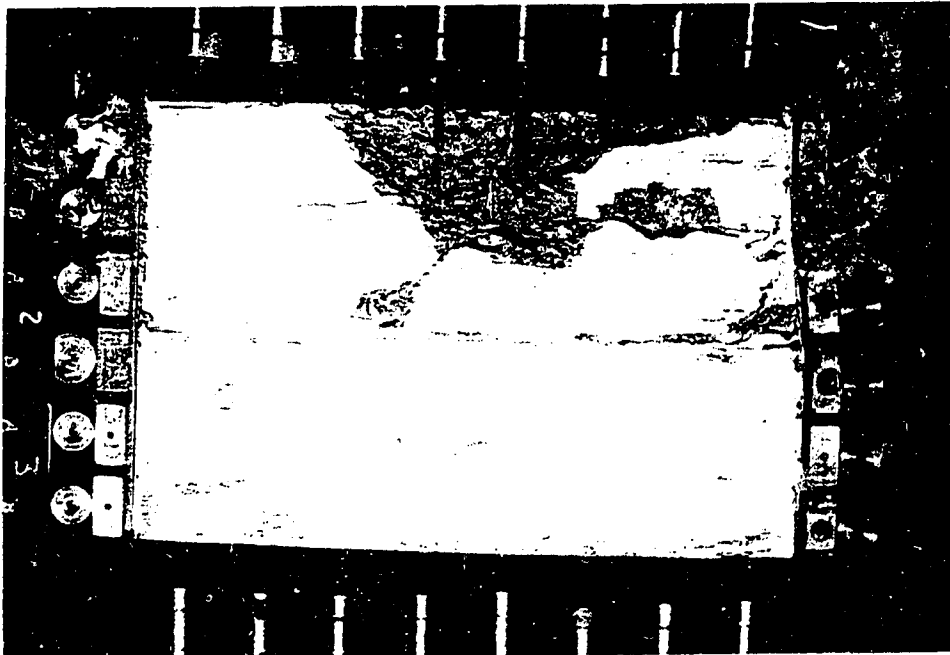
SPECIMEN 30

U OF A

11 DEC 90

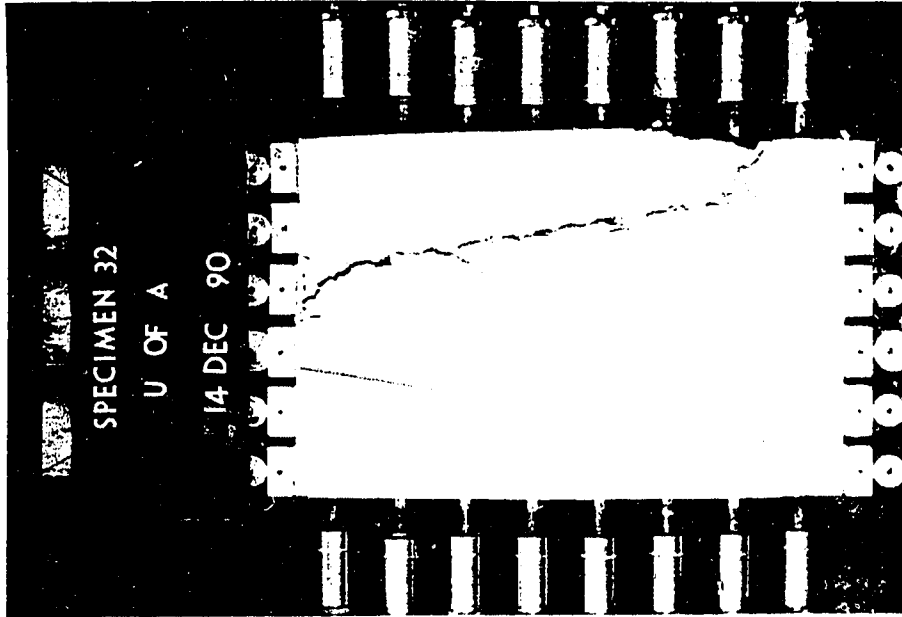
$$\frac{V_u}{bhf_c} = 0.694, \epsilon_t = 0.0098$$

Specimen #30



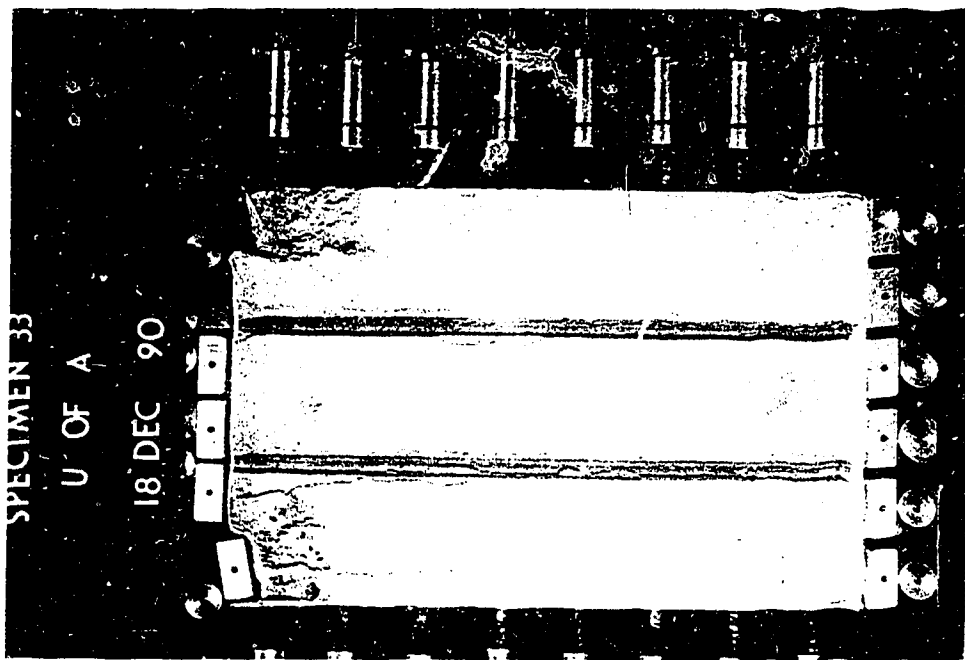
$$\frac{V_u}{bhf_c} = 0.732, \epsilon_t = 0.0099$$

Specimen #31



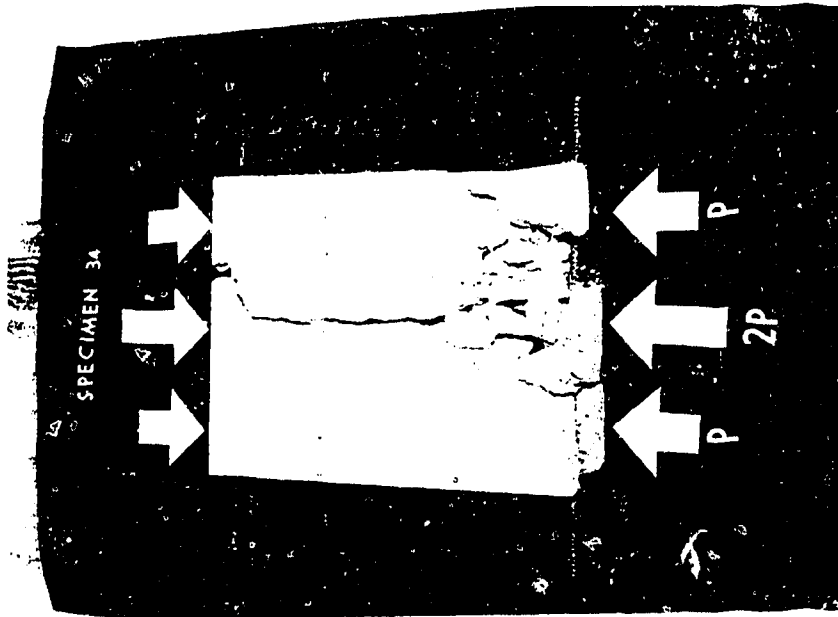
$$\frac{V_u}{bhf_c} = 0.701, \epsilon_t = 0.0044$$

Specimen #32



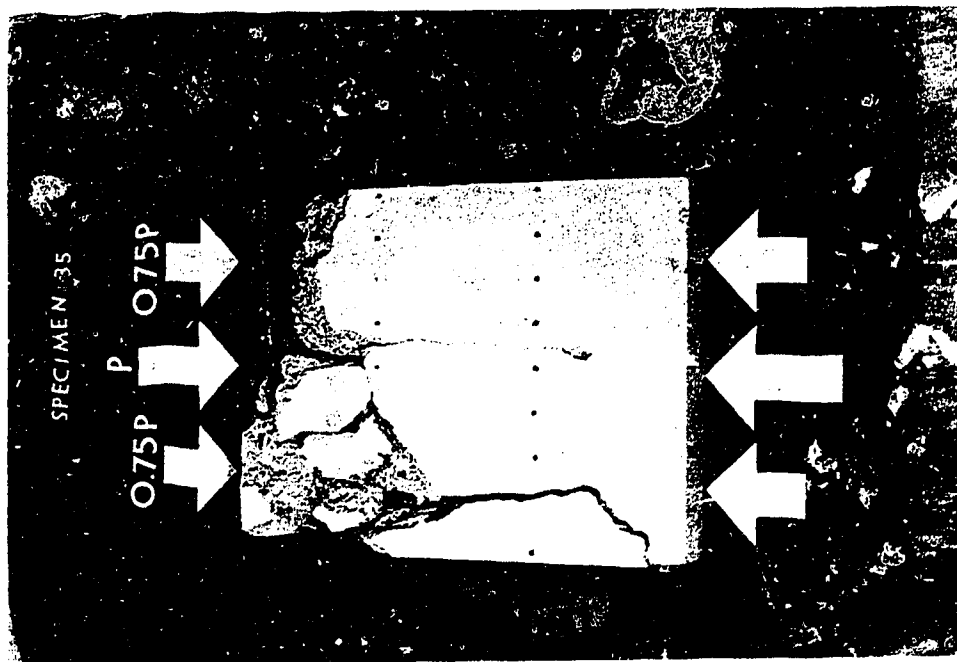
$$\frac{V_u}{bhf_c} = 0.636, \epsilon_t = 0.0067$$

Specimen #33



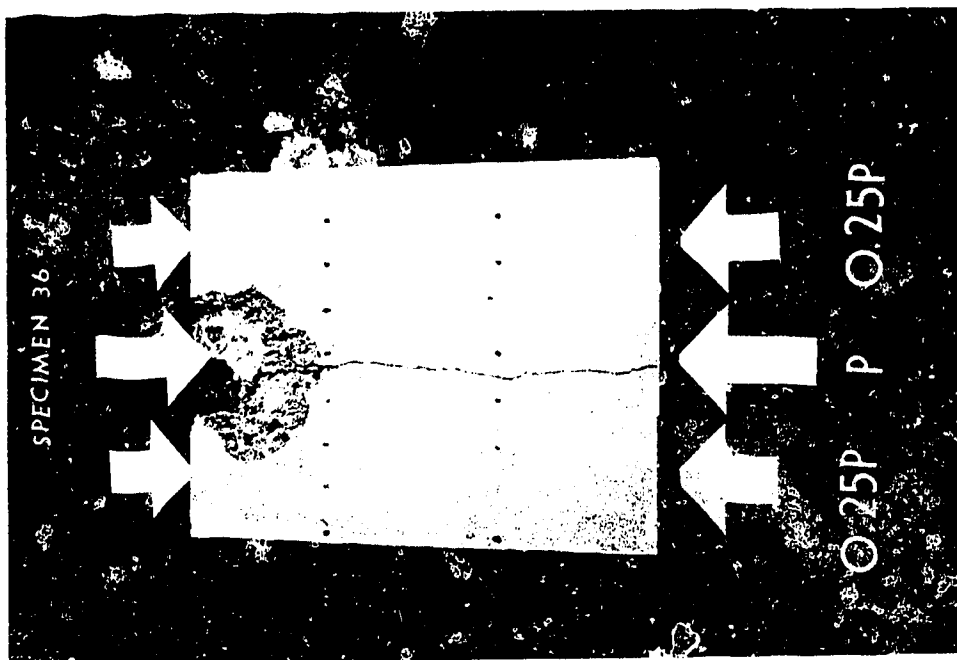
$$\frac{V_u}{bhf_c} = 0.858, \epsilon_t = 0.0060$$

Specimen #34



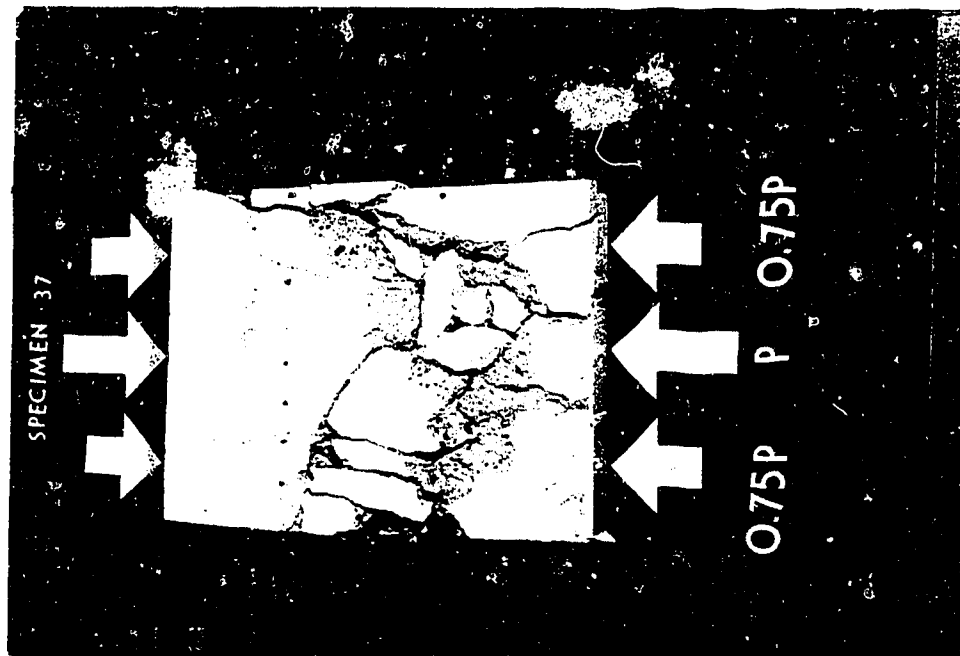
$$\frac{V_u}{bh f_c} = 0.981, \epsilon_t = 0.0023$$

Specimen #35



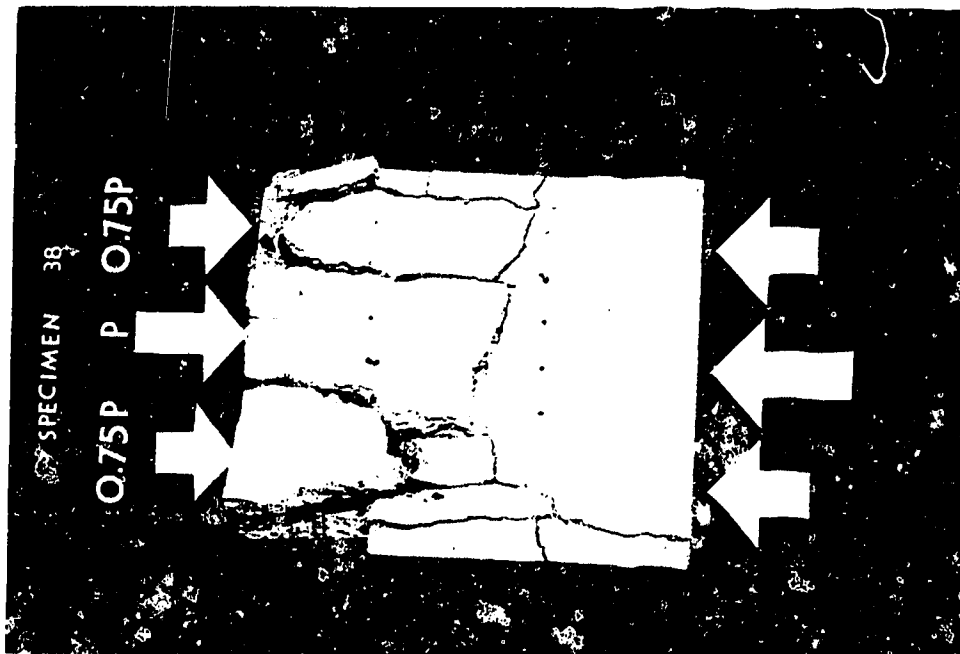
$$\frac{V_u}{bh f_c} = 0.731, \epsilon_t = 0.0000$$

Specimen #36



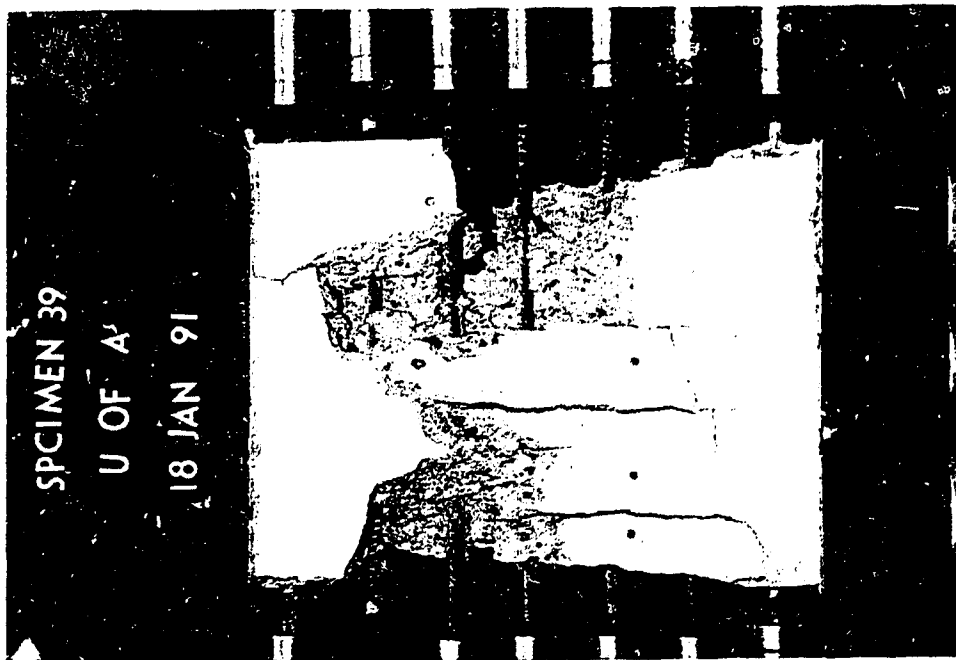
$$\frac{V_u}{bhf_c} = 0.703, \epsilon_t = 0.0079$$

Specimen #37



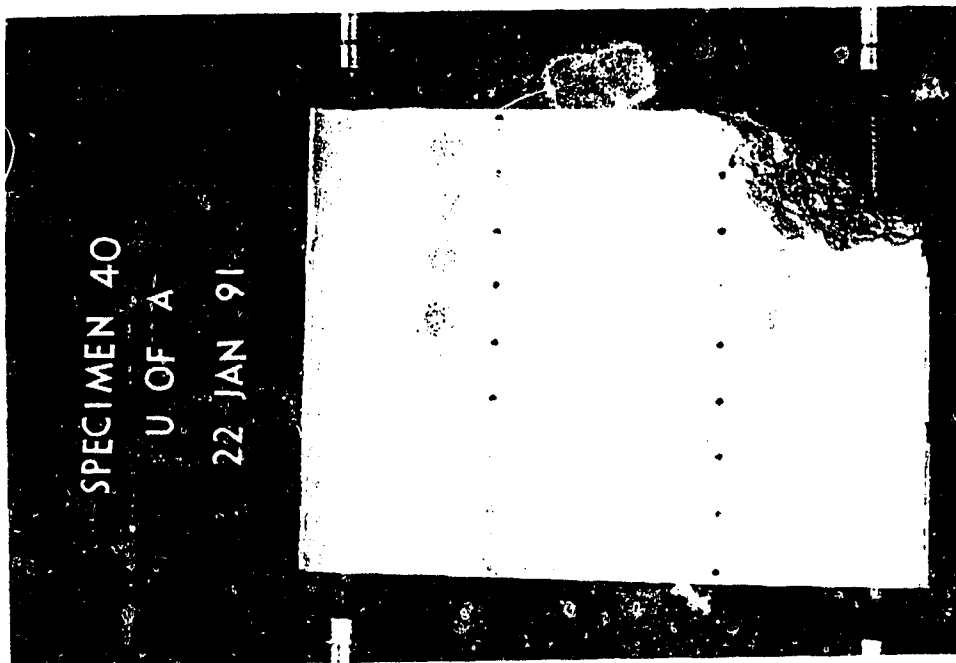
$$\frac{V_u}{bhf_c} = 0.838, \epsilon_t = 0.0081$$

Specimen #38



$$\frac{V_u}{bhf_c} = 0.622, \epsilon_t = 0.0150$$

Specimen #39



$$\frac{V_u}{bhf_c} = 1.036, \epsilon_t = 0.0000$$

Specimen #40

APPENDIX C

CRACK PATTERNS OF THE TEST BEAMS

BY SCORDELIIS AND BRESLER

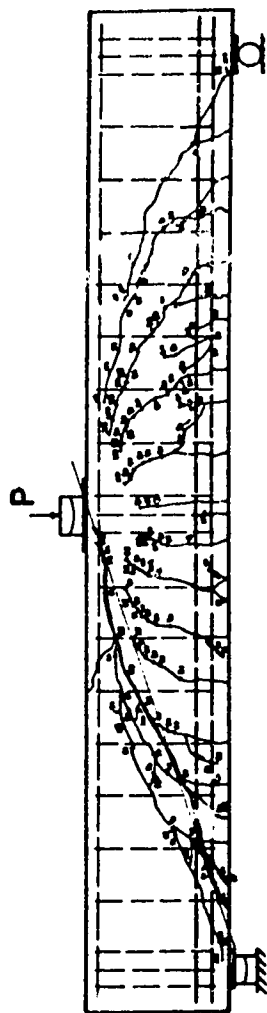


Figure C-1 Specimen A-1

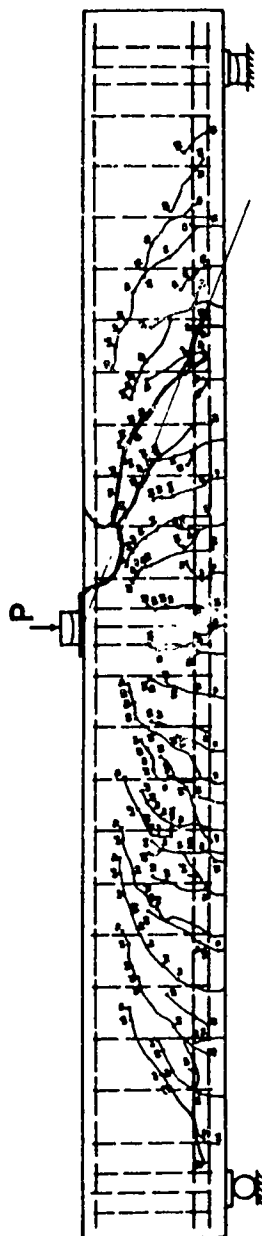


Figure C-2 Specimen A-2

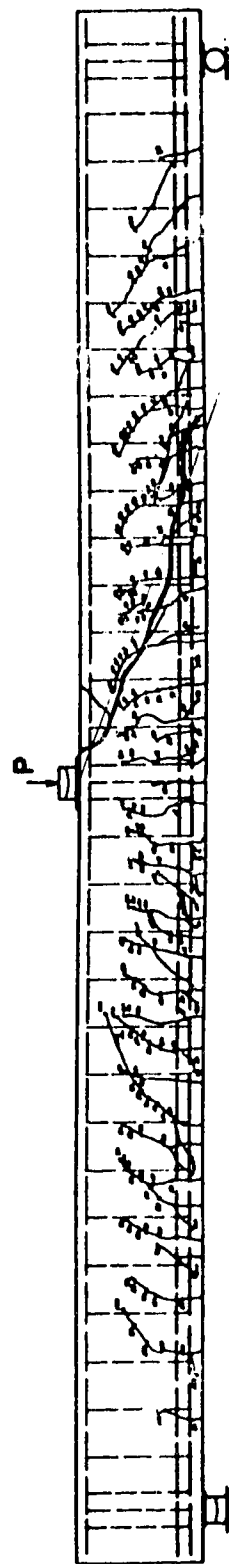


Figure C-3 Specimen A-3

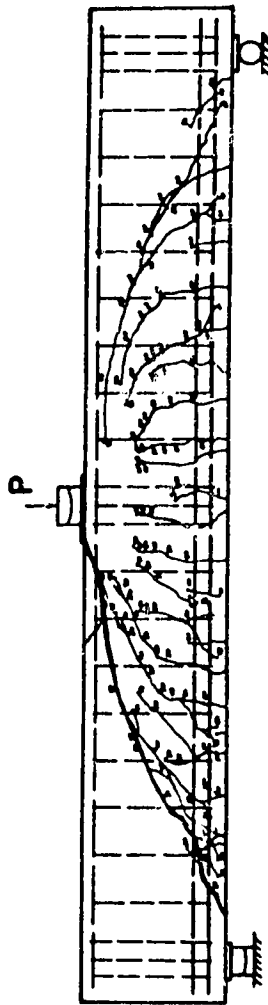


Figure C-4 Specimen B-1

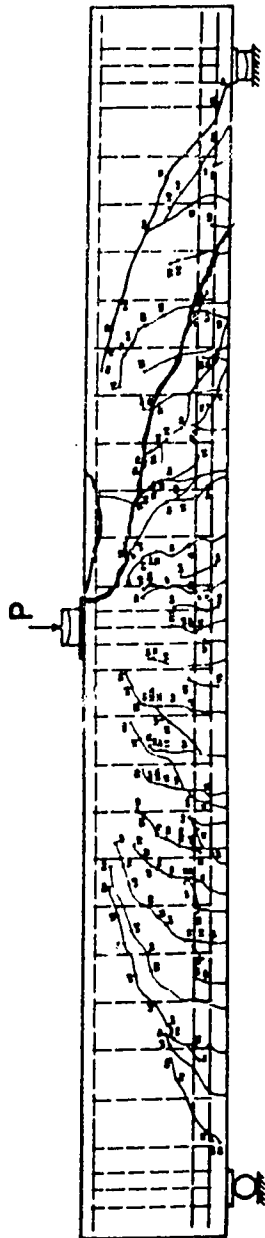


Figure C-5 Specimen B-2

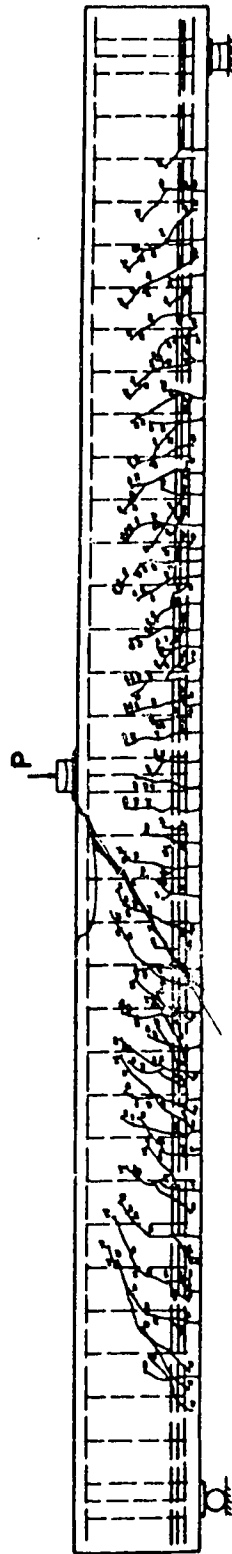


Figure C-6 Specimen B-3

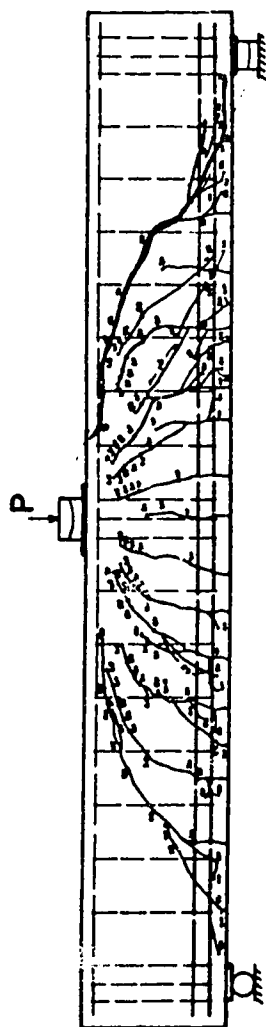


Figure C-7 Specimen C-1

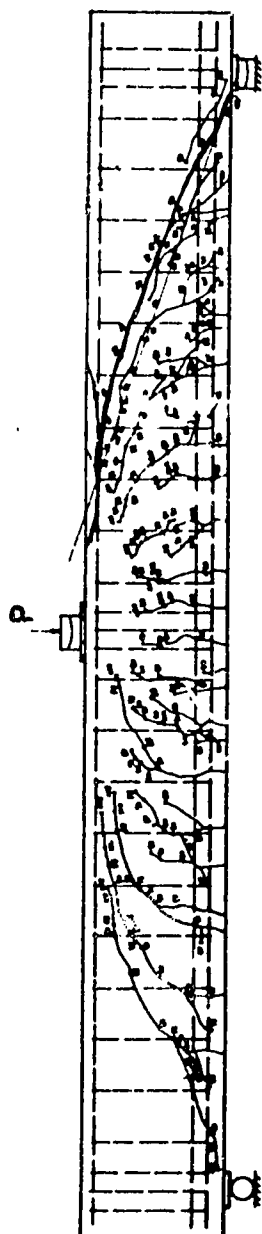


Figure C-8 Specimen C-2

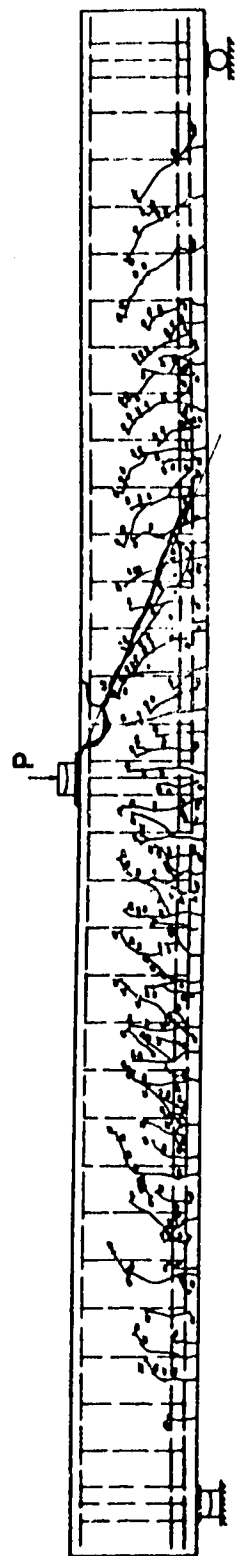
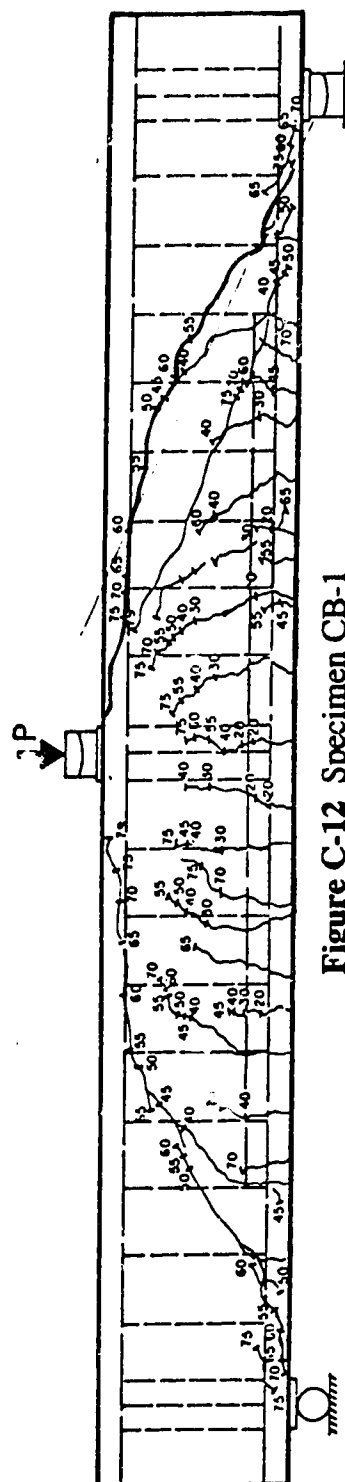
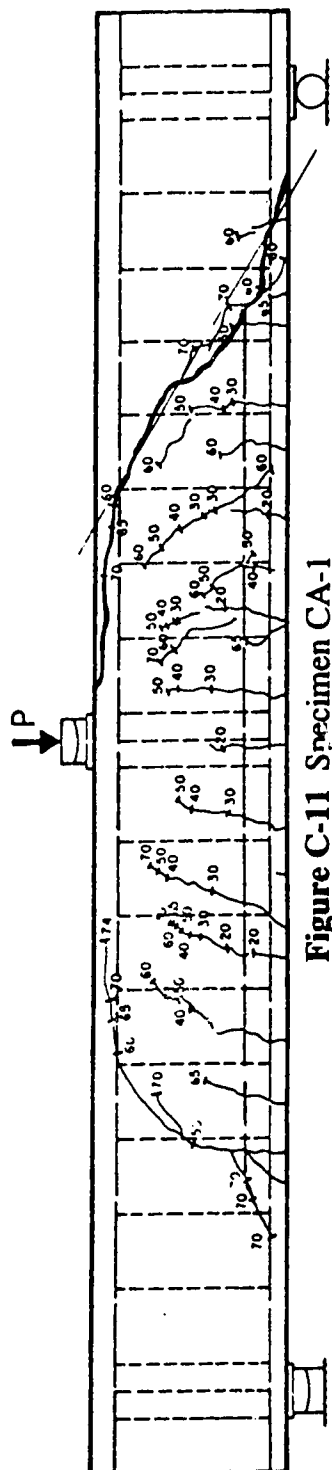
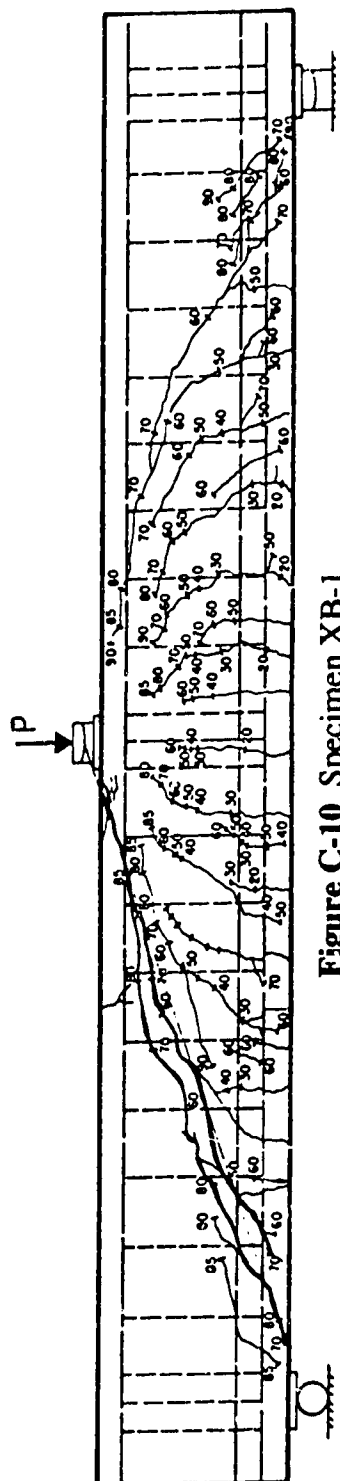


Figure C-9 Specimen C-3



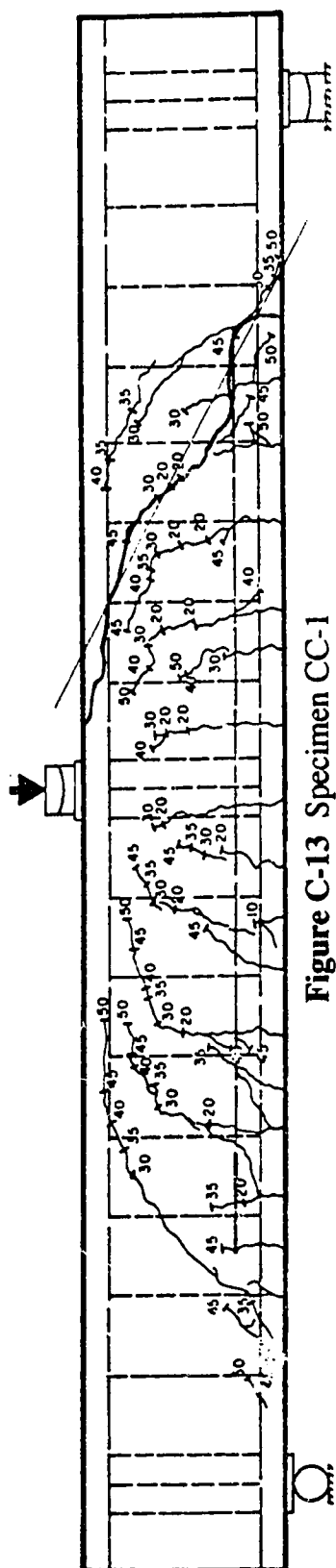


Figure C-13 Specimen CC-1

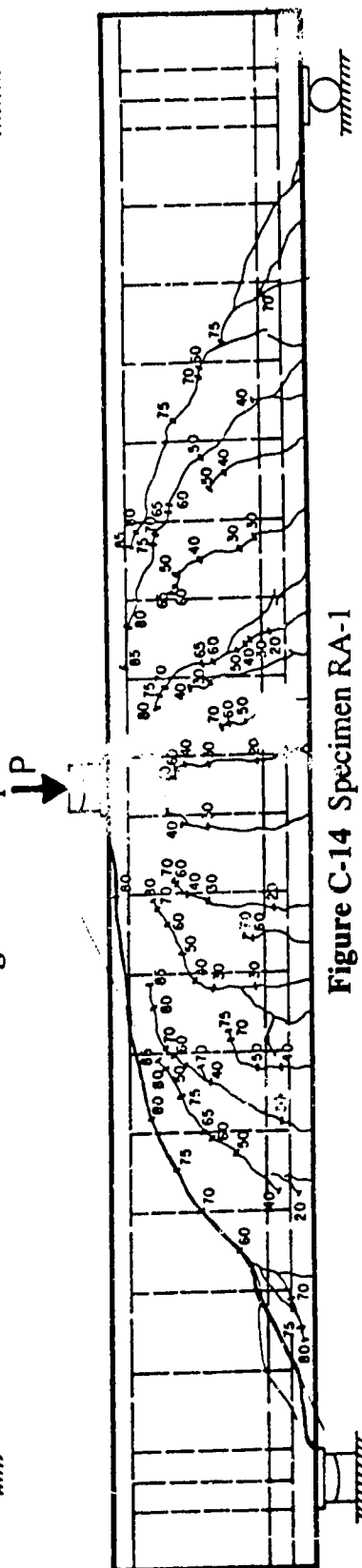


Figure C-14 Specimen RA-1

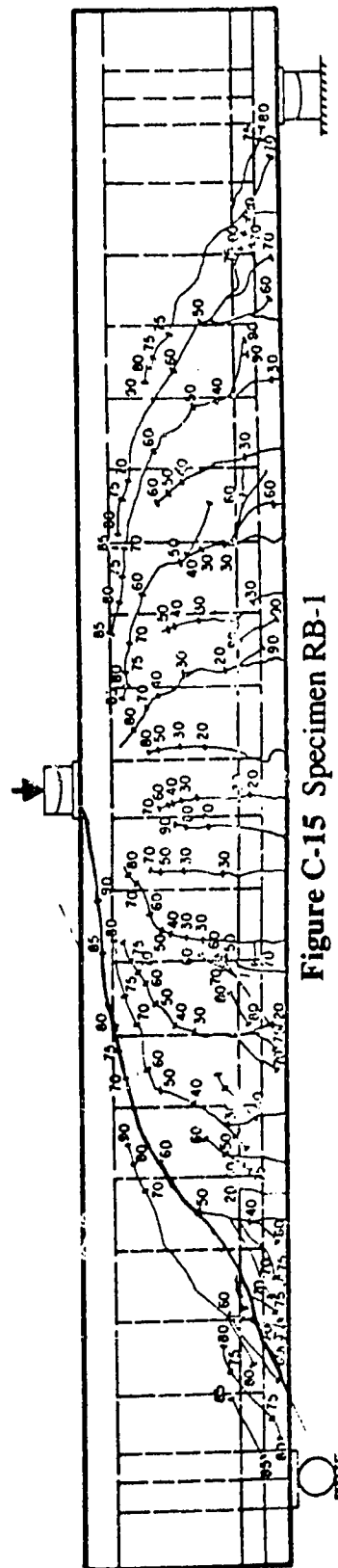


Figure C-15 Specimen RB-1

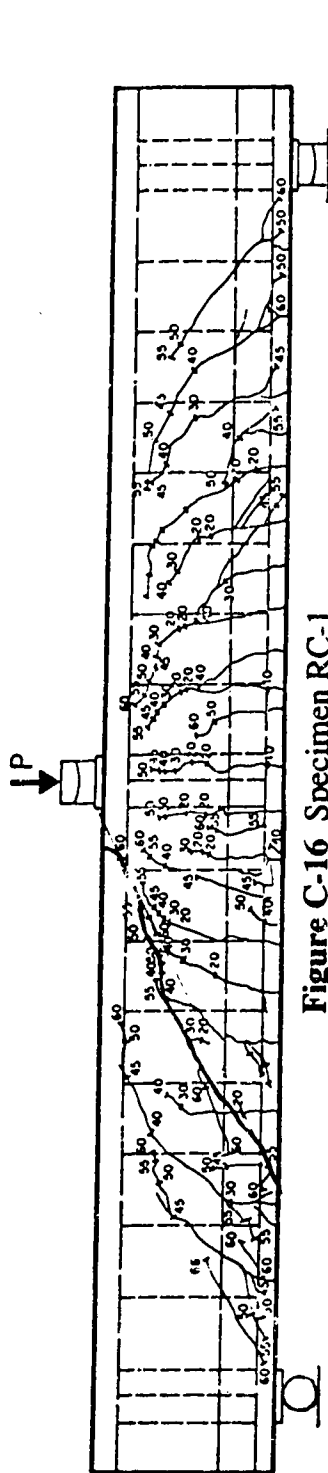


Figure C-16 Specimen RC-1

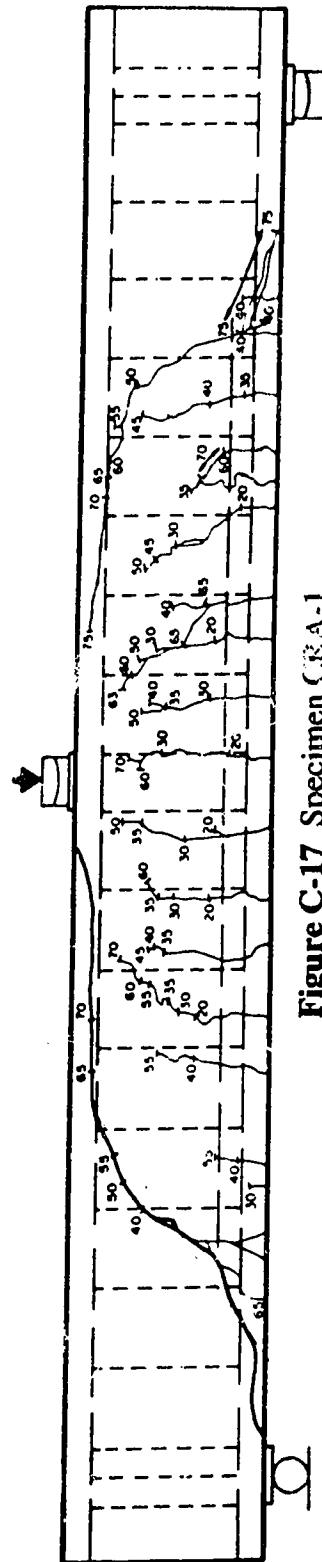


Figure C-17 Specimen CRA-1

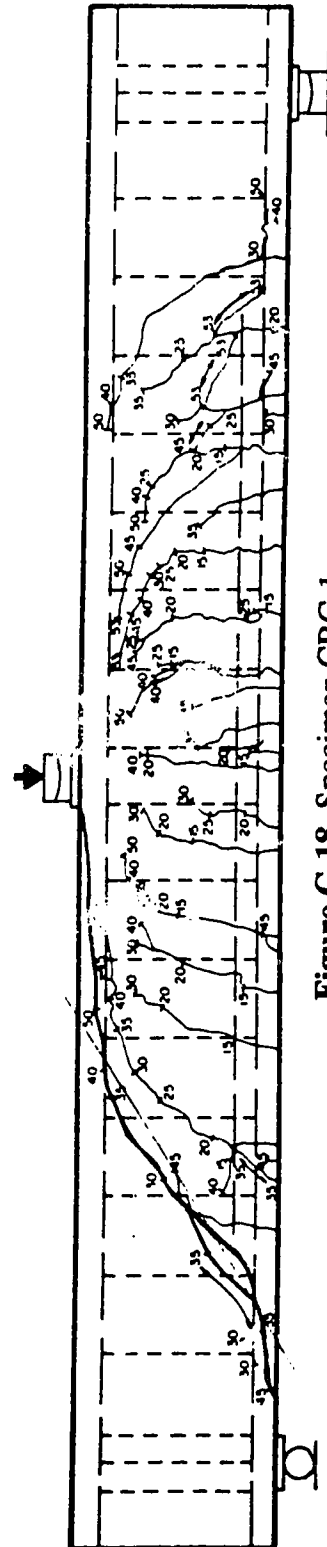
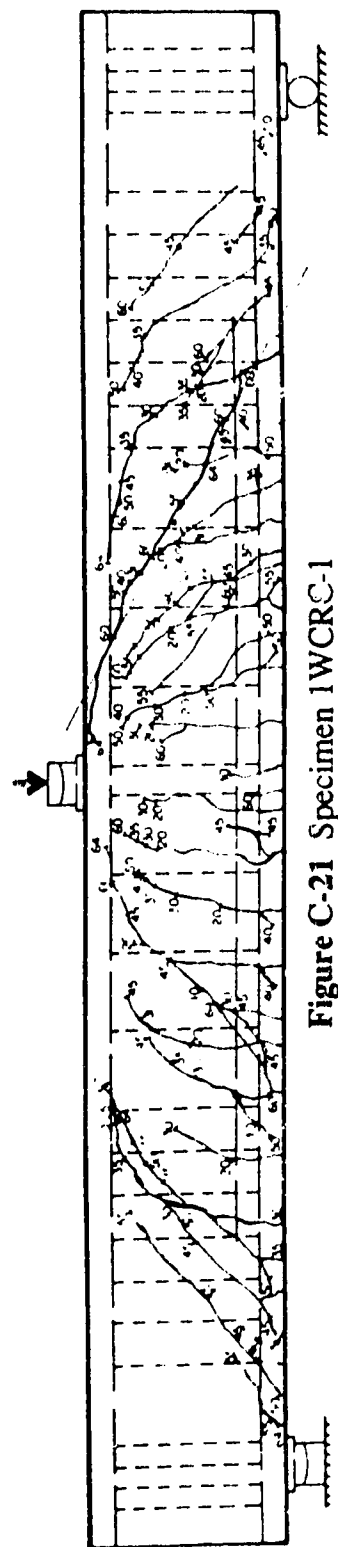
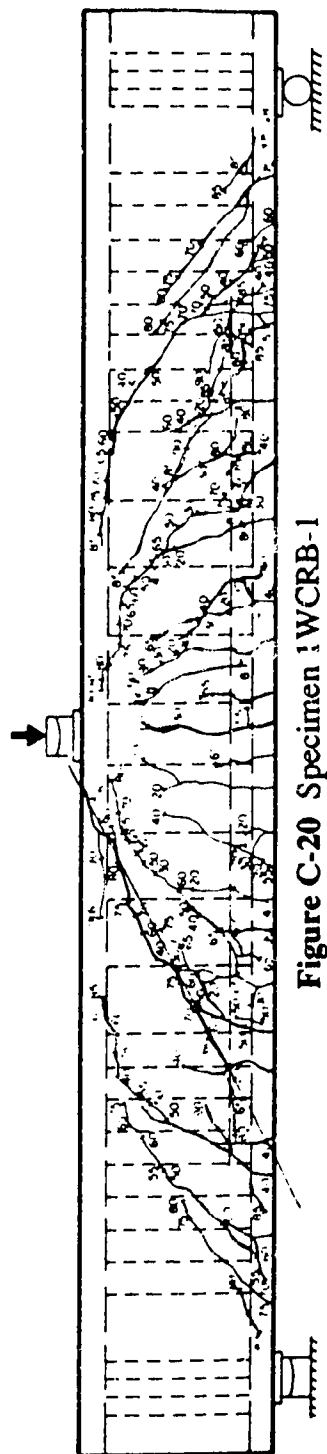
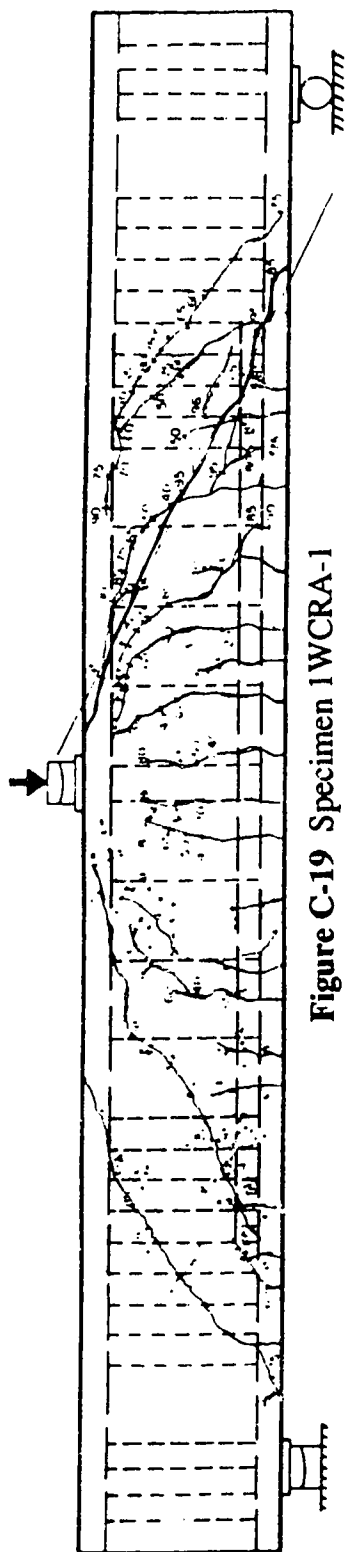


Figure C-18 Specimen CRC-1



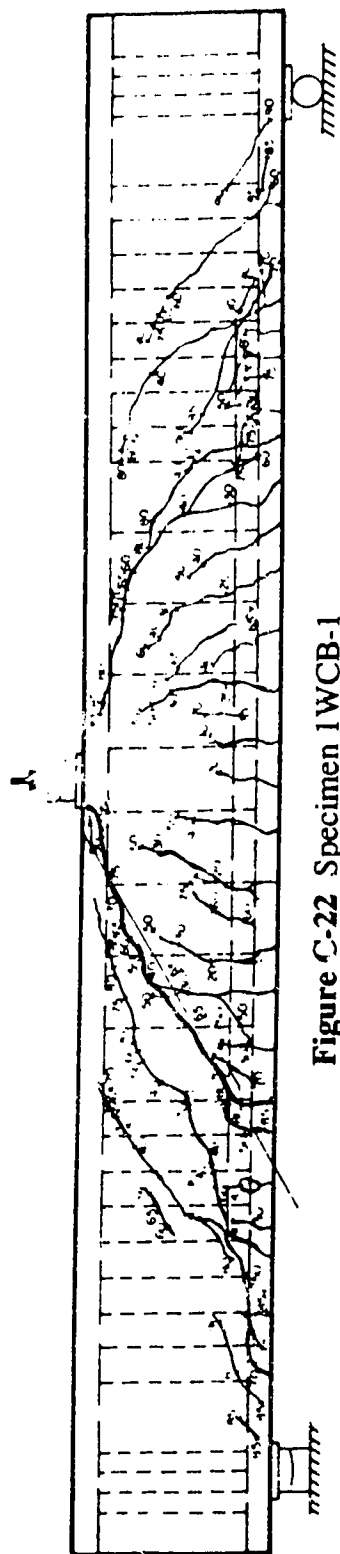


Figure C-22 Specimen 1WCB-1

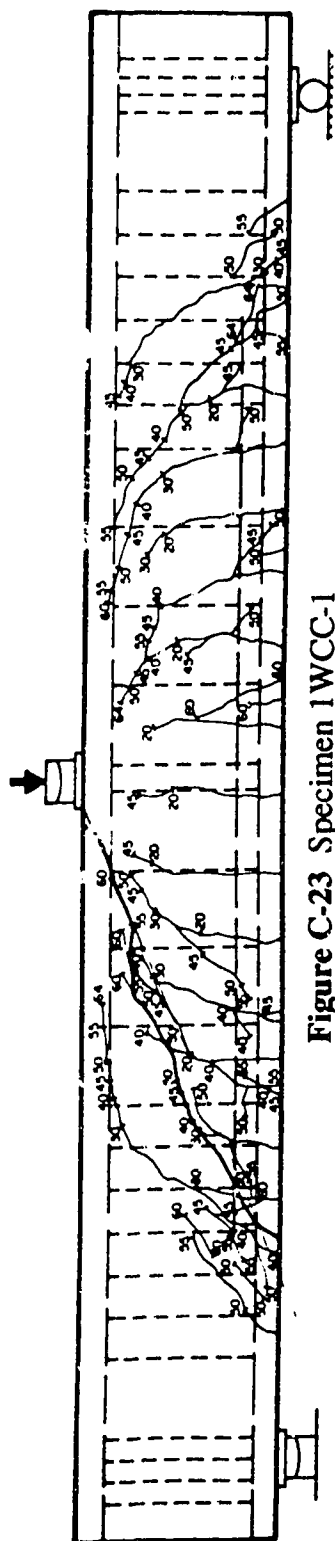


Figure C-23 Specimen 1WCC-1

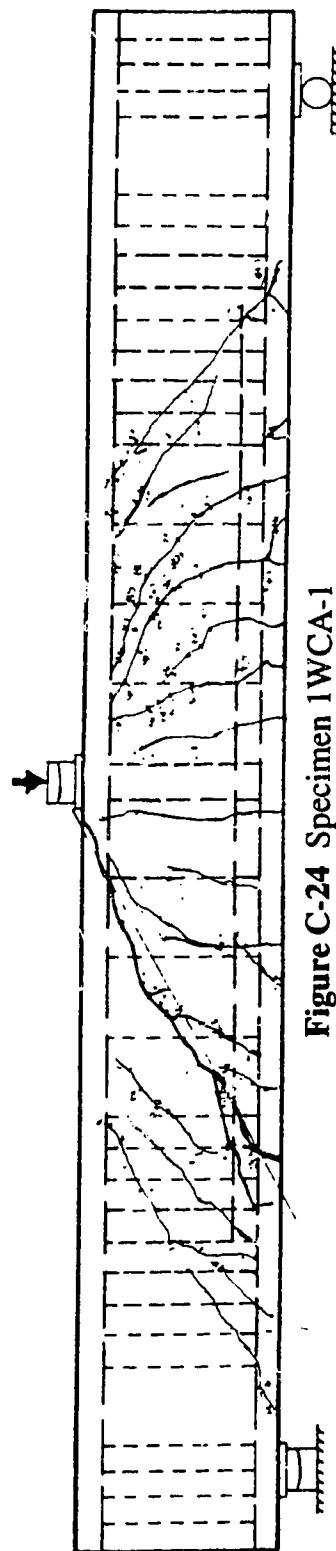


Figure C-24 Specimen 1WCA-1

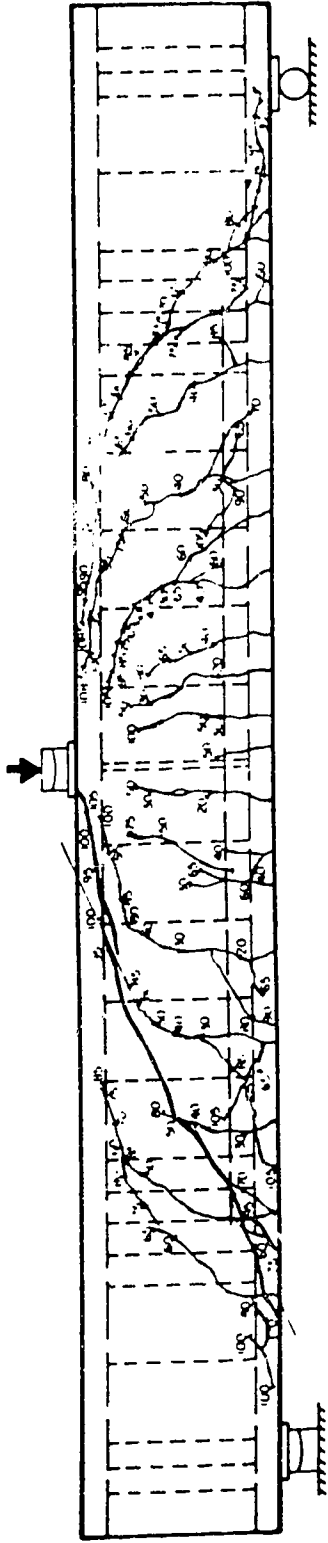


Figure C-25 Specimen 2WCA-1

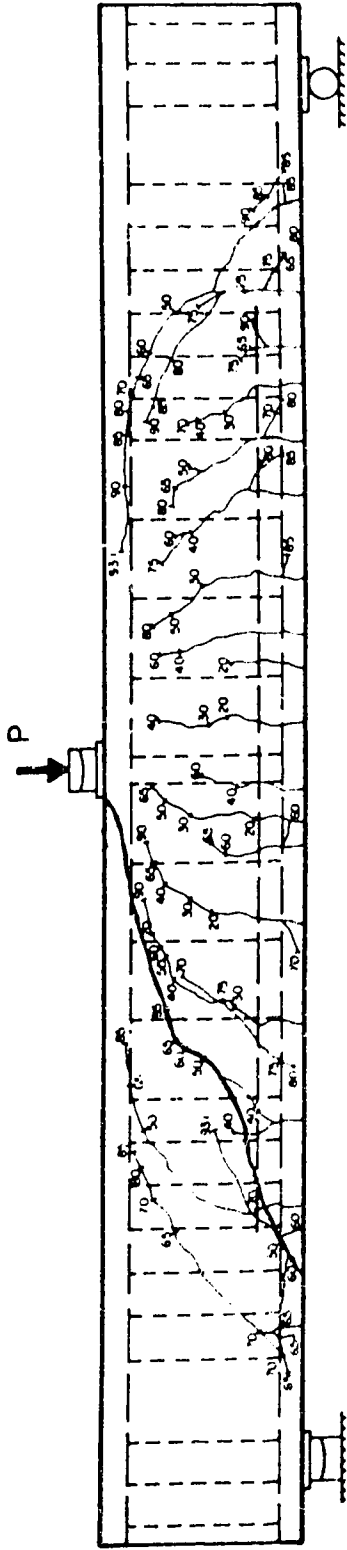


Figure C-26 Specimen 3WCA-1